Structure and functional insights of a recombinant bifunctional α-L-arabinofuranosidase (*Bo*GH43_35) with endo-xylanase activity from *Bacteroides ovatus* ATCC 8483 and its application in fruit juice clarification and waste peel saccharification

Ph.D. Thesis

by

Madhulika Shrivastava

May 2025

DEPARTMENT OF BIOSCIENCES AND BIOENGINEERING
INDIAN INSTITUTE OF TECHNOLOGY GUWAHATI
GUWAHATI – 781039, ASSAM, INDIA

Structure and functional insights of a recombinant bifunctional α-L-arabinofuranosidase (*Bo*GH43_35) with endo-xylanase activity from *Bacteroides ovatus* ATCC 8483 and its application in fruit juice clarification and waste peel saccharification

A Thesis

Submitted for partial fulfilment
of the requirements for the award of

Doctor of Philosophy

by

Madhulika Shrivastava

Under the supervision of

Prof. Arun Goyal

May 2025

DEPARTMENT OF BIOSCIENCES AND BIOENGINEERING
INDIAN INSTITUTE OF TECHNOLOGY GUWAHATI
GUWAHATI – 781039, ASSAM, INDIA

INDIAN INSTITUTE OF TECHNOLOGY GUWAHATI

DEPARTMENT OF BIOSCIENCES AND BIOENGINEERING

STATEMENT

I do hereby declare that the content embodied in this thesis entitled "**Structure and functional insights of a recombinant bifunctional α-L-arabinofuranosidase (*Bo*GH43_35) with endo-xylanase activity from *Bacteroides ovatus* ATCC 8483 and its application in fruit juice clarification and waste peel saccharification"** is the result of investigations carried out by me at Department of Biosciences and Bioengineering, Indian Institute of Technology Guwahati, Guwahati, India under the guidance of **Prof. Arun Goyal**. In keeping with the general practice of reporting scientific observations, due acknowledgements have been made wherever the work described is based on the findings of other investigators.

Madhulika

May, 2025

Madhulika Shrivastava
(Roll No.: 206106027)

INDIAN INSTITUTE OF TECHNOLOGY GUWAHATI

DEPARTMENT OF BIOSCIENCES AND BIOENGINEERING

CERTIFICATE

This is to certify that the work described in this thesis entitled "**Structure and functional insights of a recombinant bifunctional α-L-arabinofuranosidase (*Bo*GH43_35) with endo-xylanase activity from *Bacteroides ovatus* ATCC 8483 and its application in fruit juice clarification and waste peel saccharification"** by **Ms. Madhulika Shrivastava** (Roll No.: 206106027) for the award of degree of Doctor of Philosophy is an authentic record of the results obtained from the research work carried out under my supervision in the Department of Biosciences and Bioengineering, Indian Institute of Technology Guwahati, India and this work has not been submitted elsewhere for a degree.

Prof. Arun Goyal *(MTech, PhD)*
FAMI, FBRS, FABP, FNABS, FNAAS, FIFIB, FMBSI, FACCTI, FSEES
(Thesis Supervisor)
Department of Biosciences and Bioengineering
Indian Institute of Technology Guwahati
Guwahati – 781039
Assam, India

Acknowledgements

I express my heartfelt gratitude to the Almighty for granting me the strength and perseverance to complete this thesis. I would also like to extend my sincere thanks to all those who have supported me throughout this journey.

First and foremost, I am deeply grateful to my supervisor, ***Prof. Arun Goyal****, whose invaluable guidance, encouragement and unwavering support have been instrumental in the successful completion of this work. His scientific insights and high ethical standards have greatly shaped my approach to research and personal development.*

I would like to express my sincere gratitude to all my doctoral committee members, ***Prof. Sachin Kumar, Dr. Kusum Kumari Singh, Dr. Rajkumar P. Thummer*** *and* ***Dr. Kapish Gupta*** *for their constructive feedback and thoughtful suggestions during my seminars and review meetings, which significantly contributed to this work.*

I owe my profound gratitude to the present and previous heads of the Department of Biosciences and Bioenigineering, IIT Guwahati, Prof. Utpal Bora, Prof. Rakhi Chaturvedi and Prof. Latha Rangan for providing me with the necessary facilities. I wish to acknowledge the support received from all the faculties, earlier and present staffs of BSBE..

I am thankful to ***Department of Biosciences and Bioengineering*** *and* ***Central Instrument Facility (CIF)*** *for providing me with facilities to carry out my research work. I am also thankful to the* ***Indian Institute of Technology Guwahati*** *for providing the advanced infrastructure and research facilities that enabled me to carry out this work. I am also thankful to Ministry of Education (MoE), Government of India for giving assistantship throughout the Ph.D tenure.*

I am thankful to my friends Ms Devashree Patel, Mr. Sahil Dhull and Mrs. Gayatri Sharma, for their immense care, encouragement, and moral support in all hard phases of my Ph.D. tenure.

I am also thankful to my former and present lab members, Dr. Kedar Sharma, Dr. Abhijeet Thakur, Dr. Kaustubh C. Khaire, Dr. Parmeshwar V.G, Dr. Jebin Ahmed, Dr. Maibam P. Devi, Yumnam Robinson, Ardhendu, Aishwarya, Shreya Biswas, Akshita Kanwar, Vishwanath Yadav, Bipasa Choudhury, Shushruta, Ashwini, Akshay, Deblina, Tiyasa, Annu and Nilakshi for all the worthy support and cooperation.

Words fall short in expressing gratitude to my mom, Mrs. Rinku Shrivastava and dad, Mr. Satish Shrivastava whose love, patience, and unwavering belief in me have been my biggest strength. I am equally thankful to my family members Swapnil Raj, Mr. Amrendra Bhushan. Adarsh Shresth and Mrs Smita Bhushan for their continued encouragement and support.

Lastly, I am immensely grateful to my beloved companion, ***Mr. Apurva Shrestha****, for being my pillar of strength and for his enduring moral support, which helped me persevere through all the ups and downs.*

Madhulika Shrivastava

May, 2025

SYNOPSIS

Introduction

The increase in lifestyle diseases has led to sophistication in people's standard of living. In response to the increasing demand for nutritious food, food manufacturers are encouraged to develop fiber-enriched food products. Dietary fiber is defined as those components of plant material in the diet which are indigestible by enzymes in the human gastrointestinal tract. It includes cellulose, noncellulosic polysaccharides such as hemicellulose, pectic substances, gums, mucilages and a non-carbohydrate component lignin. Cellulose is the most abundant biopolymer and the major component of plant cell wall. Cellulosic chains are mainly composed of unbranched β-(1,4)-glucosyl residues. The cellulosic chains are linked through intermolecular and intramolecular hydrogen bonds, which result in the formation of crystalline linear aggregates known as cellulose microfibrils. Hemicelluloses, a diverse group of polysaccharides that include various sugar monomers other than glucose, are closely associated with cellulose in the plant cell wall matrix. Hemicellulose includes linear and branched polymers such as xylan, arabinoxylan, glucuronoxylan, xyloglucan, mannan, glucomannan, galactan, galactomannan, galactoglucomannan, arabinan and arabinogalactan. Arabinoxylans are the non-starch polysaccharides in cereals and they impact the grain quality with their physico-chemical properties. The main cereal grains include wheat, rye, corn, barley, sorghum, rice and oats. Arabinoxylans are hemicellulose consisting of β-1,4-linked xylose backbone with substitutions of L-arabinofuranosyl residues. The arabinofuranosyl residues are attached to the xylose backbone by α-1,2 and α-1,3 glycosidic linkages. Due to the nature that arabinoxylans

cannot be degraded by mammalian enzymes, they end up in the colon and are degraded by gut microbiota into SCFAs and other products. The fermentation of arabinoxylans occurs mainly through the interaction with gut microbiota and catalyzed by backbone xylan depolymerizing species, especially Bacteroidetes

Hemicellulolytic enzymes or hemicellulases can be divided into two groups: (1) enzymes that cleave the backbone are termed as core enzymes and (2) enzymes that remove the side-chain substitution are termed as ancillary or auxiliary enzymes. The presence of side chains in hemicellulose often poses a steric hindrance to the depolymerizing core enzymes, therefore ancillary enzymes are used to remove the side chains, which increases the amount of reducing sugars upon hydrolysis. α-L-Arabinofuranosidase (EC 3.2.1.55) is a hemicellulose degrading enzyme that cleaves arabinosyl residues present in the side chain on a xylan backbone. These enzymes are essential components of a group of glycosidases needed for the complete breakdown of polymeric substrates like arabinan, arabinoxylan and arabinogalactan, which are present in plant cell walls. In 1970, the first α-L-arabinofuranosidase was isolated from *Aspergillus niger* and was crystallized. They reported that the isolated α-L-arabinofuranosidase removed arabinofuranosyl residue from beet arabinan or arabinoxylan. α-L-Arabinofuranosidases are assigned to various glycoside hydrolase (GH) families, specifically GH2, GH3, GH43, GH51, GH54 and GH62 based on amino acid sequence similarities. GH43 family is known for its polyspecificity, with more than 10 reported activities such as β-1,4-xylosidase, β-1,3-xylosidase, endo-β-1,4-xylanase, galactan-1,3-β-galactosidase, endo-α-L-arabinanase, exo-α-1,5-L-arabinanase, bifunctional α-L-arabinofuranosidase/β-D-xylosidase, bifunctional α-L-arabinofuranosidase/endo-β-xylanase activities spread across 39 subfamilies. GH43

family also accommodates bifunctional xylanolytic enzymes such as β-xylosidase/α-L-arabinofuranosidases from *Clostridium stercorarium*, rumen metagenome, *Thermotoga thermarum*, *Bifidobacterium animalis* subsp. *lactis* BB-12, *Humicola insolens*. The family GH43 is further classified into 39 subfamilies based on the occurrence of conserved sequence as well as the structural and functional analyses. A total of 271 gene sequences are reported in subfamily 35, out of which only 5 are characterized to date (http://www.cazy.org/GH43_35_all.html).

The three-dimensional structure of the N-terminal catalytic module of GH43 members, in all the subfamilies, displays a similar five-bladed β-propeller fold. However, the difference in their structure lies at the C-terminal of GH43, where some of members have a β-sandwich fold, while others do not. Based on the occurrence of C-terminal domain and their amino acid sequence similarities, GH43 members are classified into different sub-families from 1 to 39. The most frequently occurring non-catalytic module at the C-terminal of GH43 family is known as the carbohydrate-binding module of family 6 (CBM6). The common structural fold adopted by CBM6 is a β-sandwich consisting of two opposing sheets of parallel or anti-parallel β-strands

Bacteroides ovatus, a Gram-negative, rod-shaped, non-spore-forming and anaerobic bacterium. It possesses an array of glycoside hydrolases. The ability of *Bacteroides* to degrade dietary and mucosal polysaccharides, as well as polysaccharides found on the surface of other gut microbes, plays a crucial role in their survival and proliferation in the environment of the gut. Among the Bacteroidetes, members of the genus *Bacteroides* are among the most dominant bacterial species residing in the human colonic microbiota. The molecular architecture of *Bo*GH43_35 with locus tag

Bovatus_02523 and Genbank Accession no. ALJ47148 from *Bacteroides ovatus* ATCC 8483 under the current study is shown below (Fig. 1).

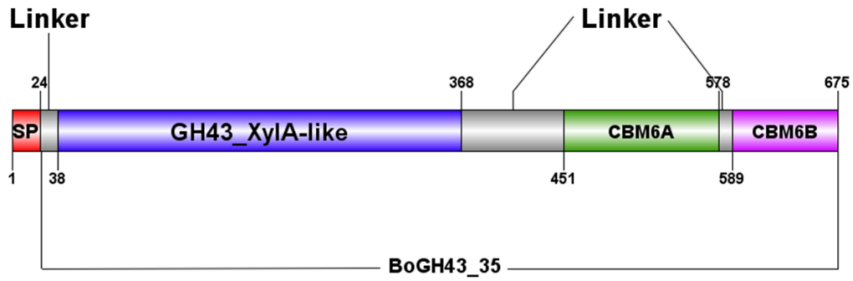

Fig. 1 Molecular architecture of a full-length amino acid sequence of *Bo*GH43_35 with locus tag Bovatus_02523 and Genbank Accession no. ALJ47148 from *Bacteroides ovatus* ATCC 8483.

Present work

The present work entitled "**Cloning, purification, biochemical, functional and structure analyses of a bifunctional α-L-arabinofuranosidase (*Bo*GH43_35) from *Bacteroides ovatus* ATCC 8483 with endo-xylanase activity**" has been divided into five chapters.

Chapter 1 introduces the concept of dietary fiber, emphasizing its increasing demand due to awareness about health and nutrition. This chapter elaborates on the definition of dietary fiber and their sources. It also includes the classification of dietary fibers as insoluble and soluble fibers. It elaborates on the interplay between the solubility and fermentability of these fibers and how they significantly influence the physiological functions of fiber. As plants are the major source of dietary fibers, this chapter covers the structure of plant cell wall with emphasis of cellulose and hemicellulose. In addition to health-related benefits, the chapter discusses the functional properties of dietary fibers from a food processing perspective. It also includes the nutritional value of arabinoxylan, a type of hemicellulose and

arabinoxylooligosaccharides, the hydrolysis products of arabinoxylan. This chapter covers topics of hemicellulolytic enzymes and their synergistic actions for the degradation of arabinoxylan. This chapter focuses on an ancillary hemicellulolytic enzyme, α-L-arabinofuranosidase and a brief review on its origin, mode of action and sources. It also mentions the Glycoside Hydrolase families containing arabinofuranosidases. A review section emphasizes on the bifunctional hemicellulases and their crucial role in the complete breakdown of arabinoxylan into fermentable pentose sugars. A significant portion of the chapter is devoted to the interaction between dietary fiber and the gut microbiome and a focus on *Bacteroides ovatus* has been included. This chapter also discusses the various applications of α-L-arabinofuranosidase. Lastly, the justification for carrying out the present thesis work has been stated with specific objectives.

Chapter 2 describes the cloning and expression of the putative α-L-arabinofuranosidase, *Bo*GH43_35, a family 43 and subfamily 35 glycoside hydrolase (GH43_35) from *Bacteroides ovatus* ATCC 8483. Whole genome analysis of *Bacteroides ovatus* ATCC 8483 revealed the presence of a gene encoding putative α-L-arabinofuranosidase, *Bo*GH43_35 located with locus tag Bovatus_02523 and Genbank Accession no. ALJ47148. The sequence analysis of *Bo*GH43_35 revealed a signal peptide (24 amino acid residues) at N-terminal followed by a GH43_XylA-like catalytic module, a carbohydrate-binding module belonging to family 6 (CBM6A) and an extended C-terminal module, CBM6-like module, CBM6B. The 1956 bp gene encoding *Bo*GH43_35 was amplified by PCR. Ligation-independent cloning was performed to clone PCR amplified product in pHTP1 vector and transformed into *E. coli* DH5α competent cells. The positive clones containing recombinant plasmid DNA

were screened by colony PCR and sequencing. The positive clone showed a DNA band of ~1.9 kb on 0.8% (w/v) agarose gel. The recombinant plasmid DNA containing gene encoding *Bo*GH43_35 was transformed into *E. coli* BL-21 (DE3) cells for expression of protein. The recombinant *Bo*GH43_35 was expressed as a soluble homogenous protein and the minimum concentration of IPTG required for the induction of protein expression was 0.25 mM. The expression of recombinant protein was checked by SDS-PAGE analysis.

Chapter 3 describes the purification and biochemical characterization of *Bo*GH43_35. *Bo*GH43_35 from *B. ovatus* was found to be a novel bifunctional α-L-arabinofuranosidase/endo-β-1,4-xylanase enzyme belonging to the GH43 family. *Bo*GH43_35 is expressed as a soluble protein of molecular mass 74.1 kDa. *Bo*GH43_35 showed mesophilic characteristics with maximum activity against wheat arabinoxylan at 37°C. *Bo*GH43_35 did not show any metal-ion dependence as its activity was not affected by the addition of metal-ions or any chelating agent. *Bo*GH43_35 hydrolyzed wheat arabinoxylan with V_{max} 5.4 U.mg^{-1} and K_M 2.7 mg.mL^{-1}. The melting temperature (T_m) of *Bo*GH43_35 was 41°C. The enzyme, *Bo*GH43_35 hydrolyzed products of wheat arabinoxylan when subjected to TLC and HPLC analysis revealed its α-L-arabinofuranosidase as well as endo-β-1,4-xylanase activities. The release of xylotetraose, xylotriose and xylobiose from beechwood xylan and the release of shorter xylooligosaccharides from cleavage of xylopentaose and xylotetraose by *Bo*GH43_35 as analyzed by TLC and MALDI-TOF MS confirmed its endo-β-1,4-xylanase activity. NMR analysis displayed that *Bo*GH43_35 removes L-arabinose at O-2 or O-3 position from mono-substituted arabinoxylan thereby categorizing it as type I α-L-arabinofuranosidase. This study makes *Bo*GH43_35 distinct from other GH43

xylanases characterized so far from *Bacteroides ovatus* ATCC 8483 owing to its initial type I α-L-arabinofuranosidase activity followed by endo-β-1,4-xylanase activity.

Chapter 4 describes the structural insights of *Bo*GH43_35 by computational and experimental methods. The amino acid sequence analysis of α-L-arabinofuranosidase/endo-β-1,4-xylanase, *Bo*GH43_35 from *B. ovatus* ATCC 8483 revealed 28.1% identity with α-L-arabinofuranosidase (*Ct*GH43) from *Clostridium thermocellum* ATCC 27405. Multiple sequence alignment of *Bo*GH43_35 with its homologous sequences showed Asp34 and Glu251 as the catalytic residues. The three-dimensional structure of *Bo*GH43_35 generated by AlphaFold2 revealed the presence 5-bladed-β-propeller fold by catalytic module followed by two consecutive jellyroll type β-sandwich fold adopted by CBM6A and CBM6B. Secondary structure analysis of *Bo*GH43_35 by Circular Dichroism showed 2.2% α-helix, 28.9% β-sheet and 68.9% random coil, which accorded with the results predicted from 2Struc and Psipred. MD simulation of the AF2 modeled structure of *Bo*GH43_35 confirmed its stability, compactness and no deformity. Molecular docking of *Bo*GH43_35 with arabino-xylooligosaccharides and xylooligosaccharides revealed the active-site pocket forming residues and maximum binding affinity with arabinose. The comparative study of MD simulated structures of *Bo*GH43_35-arabinose complex and the only *Bo*GH43_35 revealed the stability of the *Bo*GH43_35-arabinose docked complex. The catalytic residues in the docked complex were also found stable with reduced RMSF. The binding analysis of *Bo*GH43_35 by fluorescence spectroscopy against wheat arabinoxylan showed an association constant, K_a of 3.11×10^2 M^{-1} and presence of two binding sites. The DLS analysis of *Bo*GH43_35 indicated that there exists as a hypothetical sphere surrounded by a hydration shell in an aqueous solution. The overall

negative charge of *Bo*GH43_35 as determined by zeta potential on the protein surface showed its stability and solubility in the aqueous environment.

Chapter 5 describes the application of *Bo*GH43_35, a bifunctional α-L-arabinofuranosidase/endo-β-1,4-xylanase from *Bacteroides ovatus* in pomegranate and mosambi fruit juice clarification and enzymatic waste peel hydrolysis for reducing sugar production. The enzyme improved the juice transparency**,** reduced viscosity and enhanced saccharification of fruit peels, paving the way for its sustainable application in food, bioenergy and waste management industries**.** The results demonstrated that *Bo*GH43_35 treatment improves juice clarity, especially at higher enzyme concentrations (1.0 mg/mL) and longer incubation time (4 h). Turbidity in *Punica granatum* (pomegranate) juice decreased from 20.1 NTU (control) to 3.8 NTU, while in *Citrus limetta* (mosambi) juice, turbidity reduced from 597 NTU to 290 NTU. The percentage of light transmittance increased significantly, indicating enhanced juice clarity. The enzymatic treatment lowered the juice viscosity, making filtration and processing more efficient. The discarded peels of pomegranate and mosambi were subjected to enzymatic saccharification, converting hemicellulose into soluble reducing sugars, which could serve as valuable substrates for various industrial applications. The combination of *Bo*GH43_35 and *Bo*ExXyl43A **(**exo-β-1,4-xylosidase from *Bacteroides ovatus*) proved most effective for maximizing TRS yield, confirming their synergistic action. Raw pomegranate peel (PP) and mosambi peel (MP) produced significant amounts of reducing sugars, with TRS yields of 66 mg/g raw PP and 60 mg/g raw MP. With the combination of *Bo*GH43_35 and *Bo*ExXyl43A treatment, the TRS yield increased up to 623 mg/g raw PP and 505 mg/g raw MP. With continued research and

industrial adoption, *Bo*GH43_35 has the potential to revolutionize fruit processing and lignocellulosic biomass utilization, contributing to a more sustainable and efficient agro-industrial sector.

Contents

Chapter 1

General Introduction

1.1 Dietary fiber

In today's world, lifestyle-induced diseases are a significant concern for global health. Among these diseases, four stand out due to their prevalence and impact: hypertension, overweight/obesity, diabetes mellitus and dyslipidemia (Maheshwari et al., 2019). The increase in the lifestyle diseases has led to sophistication in people's standard of living (Yang et al., 2017). In response to the increasing demand for nutritious food, the food manufacturers are encouraged to develop fiber-enriched food products (Redgwell & Fischer, 2005). Dietary fiber is defined as those components of plant material in the diet which are indigestible by enzymes in the human gastrointestinal tract (McKee & Latner, 2000). It includes cellulose, noncellulosic polysaccharides such as hemicellulose, pectic substances, gums, mucilages and a non-

carbohydrate component lignin (Dhingra et al., 2012). Dietary fiber is a crucial part of a balanced diet, renowned for its numerous health benefits (Snauwaert et al., 2023). It was originally defined by Trowell in 1972 as 'the portion of food which is derived from cellular walls of plants which are digested very poorly by human beings (Trowell, 1972). The dietary fibers cannot be broken down into absorbable elements in the upper alimentary canal by human digestive enzymes (Yangılar, 2013). According to Codex Alimentarius Commission (CAC, 2006), dietary fiber means carbohydrate polymers with a degree of polymerization not lower than 3, which are neither digested nor absorbed in the small intestine (Mudgil & Barak, 2013).

A significant portion of dietary fiber is derived from the cell walls of plants. These fibers play a fundamental role in providing structural integrity and ensuring proper functionality within the plant (Williams et al., 2017). They serve as a framework that supports the plant's overall form, allowing it to maintain its shape, withstand external pressures and facilitate vital biological processes. Dietary fibers can be categorized into either insoluble or soluble fiber based on chemical, physical and functional properties (Padayachee et al., 2017).

1.2 Soluble and insoluble dietary fibers

Soluble dietary fibers resist enzymatic digestion in the gastrointestinal tract and pass through the small intestine to reach the colon and they are more easily fermented by the microbiota in the large intestine (Padayachee et al., 2017). They have the ability to absorb water, forming gels or viscous solutions (Brownlee, 2011). Pectin, a key soluble fiber found in the plant cell walls of fruits and vegetables, exemplifies this category. Soluble fibers have more pronounced effects in the upper gastro intestinal tract as compared with their insoluble counterparts, influencing the rate of food passage,

the viscosity of digestive contents and interactions with enzymes and bile salts within the stomach and small intestine (Mikkelsen et al., 2011). Whereas, insoluble dietary fibers are a type of non-starch polysaccharides that do not dissolve in water and gastric-intestinal fluids (Dai & Chau, 2017). Since the human digestive system lacks the necessary enzymes to break down plant cell wall fibers, they remain largely unchanged as they pass through the upper gastrointestinal tract (GIT) and reach the colon (Padayachee et al., 2017). These fibers generally exist in the form of dense particles that are resistant to penetration by colonic microorganisms, making them highly resistant to fermentation. This characteristic enables insoluble fibers to perform vital functions such as cleansing the bowel, supporting the health of colonic epithelial cells by promoting regular bowel movements and contributing to the formation of bulkier stools. These insoluble fibres are often rich in cellulose, hemicelluoses, resistant starch and lignin polymers (McCleary et al., 2012). Cellulose, the primary structural component of plant cell walls, constitutes approximately, 25% of the fiber content in grains and fruits and about one-third in vegetables and nuts (Jr & W, 2016). It is notably an abundant fiber in cereal bran. Hemicelluloses, a diverse group of polysaccharides that include various sugar monomers other than glucose, are closely associated with cellulose in the plant cell wall matrix. They occur in both water soluble and insoluble forms and account for roughly one-third of the total fiber content in vegetables, fruits, legumes and nuts (Fuentes-Zaragoza et al., 2010).

1.3 Physico-chemical properties of dietary fibers

Dietary fibers can be consumed either in their natural form as part of plant cell walls or in purified or semi-purified forms (Eastwood & Morris, 1992). To understand their behavior during digestion, it is important to consider certain physicochemical

properties, such as particle size, solubility, hydration capacity and viscosity (Capuano, 2017). Particle size is important because it influences various digestive processes, including transit time, fermentation and fecal excretion. The particle size of fiber depends on the type of cell walls in the food and its processing level (Guillon & Champ, 2000). It can also change during digestion due to chewing, stomach grinding and bacterial breakdown in the large intestine. Generally, dietary fibers increase the viscosity of intestinal contents and fecal volume, which helps to dilute potentially harmful substances. This process shortens the duration of proteolytic fermentation, reduces the production of harmful by-products and limits the exposure of mucosal cells to these substances (An et al., 2022). The porosity and surface area of dietary fibers also play a role in their fermentation in the colon, as they affect microbial degradation. Additionally, the surface regio-chemistry may influence certain properties, such as the ability to adsorb or bind molecules, contributing to the physiological effects of dietary fiber (Guillon & Champ, 2000). The solubility of dietary fibers depends on their chemical structure and interaction with water molecules. For instance, linear fibers that adopt ordered (semi) crystalline structures in solution, such as cellulose, have limited solubility. Whereas, branched fibers are less likely to form such ordered structures, making them more soluble in water (Capuano, 2017). Insoluble fibers, such as cellulose, hemicellulose and lignin, are mostly unfermentable by colonic microflora and increase fecal bulk by their particle formation and water-holding capacity (Mudgil & Barak, 2013). Plants are the major source of dietary fibers and exists as part of their cell walls, a polysaccharide-rich structure outside of the plant plasma membrane (An et al., 2022).

1.4 Plant cell wall

Plant cells encase themselves in a complex and semi-rigid structure, known as cell wall (Cosgrove, 2005). It surrounds the cytoplasmic membrane and allows the cell to resist internal or external pressure along with providing structural barrier to some molecules and insect invasion (Heredia et al., 1995). The cell wall composition and architecture vary according to species type, cell type, developmental stage and function of the tissue (Rodrigues Mota et al., 2018). The plant cell wall is made up of three primary layers: the middle lamella, the primary wall and the secondary wall, each differing in thickness and structural composition (Bailey, 1938). The plant cell wall structure is shown in Fig. 1.1. Monocot plants, such as cereal grains and grasses, are vital sources of food and renewable energy and their primary cell walls are predominantly composed of cellulose, with notable quantities of arabinoxylans and mixed-linkage of β-1,3- and β-1,4- β-D-glucans. On the other hand, the primary cell walls of dicot plants, which include fruits, vegetables, nuts and legumes, have a different structural makeup, featuring high levels of pectins, xyloglucans and mannans (Hu et al., 2022). In young tissues, the primary cell walls encase the expanding cells, while the secondary cell walls provide structural strength once cell growth has stopped in mature tissues (Pettolino et al., 2012).

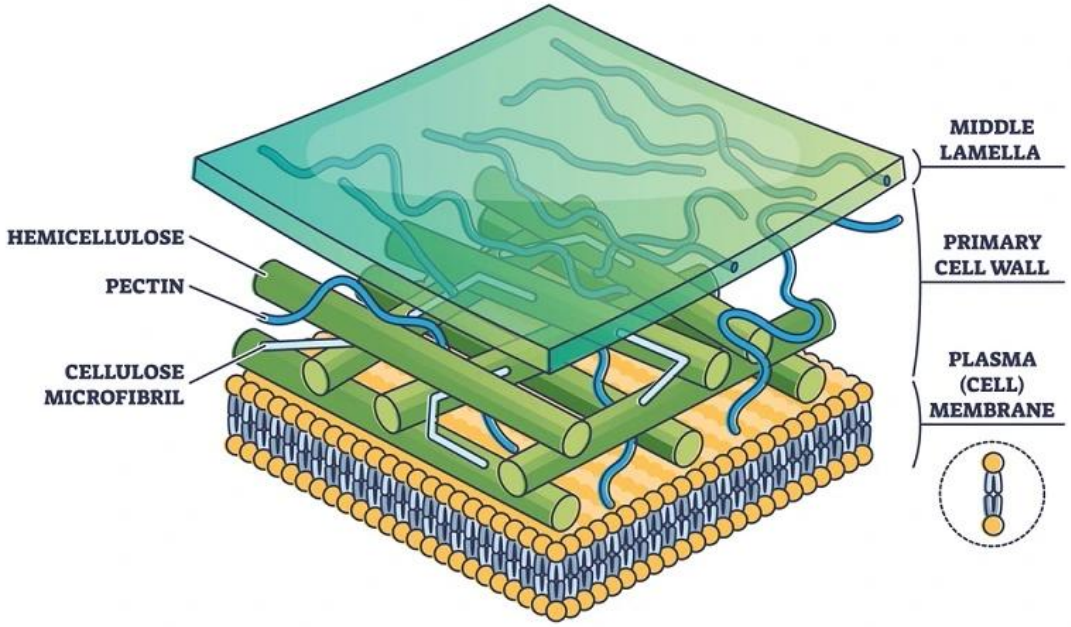

Fig. 1.1 Plant cell wall structure showing cellulose, hemicellulose and pectin in primary cell wall. (Image Source: Microbial notes)

1.4.1 Cellulose

Cellulose is the most abundant biopolymer and major component of plant cell wall. Cellulosic chains are mainly composed of unbranched β-(1,4)-glucosyl residues (Williams et al., 2017). The cellulosic chains are linked through intermolecular and intramolecular hydrogen bonds, which result in the formation of crystalline linear aggregates known as cellulose microfibrils (Hamaker & Tuncil, 2014). The molecular structures of cellulose and other polysaccharides allow them to align and cluster together by forming both inter- and intra-molecular hydrogen bonds, as well as hydrophobic interactions. This results in the formation of a network-like matrix structure (Hu et al., 2022). In contrast to the secondary cell walls, the cellulose microfibrils in the primary cell wall exhibit a higher degree of crystallinity. Additionally, these microfibrils are aligned in a parallel orientation to the axis of cell elongation, playing a crucial role in maintaining the structural integrity and facilitating

the growth process (An et al., 2022). Cellulose makes up about a quarter of dietary fiber in grains and fruit and a third in vegetables asnd nuts. Wheat bran is a rich source of insoluble cellulose, which binds water, increasing fecal volume and promoting regular bowel movements (Mudgil & Barak, 2013). While humans cannot digest cellulose directly, it is partially broken down by gut microflora, with about 50% degraded in the colon, producing short-chain fatty acids that nourish intestinal cells (Wallace et al., 2017).

1.4.2 Hemicellulose

Hemicellulose is a vast group of diverse complex polysaccharides present in the plant cell wall. It is the second most abundant class of lignocellulosic polymer and is categorized based on monosaccharides present in the hemicellulosic fraction (Saha, 2003). Hemicellulose includes linear and branched polymers such as xylan, arabinoxylan, glucuronoxylan, xyloglucan, mannan, glucomannan, galactan, galactomannan, galactoglucomannan, arabinan and arabinogalactan (Collins et al., 2005). Upon hydrolysis of these hemicellulosic polymers, the predominant monomers produced are xylose, mannose, glucose, galactose, glucuronic acid, galacturonic acid and arabinose (Beg et al., 2001). Hemicellulose is more soluble in water than cellulose due to its branched structure and the presence of different sugar residues, which disrupt the hydrogen bonding that allows cellulose to form stable, crystalline structures (Boukid, 2024). Hemicelluloses make up roughly one third of the dietary fiber in vegetables, fruits, legumes and nuts. They help promote regular bowel movements by enhancing stool hydration and also play a role in reducing cholesterol absorption by binding to cholesterol in the gut (Mudgil & Barak, 2013).

1.4.3 Arabinoxylan

Arabinoxylans are the non-starch polysaccharides in cereals and they impact the grain quality with their physico-chemical properties (Mendis & Simsek, 2014). The main cereal grains include wheat, rye, corn, barley, sorghum, rice and oat (Zannini et al., 2022). They are mostly originated from the bran and starchy endosperm and cannot be degraded by mammalian enzymes (Chen et al., 2019). Arabinoxylans are hemicellulose consisting of β-1,4-linked xylose backbone with substitutions of L-arabinofuranosyl residues (Lu et al., 2000). The arabinofuranosyl residues are attached to the xylose backbone by α-1,2 and α-1,3 glycosidic linkages as illustrated in Fig. 1.2 (Broekaert et al., 2011). The β-D-xylopyranoside residues of arabinoxylan backbone are either unsubstituted, monosubstituted with single α-L-arabinofuranoside at either C-(O)-2 or C-(O)-3, or disubstituted with α-L-arabinofuranoside residues at both C-(O)-2 or C-(O)-3 (Broekaert et al., 2011). Arabinoxylan, primarily composed of xylose and arabinose, is often called pentosans. Phenolic acids, like ferulic acid can be esterified at the C(O)-5 position of arabinose (Mendis & Simsek, 2014). Apart from xylose and arabinose, there are slight traces of glucose, galactose and mannose (He et al., 2021). The pattern and degree of substitution of arabinose along the xylose backbone vary with cereal sources and tissue location in the grain (Niño-Medina et al., 2010).

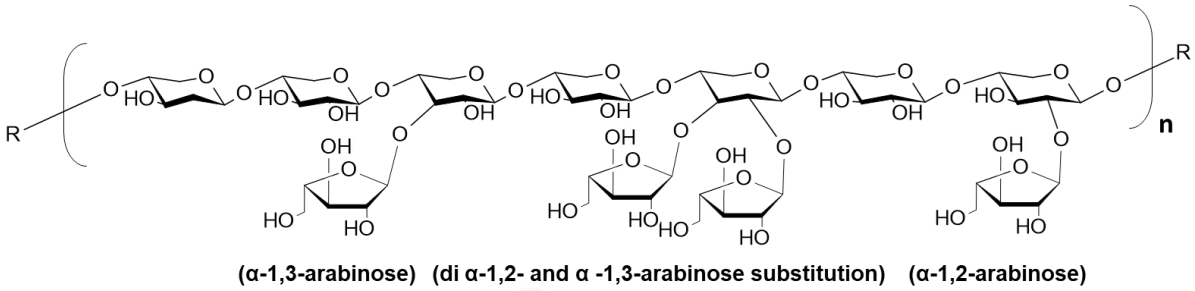

Fig. 1.2 Structure of arabinoxylan.

1.5 Nutritional value of arabinoxylan and arabinoxylooligosaccharides

There has been growing interest in the use of arabino-xylooligosaccharides, the hydrolysis products of arabinoxylan, as prebiotics due to their potential to promote the growth of *Bifidobacteria* in the human colon (Hamaker & Tuncil, 2014). A prebiotic is defined as "a selectively fermented ingredient that induces specific changes in the composition and/or activity in the gastrointestinal microbiota, conferring benefits to the host's health and well-being" (Gibson & Roberfroid, 1995). The consumption of prebiotics typically leads to modulation in the composition of the intestinal microbiota, often resulting in an increased abundance of beneficial bacteria, such as *Bifidobacteria* and/or *Lactobacillus* species. This alteration in the gut microbial community is linked to several positive health outcomes, including enhanced gut health, a reduction in the incidence of intestinal infections, improved mineral absorption and a potential reduction in the risk of colon cancer initiation (Broekaert et al., 2011). Most prebiotics selectively promote the growth and activity of beneficial gut bacteria in the gut while also inhibiting the proliferation of harmful bacteria, often through the production of short-chain fatty acids (SCFAs) (Lin et al., 2021). SCFAs such as acetate, butyrate, propionate are the fermentation products of the prebiotics by the colonic bacteria (Van Craeyveld et al., 2008). *Bifidobacteria* are the predominant group of microflora that

produce these SCFAs through the fermentation of dietary fibers causing acidic pH in the intestine which eradicates the potentially pathogenic bacteria (Mendis & Simsek, 2014).

Arabinoxylans cannot be degraded by mammalian enzymes, therefore they end up in colon and are degraded by gut microbiota into SCFAs and other products. The fermentation of arabinoxylans occur mainly through the interaction with gut microbiota and catalyzed by backbone xylan depolymerizing species, especially Bacteroidetes (Chen et al., 2019). Studies have shown that arabinoxylans demonstrate antioxidant properties, with those having a lower molecular weight and fewer substitutions exhibiting enhanced antioxidant capacity. The phenolic compounds (e.g., *p*-coumaric acids and ferulic acids) contribute to the antioxidant activity of the arabinoxylans (Snelders et al., 2013). Moreover, studies have shown that wheat bran extract enriched in arabino-xylooligosaccharides modulated the gut microbiota by stimulating the growth of *Lactococcus* sp. and several species of the *Clostridium* genus while suppressing the growth of *Aeromonas sp.*, *C. freundii* and *E. coli* in the hindgut of sturgeon (He et al., 2021).

1.6 Hemicellulolytic enzymes

Hemicellulolytic enzymes or hemicellulases can be divided into two groups: 1) enzymes that cleave the backbone are termed as core enzymes and 2) enzymes that remove the side-chain substitution are termed as ancillary or auxiliary enzymes (Moreira & Filho, 2016). The presence of side chains in hemicellulose often poses a steric hindrance to the depolymerizing core enzymes, therefore ancillary enzymes are used to remove the side chains, which increases the amount of reducing sugars upon hydrolysis (Rezania et al., 2020).

The synergistic actions of core and ancillary hemicellulases are essential for the degradation of arabinoxylan due to its intrinsic complexity and heterogeneity. The two core enzymes involved in the hydrolysis of the arabinoxylan backbone are endo-β-1,4-xylanase (EC 3.2.1.8) and β-xylosidase (EC 3.2.1.37). Endo-β-1,4-xylanase acts on the backbone of arabinoxylan composed of β-1,4 linked xylose residues and releases xylo-oligosaccharides of different degrees of polymerization (Collins et al., 2005). β-Xylosidase hydrolyses xylooligosaccharides from the non-reducing end releases xylose and also cleaves xylobiose to xylose (Collins et al., 2005). Various xylanolytic enzymes that are required for the hydrolysis of hemicellulose are given in Table 1.1.

Table 1.1 Xylanolytic enzymes on the basis of their substrate and mode of action.

Hemicellulase	EC No.	Substrates	Mode of action	Reference
Endo-β-xylanase	3.2.1.8	Xylan	Hydrolyzes the internal β-1,4 glycosidic linkage of xylan backbone	(Collins et al., 2005)
α-Arabinofuranosidase	3.2.1.55	Arabinoxylan, arabinan and arabinogalactan	Hydrolyzes non-reducing α-1,2-, α-1,3, α-1,5- linked arabinofuranosyl residues	(Lee et al., 2011)
β-Xylosidase	3.2.1.37	Xylooligosaccharide, xylobiose	Hydrolyzes β-1,4- linked xylooligosaccharides	(Zhang et al., 2019)
α-Glucuronidase	3.2.1.139	Glucuronoxylan	Hydrolyzes α-1,2-linked methyl-D-glucuronic acid from glucuronoxylan	(Shallom & Shoham, 2003)
Acetyl xylan esterase	3.1.1.72	Acetylated xylan	Hydrolyzes ester linkages between acetic acid and xylose	(Nakamura et al., 2017)
Ferulic acid esterase	3.1.1.73	Ferulic acid substituted xylan	Hydrolyzes ester linkages between ferulic acid and arabinose or ether linkages between ferulic acid and lignin	(MacKenzie et al., 1987)
p-Coumaric acid esterase	3.1.1.-	*p*-coumaric acid substituted xylan	Hydrolyzes ester linkages between *p*-coumaric acid and arabinofuranosyl residues	(Dodd & Cann, 2009)

1.6.1 Xylanases

Xylanases, originally termed 'pentosanases' were recognized by the International Union of Biochemistry and Molecular Biology (IUBMB) in 1961 and were assigned the enzyme code EC 3.2.1.8 (Collins et al., 2005). Xylanases are produced by bacteria (*Bacillus* spp., *Streptomyces* spp., *Pseudomonas* spp.), yeasts, filamentous fungi (*Aspergillus* spp., *Fusarium* spp.), snails, crustaceans, marine algae and protozoa. But fungi and bacteria are major sources of xylanases (Popa et al., 2016). Xylanase is traditionally defined as a hydrolase that catalyzes endo-hydrolysis of the homopolymeric backbone of xylan by cleaving internal β-1,4 glycosidic linkages between the β-D-xylopyranosyl units. Therefore, endo-β-1,4-xylanases are commonly termed xylanases (Collins et al., 2005).

1.6.2 Arabinofuranosidase

α-L-Arabinofuranosidase (EC 3.2.1.55) is a hemicellulose degrading enzyme that cleaves arabinosyl residues present in the side chain on a xylan backbone as shown in Fig. 1.3 (Shrivastava et al., 2023). These enzymes are essential components of a group of glycosidases needed for the complete breakdown of polymeric substrates like arabinan, arabinoxylan and arabinogalactan, which are present in plant cell walls (Margolles & de los Reyes-Gavilán, 2003). Arabinan has an α-1,5-linked arabinose backbone that is branched via α-1,2- or α-1,3-linked arabinofuranose side chains (Miyanaga et al., 2004). Endo-L-arabinanases are the only enzymes hydrolysing (1 → 5) α-L-arabinofuranosyl bonds within the arabinan polysaccharide (Seiboth & Metz, 2011). Whereas, α-L-arabinofuranosidases catalyze the hydrolysis of α-1,2-, α-1,3- and α-1,5-arabinofuranosidic bonds in L-arabinose-containing hemicelluloses such as arabinoxylan and L-arabinan (Miyanaga et al., 2004). In 1970, the first α-L-

arabinofuranosidase was isolated from *Aspergillus niger* and was crystallized (Tagawa & Kaji, 1969). They reported that the isolated α-L-arabinofuranosidase removed arabinofuranosyl residue from beet arabinan or arabinoxylan. α-L-Arabinofuranosidases work in concert with other hemicellulolytic enzymes for the complete and efficient hydrolysis of hemicelluloses (Lee et al., 2011). α-L-Arabinofuranosidases have been purified from several bacteria, fungi and plants (Numan & Bhosle, 2006). The biochemical properties of a few recombinant α-L-arabinofuranosidase from various bacteria and fungi are listed in Table 1.2.

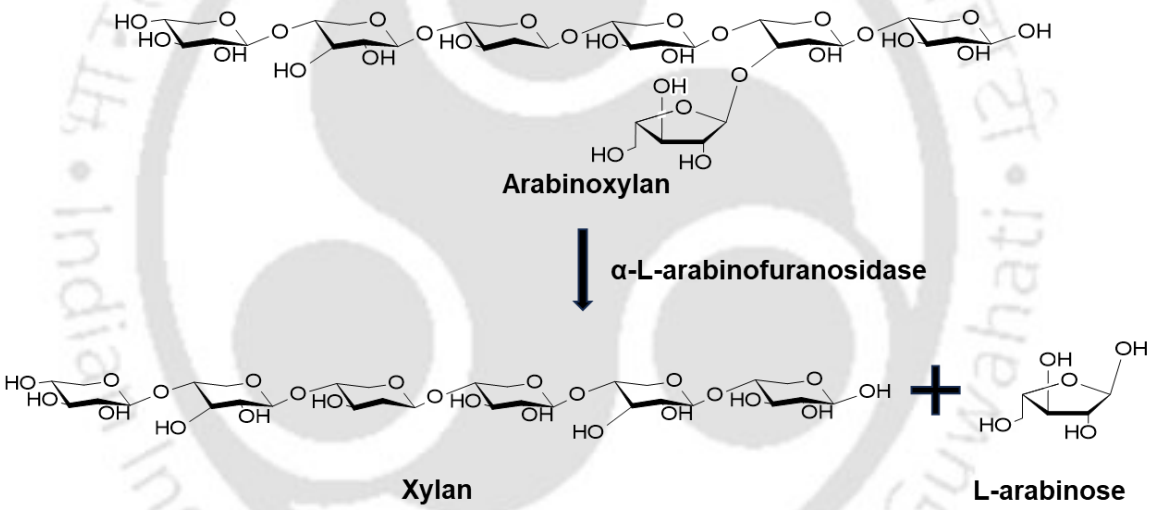

Fig. 1.3 Mode of action of α-L-arabinofuranosidase.

Table 1.2 Biochemical properties of α-L-arabinofuranosidase from bacteria and fungi.

Organism	Temp.	pH	GH Family	Reference
Bacteria				
Bacillus subtilis 168	40	5.0	GH51	(Zhang et al., 2021)
Bacillus stearothermophilus T-6	70	5.5	-	(Gilead & Shoham, 1995)
Bifidobacterium longum B667	45	6.0	GH51	(Margolles & de los Reyes-Gavilán, 2003)
Caldicellulosiruptor saccharolyticus	70	6.0	GH43	(Saleh et al., 2022)
Clostridium thermocellum ATCC 27405	50	5.7	GH43	(Ahmed et al., 2013)
Paenibacillus polymyxa	40	6.5	GH51	(Hu et al., 2018)
Pseudopedobacter saltans	50	6.5	GH43	(Thakur et al., 2020)
Streptomyces sp. SWU10	50	5.0	GH 62	(Phuengmaung et al., 2018)
Fungi				
Aspergillus awamori	50	5.0	GH51	(Li et al., 2023)
Aspergillus nidulans	60	5.5	GH62	(Contesini et al., 2017)
Eupenicillium parvum	55	4.5	GH62	(Long et al., 2022)
Humicola insolens	53	6.7	GH51	(Sørensen et al., 2006)
Penicillium chrysogenum	20	5.0	GH43	(Sakamoto et al., 2011)
Talaromyces amestolkiae	60	4.0	GH62	(Méndez-Líter et al., 2023)

Arabinofuranosidases are found in various GH families, specifically GH2, GH3, GH30, GH43, GH51, GH54, GH62 and GH93 based on amino acid sequences (Shallom et al., 2002). GH43 family is known for its polyspecificity, reported with more than 10 activities. These include β-1,4-xylosidase, β-1,3-xylosidase, endo-β-1,4-xylanase, galactan-1,3-β-galactosidase, endo-α-L-arabinanase, exo-α-1,5-L-arabinanase and bifunctional α-L-arabinofuranosidase/β-D-xylosidase activities spread across 39 subfamilies of GH43 family (Wang et al., 2014). GH43 enzymes, α-L-arabinofuranosidases and β-D-xylosidases work by inverting the stereochemical configuration of the anomeric carbon whereas the GH51 and GH54 enzymes cleave the

glycosidic bond by retaining the anomeric configuration through double displacement mechanism involving two glutamic acid residues in catalysis (Shallom et al., 2002). In the arabinofuranosidases following inverting mechanism, the catalytic residues are approximately, 8-10 Å apart and the reaction proceeds through a single displacement mechanism (Fig. 1.4A). The general acid protonates the glycosidic oxygen and the departure of the leaving group is accompanied by the nucleophilic attack of a water molecule that has been deprotonated by the general base (Lagaert et al., 2014). Whereas in the retaining mechanism, one carboxylic acid group acts as the catalytic nucleophile and the other carboxylic acid, approximately, 5 Å away, as the general acid/base catalyst (Fig. 1.4B). In the first step, the general acid protonates the glycosidic oxygen while the second catalytic residue performs a nucleophilic attack at the anomeric carbon. This leads to the departure of the leaving group and the formation of a covalent intermediate. In the second step, the first catalytic residue now acts as a base and deprotonates an incoming water molecule, which hydrolyzes the glycosyl-enzyme intermediate (Yip & Withers, 2004). Based on the structural analysis, some of the GH families are further classified into various Glycoside Hydrolase clans. From these, GH-A (GH2, GH30 and GH51) displays a $(\beta/\alpha)_8$ TIM barrel fold, GH-E (GH93) enzymes adopt a six-bladed β-propeller fold (Wang et al., 2014) and GH-F (GH43 and GH62) enzymes display a five-bladed β-propeller fold such as *Ps*GH43_12 from *Pseudopedobacter saltans* (Thakur et al., 2020). The versatility of some GH51 and GH54 enzymes is marked by their capability of hydrolyzing monosubstituted α-1,2- as well as α-1,3-arabinofuranosyl residues from arabinoxylans and even doubly substituted arabinoxylans (Shallom et al., 2002). Depending upon the substrate

specificity, AFs are classified into three types: Type-A arabinofuranosidases are active on α-1,5-L-arabinoxylooligosaccharides and *para*-nitrophyl-α-L-arabinofuranoside (*p*NPA), while Type-B arabinofuranosidases are also active on L-arabinan and arabino-oligosaccharides (Sakamoto et al., 2011). The third type of arabinofuranosidases are active on mono- or di-substituted arabinose in arabinoxylans are rare (Sakamoto et al., 2011).

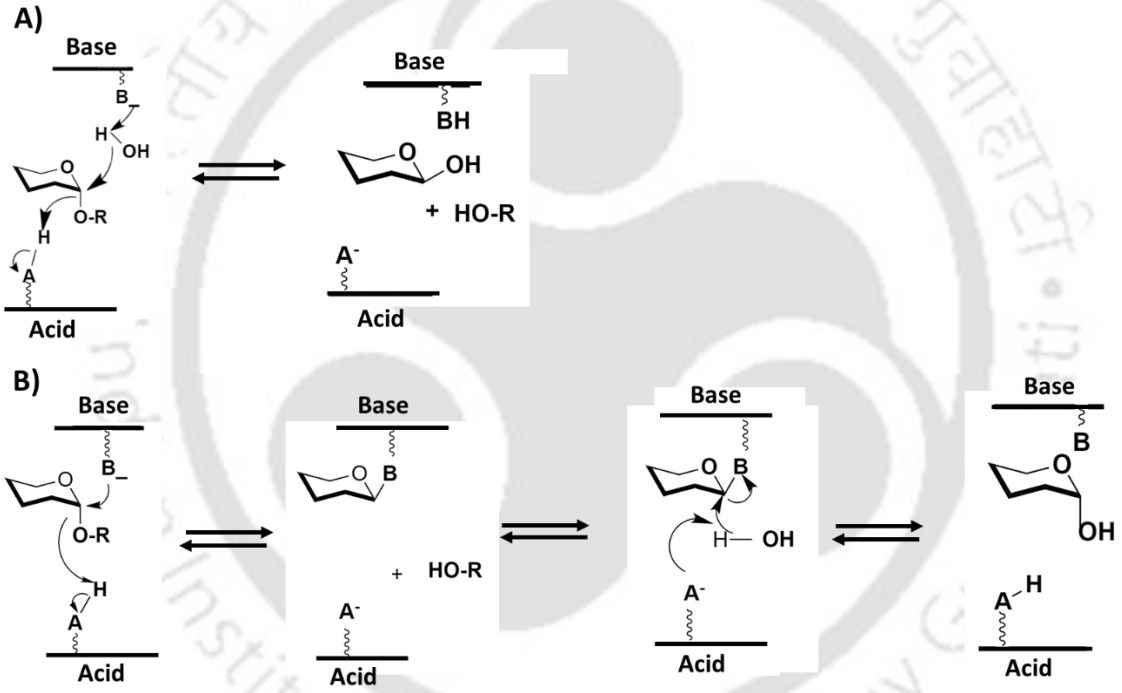

Fig. 1.4 Mechanism of action of hemicellulolytic enzymes. A) inverting type mechanism and B) retaining type mechanism (Shrivastava et al., 2023).

1.6.3 Xylosidases

Xylans are hydrolyzed by endoxylanases to produce xylooligosaccharides that are further acted upon by xylosidases to release single xylose moieties. The complete xylan hydrolysis requires the synergistic action of both endo-β-1,4-xylanases and β-1,4-xylosidases. β-Xylosidases are hydrolytic enzymes that cleave the xylose residues in an exo-acting manner from the non-reducing end of xylooligosaccharides (Collins et

al., 2005). β-1,4-D-Xylosidase (EC 3.2.1.37) catalyzes the hydrolysis of β-1,4-linked xylose residues from xylooligosaccharides whereas, β-1,3-D-xylosidases (EC 3.2.1.72) act on β-1,3-linked xylose residues such as xylan in green algae but are rarely reported (Zhang et al., 2019). β-1,4-Xylosidases are produced by variety of sources such as plants, animals, bacteria and fungi, from which mostly filamentous fungi and bacteria are used for the high-scale production at industrial level. The bacterial genera *Bacillus, Streptomyces* and *Clostridium* are majorly involved in the production of β-1,4-xylosidase, a cell wall depolymerizing enzyme. Filamentous fungi such as *Aspergillus spp., Humicola spp., Trichoderma spp.* have been extensively studied for the production of β-1,4-xylosidases (Kousar et al., 2013).

1.6.4 Bifunctional hemicellulases

The complete breakdown of arabinoxylan involves the concerted action of a xylanolytic enzyme system having various activities and mechanisms, including endoxylanases, β-xylosidases and α-L-arabinofuranosidases (Shrivastava et al., 2023). Bifunctional xylanolytic enzymes play a crucial role in the complete breakdown of arabinoxylan into fermentable pentose sugars. These sugars are then utilized by gut microbes to produce various beneficial compounds for health such as lactic acid, acetate, propionate and butyrate (Limsakul et al., 2021).

A bifunctional enzyme contains two distinct catalytic capacities in the same polypeptide chain (Khandeparker & Numan, 2008). They hydrolyze complex polymer, exhibiting two activities that are often complementary and allow enzyme to catalyze consecutive reactions (Bouraoui et al., 2016). Enzymatic diversity in nature has resulted in the development of bifunctional xylanases, which serve as potential candidates for efficiently breaking down complex arabinoxylans. In 2015, a novel bifunctional GH51

exo-α-L-arabinofuranosidase/endo-xylanase from *Alicyclobacillus* sp. A4 was reported (Yang et al., 2015). A multifunctional xylanolytic enzyme, *Pc*Axy43B from *Paenibacillus curdlanolyticus* B-6 was reported to exhibit α-L-arabinofuranosidase, endoxylanase and β-1,4-xylosidase activities (Limsakul et al., 2021). Two bifunctional β-xylosidase/α-L-arabinofuranosidase, *Pp*Xyl43A and *Pp*Xyl43B, from *Paenibacillus physcomitrellae* XB displayed different xylan degrading ability on substrates such as corncob xylan, oat spelt xylan, wheat flour arabinoxylan and beechwood xylan (Zhang et al., 2021). A bifunctional enzyme belonging to GH43 family, rAbf43A, cloned from bacterial consortium exhibited both arabinofuranohydrolase as well as endoxylanase activities (Wang et al., 2023).

Apart from naturally occurring bifunctional hemicellulases, protein engineering strategies have been exploited to create multifunctional xylanases. The catalytic domain of a xylanase (from *Clostridium thermocellum*) was fused with a dual functional arabinofuranosidase/xylosidase (from a compost starter mixture) using a flexible peptide linker to generate a multifunctional enzyme (Fan et al., 2009). The constructed chimera was reported to be more active than the parental enzyme mixture in the hydrolysis of natural xylans and corn stover. A trifunctional xylanolytic enzyme from *Ruminiclostridium josui*, Abf62A-Axe6A, exhibiting α-L-arabinofuranosidase, endoxylanase and acetylxylan esterase activities was constructed (Wang et al., 2018). The trifunctional enzyme, Abf62A-Axe6A was highly active towards arabinoxylan and moderately active towards sugar beet arabinan, releasing arabinose. Abf62A-Axe6A released α-1,2- and α-1,3-linked arabinofuranose from both mono- and di-substituted xylosyl residues and also demonstrated the endoxylanase activity toward birchwood and beechwood xylans and xylooligosaccharides.

1.6.5 Carbohydrate binding modules

In addition to the catalytic modules of hemicellulases, there are also various other structural and non-functional modules such as the carbohydrate-binding module, CBM (https://www.cazy.org/Carbohydrate-Binding-Modules.html). CBMs serve as a targeting agent facilitating binding of the catalytic module of a hemicellulase to polysaccharide substrate (Tomme et al., 2000). It has also been suggested that the binding of CBMs to polysaccharide disrupts their structural integrity and enhances their hydrolysis (Singh et al., 2021). The catalytic module of a hemicellulolytic enzyme could either have glycoside hydrolase or carbohydrate esterase activity (Shallom & Shoham, 2003). Typically, hemicellulase enzymes contain a catalytic module involved in the hydrolytic action and CBM at either the amino terminal or carboxy terminal, connected to the catalytic module by a peptide linker. Enzymes without CBMs are also found in the nature (Singh et al., 2021). Binding of the CBM to the substate increases the proximity between the enzyme (and thus the catalytic core) and the substrate thus prolonging the duration of their interaction. Majority of the CBMs display a β-jelly roll structure (You et al., 2024). Till date, 106 families of CBMs are known (http://www.cazy.org/). The complexity of a particular enzyme is determined by the number of CBMs and catalytic modules present in single polypeptide chain (Singh et al., 2021).

1.7 Gut microbiota and dietary fibers

The colon or large intestine serves as an anaerobic fermentation chamber populated by diverse microorganisms, which not only enhances the host's digestive capacity but also influences the various biological processes beyond digestion (Ye et al., 2022). The composition of microbial communities in the gut is shaped by multiple

factors, including the individual's genetic predisposition, physiological conditions, environmental factors such as lifestyle and diet and pharmacological influences. Dietary fiber is consumed by commensal bacteria abundantly present in the large intestine and is thus an energy source for these bacteria, resulting in a change in gut bacterial composition (Chudan et al., 2023). The degree of polymerization, particle size, solubility, viscosity and other characteristics of dietary fiber may influence the fiber fermentability and the fiber-specific gut microbiota (Tuncil et al., 2020). Genomes of the resident microbes in the large intestine encode a large repertoire of carbohydrate active enzymes (CAZymes), enabling them to efficiently metabolize the dietary fibers through fermentation process (Hamaker & Tuncil, 2014). These intestinal bacteria, specialized in degrading dietary fibers include species from genera *Lactobacilli*, *Bacteroides* and non-pathogenic *Clostridia* (Grootaert et al., 2007). Firmicutes and Bacteroidetes represent the predominant bacterial phyla within the gut microbiota, playing crucial roles in maintaining intestinal homeostasis. Firmicutes, the most diverse and expansive phylum, contribute significantly to the microbial phylogenetic diversity, accounting for approximately, 70% of the total bacterial composition in the gut (Cheng et al., 2022). In contrast, Bacteroidetes, comprising key genera such as *Bacteroides*, *Alistipes*, *Parabacteroides* and *Prevotella*, exhibit a greater capacity for polysaccharide degradation, facilitated by their extensive repertoire of polysaccharide-degrading enzymes (Cheng et al., 2022). This distinction underscores their fundamental roles in carbohydrate metabolism and energy extraction within the gut ecosystem.

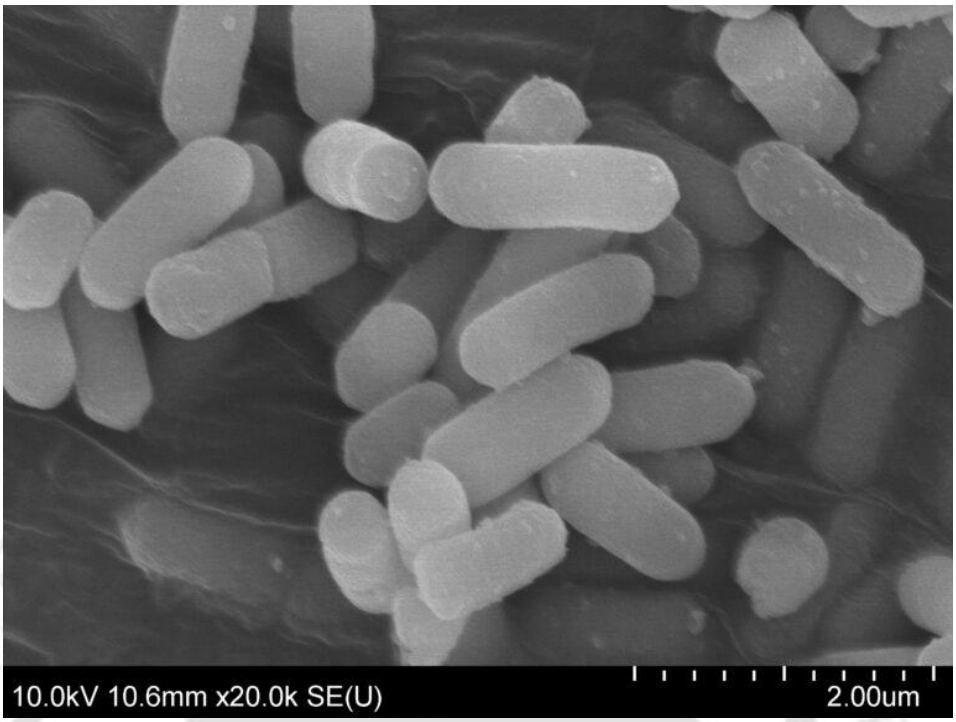

Fig. 1.4 Scanning electron micrograph of *Bacteroides sp.* (Image source: Probio).

The ability of *Bacteroides* to degrade dietary and mucosal polysaccharides, as well as polysaccharides found on the surface of other gut microbes, plays a crucial role in their survival and proliferation in the environment of the gut (Martens et al., 2008). Among the Bacteroidetes, members of the genus *Bacteroides* (Fig. 1.5) are among the most dominant bacterial species residing in the human colonic microbiota. Notably, *Bacteroides ovatus*, a Gram-negative, rod-shaped, non-spore-forming and anaerobic bacterium, is detected in over 90% of individuals (Wegmann et al., 2016). To facilitate the breakdown of hemicelluloses, *Bacteroides ovatus* harbors numerous polysaccharide utilization loci (PULs), which encode specialized enzymes involved in the degradation of hemicelluloses (Martens et al., 2008). Further studies have demonstrated the substrate specificity of *B. ovatus*, particularly in relation to hemicellulose degradation. Centanni et al. in 2017 reported that *B. ovatus* efficiently utilizes a variety of xylan-

based substrates, including beechwood xylan, wheat arabinoxylan and highly branched xylan derived from Phormium spp. commonly referred to as New Zealand flax (Centanni et al., 2017).

1.8 Applications of arabinofuranosidases

α-L-Arabinofuranosidases have received much attention due to their role in the degradation of arabinoxylans. These are accessory enzymes that either act on α-L-arabinofuranosidic linkages alone or in synergy with other hemicellulases and pectin degrading enzymes for the complete hydrolysis of hemicelluloses and pectins (Numan & Bhosle, 2006). Since, L-arabinose side chains present on xylans can hinder the action of xylanase, α-L-arabinofuranosidase acts in synergy with endoxylanase resulting in more effective degradation of the xylan chains from which arabinose moieties are removed (Fehér, 2018). Arabinofuranosidases have demonstrated significant utility in various biotechnological applications (Fig. 1.6). Some of them are described below.

Fig. 1.6 Biotechnological applications of α-L-arabinofuranosidase

1.8.1 Flavor enhancer in wine industry

Arabinofuranosidases are used in wine industry, particularly for enhancing the flavor profile of the wine. Among the key factors that influences the overall quality of wine is the aroma that stands out as one of the most important aspects. The primary aromas of wine, often referred to as varietal aromas, stem from the presence of free terpenes. The terpenes are found in both grape must and wine, but these terpenes exist alongside varying amounts of their glycosylated forms, which are typically odorless (Zietsman et al., 2011). The release of these bound terpenes plays a crucial role in enhancing the aroma and taste of the wine. The bound terpenes are linked to mono- or di-saccharides (Sarry & Günata, 2004). The glycosylated terpenes contain sugars, specifically monosaccharides or disaccharides, which prevent them from being aromatic. To release the free terpenes and unlock their fragrance, certain enzymatic activities are necessary. In the first step, depending on the nature of the sugar at the non-reducing end, the enzymes α-L-arabinofuranosidase, α-L-rhamnosidase, β-1,4-xylosidase or a β-D-apiosidase liberate the sugars arabinose, rhamnose, xylose or apiose, respectively. In the second step, β-glucosidase hydrolyses the remaining glycosidic bond releasing the terpene (Gunata et al., 1988).

1.8.2 Improving texture of bread

Wheat flour contains two types of arabinoxylans, one that dissolves in water and other that is insoluble. The insoluble fraction of arabinoxylan interferes with gluten, a protein network formation during dough mixing. Insoluble arabinoxylans compete for water which gluten proteins also need for dough's elasticity and ability to trap gas during fermentation. This physical blocking of gluten structure results in the lower quality of dough (Akram et al., 2024). Endo-xylanases convert the water insoluble

arabinoxylan into soluble form, that increases the dough volume, decreases the dough firmness and create finer and uniform crumbs (Ramalingam, 2010). Moreover, there are reports on addition of α-L-arabinofuranosidases to improve the bread quality. It was demonstrated that supplementation of fusion enzyme created by fusing a xylan specific-Carbohydrate binding domain 6 (XBD6) from *Clostridium thermocellum* to α-L-arabinofuranosidase (TmAra) from *Thermotoga maritima* improved the texture and volume in the steamed bread, which was a consequence of the increased strength of the dough (Zhou et al., 2019). Fusion enzyme reduced crumb (inner part of baked bread loaf) firmness and increased the specific volume with higher springiness, cohesiveness and crumb chewiness.

1.8.3 Pulp bleaching in paper industry

Pulp bleaching using enzymes is an important step in paper production. It is the process of removing color (mainly due to lignin) from wood pulp to produce white or lighter-colored paper (Zhang & Naebe, 2021). Traditionally, pulp was bleached by treatment with chlorine or chlorine dioxide (Bezalel et al., 1993). Bio-bleaching of pulp uses hemicellulases, usually xylanases, to break bonds with lignin, releasing the coloured lignin attached to oligosaccharides (Bezalel et al., 1993). Application of α-L-arabinofuranosidase enhances the delignification of pulp as the enzyme releases the arabinose side chain whose presence otherwise retards the action of other bleaching enzymes (Numan & Bhosle, 2006). The purified α-L-arabinofuranosidase from *Bacillus stearothermophilus* was shown to partially delignify the softwood kraft pulp (Bezalel et al., 1993). The simultaneous use of α- L-arabinofuranosidase from *Aureobasidium pullulans* NRRL Y-12974 and xylanase from *Trichoderma longibrachiatum* resulted in a greater release of reducing sugar from pulp as compared

to the additive effects of using α-L-arabinofuranosidase and xylanase independently suggesting a synergy (Makkonen & Nakas, 2005).

1.8.4 Digestibility of animal feedstock

The breakdown of feedstuffs by ruminal microorganisms leads to the production of acids and allow the rumen microbial population to multiply (Dehority & Scott, 1967). Hemicelluloses that contribute as feedstock for animals are less consumed due to low digestibility (Numan & Bhosle, 2006). A strong correlation was observed between the increased digestibility of feedstuffs and a reduction in the degree to which hemicellulose polymers are substituted with arabinosyl residues (Greve et al., 1984). Studies have shown that the commercial enzyme preparations containing α-L-arabinofuranosidase can enhance the performance of xylanase on feedstuffs used in poultry feeding. This is because xylanase preferentially acts on unsubstituted regions of xylan, which helps in reducing the viscosity of the feedstuffs, thereby improving their digestibility (Mathlouthi et al., 2002). Furthermore, Cotta (1993) reported that α-L-arabinofuranosidase isolated from *Ruminococcus albus* 8 effectively removed arabinosyl residues from alfalfa cell walls, as well as from pectic and hemicellulosic polysaccharides. This enzymatic action makes these substrates more vulnerable to degradation by other glycanases, further aiding in their breakdown and enhancing the overall digestibility of the feed (Cotta, 1993).

1.8.5 Fruits juice industry

Fruit juices prepared by simple extraction are cloudy, viscous and turbid due to the presence of polysaccharides such as starch, pectin, cellulose, hemicelluloses and bound lignin (Rosmine et al., 2017). The cloudy juices give lower yields, less acceptable and are difficult to pasteurise and concentrate (Numan & Bhosle, 2006). A

combination of macerating enzymes (cellulases, xylanases and pectinases) have been used in fruit juice clarification to increase the yield, clarity and decrease the viscosity of juice (Nagar et al., 2012). Low-viscosity juices with high clarity are more appealing to consumers and are more nutritive with increased bioavailability of sugars. Increase in clarity and decrease in viscosity of fruit juices using xylanases from *Bacillus stearothermophilus* has been reported (Dhiman et al., 2011). An α-L-arabinofuranosidase from *Chthonomonas calidirosea* T49 for clarification process of ginkgo kernel juice fermented with *L. plantarum* Y2 was reported (Chen et al., 2024). The changes in constituent and content of volatile flavor compounds also made the flavor of the fermentation broth more mellow and rich and improved the acceptance of consumers to the fermented ginkgo kernel juice (Chen et al., 2024)

1.8.6 Production of fermentable sugars for bioethanol industry

Lignocellulosic biomass predominantly comprises of cellulose, hemicellulose and lignin, which form complex polymers naturally recalcitrant to enzymatic conversion (Jaafar et al., 2021). The conversion of arabinoxylan, into a fermentable hydrolysate is crucial for using hemicellulose in the production of ethanol or other value-added products (Sørensen et al., 2005). While acid hydrolysis can entirely break down arabinoxylans into monosaccharides, the enzymatic hydrolysis is favoured because it reduces the formation of byproducts that could hinder the subsequent microbial fermentation (de Sousa Paredes et al., 2015). A study highlighted that endo-xylanase (XynC) from *Penicillium funiculosum* and α-L-arabinofuranosidase (AbfB) from *Aspergillus niger* acted synergistically on sugarcane bagasse pulp and arabinoxylan degradation with respect to the release of arabinose and xylooligosaccharides (Gonçalves et al., 2012). It was reported that two GH62 α-L-

arabinofuranosidases (ARA-1 and ARA-2) from *Talaromyces amestolkiae* acted synergistically with a *T. amestolkiae* endoxylanase for enhancing arabinose and xylooligosaccharides release from arabinoxylan (Méndez-Líter et al., 2023).

1.9 Significance and objectives of the present study

1.9.1 Significance of Investigation

The exploration of new xylanolytic enzymes hydrolysing the complex dietary fibers is of paramount importance. These enzymes play a key role in breaking down dietary polysaccharides which are otherwise resistant to human digestion. These xylanolytic enzymes facilitate the pre-hydrolysis of non-digestible fibers in animal feed, enhancing digestibility and contribute to the production of sugar syrups from lignocellulosic biomass. From a technological perspective, arabinofuranosidases, endoxylanases and xylosidases serve a potential role in various industrial applications. The investigation into novel arabinofuranosidase holds immense scientific and industrial significance due to its potential to efficiently degrade complex plant-based polysaccharides, particularly arabinoxylans, which are abundant in cereal grains and agricultural residues. It also supports the development of arabinose and arabino-xylooligosaccharides, with more effective prebiotic properties. Such prebiotics can enhance human health by targeting and modulating the gut microbiota. (Yoo et al., 2024). α-L-Arabinofuranosidases play a crucial role in the debranching of these arabinose residues, thereby enhancing the access of other enzymes like xylosidases to the main xylan chain. Therefore, a detailed study and characterization of novel arabinofuranosidase is important as studying them helps advance our understanding of their biochemical and structural properties. *Bacteroides ovatus*, a prominent gut bacterium known for its polysaccharide-degrading capacity, encodes several carbohydrate-active enzymes, including α-L-arabinofuranosidases. The gene encoding a putative α-L-arabinofuranosidase of family 43 glycoside hydrolase (*Bo*GH43_35) was identified in *Bacteroides ovatus* ATCC 8483 genome. Therefore, in the proposed

work, the gene encoding a family 43 glycoside hydrolase (GenBank Accession number ALJ47148) from *Bacteroides ovatus* will be cloned, expressed and purified. The biochemical and functional characterization of α-L-arabinofuranosidase, *Bo*GH43_35 of family 43 glycoside hydrolase from *Bacteroides ovatus* will be carried out to determine its specificity and ability to degrade various complex natural and synthetic xylan substrates. Moreover, understanding its efficiency and stability under different pH and temperature conditions will be crucial for industrial applications. The structural studies of *Bo*GH43_35 by computational methods will help predict its three-dimensional structure and its interaction with suitable ligands through molecular docking analyses. Furthermore, the regioselectivity analysis of *Bo*GH43_35 using proton-nuclear magnetic resonance will unravel its specificity for O-2 or O-3 or both O-2 and O-3 L-arabinose substitutions on arabinoxylan. Dynamic Light Scattering will be used to measure the hydrodynamic radius of *Bo*GH43_35 in different protein concentrations and assess the oligomeric state in solution. The effect of α-L-arabinofuranosidase on fruit juice clarification will be analysed. Moreover, its efficiency alone or in combination with xylosidase in the fruit peel biomass hydrolysis is also proposed for the production of xylooligosaccharides. The specific objectives that are formulated for the proposed work are given below.

1.9.2 Specific objectives

1) Cloning of gene encoding, a putative α-L-arabinofuranosidase, *Bo*GH43_35, from *Bacteroides ovatus*, its expression and purification.
2) Biochemical characterization of recombinant α-L-arabinofuranosidase (*Bo*GH43_35).
3) Mode of action and regioselectivity analyses of α-L-arabinofuranosidase (*Bo*GH43_35).
4) Structure analysis of α-L-arabinofuranosidase (*Bo*GH43_35) by computational and experimental methods.
5) Application of α-L-arabinofuranosidase (*Bo*GH43_35) in pomegranate and sweet lemon juice clarification.
6) Application of *Bo*GH43_35 for saccharification of peels of pomegranate and sweet lemon.

1.10 References

Ahmed, S., Luis, A. S., Bras, J. L. A., Ghosh, A., Gautam, S., Gupta, M. N., Fontes, C. M. G. A., & Goyal, A. (2013). A novel α-L-Arabinofuranosidase of family 43 Glycoside Hydrolase (*ss*43Araf) from *Clostridium thermocellum*. *PLOS ONE*, *8*(9), e73575. https://doi.org/10.1371/journal.pone.0073575

Akram, F., Fatima, T., Ibrar, R., Shabbir, I., Shah, F. I., & Haq, I. ul. (2024). Trends in the development and current perspective of thermostable bacterial hemicellulases with their industrial endeavors: A review. *International Journal of Biological Macromolecules*, *265*, 130993. https://doi.org/10.1016/j.ijbiomac.2024.130993

An, Y., Lu, W., Li, W., Pan, L., Lu, M., Cesarino, I., Li, Z., & Zeng, W. (2022). Dietary fiber in plant cell walls—The healthy carbohydrates. *Food Quality and Safety*, *6*, fyab037. https://doi.org/10.1093/fqsafe/fyab037

Bailey, I. W. (1938). Cell Wall Structure of Higher Plants. *Industrial & Engineering Chemistry*, *30*(1), 40–47. https://doi.org/10.1021/ie50337a009

Beg, Q. K., Kapoor, M., Mahajan, L., & Hoondal, G. S. (2001). Microbial xylanases and their industrial applications: A review. *Applied Microbiology and Biotechnology*, *56*(3–4), 326–338. https://doi.org/10.1007/s002530100704

Bezalel, L., Shoham, Y., & Rosenberg, E. (1993). Characterization and delignification activity of a thermostable α-l-arabinofuranosidase from *Bacillus stearothermophilus*. *Applied Microbiology and Biotechnology*, *40*(1), 57–62. https://doi.org/10.1007/BF00170429

Birgisson, H., Fridjonsson, O., Bahrani-Mougeot, F. K., Hreggvidsson, G. O., Kristjansson, J. K., & Mattiasson, B. (2004). A new thermostable α-L-arabinofuranosidase from a novel thermophilic bacterium. *Biotechnology Letters*, *26*(17), 1347–1351. https://doi.org/10.1023/B:BILE.0000045631.57073.79

Boukid, F. (2024). Comprehensive review of barley dietary fibers with emphasis on arabinoxylans. *Bioactive Carbohydrates and Dietary Fibre*, *31*, 100410. https://doi.org/10.1016/j.bcdf.2024.100410

Bouraoui, H., Desrousseaux, M.-L., Ioannou, E., Alvira, P., Manaï, M., Rémond, C., Dumon, C., Fernandez-Fuentes, N., & O'Donohue, M. J. (2016). The GH51 α-L-arabinofuranosidase from *Paenibacillus* sp. THS1 is multifunctional, hydrolyzing main-chain and side-chain glycosidic bonds in heteroxylans. *Biotechnology for Biofuels*, *9*(1), 140. https://doi.org/10.1186/s13068-016-0550-x

Broekaert, W. F., Courtin, C. M., Verbeke, K., Van De Wiele, T., Verstraete, W., & Delcour, J. A. (2011). Prebiotic and other health-related effects of cereal-derived Arabinoxylans, arabinoxylan-oligosaccharides and xylooligosaccharides. *Critical Reviews in Food Science and Nutrition*, *51*(2), 178–194. https://doi.org/10.1080/10408390903044768

Brownlee, I. A. (2011). The physiological roles of dietary fibre. *Food Hydrocolloids*, *25*(2), 238–250. https://doi.org/10.1016/j.foodhyd.2009.11.013

Capuano, E. (2017). The behavior of dietary fiber in the gastrointestinal tract determines its physiological effect. *Critical Reviews in Food Science and Nutrition*, *57*(16), 3543–3564. https://doi.org/10.1080/10408398.2016.1180501

Centanni, M., Hutchison, J. C., Carnachan, S. M., Daines, A. M., Kelly, W. J., Tannock, G. W., & Sims, I. M. (2017). Differential growth of bowel commensal *Bacteroides* species on

plant xylans of differing structural complexity. *Carbohydrate Polymers*, *157*, 1374–1382. https://doi.org/10.1016/j.carbpol.2016.11.017

Chen, J., Wang, Q., Zhou, J., Yang, J., Xu, L., Huo, D., & Wei, Z. (2024). Optimization of α-L-arabinofuranosidase CcABF on clarification and beneficial active substances in fermented ginkgo kernel juice by artificial neural network and genetic algorithm. *Food Chemistry*, *450*, 139386. https://doi.org/10.1016/j.foodchem.2024.139386

Chen, Z., Li, S., Fu, Y., Li, C., Chen, D., & Chen, H. (2019). Arabinoxylan structural characteristics, interaction with gut microbiota and potential health functions. *Journal of Functional Foods*, *54*, 536–551. https://doi.org/10.1016/j.jff.2019.02.007

Cheng, J., Hu, J., Geng, F., & Nie, S. (2022). *Bacteroides* utilization for dietary polysaccharides and their beneficial effects on gut health. *Food Science and Human Wellness*, *11*(5), 1101–1110. https://doi.org/10.1016/j.fshw.2022.04.002

Chudan, S., Ishibashi, R., Nishikawa, M., Tabuchi, Y., Nagai, Y., Ikushiro, S., & Furusawa, Y. (2023). Effect of wheat-derived arabinoxylan on the gut microbiota composition and colonic regulatory T Cells. *Molecules*, *28*(7), Article 7. https://doi.org/10.3390/molecules28073079

Collins, T., Gerday, C., & Feller, G. (2005). Xylanases, xylanase families and extremophilic xylanases. *FEMS Microbiology Reviews*, *29*(1), 3–23. https://doi.org/10.1016/j.femsre.2004.06.005

Contesini, F. J., Liberato, M. V., Rubio, M. V., Calzado, F., Zubieta, M. P., Riaño-Pachón, D. M., Squina, F. M., Bracht, F., Skaf, M. S., & Damasio, A. R. (2017). Structural and functional characterization of a highly secreted α-L-arabinofuranosidase (GH62) from *Aspergillus nidulans* grown on sugarcane bagasse. *Biochimica et Biophysica Acta (BBA) - Proteins and Proteomics*, *1865*(12), 1758–1769. https://doi.org/10.1016/j.bbapap.2017.09.001

Cosgrove, D. J. (2005). Growth of the plant cell wall. *Nature Reviews Molecular Cell Biology*, *6*(11), 850–861. https://doi.org/10.1038/nrm1746

Cotta, M. A. (1993). Utilization of xylooligosaccharides by selected ruminal bacteria. *Applied and Environmental Microbiology*, *59*(11), 3557–3563. https://doi.org/10.1128/aem.59.11.3557-3563.1993

Dai, F.-J., & Chau, C.-F. (2017). Classification and regulatory perspectives of dietary fiber. *Journal of Food and Drug Analysis*, *25*(1), 37–42. https://doi.org/10.1016/j.jfda.2016.09.006

de Sousa Paredes, R., da Rocha Olivieri de Barros, R., Inoue, H., Yano, S., & da Silva Bon, E. P. (2015). Production of xylanase, α-L-arabinofuranosidase, β-xylosidase, and β-glucosidase by *Aspergillus awamori* using the liquid stream from hot-compressed water treatment of sugarcane bagasse. *Biomass Conversion and Biorefinery*, *5*(3), 299–307. https://doi.org/10.1007/s13399-015-0159-5

Debeche, T., Cummings, N., Connerton, I., Debeire, P., & O'Donohue, M. J. (2000). Genetic and biochemical characterization of a highly thermostable α-L-arabinofuranosidase from *Thermobacillus xylanilyticus*. *Applied and Environmental Microbiology*, *66*(4), 1734–1736. https://doi.org/10.1128/AEM.66.4.1734-1736.2000

Dehority, B. A., & Scott, H. W. (1967). Extent of cellulose and hemicellulose digestion in various forages by pure cultures of rumen bacteria. *Journal of Dairy Science*, *50*(7), 1136–1141. https://doi.org/10.3168/jds.S0022-0302(67)87579-9

Dhiman, S. S., Garg, G., Sharma, J., & Mahajan, R. (2011). Characterization of statistically produced xylanase for enrichment of fruit juice clarification process. *New Biotechnology*, *28*(6), 746–755. https://doi.org/10.1016/j.nbt.2010.11.004

Dhingra, D., Michael, M., Rajput, H., & Patil, R. T. (2012). Dietary fibre in foods: A review. *Journal of Food Science and Technology*, *49*(3), 255–266. https://doi.org/10.1007/s13197-011-0365-5

Dodd, D., & Cann, I. K. O. (2009). Enzymatic deconstruction of xylan for biofuel production. *GCB Bioenergy*, *1*(1), 2–17. https://doi.org/10.1111/j.1757-1707.2009.01004.x

Eastwood, M., & Morris, E. (1992). Physical properties of dietary fiber that influence physiological function: A model for polymers along the gastrointestinal tract. *The American Journal of Clinical Nutrition*, *55*(2), 436–442. https://doi.org/10.1093/ajcn/55.2.436

Fan, Z., Werkman, J. R., & Yuan, L. (2009). Engineering of a multifunctional hemicellulase. *Biotechnology Letters*, *31*(5), 751–757. https://doi.org/10.1007/s10529-009-9926-3

Fehér, C. (2018). Novel approaches for biotechnological production and application of L-arabinose. *Journal of Carbohydrate Chemistry*, *37*(5), 251–284. https://doi.org/10.1080/07328303.2018.1491049

Fuentes-Zaragoza, E., Riquelme-Navarrete, M. J., Sánchez-Zapata, E., & Pérez-Álvarez, J. A. (2010). Resistant starch as functional ingredient: A review. *Food Research International*, *43*(4), 931–942. https://doi.org/10.1016/j.foodres.2010.02.004

Gibson, G. R., & Roberfroid, M. B. (1995). Dietary modulation of the human colonic microbiota: Introducing the concept of prebiotics. *The Journal of Nutrition*, *125*(6), 1401–1412. https://doi.org/10.1093/jn/125.6.1401

Gilead, S., & Shoham, Y. (1995). Purification and characterization of alpha-L-arabinofuranosidase from *Bacillus stearothermophilus* T-6. *Applied and Environmental Microbiology*, *61*(1), 170–174. https://doi.org/10.1128/aem.61.1.170-174.1995

Gonçalves, T. A., Damásio, A. R. L., Segato, F., Alvarez, T. M., Bragatto, J., Brenelli, L. B., Citadini, A. P. S., Murakami, M. T., Ruller, R., Paes Leme, A. F., Prade, R. A., & Squina, F. M. (2012). Functional characterization and synergic action of fungal xylanase and arabinofuranosidase for production of xylooligosaccharides. *Bioresource Technology*, *119*, 293–299. https://doi.org/10.1016/j.biortech.2012.05.062

Greve, L. C., Labavitch, J. M., & Hungate, R. E. (1984). Alpha-L-arabinofuranosidase from *Ruminococcus albus* 8: Purification and possible role in hydrolysis of alfalfa cell wall. *Applied and Environmental Microbiology*, *47*(5), 1135–1140. https://doi.org/10.1128/aem.47.5.1135-1140.1984

Grootaert, C., Delcour, J. A., Courtin, C. M., Broekaert, W. F., Verstraete, W., & Van de Wiele, T. (2007). Microbial metabolism and prebiotic potency of arabinoxylan oligosaccharides in the human intestine. *Trends in Food Science & Technology*, *18*(2), 64–71. https://doi.org/10.1016/j.tifs.2006.08.004

Guillon, F., & Champ, M. (2000). Structural and physical properties of dietary fibres, and consequences of processing on human physiology. *Food Research International*, *33*(3), 233–245. https://doi.org/10.1016/S0963-9969(00)00038-7

Gunata, Z., Bitteur, S., Brillouet, J.-M., Bayonove, C., & Cordonnier, R. (1988). Sequential enzymic hydrolysis of potentially aromatic glycosides from grape. *Carbohydrate Research*, *184*, 139–149. https://doi.org/10.1016/0008-6215(88)80012-0

Hamaker, B. R., & Tuncil, Y. E. (2014). A perspective on the complexity of dietary fiber structures and their potential effect on the gut microbiota. *Journal of Molecular Biology*, *426*(23), 3838–3850. https://doi.org/10.1016/j.jmb.2014.07.028

He, H.-J., Qiao, J., Liu, Y., Guo, Q., Ou, X., & Wang, X. (2021). Isolation, structural, functional, and bioactive properties of cereal arabinoxylan─A critical review. *Journal of Agricultural and Food Chemistry*, *69*(51), 15437–15457. https://doi.org/10.1021/acs.jafc.1c04506

Heredia, A., Jiménez, A., & Guillén, R. (1995). Composition of plant cell walls. *Zeitschrift Für Lebensmittel-Untersuchung Und Forschung*, *200*(1), 24–31. https://doi.org/10.1007/BF01192903

Hu, X., Zhang, G., Hamaker, B. R., & Miao, M. (2022). The contribution of intact structure and food processing to functionality of plant cell wall-derived dietary fiber. *Food Hydrocolloids*, *127*, 107511. https://doi.org/10.1016/j.foodhyd.2022.107511

Hu, Y., Zhao, Y., Tian, S., Zhang, G., Li, Y., Li, Q., & Gao, J. (2018). Screening of a novel Glycoside Hydrolase family 51 α-L-arabinofuranosidase from *Paenibacillus polymyxa* KF-1: Cloning, expression, and characterization. *Catalysts*, *8*(12), Article 12. https://doi.org/10.3390/catal8120589

Jaafar, N. R., Ayob, S. N., Abd Rahman, N. H., Abu Bakar, F. D., Murad, A. M. A., & Illias, R. M. (2021). Rational protein engineering of α-L-arabinofuranosidase from *Aspergillus niger* for improved catalytic hydrolysis efficiency on kenaf hemicellulose. *Process Biochemistry*, *102*, 349–359. https://doi.org/10.1016/j.procbio.2020.12.012

Jr, P., & W, Y. (2016). A Review of Physiological Effects of Soluble and Insoluble Dietary Fibers. *Journal of Nutrition & Food Sciences*, *06*(02). https://doi.org/10.4172/2155-9600.1000476

Khandeparker, R., & Numan, M. T. (2008). Bifunctional xylanases and their potential use in biotechnology. *Journal of Industrial Microbiology and Biotechnology*, *35*(7), 635–644. https://doi.org/10.1007/s10295-008-0342-9

Kousar, S., Mustafa, G., & Jamil, A. (2013). Microbial xylosidases: Production and biochemical characterization. *Pakistan Journal of Life and Social Sciences (Pakistan)*, *11*(2). https://agris.fao.org/search/en/providers/122650/records/647369c308fd68d546063755

Lagaert, S., Pollet, A., Courtin, C. M., & Volckaert, G. (2014). β-Xylosidases and α-L-arabinofuranosidases: Accessory enzymes for arabinoxylan degradation. *Biotechnology Advances*, *32*(2), 316–332. https://doi.org/10.1016/j.biotechadv.2013.11.005

Lee, D.-S., Wi, S.-G., Lee, Y.-G., Cho, E.-J., Chung, B.-Y., & Bae, H.-J. (2011). Characterization of a new α-L-arabinofuranosidase from *Penicillium* sp. LYG 0704, and their application in lignocelluloses degradation. *Molecular Biotechnology*, *49*(3), 229–239. https://doi.org/10.1007/s12033-011-9396-4

Li, C., Cao, H., Wu, W., Meng, G., Zhao, C., Cao, Y., & Yuan, J. (2023). Expression and characterization of α-L-arabinofuranosidase derived from *Aspergillus awamori* and its

enzymatic degradation of corn byproducts with xylanase. *Bioresource Technology*, *384*, 129278. https://doi.org/10.1016/j.biortech.2023.129278

Limsakul, P., Phitsuwan, P., Waeonukul, R., Pason, P., Tachaapaikoon, C., Poomputsa, K., Kosugi, A., & Ratanakhanokchai, K. (2021). A novel multifunctional arabinofuranosidase/endoxylanase/β-xylosidase GH43 enzyme from *Paenibacillus curdlanolyticus* B-6 and its synergistic action to produce arabinose and xylose from cereal arabinoxylan. *Applied and Environmental Microbiology*, *87*(24), e01730-21. https://doi.org/10.1128/AEM.01730-21

Lin, S., Agger, J. W., Wilkens, C., & Meyer, A. S. (2021). Feruloylated arabinoxylan and oligosaccharides: Chemistry, nutritional functions, and options for enzymatic modification. *Annual Review of Food Science and Technology*, *12*(Volume 12, 2021), 331–354. https://doi.org/10.1146/annurev-food-032818-121443

Long, L., Sun, L., Liu, Z., Lin, Q., Wang, J., & Ding, S. (2022). Functional characterization of a GH62 family α-L-arabinofuranosidase from *Eupenicillium parvum* suitable for monosaccharification of corncob arabinoxylan in combination with key enzymes. *Enzyme and Microbial Technology*, *154*, 109965. https://doi.org/10.1016/j.enzmictec.2021.109965

Lu, Z. X., Walker, K. Z., Muir, J. G., Mascara, T., & O'Dea, K. (2000). Arabinoxylan fiber, a byproduct of wheat flour processing, reduces the postprandial glucose response in normoglycemic subjects. *The American Journal of Clinical Nutrition*, *71*(5), 1123–1128. https://doi.org/10.1093/ajcn/71.5.1123

MacKenzie, C. R., Bilous, D., Schneider, H., & Johnson, K. G. (1987). Induction of cellulolytic and xylanolytic enzyme systems in *Streptomyces* spp. *Applied and Environmental Microbiology*, *53*(12), 2835–2839. https://doi.org/10.1128/aem.53.12.2835-2839.1987

Maheshwari, G., Sowrirajan, S., & Joseph, B. (2019). β-Glucan, a dietary fiber in effective prevention of lifestyle diseases – An insight. *Bioactive Carbohydrates and Dietary Fibre*, *19*, 100187. https://doi.org/10.1016/j.bcdf.2019.100187

Makkonen, H. P., & Nakas, J. P. (2005). Use of xylanase and arabinofuranosidase for arabinose removal from unbleached kraft pulp. *Biotechnology Letters*, *27*(21), 1675–1679. https://doi.org/10.1007/s10529-005-2728-3

Margolles, A., & de los Reyes-Gavilán, C. G. (2003). Purification and functional characterization of a novel α-L-arabinofuranosidase from *Bifidobacterium longum* B667. *Applied and Environmental Microbiology*, *69*(9), 5096–5103. https://doi.org/10.1128/AEM.69.9.5096-5103.2003

Martens, E. C., Chiang, H. C., & Gordon, J. I. (2008). Mucosal glycan foraging enhances fitness and transmission of a Saccharolytic human gut bacterial symbiont. *Cell Host & Microbe*, *4*(5), 447–457. https://doi.org/10.1016/j.chom.2008.09.007

Mathlouthi, N., Saulnier, L., Quemener, B., & Larbier, M. (2002). Xylanase, β-glucanase, and other side enzymatic activities have greater effects on the viscosity of several feedstuffs than xylanase and β-glucanase used alone or in combination. *Journal of Agricultural and Food Chemistry*, *50*(18), 5121–5127. https://doi.org/10.1021/jf011507b

McCleary, B. V., DeVries, J. W., Rader, J. I., Cohen, G., Prosky, L., Mugford, D. C., Champ, M., & Okuma, K. (2012). Determination of insoluble, soluble, and total dietary fiber (CODEX Definition) by enzymatic-gravimetric method and liquid chromatography: Collaborative study. *Journal of AOAC INTERNATIONAL*, *95*(3), 824–844. https://doi.org/10.5740/jaoacint.CS2011_25

McKee, L. H., & Latner, T. A. (2000). Underutilized sources of dietary fiber: A review. *Plant Foods for Human Nutrition*, *55*(4), 285–304. https://doi.org/10.1023/A:1008144310986

Méndez-Líter, J. A., de Eugenio, L. I., Nieto-Domínguez, M., Prieto, A., & Martínez, M. J. (2023). Expression and characterization of two α-L-arabinofuranosidases from *Talaromyces amestolkiae*: Role of these enzymes in biomass valorization. *International Journal of Molecular Sciences*, *24*(15), Article 15. https://doi.org/10.3390/ijms241511997

Mendis, M., & Simsek, S. (2014). Arabinoxylans and human health. *Food Hydrocolloids*, *42*, 239–243. https://doi.org/10.1016/j.foodhyd.2013.07.022

Mikkelsen, D., Gidley, M. J., & Williams, B. A. (2011). In vitro fermentation of bacterial cellulose composites as model dietary fibers. *Journal of Agricultural and Food Chemistry*, *59*(8), 4025–4032. https://doi.org/10.1021/jf104855e

Miyanaga, A., Koseki, T., Matsuzawa, H., Wakagi, T., Shoun, H., & Fushinobu, S. (2004). Crystal structure of a family 54 α-L-arabinofuranosidase reveals a novel Carbohydrate-binding Module that can bind arabinose. *Journal of Biological Chemistry*, *279*(43), 44907–44914. https://doi.org/10.1074/jbc.M405390200

Moreira, L. R. S., & Filho, E. X. F. (2016). Insights into the mechanism of enzymatic hydrolysis of xylan. *Applied Microbiology and Biotechnology*, *100*(12), 5205–5214. https://doi.org/10.1007/s00253-016-7555-z

Mudgil, D., & Barak, S. (2013). Composition, properties and health benefits of indigestible carbohydrate polymers as dietary fiber: A review. *International Journal of Biological Macromolecules*, *61*, 1–6. https://doi.org/10.1016/j.ijbiomac.2013.06.044

Nagar, S., Mittal, A., & Gupta, V. K. (2012). Enzymatic clarification of fruit juices (Apple, Pineapple, and Tomato) using purified *Bacillus pumilus* SV-85S xylanase. *Biotechnology and Bioprocess Engineering*, *17*(6), 1165–1175. https://doi.org/10.1007/s12257-012-0375-9

Nakamura, A. M., Nascimento, A. S., & Polikarpov, I. (2017). Structural diversity of carbohydrate esterases. *Biotechnology Research and Innovation*, *1*(1), 35–51. https://doi.org/10.1016/j.biori.2017.02.001

Niño-Medina, G., Carvajal-Millán, E., Rascon-Chu, A., Marquez-Escalante, J. A., Guerrero, V., & Salas-Muñoz, E. (2010). Feruloylated arabinoxylans and arabinoxylan gels: Structure, sources and applications. *Phytochemistry Reviews*, *9*(1), 111–120. https://doi.org/10.1007/s11101-009-9147-3

Numan, M. T., & Bhosle, N. B. (2006). α-L-Arabinofuranosidases: The potential applications in biotechnology. *Journal of Industrial Microbiology and Biotechnology*, *33*(4), 247–260. https://doi.org/10.1007/s10295-005-0072-1

Padayachee, A., Day ,L., Howell ,K., & and Gidley, M. J. (2017). Complexity and health functionality of plant cell wall fibers from fruits and vegetables. *Critical Reviews in Food Science and Nutrition*, *57*(1), 59–81. https://doi.org/10.1080/10408398.2013.850652

Pettolino, F. A., Walsh, C., Fincher, G. B., & Bacic, A. (2012). Determining the polysaccharide composition of plant cell walls. *Nature Protocols*, *7*(9), 1590–1607. https://doi.org/10.1038/nprot.2012.081

Phuengmaung, P., Kunishige, Y., Sukhumsirichart, W., & Sakamoto, T. (2018). Identification and characterization of GH62 bacterial α-L-arabinofuranosidase from thermotolerant *Streptomyces* sp. SWU10 that preferentially degrades branched L-arabinofuranoses in wheat arabinoxylan. *Enzyme and Microbial Technology*, *112*, 22–28. https://doi.org/10.1016/j.enzmictec.2018.01.009

Popa, A., Israel-Roming, F., & Cornea, C. P. (2016). Microbial xylanase: A review. *Scientific Bulletin. Series F. Biotechnologies*, *20*, 335–342.

Ramalingam, C. and Harris. A. D. (2010). Xylanases and its application in food industry: A Review. *Journal of Experimental Sciences*. https://updatepublishing.com/journal/index.php/jes/article/view/1737

Redgwell, R. J., & Fischer, M. (2005). Dietary fiber as a versatile food component: An industrial perspective. *Molecular Nutrition & Food Research*, *49*(6), 521–535. https://doi.org/10.1002/mnfr.200500028

Rezania, S., Oryani, B., Cho, J., Talaiekhozani, A., Sabbagh, F., Hashemi, B., Rupani, P. F., & Mohammadi, A. A. (2020). Different pretreatment technologies of lignocellulosic biomass for bioethanol production: An overview. *Energy*, *199*, 117457. https://doi.org/10.1016/j.energy.2020.117457

Rodrigues Mota, T., Matias De O, Marchiosi, R., Ferrarese-Filho, O., & Santos, W. D. D. (2018). Plant cell wall composition and enzymatic deconstruction. *AIMS Bioengineering*, *5*(1), 63–77. https://doi.org/10.3934/bioeng.2018.1.63

Rosmine, E., Sainjan, N. C., Silvester, R., Alikkunju, A., & Varghese, S. A. (2017). Statistical optimisation of xylanase production by estuarine *Streptomyces* sp. and its application in clarification of fruit juice. *Journal of Genetic Engineering and Biotechnology*, *15*(2), 393–401. https://doi.org/10.1016/j.jgeb.2017.06.001

Saha, B. C. (2003). Hemicellulose bioconversion. *Journal of Industrial Microbiology and Biotechnology*, *30*(5), 279–291. https://doi.org/10.1007/s10295-003-0049-x

Sakamoto, T., Ogura, A., Inui, M., Tokuda, S., Hosokawa, S., Ihara, H., & Kasai, N. (2011). Identification of a GH62 α-L-arabinofuranosidase specific for arabinoxylan produced by *Penicillium chrysogenum*. *Applied Microbiology and Biotechnology*, *90*(1), 137–146. https://doi.org/10.1007/s00253-010-2988-2

Saleh, M. A., Mahmud, S., Albogami, S., El-Shehawi, A. M., Paul, G. K., Islam, S., Dutta, A. K., Uddin, M. S., & Zaman, S. (2022). Biochemical and molecular dynamics study of a novel GH 43 α-L-arabinofuranosidase/β-xylosidase from *Caldicellulosiruptor saccharolyticus* DSM8903. *Frontiers in Bioengineering and Biotechnology*, *10*. https://doi.org/10.3389/fbioe.2022.810542

Sarry, J.-E., & Günata, Z. (2004). Plant and microbial glycoside hydrolases: Volatile release from glycosidic aroma precursors. *Food Chemistry*, *87*(4), 509–521. https://doi.org/10.1016/j.foodchem.2004.01.003

Seiboth, B., & Metz, B. (2011). Fungal arabinan and L-arabinose metabolism. *Applied Microbiology and Biotechnology*, *89*(6), 1665–1673. https://doi.org/10.1007/s00253-010-3071-8

Shallom, D., Belakhov, V., Solomon, D., Gilead-Gropper, S., Baasov, T., Shoham, G., & Shoham, Y. (2002). The identification of the acid–base catalyst of α-arabinofuranosidase from *Geobacillus stearothermophilus* T-6, a family 51 glycoside

hydrolase. *FEBS Letters*, *514*(2–3), 163–167. https://doi.org/10.1016/S0014-5793(02)02343-8

Shallom, D., & Shoham, Y. (2003). Microbial hemicellulases. *Current Opinion in Microbiology*, *6*(3), 219–228. https://doi.org/10.1016/S1369-5274(03)00056-0

Shrivastava, M., Maibam, P. D., Aishwarya, A., & Goyal, A. (2023). Hemicellulases and auxiliary activities for biomass hydrolysis. In V. Bisaria (Ed.), *Handbook of Biorefinery Research and Technology* (pp. 1–23). Springer Netherlands. https://doi.org/10.1007/978-94-007-6724-9_36-1

Singh, N., Mathur, A. S., Gupta, R. P., Barrow, C. J., Tuli, D. K., & Puri, M. (2021). Enzyme systems of thermophilic anaerobic bacteria for lignocellulosic biomass conversion. *International Journal of Biological Macromolecules*, *168*, 572–590. https://doi.org/10.1016/j.ijbiomac.2020.12.004

Snauwaert, E., Paglialonga, F., Vande Walle, J., Wan, M., Desloovere, A., Polderman, N., Renken-Terhaerdt, J., Shaw, V., & Shroff, R. (2023). The benefits of dietary fiber: The gastrointestinal tract and beyond. *Pediatric Nephrology*, *38*(9), 2929–2938. https://doi.org/10.1007/s00467-022-05837-2

Snelders, J., Dornez, E., Delcour, J. A., & Courtin, C. M. (2013). Ferulic acid content and appearance determine the antioxidant capacity of arabinoxylanoligosaccharides. *Journal of Agricultural and Food Chemistry*, *61*(42), 10173–10182. https://doi.org/10.1021/jf403160x

Sørensen, H. R., Jørgensen, C. T., Hansen, C. H., Jørgensen, C. I., Pedersen, S., & Meyer, A. S. (2006). A novel GH43 α-L-arabinofuranosidase from *Humicola insolens*: Mode of action and synergy with GH51 α-L-arabinofuranosidases on wheat arabinoxylan. *Applied Microbiology and Biotechnology*, *73*(4), 850–861. https://doi.org/10.1007/s00253-006-0543-y

Sørensen, H. R., Pedersen, S., Viksø-Nielsen, A., & Meyer, A. S. (2005). Efficiencies of designed enzyme combinations in releasing arabinose and xylose from wheat arabinoxylan in an industrial ethanol fermentation residue. *Enzyme and Microbial Technology*, *36*(5), 773–784. https://doi.org/10.1016/j.enzmictec.2005.01.007

Tagawa, K., & Kaji, A. (1969). Preparation of L-arabinose-containing polysaccharides and the action of an α-L-arabinofuranosidase on these polysaccharides. *Carbohydrate Research*, *11*(3), 293–301. https://doi.org/10.1016/S0008-6215(00)80570-4

Thakur, A., Sharma, K., Jaiswal, K., & Goyal, A. (2020). Structure and dynamics analysis of a family 43 glycoside hydrolase α-L-arabinofuranosidase (*Ps*GH43_12) from *Pseudopedobacter saltans* by computational modeling and small-angle X-ray scattering. *International Journal of Biological Macromolecules*, *163*, 582–592. https://doi.org/10.1016/j.ijbiomac.2020.07.007

Thakur, A., Sharma, K., Jamaldheen, S. B., & Goyal, A. (2020). Molecular characterization, regioselective and synergistic action of first recombinant type III α-L-arabinofuranosidase of family 43 Glycoside Hydrolase (*Ps*GH43_12) from *Pseudopedobacter saltans*. *Molecular Biotechnology*, *62*(9), 443–455. https://doi.org/10.1007/s12033-020-00263-x

Tomme, P., Boraston, A., Kormos, J. M., Warren, R. A. J., & Kilburn, D. G. (2000). Affinity electrophoresis for the identification and characterization of soluble sugar binding by carbohydrate-binding modules. *Enzyme and Microbial Technology*, *27*(7), 453–458. https://doi.org/10.1016/S0141-0229(00)00246-5

Trowell, H. (1972). Ischemic heart disease and dietary fiber. *The American Journal of Clinical Nutrition*, *25*(9), 926–932. https://doi.org/10.1093/ajcn/25.9.926

Tuncil, Y. E., Thakkar, R. D., Arioglu-Tuncil, S., Hamaker, B. R., & Lindemann, S. R. (2020). Subtle variations in dietary-fiber fine structure differentially influence the composition and metabolic function of gut microbiota. *mSphere*, *5*(3), 10.1128/msphere.00180-20. https://doi.org/10.1128/msphere.00180-20

Van Craeyveld, V., Swennen, K., Dornez, E., Van de Wiele, T., Marzorati, M., Verstraete, W., Delaedt, Y., Onagbesan, O., Decuypere, E., Buyse, J., De Ketelaere, B., Broekaert, W. F., Delcour, J. A., & Courtin, C. M. (2008). Structurally different wheat-derived arabinoxylooligosaccharides have different prebiotic and fermentation properties in rats. *The Journal of Nutrition*, *138*(12), 2348–2355. https://doi.org/10.3945/jn.108.094367

Wallace, T. C., Marzorati ,Massimo, Spence ,Lisa, Weaver ,Connie M., & and Williamson, P. S. (2017). New frontiers in fibers: Innovative and emerging research on the gut microbiome and bone health. *Journal of the American College of Nutrition*, *36*(3), 218–222. https://doi.org/10.1080/07315724.2016.1257961

Wang, R., Zhang, Y., Liu, L., Yang, J., & Yuan, H. (2023). Discovery of a bifunctional xylanolytic enzyme with arabinoxylan arabinofuranohydrolase-d3 and endo-xylanase activities and its application in the hydrolysis of cereal arabinoxylans. *Microbial Biotechnology*, *16*(7), 1536–1547. https://doi.org/10.1111/1751-7915.14267

Wang, W., Mai-Gisondi, G., Stogios, P. J., Kaur, A., Xu, X., Cui, H., Turunen, O., Savchenko, A., & Master, E. R. (2014). Elucidation of the molecular basis for arabinoxylan-debranching activity of a thermostable family GH62 α-L-arabinofuranosidase from *Streptomyces thermoviolaceus*. *Applied and Environmental Microbiology*, *80*(17), 5317–5329. https://doi.org/10.1128/AEM.00685-14

Wang, Y., Sakka, M., Yagi, H., Kaneko, S., Katsuzaki, H., Kunitake, E., Kimura, T., & Sakka, K. (2018). *Ruminiclostridium josui* Abf62A-Axe6A: A tri-functional xylanolytic enzyme exhibiting α-L-arabinofuranosidase, endoxylanase, and acetylxylan esterase activities. *Enzyme and Microbial Technology*, *117*, 1–8. https://doi.org/10.1016/j.enzmictec.2018.05.016

Wegmann, U., Goesmann, A., & Carding, S. R. (2016). Complete genome sequence of *Bacteroides ovatus* V975. *Genome Announcements*, *4*(6), 10.1128/genomea.01335-16. https://doi.org/10.1128/genomea.01335-16

Williams, B. A., Grant, L. J., Gidley, M. J., & Mikkelsen, D. (2017). Gut fermentation of dietary fibres: Physico-chemistry of plant cell walls and implications for health. *International Journal of Molecular Sciences*, *18*(10), Article 10. https://doi.org/10.3390/ijms18102203

Yang, W., Bai, Y., Yang, P., Luo, H., Huang, H., Meng, K., Shi, P., Wang, Y., & Yao, B. (2015). A novel bifunctional GH51 exo-α-L-arabinofuranosidase/endo-xylanase from *Alicyclobacillus sp*. A4 with significant biomass-degrading capacity. *Biotechnology for Biofuels*, *8*(1), 197. https://doi.org/10.1186/s13068-015-0366-0

Yang, Y., Ma, S., Wang, X., & Zheng, X. (2017). Modification and application of dietary fiber in foods. *Journal of Chemistry*, *2017*, 1–8. https://doi.org/10.1155/2017/9340427

Yangılar, F. (2013). The Application of Dietary Fibre in Food Industry: Structural features, effects on health and definition, obtaining and analysis of dietary fibre: A Review. *Journal of Food and Nutrition Research*. https://www.semanticscholar.org/paper/The-

Application-of-Dietary-Fibre-in-Food-Industry%3A-Yang%C4%B1lar/212e146521fee70a1bae5b39b87b8f927bec7c51

Ye, S., Shah, B. R., Li, J., Liang, H., Zhan, F., Geng, F., & Li, B. (2022). A critical review on interplay between dietary fibers and gut microbiota. *Trends in Food Science & Technology*, *124*, 237–249. https://doi.org/10.1016/j.tifs.2022.04.010

Yoo, S., Jung, S.-C., Kwak, K., & Kim, J.-S. (2024). The role of prebiotics in modulating gut microbiota: Implications for human health. *International Journal of Molecular Sciences*, *25*(9), 4834. https://doi.org/10.3390/ijms25094834

You, Y., Kong, H., Li, C., Gu, Z., Ban, X., & Li, Z. (2024). Carbohydrate binding modules: Compact yet potent accessories in the specific substrate binding and performance evolution of carbohydrate-active enzymes. *Biotechnology Advances*, *73*, 108365. https://doi.org/10.1016/j.biotechadv.2024.108365

Y. Yip, V. L., & G. Withers, S. (2004). Nature's many mechanisms for the degradation of oligosaccharides. *Organic & Biomolecular Chemistry*, *2*(19), 2707–2713. https://doi.org/10.1039/B408880H

Zannini, E., Bravo Núñez, Á., Sahin, A. W., & Arendt, E. K. (2022). Arabinoxylans as functional food ingredients: A Review. *Foods*, *11*(7), Article 7. https://doi.org/10.3390/foods11071026

Zhang, R., Li, N., Xu, S., Han, X., Li, C., Wei, X., Liu, Y., Tu, T., Tang, X., Zhou, J., & Huang, Z. (2019). Glycoside Hydrolase family 39 β-Xylosidases exhibit β-1,2-xylosidase activity for transformation of notoginsenosides: A new EC subsubclass. *Journal of Agricultural and Food Chemistry*, *67*(11), 3220–3228. https://doi.org/10.1021/acs.jafc.9b00027

Zhang, R., Tan, S. Q., Zhang, B. L., Guo, Z. Y., Tian, L. Y., Weng, P., & Luo, Z. Y. (2021). Two key amino acids variant of α-L-arabinofuranosidase from *Bacillus subtilis* Str. 168 with altered activity for selective conversion of ginsenoside Rc to Rd. *Molecules*, *26*(6), Article 6. https://doi.org/10.3390/molecules26061733

Zhang, X. J., Wang, L., Wang, S., Chen, Z. L., & Li, Y. H. (2021). Contributions and characteristics of two bifunctional GH43 β-xylosidase /α-L-arabinofuranosidases with different structures on the xylan degradation of *Paenibacillus physcomitrellae* strain XB. *Microbiological Research*, *253*, 126886. https://doi.org/10.1016/j.micres.2021.126886

Zhang, Y., & Naebe, M. (2021). Lignin: A review on structure, properties, and applications as a light-colored UV absorber. *ACS Sustainable Chemistry & Engineering*, *9*(4), 1427–1442. https://doi.org/10.1021/acssuschemeng.0c06998

Zhou, T., Xue ,Yemin, Zhang ,Zonghui, Dong ,Yuanyuan, Gao ,Rui, & Li, Y. (2019). Improvement of the characteristics of steamed bread by supplementation of recombinant α-L-arabinofuranosidase containing xylan-binding domain. *Food Biotechnology*, *33*(1), 34–53. https://doi.org/10.1080/08905436.2018.1553048

Zietsman, A. J. J., de Klerk, D., & van Rensburg, P. (2011). Coexpression of α-L-arabinofuranosidase and β-glucosidase in *Saccharomyces cerevisiae*. *FEMS Yeast Research*, *11*(1), 88–103. https://doi.org/10.1111/j.1567-1364.2010.00694.x

Chapter 2

Cloning and expressions of an α-L-arabinofuranosidase (*Bo*GH43_35) from *Bacteroides ovatus* ATCC 8483

2.1 Introduction

Recalcitrant dietary fibers are plant-derived polysaccharides that remain mostly unaffected in the human gut by alimentary enzymes (Kritchevsky, 1988). The predominant bacterial genus colonizing the human gut are *Bacteroides, Bifidobacteria* and *Prevotella* (Fultz et al., 2021; Zeybek et al., 2020). *Bacteroides* spp. are the model group for exploring microbial colonization due to their inherent capability to digest various complex polysaccharides in the human gut (Zeybek et al., 2020). *Bacteroides* spp. harbor various genes encoding glycoside hydrolases (GH) involved in degrading the complex dietary polysaccharides, cellulose and hemicellulose (Hamaker & Tuncil, 2014). The potent species of *Bacteroides* genus are *Bacteroides ovatus, Bacteroides*

cellulosilyticus, Bacteroides vulgatus and *Bacteroides thetaiotaomicron* that degrade wide range of dietary fibers (Martens et al., 2014).

The dietary polysaccharides are predominantly found in the cell walls of plants where cellulose, non-cellulosic polysaccharides, such as hemicellulose and pectin, and phenolic polymer lignin are the principal components (Bach Knudsen, 2001). Hemicelluloses, one of the major dietary polysaccharides, are linear and branched polymers such as xylans, arabinoxylans, xyloglucans, mannan, galactan, arabinogalactan (Collins et al., 2005). Xylan, being the second most abundant component of plant cell wall polysaccharide serves as a major substrate for microbial fermentation in human gut (Dodd et al., 2011). The xylan main chain is built of β-1,4-linked D-xylopyranosyl (Xylp) residues (Shrivastava et al., 2023). Furthermore, the mono-substitution or di-substitution of D-xylopyranosyl residues at the O-2 and/or O-3 positions with α-L-arabinofuranose units makes it arabinoxylan (He et al., 2021). A variety of glycoside hydrolases play an indispensable role in the complete hydrolysis of arabinoxylan. Among them, endo-β-1,4-xylanases (EC 3.2.1.8) target the β-1,4-linkage between D-xylopyranosyl residues of xylan and produce xyloligosaccharides (degree of polymerization <2) whereas, β-xylosidases (EC 3.2.1.37) degrade these short xylooligosaccharides to release xylose residues (Biely et al., 2023). α-L-Arabinofuranosidases (EC 3.2.1.55) hydrolyze the terminal α-1,2- and/or α-1,3-, L-arabinose side-chains from arabinoxylans (Ahmed et al., 2013).

α-L-Arabinofuranosidases (AFs) are assigned to various GH families, specifically GH2, GH3, GH43, GH51, GH54 and GH62 based on amino acid sequence similarities (Shallom et al., 2002). GH43 family is known for its polyspecificity, with

more than 10 reported activities such as β-1,4-xylosidase, β-1,3-xylosidase, endo-β-1,4-xylanase, galactan-1,3-β-galactosidase, endo-α-L-arabinanase, exo-α-1,5-L-arabinanase, bifunctional α-L-arabinofuranosidase/β-D-xylosidase, bifunctional α-L-arabinofuranosidase/endo-β-xylanase activities spread across 39 subfamilies (Shrivastava et al., 2025). The family GH43 is further classified into 39 subfamilies based on the occurrence of conserved sequence as well as the structural and functional analyses (Mewis et al., 2016). A total of 271 gene sequences are reported in subfamily 35, out of which only 5 are characterized to date (http://www.cazy.org/GH43_35_all.html).

The genome analysis of *Bacteroides ovatus* ATCC 8483, revealed a putative α-L-arabinofuranosidase, belonging to family GH43 and subfamily 35 (*Bo*GH43_35). In the current study, a gene responsible for encoding a putative α-L-arabinofuranosidase *Bo*GH43_35 derived from *Bacteroides ovatus* ATCC 8483 with GenBank Accession Number ALJ47148 and locus tag Bovatus_02523 was recognized and its gene sequence was obtained from NCBI database. The gene encoding putative α-L-arabinofuranosidase, *Bo*GH43_35 was cloned in a pHTP1 vector and subsequently expressed in *E. coli* BL-21 (DE3) cells.

2.2 Materials and methods

2.2.1 Bacterial cells, vector, reagents, chemicals and kits

The genomic DNA of *Bacteroides ovatus* ATCC 8483, the pHTP1 expression vector, Supreme NZYProof DNA polymerase master mix, the oligonucleotide primers utilized for PCR amplification of gene encoding *Bo*GH43_35, NZYDNA Ladder VIII (200-5000 bp) and NZYTech Easy cloning and expression kit were obtained from NZYTech genes and enzymes (Lisbon, Portugal). *Escherichia coli* DH5α cells employed for transformation of the recombinant plasmid and *E. coli* BL21 (DE3) cells for expressing the recombinant plasmid were acquired from Novagen (Madison, WI). QIAprep spin miniprep kit for plasmid DNA isolation was purchased from QIAGEN, Valencia, USA, GenElute gel-extraction kit, ethidium bromide, low EEO agarose, bromophenol blue, xylene cyanol, ammonium persulphate, acrylamide, N,N-methylenebis(acrylamide), Bovine serum albumin and nuclease-free water (pH 8.0) were purchased from Sigma-Aldrich, USA. Isopropyl-β-D-thiogalactopyranoside (IPTG), Bradford reagent R-250, sodium chloride, calcium chloride, magnesium chloride, Luria-Bertani (LB) broth, sodium lauryl sulphate, pre-stained protein marker, Coomassie Brilliant Blue-R250, disodium ethylenediamine tetra acetate (EDTA), sodium hydroxide, Nickel sulphate, Trizma base and agar were bought from Hi-Media Laboratories Pvt. Ltd. (India). Kanamycin, methanol, glacial acetic acid, imidazole, hydrochloric acid, glycerol and dimethyl sulfoxide (DMSO) were procured from Sisco Research Laboratories Pvt. Ltd. (India). A thermal cycler for Polymerase Chain Reaction and Mini-PROTEAN Tetra Cell apparatus for conducting SDS-PAGE were obtained from Bio-Rad Laboratories, Inc., USA.

2.2.2 Sequence analysis of *Bo*GH43_35

The whole genome of *Bacteroides ovatus* ATCC 8483 was analyzed for the selection of family 43 glycoside hydrolase encoding genes. The gene sequence encoding *Bo*GH43_35 from *Bacteroides ovatus* is located in the locus tag Bovatus_02523 with Genbank accession no. ALJ47148. Both nucleotide and amino acid sequences were retrieved from NCBI. BLASTp analysis of *Bo*GH43_35 was performed against PDB database and UniProtKB/ SwissProt database to determine its coding region by comparison with its closest homologues. The boundaries of the conserved domains of *Bo*GH43_35 were predicted by feeding the amino acid sequence of *Bo*GH43_35 in the interface of NCBI-Conserved Domains Database (https://www.ncbi.nlm.nih.gov/cdd/). InterProScan web service was also accessed to obtain the conserved domains of *Bo*GH43_35 (https://www.ebi.ac.uk/interpro/search/sequence/). SignalP 6.1 server was referred to obtain the subcellular localization of *Bo*GH43_35 (https://services.healthtech.dtu.dk/services/SignalP-6.0/). Molecular mass, theoretical pI, molar extinction coefficient and amino acid composition of *Bo*GH43_35 were analysed by employing ProtParam server (https://web.expasy.org/protparam/).

2.2.3 PCR amplification of gene encoding *Bo*GH43_35

The gene (1956 bp) encoding *Bo*GH43_35 without signal peptide was amplified by Supreme NZYProof 2x master mix kit using a thermal cycler (Bio-Rad Laboratories, Inc.) by utilizing genomic DNA of *Bacteroides ovatus* ATCC 8483. The oligo-nucleotide primers for gene amplification by PCR are given in Table 2.1. The underlined sequences of the forward and reverse primers are pHTP1 vector-complementary sequence which are exploited for ligase-independent cloning. The PCR

reaction composition and the PCR cycle conditions for amplification are mentioned in Table 2.2 and 2.3, respectively.

Table 2.1 Oligonucleotide primers for PCR amplification.

Primer	Primer sequence
Forward	5'- TCAGCAAGGGCTGAGGCAGAATGCAAATCCTTATCTG-3′
Reverse	5′- TCAGCGGAAGCTGAGGCTATTTACTTCTCACTGCGAAG-3′

Table 2.2 PCR mixture components for amplification of gene encoding *Bo*GH43_35 from *Bacteroides ovatus.*

PCR components	Volume (µL)	Final concentrations
2x Supreme Proof Master mix	25	1x
Genomic DNA (25 ng/µL)	2	50 ng
Primer Fw (10 µM)	2.5	0.5 µM
Primer Rv (10 µM)	2.5	0.5 µM
DMSO (100 %)	1.5	3%
Nuclease-free water	16.5	-
Total Volume	50	-

Table 2.3 PCR conditions for amplification of gene encoding *Bo*GH43_35 from *Bacteroides ovatus.*

	Steps	Temperature (ºC)	Time
I.	Initial Denaturation	98	30 sec
II.	35 cycles		
	i) Denaturation	98	10 sec
	ii) Annealing	62	30 sec
	iii) Elongation	72	1 min 30 sec
III.	Final elongation	72	10 min
IV.	Hold	4	Infinite

2.2.4 Agarose gel electrophoresis of PCR amplified products

The PCR amplified gene encoding *Bo*GH43_35 from *Bacteroides ovatus* was loaded in 0.8 % (w/v) agarose gel, which was prepared using 1x TAE buffer. The composition of 10 x TAE buffer (Sambrook & Russell, 2001) is listed in Table 2.4. The 0.8 % (w/v) agarose gel was prepared by adding 0.4 g of agarose in 50 mL 1x TAE

buffer and dissolved by heating it in a microwave oven. After cooling down the solution to 45-50ºC, 5.0 µL of ethidium bromide solution (5 mg/mL) was added, mixed and poured in the gel casting tray. The comb of the gel casting apparatus (Genaxy Scientific Pvt. Ltd, India) was properly placed and the gel was allowed to solidify. The PCR amplified product was mixed in a ratio of 4:1 with 5x DNA loading dye and loaded into wells of agarose gel. The gel was immersed in 1x TAE buffer and run under constant voltage, 50 volts till the dye migrated 70% distance of the gel. The gel was subjected for DNA analysis under UV light in a gel documentation system (Bio-RAD XR, USA). After locating the band of PCR amplicon, it was excised from the gel with the help of a scalpel and purified for further use.

Table 2.4 10x TAE buffer composition.

Components	Quantity for 1L	Concentration
Trizma base	242 g	400 mM
Glacial acetic acid	57.1 mL	-
EDTA (pH 8.0)	7.43 g	50 mM

2.2.5 DNA loading dye buffer

The 5x DNA loading dye buffer was formulated by mixing the components outlined in Table 2.5. A 5x stock solution of DNA loading buffer was prepared and 1 volume of it mixed with 4 volumes of the amplified DNA to achieve a final dye concentration of 1x prior to loading on to the agarose gel. The final pH of the DNA loading dye was adjusted to pH 8.0.

Table 2.5 5x DNA loading dye composition.

Components	Final concentration (5x)
Tris-HCl	50 mM
Glycerol	25% (w/v)
EDTA	5.0 mM
Bromophenol blue	0.2% (w/v)
Xylene cyanol	0.2% (w/v)

2.2.6 DNA extraction from agarose gel

The PCR amplified DNA was purified from agarose gel using the GenElute Gel extraction kit (Sigma, USA), following the manufacturer's protocol. The purification process was carried out in the following steps.

1. The excised agarose gel piece was transferred to a sterile pre-weighed microcentrifuge tube.
2. To the excised gel, three volumes of gel solubilisation solution was added for every 1 volume of gel (approximately 100 mg ~ 100 µl) in the microcentrifuge tube.
3. The tube was then incubated at 50°C for 10 min to facilitate complete dissolution the agarose gel.
4. Isopropanol (100%) equal to single gel volume was added to the same tube and mixed.
5. The GenElute Binding Column G was prepared by placing it to a 2 mL collection tube which was provided with the gel extraction kit. To activate the column, 500 µL of column preparation solution was added to the column and centrifuged at 13000g for 1 min.
6. The flow through from the column was discarded and solution containing PCR amplified DNA was added to the prepared column and centrifuged at 13000g for 1 min at 25°C.
7. The column was then washed with 700 µL of Wash solution, centrifuged at 13000g for 1 min and flow through was discarded. The empty column was again centrifuged to remove remaining ethanol.

8. Now, the DNA-bound column was transferred to a new sterile 1.5 mL microcentrifuge tube and 30 µl of pre-warmed nuclease-free water from Sigma-Aldrich Co. LLC., USA was added at the centre of the column. The column was kept at room temperature for 5 min and then centrifuged at 13000g for 1 min for elution.
9. The eluted DNA was stored at -20°C for further use.

2.2.7 Ligase-Independent Cloning of gene encoding *Bo*GH43_35 in pHTP1 vector

pHTP1 vector was used for Ligase-Independent Cloning. pHTP1 is a ready-to-use linearized vector containing bacteriophage T7 promoter that is specifically recognized by T7 RNA polymerase (Fig. 2.1). pHTP1 vector contains two poly-histidine (6xHis) tags (N- and C-terminal) which allow subsequent recombinant protein purification by immobilized metal-ion affinity chromatography (IMAC). The quantity of the purified PCR product was determined by using Nano drop (Implen, Germany). The quantity of purified PCR product required for cloning into linearized pHTP1 vector was determined by the following formula:

$$\text{ng of insert} = \frac{[\text{ng of vector}] \times [\text{kb size of insert}]}{[\text{kb size of vector}]} \times \text{molar ratio of } \frac{[\text{insert}]}{[\text{vector}]}$$

$$\frac{100\ (\text{ng}) \times 1.9(\text{ng})}{5.332\ (\text{kb})} \times \frac{10}{1} = 356\ \text{ng}\ (Bo\text{GH43\_35})$$

Upon combining the PCR product with linearized pHTP1 vector, in the presence of NZYEasy enzyme mix, the two DNA molecules anneal through base-pair complementation of the single strand regions. The reaction occurs in a single tube across three temperature-dependent steps. Circular recombinant vector containing the fragment of interest is obtained by transforming the annealed plasmid DNA into competent *E. coli* cells.

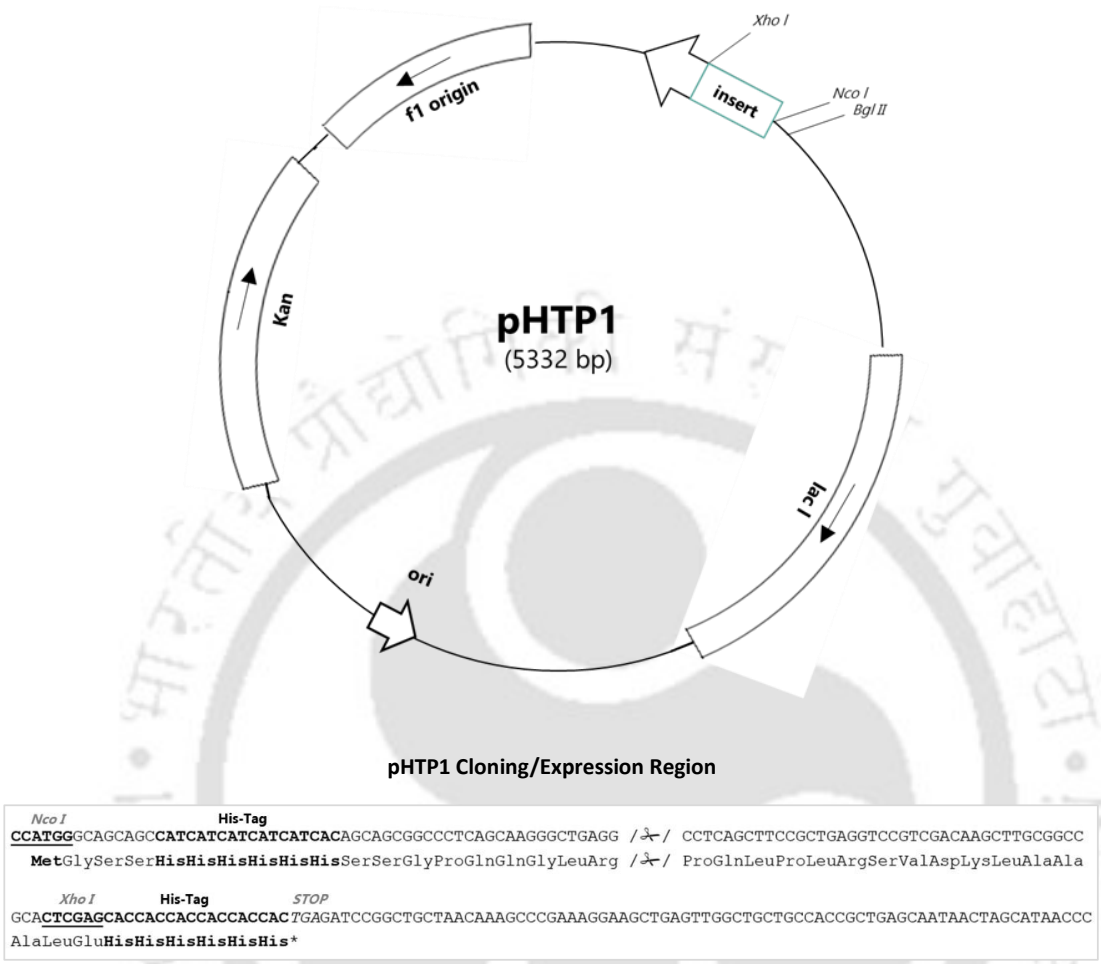

✂ Represents the site where the gene will be inserted.

Fig. 2.1 Restriction map of the pHTP1 expression vector showing cloning site between the restriction enzyme site of *NcoI* and *XhoI*. pHTP1 cloning and expression region showing restriction enzyme site of *NcoI*, N-terminal His_6-Tag coding sequence followed by site of gene insertion, restriction enzyme site of *XhoI*, C-terminal His_6-Tag coding sequence and stop codon.

The steps followed for cloning are as follows:

1. The reaction mixture was prepared by combining the components mentioned in Table 2.6 in a sterile, nuclease-free PCR tube on ice.
2. The PCR tube containing all the components was subjected to a short spin in a centrifuge to collect all the contents at the bottom of the tube.
3. The cloning reaction was performed in a thermal cycler by following the reaction conditions mentioned in Table 2.7.
4. The cloned product obtained was used for transformation.

Table 2.6 Components of reaction for cloning in a thermocycler.

Components	Final volume (µL)
10x Reaction buffer	2
Insert (34 ng/ µL)	10
pHTP1 vector (100 ng)	1
NZYEasy enzyme mix	1
Nuclease free water	6
Total volume	20

Table 2.7 Reaction conditions for cloning in a thermocycler.

Temperature (°C)	Time (min)
37	60
80	10
30	10
4	Infinite

2.2.8 Preparation of culture medium

E. coli DH5α and BL-21 (DE3) cells containing recombinant plasmid were grown in the most commonly used culture medium, Luria Bertani (LB) medium. To prepare the LB medium, the components listed in Table 2.8 (Sambrook et al., 1989) were dissolved in 120 ml of deionized water. After adjusting the pH to 7.2, the final volume was made up to 200 mL. The medium was dispensed into a 500 mL conical flask and autoclaved at 121°C at 15 psi for 20 min. The filter sterilized antibiotic (Kanamycin; 50 µg/ml) was added to autoclaved and cooled LB medium prior to the culture inoculation.

Table 2.8 Composition of Luria-Bertani medium (Sambrook *et al.*, 1989)

Component	Final concentration (%, w/v)
Tryptone	1.0
Yeast extract powder	0.5
Sodium chloride	1.0

LB agar medium was prepared by adding 2% (w/v) Agar Agar type I in LB broth. The resulting mixture was then autoclaved as outlined earlier, then cooled to around 50-55°C. The prepared medium was supplemented with the antibiotic (Kanamycin; 50 µg/ml) under the laminar air flow and were poured (approximately 25 mL) in the sterile petri plates and allowed to solidify for 30-40 min.

2.2.9 *E. coli* DH5α competent cells preparation by CaCl2 method

Day 1

1. *E. coli* DH5α cells (100 µL) from glycerol stock were inoculated in a test tube containing 10.0 ml LB medium (Sambrook et al., 1989). The culture was grown at 37ºC and 180 rpm for 12-14 h.
2. The solutions that are used in competent cells preparation, *viz*., 0.1 M $CaCl_2$, 0.1 M $MgCl_2$, and 0.1 M CaCl2 containing 15% glycerol (v/v) were filtered by passing through Whatman No.1 filter paper, autoclaved and kept in refrigerator. 1.5 ml micro-centrifuge tubes, 50 ml centrifuge tubes (round bottom) and micro tips were autoclaved and kept in laminar hood.

Day 2

3. Next day, 2.0 mL culture from primary culture was inoculated in 200 mL LB medium and incubated at 37°C in a shaking incubator at 180 rpm till its OD600 reached 0.4-0.6.
4. The culture was chilled on ice for 30 min and then 40 ml culture was transferred aseptically to 50 mL round bottom centrifuge tubes and harvested by centrifugation at 2,710g at 4ºC for 10 min.
5. The supernatant was discarded and the step was repeated for entire 200 mL culture.
6. The cell pellet was gently resuspended in 5 mL of chilled 0.1 M $CaCl_2$ solution followed by 5 mL 0.1 M $MgCl_2$. The cell suspension was kept on ice for 10 min.
7. The tube containing cell suspension was subjected to centrifugation at 2,710g at 4ºC for 10 min.
8. The supernatant was gently removed and the cell pellet was resuspended in 3.0 ml of ice-cold 0.1 M $CaCl_2$ solution.

9. The cell suspension was kept on ice for 10 min and centrifuged at 2,710g at 4ºC for 10 min.
10. The supernatant was carefully discarded and the cell pellet was resuspended in 0.1 M $CaCl_2$ solution containing 15% (v/v) glycerol. Aliquots of 100 µL of competent cells were done in 1.5 ml microcentrifuge tubes and kept at -80ºC for further use. Similarly, competent cells of *E. coli* BL-21 (DE3) bacterial strain were made.

2.2.10 Transformation of the recombinant DNA into *E. coli* DH5α cells

The reaction mixture obtained in Section 2.2.7 was transformed into the *E. coli* DH5α competent cells, which were prepared as described in Section 2.2.8. The transformation was carried out using the heat shock method.

1. The micro-centrifuge tube containing 100 µl *E. coli* DH5α competent cells was taken out from -80°C and placed on ice for 10 min for thawing.
2. After thawing 10 µl of the reaction mixture was added to 100 µl *E. coli* DH5α competent cells under sterile conditions in the laminar air flow.
3. The tube was gently tapped 2-3 times and was incubated for 30 min on ice.
4. Heat shock at 42°C for 42 sec was given to the cells followed by immediate incubation on ice for 5 min.
5. The transformed cells were added with 1.0 mL of autoclaved LB medium and incubated at 37°C with shaking for 60 min at 180 rpm.
6. The cells were then centrifuged at 3,000g for 5 min at 25°C.
7. 900 µL of supernatant was carefully removed and the cell pellet was re-suspended in remaining 100 µL supernatant.
8. The resuspended cells were then spread onto LB agar plates supplemented with the kanamycin at 50 µg/mL and incubated at 37°C for 16h under static condition.
9. The transformation efficiency was calculated using the following equation,

$$Transformation\ efficiency = \frac{No.of\ colonies\ on\ LB\ agar\ plate \times Dilution\ factor}{\mu g\ of\ insert\ DNA} = cfu/\ \mu g$$

2.2.11 Screening of positive recombinant clones by colony PCR

The screening of positive recombinant clones was achieved through colony PCR. The colonies with different phenotypes were selected for colony PCR. The details of reaction mixture to carry out colony PCR is mentioned in Table 2.9. 20 µL of the total reaction mixture was aliquoted in 16 PCR tubes. Each colony selected was divided in two parts, one was resuspended in the PCR tube containing 20 µL reaction mixture, whereas other half was used for streaking on a LB agar master plate supplemented with kanamycin (50 µg/mL), incubated at 37°C for 12h under static condition and then stored at 4°C for further use. The reaction conditions followed for colony PCR are mentioned in Table 2.10. The colony PCR products obtained were run on 0.8% (w/v) agarose gel and were visualized under UV transilluminator. The positive clones for the respective recombinant derivatives (insert and vector) were identified based on their size. The respective colonies of the positive clones were identified from the LB agar master plate. The colony was picked and inoculated in 10 mL LB medium supplemented with kanamycin (50 µg/mL), incubated at 37°C with shaking for 12 h at 180 rpm. Glycerol stock of 1 mL *E. coli* DH5α containing the recombinant plasmids was prepared by keeping the final concentration of autoclaved glycerol to 20-25%. Rest of the culture was used for plasmid DNA isolation. The isolated DNA was sent for Sanger's sequencing for clone confirmation.

Table 2.9 Colony PCR mixture components for screening of recombinant clones.

PCR components	Volume (µL) (x16)	Final concentrations
2x Supreme Proof Master mix	10 (160 µL)	1x
Primer Fw (10 µM)	0.9 (14.4 µL)	0.45 µM
Primer Rv (10 µM)	0.9 (14.4 µL)	0.45 µM
Nuclease-free water	8.2 (131.2 µL)	-
Total Volume	20 (320 µL)	-

Table 2.10 PCR cycles for screening of recombinant clones.

	Steps	Temperature (ºC)	Time
V.	Initial Denaturation	95	15 min
VI.	30 cycles		
	iv) Denaturation	95	15 sec
	v) Annealing	50	15 sec
	vi) Elongation	72	1 min
VII.	Final elongation	72	10 min
VIII.	Hold	20	Infinite

2.2.12 Plasmid isolation protocol (QIAGEN, Valencia, USA)

The plasmid DNA from 9 mL of an overnight grown culture was isolated using a miniprep kit from QIAGEN (Valencia, USA) by following the protocol mentioned below.

1. 9 mL of an overnight grown *E. coli* culture was pelleted by centrifugation at 6000g for 1 min at 4°C in 1.5 mL microcentrifuge tube.
2. The bacterial cell pellet was resuspended in 0.3 mL resuspension buffer P1.
3. 0.3 mL of lysis buffer P2 was added to the same resuspension and mixed thoroughly by inverting 4-6 times. It was incubated at room temperature (15-25°C) for 5 min.
4. 0.3 mL of prechilled neutralization buffer P3 was added and mixed by inverting 4-6times. The tube was incubated on ice for 5 min.
5. After incubation, it was centrifuged at 13,000g for 10 min at 4°C.
6. A QIAGEN-tip 20 column, provided with kit, was added with 1 mL buffer QBT and centrifuged at 13,000g for 1 min. Flow-through was discarded.

7. The supernatant (0.5 mL) obtained in step 5 was applied to the QIAGEN-tip 20 column prepared in step 6 and centrifuged at 13,000g for 1 min. Flow-through was discarded. This step was repeated until all the supernatant was centrifuged.
8. The column was washed with 0.5 mL washing buffer QC (ethanol added). It was centrifuged at 13,000g for 1 min. Flow-through was discarded.
9. The DNA was eluted by adding 50 µL pre-warmed nuclease-free water. It was collected in a fresh 1.5 mL microcentrifuge tube.
10. The eluted DNA was stored at -20°C for further use.

2.2.13 Transformation of *E. coli* BL21 (DE3) cells by recombinant plasmid DNA into and expression of *Bo*GH43_35

1 µL of the recombinant plasmid with gene encoding (*Bo*GH43_35) isolated in Section 2.2.12 was transformed in 100 µl *E. coli* BL21(DE3) competent cells by heat shock method according to the protocol outlined in section 2.2.10. The cells were spread on LB agar plate supplemented with kanamycin (50 µg/ml) and incubated at 37°C for 12 h. The colonies were randomly picked from LB agar plate and inoculated in 10 mL of LB medium supplemented with kanamycin (50 µg/ml) and incubated at 37°C, 180 rpm for 12 h. Once the cell culture reached mid exponential phase (A_{600} = 0.4), the culture were cooled to 24°C and induced by adding isopropyl-β-D-thiogalactopyranoside (IPTG) at a final concentration varying from 0.25 to 1.0 mM. After IPTG induction, the cells were further incubated at 24°C for 18 h at 180 rpm. From each tube 200 µL of culture medium was collected and centrifuged at 13,000g for 5 min. The supernatant was discarded and the cells were resuspended in 200 µL water by vortexing. The tubes were again centrifuged at 13,000g for 5 min. The supernatant was discarded and the cells were resuspended in 40 µL water. The expression of recombinant protein was confirmed by comparing the uninduced and induced cell samples on polyacrylamide gel electrophoresis (SDS-PAGE).

2.2.14 Analysis of recombinant *Bo*GH43_35 protein expression by Sodium dodecyl sulphate-Polyacrylamide gel electrophoresis (SDS-PAGE)

2.2.14.1 Preparation of SDS-PAGE gel

The recombinant protein expression was analyzed by SDS-PAGE on 12% (w/v) gel (Laemmli, 1970; Sambrook et al., 1989). The over-expression of *Bo*GH43_35 was confirmed by comparing the induced and uninduced *E. coli* BL21 (DE3) cells on the gel. The resolving and stacking gels were prepared by following the protocols from Sambrook *et al* (1989). The resolving gel (12%, w/v) was prepared by adding all the ingredients mentioned in Table. 2.2.11. The stacking gel (4%, w/v) was prepared by mixing all the components listed in Table 2.11.

The acrylamide solution, 30% (w/v) used in preparing the resolving and stacking gels was prepared by weighing 0.8g of N,N-methylene-bis(acrylamide) and dissolving it completely in 50 mL deionized water. Acrylamide (29.2g) was weighed and added to it and dissolved completely till the solution became clear. The final volume was made up to 100 mL, filtered using Whatman No. 1 filter paper and stored in an ambered bottle at 4°C as acrylamide is photo-sensitive.

Table 2.11 Components of resolving and stacking gel for 12% (w/v) SDS-PAGE.

Components	Volume (mL) for resolving gel	Volume (mL) for stacking gel
Acrylamide solution (30%, w/v)	4.0	0.7
Deionized water	0.6	2.8
SDS (10%, w/v)	1.0	0.5
Glycerol (50%, v/v)	1.0	-
1.5 M Tris-HCl (pH 8.8)	3.3	-
1.5 M Tris-HCl (pH 6.8)	-	1.0
Ammonium persulfate (10%, w/v)	0.1	0.05
N,N,N',N'-tetramethylethylenediamine (TEMED)	0.01	0.005
Total	**10.0**	**5.0**

2.2.14.2 Preparation of SDS-PAGE sample loading buffer and running buffer

The stock solution of 5x sample loading buffer was prepared by dissolving the components as described in Table 2.12 (Laemmli, 1970). The final pH of the buffer was adjusted to 6.8. the final concentration of the loading buffer was kept 1x by mixing 4 volumes of the protein sample and 1 volume of the buffer before loading on to SDS-PAGE gel.

The stock solution of 10x running buffer was prepared as described in Table 2.13. The final pH of the buffer was adjusted to 8.3. After preparing, the buffer was filtered through Whatman, Filter No. 1 and stored at 4°C. While running the SDS-PAGE gels, 1x of the running buffer was prepared by diluting the 10x stock.

Table 2.12 Composition of 5x sample loading buffer.

Components	Final concentration (5x)
Tris-base	62.5 mM
Glycerol	20.0% (v/v)
SDS	2.0% (w/v)
Bromophenol blue	0.025% (w/v)
B-mercaptoethanol	5.0% (w/v)

Table 2.13 Composition of 10x Tris-Glycine or running buffer.

Components	Final concentration (10x)
Tris-base	0.25 M
Glycine	2.5 M
SDS	1.0% (w/v)

2.2.14.3 Preparation of staining and de-staining solutions

The staining solution for SDS-PAGE gel was prepared by dissolving 0.25g Coomassie Brilliant Blue (CBB) R-250 dye (0.25%, w/v) in 100 mL solution of deionized water, methanol and glacial acetic acid in a ratio of 5:4:1. The staining solution was stirred continuously on a magnetic stirrer, overnight to ensure complete dissolution and proper mixing of the components. Then the solution was filtered through Whatman, Filter No. 1 to remove any undissolved particles or impurities. The SDS-PAGE gels were de-stained by immersing the gel in de-staining solution which consisted of deionized water, methanol and glacial acetic acid in 5:4:1. The gel was left in the de-staining solution, allowing the excess dye to be gradually removed, and the bands to become more distinct and visible. This process was carried out until the background was sufficiently cleared, revealing the protein bands on the gel.

2.3 Results and Discussion

2.3.1 Sequence analysis of *Bo*GH43_35

The nucleotide (1965 bp) and protein (675 amino acid residues) sequences of *Bo*GH43_35, a putative α-L-arabinofuranosidase from Bacteroides ovatus ATCC 8483 with Genbank Accession no. ALJ47148 was obtained from NCBI database. SignalP 6.0 identified a signal peptide of 24 amino acids at the N-terminal region (residues 1-24) of the *Bo*GH43_35 sequence (Fig. 1a). The signal peptide analysis gave an insight about the cleavage site between Ala24 and Glu25. Conserved domain analysis using NCBI-Conserved Domain Database search revealed *Bo*GH43_35 as a modular enzyme with the presence of an N-terminal GH43_XylA-like catalytic module, belonging to family 43 glycoside hydrolase (residues 38-368), followed by carbohydrate binding module 6, referred here as CBM6A (residues 450-578) and an extended C-terminal module, CBM6-like module, referred here as CBM6B (residues 589-675) as shown in Fig. 2.2.

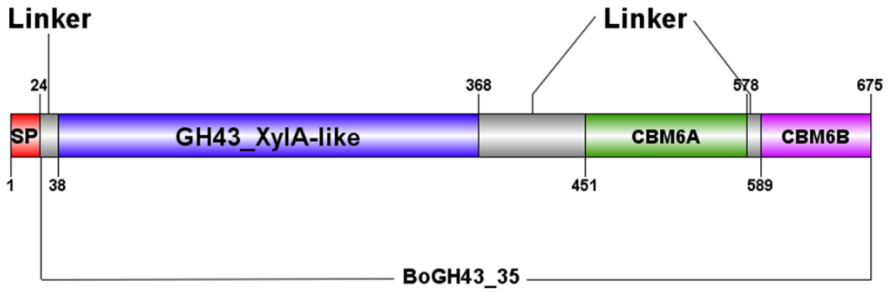

Fig. 2.2 Molecular architecture of a full length *Bo*GH43_35 consisting of 675 amino acids. It shows a signal peptide (SP) at N-terminal followed by a GH43 catalytic domain ranging from amino acid 38-368, a Carbohydrate binding module 6 (CBM6A) from amino acid 450-578 and a C-terminal CBM6B ranging from amino acid 589 to 675.

2.3.2 PCR amplification of *Bo*GH43_35

The PCR amplified gene encoding *Bo*GH43_35, 1956 bp was obtained from the genomic DNA of *Bacteroides ovatus* ATCC 8483 using the protocol outlined in section 2.2.3. The PCR product was then analyzed by running it on 0.8% (w/v) agarose gel as shown in Fig. 2.3. The resulting amplicon exhibited a clear band corresponding to a size of approximately 1.9 kb. The amplified product was excised from gel and purified by following the steps mentioned in section 2.2.6. and stored in -20°C for further use.

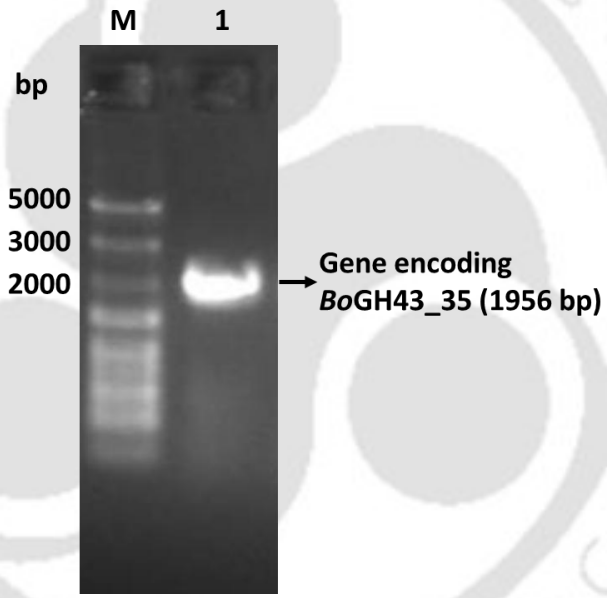

Fig. 2.3 Agarose gel (0.8%, w/v) showing Lane M- DNA Marker (NZYDNA Ladder VIII, 200-5000 bp) and Lane 1- PCR amplified gene encoding *Bo*GH43_35 of 1.9 kb.

2.3.3 Ligase-Independent Cloning of gene encoding *Bo*GH43_35 in pHTP1 vector

The purified PCR amplified gene encoding *Bo*GH43_35 was subjected to ligase independent cloning using pHTP1 vector. The ligated *Bo*GH43_35-pHTP1 was obtained by following the protocol described in section 2.2.7. The ligated *Bo*GH43_35-pHTP1 plasmid was introduced into *E. coli* DH5α competent cells through transformation and grown on LB agar plated at 37°C under static conditions for 16 h.

The transformation efficiency of the *E. coli* DH5α competent cells was determined to be 8.5×10^6 cfu/µg.

2.3.4 Screening of positive clones by colony PCR

The *E. coli* DH5α colonies transformed with the gene encoding *Bo*GH43_35 into pHTP1 were subjected to colony PCR. The amplicons obtained by colony PCR were run on 0.8% (w/v) agarose gel as mentioned in section 2.2.11. and visualized under UV transilluminator (Fig. 2.4). Positive clones showed the band of 1956 bp and were also validated by Sanger's sequencing with no mutation.

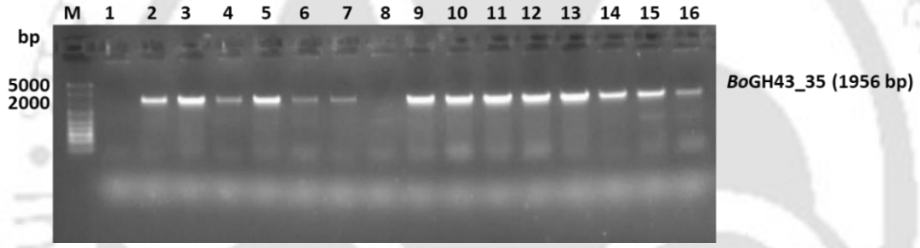

Fig. 2.4 Agarose gel (0.8%, w/v) showing Lane M- DNA Marker (NZYDNA Ladder VIII, 200-5000 bp) and Lane 1-16 Clone confirmation by colony PCR of 16 colonies.

2.3.5 Expression of recombinant protein BoGH43_35 and IPTG concentration optimization

The sequencing results confirmed that the gene encoding *Bo*GH43_35 protein is composed of 670 amino acids. This includes a 19 amino acid sequence (MGSSHHHHHHSSGPQQGLR) from pHTP1 vector at the N-terminal including His_6-tag. This is followed by GH43_XylA-like catalytic module (residue 38-363) and two CBM modules, CBM6A (residue 445-573) followed by CBM6B (residue 584 to 670) at the C-terminal (as illustrated in Fig. 2.5).

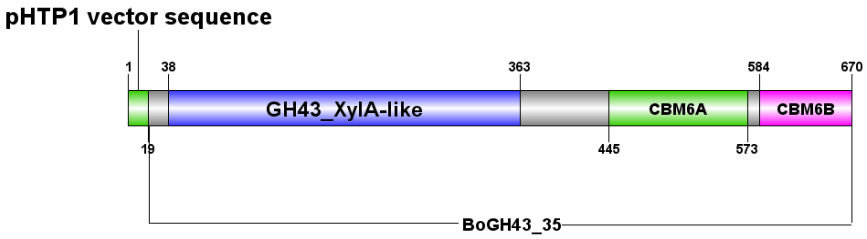

Fig. 2.5 Molecular architecture of cloned *Bo*GH43_35 consisting of 670 amino acids. It shows pHTP1 vector sequence at N-terminal followed by a GH43 catalytic domain, a Carbohydrate binding module 6 (CBM6A) and a C-terminal CBM6B ranging from amino acid 584 to 670.

The transformed *E. coli* BL21 (DE3) competent cells (transformation efficiency of 5.5×10^6 cfu/µg) harbouring the recombinant *Bo*GH43_35-pHTP1 plasmid was checked for protein expression with varying concentrations of IPTG (0.25-1.0 mM) as mentioned in section 2.2.13. *Bo*GH43_35 was expressed in the induced cells with a molecular mass of approximately, 74 kDa which was in agreement with its theoretical molecular mass of 74.1 kDa, obtained from Expasy server. The minimum final concentration of IPTG required for protein expression of *Bo*GH43_35 was 0.25 mM (Fig. 2.6).

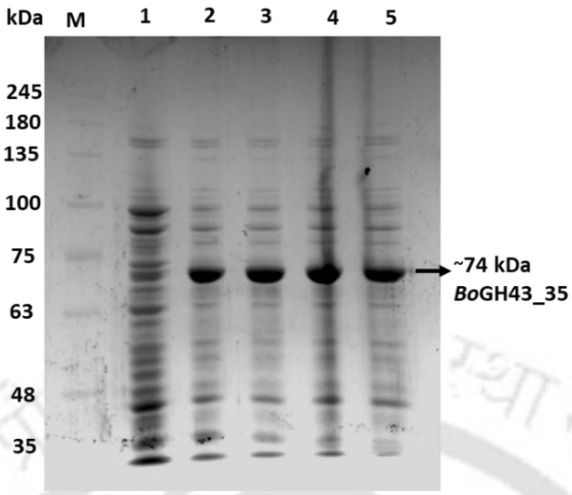

Fig. 2.6 SDS-PAGE (12% w/v gel) showing expression of *Bo*GH43_35 and IPTG concentration optimization. Lane M- Pre-stained Protein marker (Himedia, India), 1- Uninduced *E. coli* BL21 (DE3) cells, 2- Induced *E. coli* BL21 (DE3) cells (0.25 mM), lane 3- Induced *E. coli* BL21 (DE3) cells (0.5 mM), 4- Induced *E. coli* BL21 (DE3) cells (0.75 mM) and 5- Induced *E. coli* BL21 (DE3) cells (1 mM IPTG)

2.4 Conclusion

Whole genome analysis of *Bacteroides ovatus* ATCC 8483 revealed the presence of a gene encoding putative α-L-arabinofuranosidase, *Bo*GH43_35 located with locus tag Bovatus_02523 and Genbank Accession no. ALJ47148. The sequence analysis of *Bo*GH43_35 revealed a signal peptide (24 amino acid residues) at N-terminal followed by a GH43_XylA-like catalytic module, a carbohydrate binding module belonging to family 6 (CBM6A) and an extended C-terminal module, CBM6-like module, CBM6B. The 1956 bp gene encoding *Bo*GH43_35 was amplified by PCR. Ligation independent cloning was performed to clone PCR amplified product in pHTP1 vector and transformed into *E. coli* DH5α competent cells. The positive clone containing recombinant plasmid DNA were screened by colony PCR and sequencing. The positive clone showed DNA band of ~1.9 kb on 0.8% (w/v) agarose gel. The recombinant plasmid DNA containing gene encoding *Bo*GH43_35 was transformed into *E. coli* BL-21 (DE3) cells for expression of protein. The recombinant *Bo*GH43_35 was expressed as soluble homogenous protein and the minimum concentration of IPTG required for the induction of protein expression was 0.25 mM. The expression of recombinant protein was checked by SDS-PAGE analysis.

2.5 References

Ahmed, S., Luis, A. S., Bras, J. L. A., Ghosh, A., Gautam, S., Gupta, M. N., Fontes, C. M. G. A., & Goyal, A. (2013). A novel α-L-arabinofuranosidase of family 43 glycoside hydrolase (*Ct*43Araf) from *Clostridium thermocellum*. *PLoS ONE*, *8*(9), e73575. https://doi.org/10.1371/journal.pone.0073575

Bach Knudsen, K. E. (2001). The nutritional significance of "dietary fibre" analysis. *Animal Feed Science and Technology*, *90*(1–2), 3–20. https://doi.org/10.1016/S0377-8401(01)00193-6

Biely, P., Šuchová, K., & Puchart, V. (2023). Diversity of microbial endo-β-1,4-xylanases. In *Glycoside Hydrolases* (pp. 135–163). Elsevier. https://doi.org/10.1016/B978-0-323-91805-3.00009-5

Collins, T., Gerday, C., & Feller, G. (2005). Xylanases, xylanase families and extremophilic xylanases. *FEMS Microbiology Reviews*, *29*(1), 3–23. https://doi.org/10.1016/j.femsre.2004.06.005

Dodd, D., Mackie, R. I., & Cann, I. K. O. (2011). Xylan degradation, a metabolic property shared by rumen and human colonic *Bacteroidetes*. *Molecular Microbiology*, *79*(2), 292–304. https://doi.org/10.1111/j.1365-2958.2010.07473.x

Fultz, R., Ticer, T., Ihekweazu, F. D., Horvath, T. D., Haidacher, S. J., Hoch, K. M., Bajaj, M., Spinler, J. K., Haag, A. M., Buffington, S. A., & Engevik, M. A. (2021). Unraveling the metabolic requirements of the gut commensal *Bacteroides ovatus*. *Frontiers in Microbiology*, *12*, 745469. https://doi.org/10.3389/fmicb.2021.745469

Hamaker, B. R., & Tuncil, Y. E. (2014). A perspective on the complexity of dietary fiber structures and their potential effect on the gut microbiota. *Journal of Molecular Biology*, *426*(23), 3838–3850. https://doi.org/10.1016/j.jmb.2014.07.028

He, H.-J., Qiao, J., Liu, Y., Guo, Q., Ou, X., & Wang, X. (2021). Isolation, structural, functional, and bioactive properties of cereal arabinoxylan─A critical review. *Journal of Agricultural and Food Chemistry*, *69*(51), 15437–15457. https://doi.org/10.1021/acs.jafc.1c04506

Kritchevsky, D. (1988). Dietary Fiber. *Annual Review of Nutrition*, *8*(1), 301–328. https://doi.org/10.1146/annurev.nu.08.070188.001505

Laemmli, U. K. (1970). Cleavage of structural proteins during the assembly of the head of bacteriophage T4. *Nature*, *227*(5259), 680–685. https://doi.org/10.1038/227680a0

Martens, E. C., Kelly, A. G., Tauzin, A. S., & Brumer, H. (2014). The devil lies in the details: How variations in polysaccharide fine-structure impact the physiology and evolution of gut microbes. *Journal of Molecular Biology*, *426*(23), 3851–3865. https://doi.org/10.1016/j.jmb.2014.06.022

Mewis, K., Lenfant, N., Lombard, V., & Henrissat, B. (2016). Dividing the large glycoside hydrolase family 43 into subfamilies: A motivation for detailed enzyme characterization. *Applied and Environmental Microbiology*, *82*(6), 1686–1692. https://doi.org/10.1128/AEM.03453-15

Sambrook, J., Fritsch, E. F., Maniatis, T., Russell, D. W., & Green, M. R. (1989). *Molecular cloning: A laboratory manual*. Cold Spring Harbor Laboratory Press.

Sambrook, J., & Russell, D. W. (2001). *Molecular cloning: A laboratory manual* (3rd ed). Cold Spring Harbor Laboratory Press.

Shallom, D., Belakhov, V., Solomon, D., Gilead-Gropper, S., Baasov, T., Shoham, G., & Shoham, Y. (2002). The identification of the acid–base catalyst of α-arabinofuranosidase from *Geobacillus stearothermophilus* T-6, a family 51 glycoside hydrolase. *FEBS Letters*, *514*(2–3), 163–167. https://doi.org/10.1016/S0014-5793(02)02343-8

Shrivastava, M., Maibam, P. D., Aishwarya, A., & Goyal, A. (2023). Hemicellulases and auxiliary activities for biomass hydrolysis. In V. Bisaria (Ed.), *Handbook of Biorefinery Research and Technology* (pp. 1–23). Springer Netherlands. https://doi.org/10.1007/978-94-007-6724-9_36-1

Zeybek, N., Rastall, R. A., & Buyukkileci, A. O. (2020). Utilization of xylan-type polysaccharides in co-culture fermentations of *Bifidobacterium* and *Bacteroides* species. *Carbohydrate Polymers*, *236*, 116076. https://doi.org/10.1016/j.carbpol.2020.116076

Chapter 3

Purification, biochemical characterization and mode of action analysis of the recombinant *Bo*GH43_35 from *Bacteroides ovatus* ATCC 8483

3.1 Introduction

The enhancement in the life style diseases there has been increasing interest and preference for natural and functional foods and medicines. These can be plant-derived recalcitrant dietary fibres that have gained popularity owing to their functional benefits, including antioxidative, antidiabetic and antitumor activities (Wang et al., 2022). The microbiota inhabiting the large intestine ferment dietary polysaccharides and convert them to short-chain fatty acids (SCFAs), in particular acetate and butyrate (Koh et al., 2016). SCFAs are key mediators in host-microbe mutualism (Nastasi et al., 2015) and play a pivotal role in maintaining low luminal pH which thereby inhibits the growth of pathogenic microorganisms in the gut (Ríos-Covián et al., 2016).

Bacteroides ovatus possesses an array of glycoside hydrolases that enables the breakdown of diverse dietary polysaccharides, into simple sugars (Collins et al., 2005). This enzymatic activity is essential for the efficient utilization of these fibers thereby

enhancing the growth of other beneficial gut microbes, contributing to overall gut health. This creates a balanced and diverse microbial community, which is associated with numerous health benefits, including improved digestion and immune function along with the reduced inflammation (Fultz et al., 2021).

In cereal grains, arabinoxylans constitute their major cell wall components and become an important part of dietary fiber for humans (Broekaert et al., 2011). The backbone structure of arabinoxylans is primarily composed of β-(1,4)-linked xylose residues. These xylose residues are further decorated with arabinose residues attached on the C(O)-2 and/or C(O)-3 position (Mendis & Simsek, 2014). Additionally, phenolic acids such as ferulic acid can form ester linkages at the C(O)-5 position of arabinose residues. The intricate architecture of dietary arabinoxylans necessitates the use of a combination of depolymerizing enzymes and ancillary enzymes for effective degradation. Consequently, multifunctional xylanolytic enzymes are of significant importance, as they efficiently breakdown the gut dietary arabinoxylans intake (Fan et al., 2009). The glycoside hydrolase family 43 (GH43) is known to accommodate such multifunctional xylanolytic enzymes.

A recombinant xylanolytic enzyme, *Pc*Axy43A from *Paenibacillus curdlanolyticus* B-6 showed multi-functionality possessing endo-xylanase, β-xylosidase, and α-L-arabinofuranosidase activities (Teeravivattanakit et al., 2016). It removed doubly substituted arabinosyl residues from the O2 and O3 positions of xylose residues. Another group also explored *Paenibacillus curdlanolyticus* B-6 and revealed a recombinant *Pc*Axy43B also being trifunctional (endoxylanase/β-xylosidase/α-L-arabinofuranosidase) showing specific activity of 3.0 U.mg-1, 1.6 U.mg-1 and 1.0 U.mg-1 against birchwood xylan, oat spelt xylan and rye arabinoxylan, respectively

(Limsakul et al., 2021). The key insights from this study included the liberation of arabinose and xylooligosaccharides in the *Pc*Axy43B hydrolysed rye arabinoxylan as analysed by thin layer chromatography. The full length *Pc*Axy43B contained GH43 catalytic module along with two carbohydrate binding modules (CBM) belonging to families 6 (CBM6) followed by CBM36. The authors reported that CBM36 play an important role in enzymatic hydrolysis of xylan substrates, as the truncated derivative of *Pc*Axy43B that contains only GH43 catalytic module and CBM6 showed far reduced specific activity against birchwood xylan (0.02 U.mg-1), oat spelt xylan (0.17 U.mg-1) and rye arabinoxylan (0.21 U.mg-1) as a result of a lack of endoxylanase activity. In addition, two bifunctional β-xylosidase/α-L-arabinofuranosidase (*Pp*xyl43A and *Pp*xyl43B) enzymes from *Paenibacillus physcomitrellae* were characterized (Zhang et al., 2021). The authors reported that both *Pp*xyl43A and *Pp*xyl43B showed activity against the synthetic substrates p-NP-β-D-xylopyranoside (p-NPX) and p-NP-α-L-arabinofuranoside (p-NPAf). However, there is no mention of activities of *Pp*xyl43A and *Pp*xyl43B against natural substrate, arabinoxylan. The bifunctional xylanolytic enzymes are not limited to bacterial sources but fungi have also been excellent producers. An enzyme, Xyl43A from a thermophilic fungus *Humicola insolens* Y1 showed bifunctional behaviour displaying β-xylosidase/α-arabinosidase activities having stability in broad pH range, 5.0-10.0 was reported (Yang et al., 2015). They reported that Xyl43A shows maximum specific activity of 20.5 U.mg-1 and 4.7 U.mg-1 against p-NPX and p-NPAf, respectively.

The exploration of new novel multifunctional enzymes hydrolysing complex dietary fibers is of paramount importance. These enzymes play a crucial role in breaking down dietary polysaccharides which are otherwise resistant to human

digestion. These multifunctional enzymes convert the complex polysaccharides into simple fermentable sugars, that can be utilised by gut bacteria (Leschonski et al., 2024). Therefore, the detailed study and characterization of novel multifunctional enzymes involved in efficient dietary fiber degradation not only advance our understanding of their biochemical properties but also pave the way for the development of more effective prebiotics that can enhance human health through targeted modulation of the gut microbiota (Yoo et al., 2024).

In the current study, a gene responsible for encoding a putative α-L-arabinofuranosidase, *Bo*GH43_35 derived from *Bacteroides ovatus* ATCC 8483 (GenBank Accession Number ALJ47148) was purified and biochemically characterized. It is hypothesized that an extensive biochemical and kinetic properties of *Bo*GH43_35 are crucial in understanding the mechanism followed by *Bacteroides ovatus* in hydrolysing complex xylan substrates present in dietary fibres. A detailed investigation on the mode of action of *Bo*GH43_35 exposed its initial α-L-arabinofuranosidase activity followed by endo-β-1,4-xylanase activity. The bifunctionality of *Bo*GH43_35 underscores its significant potential in the complete and efficient degradation of dietary polysaccharides by involving single enzyme exhibiting dual activities. Furthermore, the regioselectivity analysis of *Bo*GH43_35 using proton-nuclear magnetic resonance (^{1}H NMR) unravelled its type I arabinofuranosidase activity. Though, the bacterium *Bacteroides ovatus* has been extensively explored earlier, however, an α-L-arabinofuranosidase with endo-β-1,4-xylanase has never been reported.

3.2 Materials and methods

3.2.1 Chemicals and substrates

L-arabinose, xylan from oat spelt, sodium dihydrogen phosphate dibasic, sodium phosphate monobasic anhydrous, nickel sulphate, sodium carbonate, sodium hydroxide, copper sulphate pentahydrate, sodium potassium tartarate, sodium bicarbonate, sodium sulphateand salts of metal ions viz. $CaCl_2$, $MgCl_2$, $CuCl_2$, $CoCl_2$, $FeCl_3$, $MgSO_4$, $MnSO_4$, $ZnSO_4$, $NiSO_4$, $CuSO_4$, NaCl and KCl were obtained from HiMedia Laboratories Pvt. Ltd., India. Wheat arabinoxylan (low viscosity), rye arabinoxylan (high viscosity), larchwood xylan, wheat arabinoxylan (insoluble), arabinan from sugar beet, *p*-Nitrophenyl-α-L-arabinofuranoside, *p*-Nitrophenyl-β-D-xylopyranoside and standards *viz.* D-xylose, xylobiose, xylotriose, xylotetraose and xylopentaose were procured from Megazyme Ltd., Ireland. 4-O-methylglucuronoxylan was purchased from Carbosynth Ltd., UK. Carboxy methyl cellulose sodium salt, Phenylmethylsulfonyl fluoride (PMSF), acrylamide, N,N-methylenebis (acrylamide), *p*-Nitrophenyl-α-L-arabinopyranoside, *p*-Nitrophenyl-β-L-arabinopyranoside and *p*-NP-β-D-glucopyranoside were purchased from Sigma-Aldrich Co. LLC., USA. Sodium arsenate, ammonium molybdate, sulphuric acid, hydrochloric acid, acetone, acetonitrile, acetic acid and Folin's reagent were purchased from Merck Limited, India. For thin layer chromatography (TLC), the Silica gel plates (60G F_{254}, 20 X 20 cm) were purchased from Merck KGaA, Darmstadt, Germany. Beechwood xylan was purchased from Sisco Research Laboratories Pvt. Ltd. (India).

3.2.2 Purification of *Bo*GH43_35 recombinant protein by affinity chromatography

The recombinant protein, *Bo*GH43_35 possessing an N-terminal His_6-tag was purified through immobilized metal-ion affinity chromatography (IMAC) following the method described below. The purification of recombinant protein was conducted using 5.0 mL sepharose column (GE Healthcare, HiTrap chelating HP). The composition of equilibration as well as elution buffers used for affinity column purification is mentioned in Table 3.1.

Table 3.1 Composition of buffers used in purification of *Bo*GH43_35 by affinity purification.

Buffer	**Composition**
Equilibration buffer	50 mM sodium phosphate, pH 7.0 300 mM NaCl, 50 mM Imidazole
Elution buffer	50 mM sodium phosphate, pH 7.0 300 mM NaCl, 300 mM Imidazole
Column cleaning buffer	50 mM sodium phosphate, pH 7.5 300 mM NaCl, 50 mM EDTA
Dialysis buffer	50 mM sodium phosphate, pH 7.0

1. The *E. coli* BL21 (DE3) cells containing the recombinant plasmid were grown in 200 mL LB medium supplemented with kanamycin (50 µg/mL) till mid-exponential phase (OD_{600}=0.6) at 37°C and 180 rpm. The recombinant gene expression was induced by adding IPTG with a final concentration of 0.25 mM and incubating the culture at 24°C and 180 rpm for 16 h.
2. The bacterial cells were harvested by centrifugation at 6000***g*** at 4°C. The cell pellet was re-suspended in 5 mL of 50 mM Sodium phosphate buffer, pH 7.0.

3. The cells were sonicated (Sonics, Vibra cells, USA) on ice for 15 min (5s on and 8s off pulse; with 33% amplitude) and centrifuged at 12,000***g*** at 4ºC for 1 h to get the crude cell-free extract.
4. The cell-free extract obtained after centrifugation was filtered through through a 0.45 µm filter membrane using a syringe filter before loading onto 5 mL HiTrap chelating HP column. The column was pre-washed with 5 volumes of filtered and degassed water to remove the alcohol.
5. Column was charged using 2.0 mL of 0.1 M $NiSO_4$ solution and the unbound Ni^{2+} ions were washed away with 2-5 volumes of water.
6. Then, the column was equilibrated with 10 volumes of equilibration buffer (Table 3.1).
7. The filtered cell-free extract of recombinant protein was loaded onto the column at a flow rate of 0.5 $mL.min^{-1}$.
8. The column was then washed with 50 column volumes of equilibration buffer to remove the unbound proteins.
9. The bound protein of interest was then eluted with elution buffer under a gradient of 0-100% imidazole concentration, and 1 mL fractions were collected (Carvalho *et al.*, 2004).
10. The column was cleaned using a cleaning buffer as mentioned in Table 3.1, washed with 5 volumes of water and incubated in 1N NaOH at 4°C for 2h. The column was then washed with 20 volumes of water to remove NaOH, and finally stored in 20% (v/v) ethanol at 4°C.

The purified recombinant protein *Bo*GH43_35 was extensively dialysed using a dialysis membrane (with a Mol. Mass cut off 12 -14 kDa) in 50 mM sodium phosphate buffer, pH 7.0 to remove the solutes. The purity and molecular mass of *Bo*GH43_35 was verified by SDS-PAGE as described in Section 2.2.14

3.2.3 Protein concentration determination of purified recombinant proteins by using Folin-Lowry and UV method

The concentration of the purified *Bo*GH43_35 was determined by Folin-Lowry method (Lowry et al., 1951) using bovine serum albumin (BSA) as standard. The BSA standard at different concentrations (10-1000 µg.mL^{-1}) and the unknown *Bo*GH43_35 fraction samples were treated with an alkaline reagent composed of sodium carbonate and copper sulfate, which binds to peptide bonds and forms a blue complex. Subsequently, the Folin-Ciocalteu reagent, which contains phosphomolybdic and phosphotungstic acids, was added, resulting in a color change due to the reduction of these acids by the tyrosine and tryptophan residues in proteins. The intensity of the resulting blue color, which develops over a 30-minute incubation period, was measured spectrophotometrically at 660 nm. By comparing the absorbance values of the samples to those of a standard curve generated from known BSA concentrations, the protein concentration in the *Bo*GH43_35 was quantified.

The composition of reagents used in Folin-Lowry method are mentioned below.

Reagent A: Sodium carbonate (2.0 g) and sodium hydroxide (0.4 g) dissolved 100 mL of distilled water.

Reagent B1: Potassium sodium tartrate tetrahydrate (2.0 g) dissolved in 10 mL distilled water.

Reagent B2: Copper sulphate pentahydrate (1.0 g) dissolved in 100 mL distilled water.

Reagent C: Freshly prepared prior the experiment by dissolving reagent B1, A and B2 in a ratio of B1:A:B2 = 1:100:1.

Folin-Ciocalteu reagent : 1 N Folin-Ciocalteu reagent.

3.2.3.1 Protocol of Folin-Lowry method for protein estimation

1. A series of dilutions of the BSA standard was prepared to generate a range of protein concentrations (10-1000 µg.mL^{-1}) for making the standard curve.
2. 0.2 mL of the protein sample or standard solution was placed into labeled test tubes.
3. 1.0 mL of freshly prepared Reagent C (Alkaline Copper Solution) was added to each tube (containing either protein standards or unknown samples). The mixtures were incubated at room temperature for 10 min to allow color development.
4. 0.1 mL of 1 N Folin-Ciocalteu reagent was added to the sample solutions. The solution was mixed and incubated at room temperature for 30 min.
5. The absorbance was measured at 660 nm using a spectrophotometer.
6. The absorbance readings of the standards were used to construct a standard curve. The protein concentration of the unknown samples were calculated by using the standard curve.

The amount of recombinant protein was estimated using the following equation,

$$\text{Protein concentration} = \frac{\Delta A_{660} \times C \times V}{v}$$

Where,

ΔA_{660} = change in absorbance of the sample
V = volume of the protein-buffer mixture (mL)
C = 1 OD equivalent of BSA from the standard plot (mg.mL^{-1})
v = volume of the protein used for assay (mL)

3.2.3.2 Protein concentration determination by UV method

The concentration of purified protein was also determined from their corresponding absorbance at 280 nm using the equation below (Layne, 1957; Stoscheck, 1990). Absorbance was measured after proper dilution of the protein using a spectrophotometer (Multiskan SkyHigh, Thermo Fisher Scientific, Waltham, MA,

USA) having a path length of 1 cm. The molar extinction co-efficient 134580 $M^{-1}cm^{-1}$for *Bo*GH43_35 was used for the calculation.

$$\text{Concentration of protein (mg.mL}^{-1}\text{)} = \frac{\text{Absorbance at 280 nm x Mol. weight (Da)}}{\text{Extinction coefficient (M}^{-1}\text{cm}^{-1}\text{) x Path length (1 cm)}}$$

3.2.4 Enzyme activity assay

3.2.4.1 Against natural substrates

The enzyme assay was performed in a 100 µL reaction mixture containing 10 µL of purified, 50 µg.mL^{-1} *Bo*GH43_35 (5 µg.mL^{-1}final concentration) in 0.05 M sodium phosphate buffer, pH 7.0 and 90 µL of 1.1% (w/v) of natural substrate dissolved in the same buffer at 1.0% (w/v) final concentration. The reaction mixtures were incubated at 37°C for the optimized time of 2 min. *Bo*GH43_35 enzyme activity was quantified by estimating the released reducing sugar by following the methods of Nelson (Nelson, 1944) and Somogyi (Somogyi, 1945). The details of preparation of the reagents are mentioned in Section 3.2.4.3. 25:1 ratio of copper reagent A (NS-A): copper reagent B (NS-B) was used to make Nelson-Somogyi-D (NS-D) solution (Nelson, 1944). After the completion of the reaction, 100 µL of NS-D reagent was added to the enzyme-substrate mixture, followed by boiling it in water bath for 20 min The mixture was allowed to cool and then added with 100 µL of NS-C reagent followed by adjusting the volume to 1 mL by adding 700 µL distilled water. The absorbance of mixture was recorded at 500 nm using a spectrophotometer (Multiskan SkyHigh, Thermo Fisher Scientific, Waltham, MA, USA). The standard curve of a mixture of equimolar L-arabinose and D-xylose was plotted for calculating the released amount of reducing sugar. All the enzyme assays were carried out in triplicate sets.

`Calculation of enzyme activity

The enzyme activity was estimated in units per millilitre ($U.mL^{-1}$), whereas specific activity was quantified in units per milligram of enzyme ($U.mg^{-1}$). Enzyme activity ($U.mL^{-1}$) of *Bo*GH43_35 refers to the quantity of enzyme per mL needed to release one µmole of arabinose/xylose per min. One unit (U or $\mu mole.min^{-1}$) of *Bo*GH43_35 enzyme is the quantity of *Bo*GH43_35 required to release one µmole of arabinose/xylose in one minute. The specific enzyme activity ($U.mg^{-1}$) is the quantity of enzyme per milligram needed to liberate one µmole of arabinose/xylose in one minute under optimum reaction conditions. The enzyme activity of *Bo*GH43_35 was calculated as described below,

$$\text{Enzyme activity } (U.mL^{-1}) = \frac{\Delta A_{500} \times C \times V}{150 \times t \times v} = (\mu mole.min^{-1}.mL^{-1})$$

where,

ΔA_{500} = change in absorbance of the sample at 500 nm
C = 1 OD equivalent L-arabinose concentration from standard plot
V = volume of the reaction mixture (mL)
t = time of reaction (min)
150 = molecular weight of D-xylose/ L-Arabinose
v = volume of the enzyme taken in assay (mL) for reducing sugar estimation.

The specific activity of *Bo*GH43_35 was calculated as described below,

$$\text{Specific activity } (U.mg^{-1}) = \frac{\text{Enzyme activity } (U.mL^{-1})}{\text{Enzyme concentration } (mg.mL^{-1})} = (\mu mole.min^{-1}.mg^{-1})$$

3.2.4.2 Against synthetic substrates

The enzyme activity of *Bo*GH43_35 was also assessed against synthetic substrates *viz*, *p*-nitrophenyl-glycosides (*p*-NP-α-L-arabinopyranoside, *p*-NP-β-D-xylopyranoside, *p*-NP-β-D-glucoside, *p*-NP-α-L-arabinofuranoside and *p*-NP-β-L-

arabinopyranoside). The substrate 90 µl each at 2 mM concentration dissolved in 0.05 M sodium phosphate buffer (pH 7.0) and 10 µl of buffer was taken as blank, whereas 10 µl of *Bo*GH43_35 (50 µg.mL^{-1}) was added for its enzyme activity analysis. After 2 min of incubation at 37°C, the reaction was stopped by adding 100 µl of 0.5 M sodium carbonate solution. Quantification of the released *p*-NP was done by measuring the absorbance at 410 nm (A_{410}) and using standard plot of *p*-NP to calculate the Molar Extinction coefficient of *p*-NP (7011 M^{-1}.cm $^{-1}$), subsequently the enzyme activity (Margolles & De Los Reyes-Gavilán, 2003). All assays were carried out in triplicate sets.

3.2.4.3 Preparation of reagents for reducing sugar estimation

Reagent A

Sodium carbonate anhydrous	6.25 g
Sodium potassium tatarate	6.25 g
Sodium bicarbonate	5.0 g
Sodium sulphate anhydrous	50.0 g

The above specified components were dissolved in 100 mL of deionized water and the total volume was adjusted to 250 mL. The resulting solution was filtered using Whatman No. 1 filter paper and stored at temperature of 30°C.

Reagent B

Reagent B was formulated by dissolving 15 g of copper sulfate ($CuSO_4$) in 50 mL of deionized water, with the addition of one or two drops of concentrated sulfuric acid. The final volume of the resulting solution was adjusted to 100 mL and filtered using Whatman No. 1 filter paper. The solution was stored at temperature of 30°C.

Reagent C

Reagent C was prepared in a dimly lit environment through a two-step process. Initially, 2.5 g of ammonium molybdate were dissolved in 45 mL of deionized water using a 100 mL beaker, followed by the addition of 2.1 mL of concentrated sulfuric acid. Simultaneously, in another beaker, 0.3 g of sodium arsenate was dissolved in 2.5 mL of deionized water. Subsequently, the sodium arsenate solution was mixed with ammonium molybdate solution resulting in a total volume of approximately 50 milliliters. The resulting solution was then filtered using Whatman No. 1 filter paper in low-light conditions and stored at 37°C. The solution was utilized after a 24 h incubation period.

Reagent D

Reagent D was prepared by combining reagent A and reagent B in a ratio of 25:1. The composite reagent D was freshly prepared for the assay.

3.2.4.4 Generation of standard plot of D-xylose/L-arabinose

The standard plot for equimolar D-xylose/ L-arabinose was created by altering its concentration within the range of 10-100 µg.mL^{-1} from the mixture of 100 µg.mL^{-1} of D-xylose and 100 µg.mL^{-1} of L-arabinose. 100 µl reaction mixture containing 50 mM sodium phosphate buffer pH 7.0 with D-xylose/ L-arabinose in a 1.5 mL microcentrifuge was added with 100 µl of solution D (Section 3.2.4.3). The reaction mixture was then heated in boiling water bath for 20 min, followed by cooling to room temperature. 100 µL of solution C (Section 3.2.4.1) was added and the components were mixed. Then 700 µL distilled water was added to adjust the final volume to 1 mL. The absorbance at 500 nm (A_{500}) was measured using UV-Visible spectrophotometer (Thermo, Multiskan) against a buffer blank. A standard plot of A_{500} versus D- xylose concentration (µg.mL^{-1}) was developed and 1 A_{500} equivalent of D- xylose (µg.mL^{-1})

was calculated. 1 A_{500} equivalent of equimolar D-xylose/ L-arabinose ($\mu g.mL^{-1}$) was converted into $mg.mL^{-1}$ for the determination of enzyme activity.

3.2.5 Biochemical characterization of *Bo*GH43_35

3.2.5.1 Substrate specificity

Various natural and synthetic substrates were employed to perform the enzyme assay of *Bo*GH43_35 to determine its substrate specificity and highest enzyme activity. The natural substrates used were beechwood xylan, larchwood xylan, xylan from oat spelts, wheat arabinoxylan (low viscosity), insoluble wheat arabinoxylan, rye arabinoxylan (high viscosity), 4-O-methyl glucuronoxylan, sugar beet arabinan and carboxy methyl cellulose (CMC)-sodium salt. The enzyme assays using natural substrates were performed by following the protocol mentioned in Section 3.2.4.1. Whereas, the enzyme assays against synthetic substrates were performed by following the protocol mentioned in Section 3.2.4.2.

3.2.5.2 Investigating optimum pH and pH resilience of *Bo*GH43_35

The determination of optimum pH of *Bo*GH43_35 was done by measuring its activity at 37°C against 1% (w/v) wheat arabinoxylan (low viscosity) as the substrate in 0.05 M sodium phosphate buffer, pH 7.0. Different buffers corresponding to different pH ranges were used, such as for pH range 3.0–6.0, 0.05M citrate phosphate, for pH range 6.0–8.0, 0.05M sodium phosphate and for pH range 8.0–9.0, 0.05 M Tris–HCl. The stability of *Bo*GH43_35 at different pH was investigated by incubating 50 µL of *Bo*GH43_35 (50 $\mu g.mL^{-1}$) in the afore-mentioned buffers for 90 min at 4°C. Following the incubation, enzyme assays were performed by taking and aliquot, 10 µL to measure the residual enzyme activity in 0.1 mL reaction mixture as mentioned in section 3.2.4.1.

All assays were performed in triplicate sets and the average value of the residual enzyme activity was presented.

3.2.5.3 Investigating optimum temperature and thermo-stability of *Bo*GH43_35

The optimum temperature of *Bo*GH43_35 was measured with in a temperature range, from 10-70°C. The assay reaction mixture, 0.1 mL containing 10 µL of enzyme (50 µg.mL^{-1}) in 1% (w/v) wheat arabinoxylan (low viscosity) dissolved in 0.05 M sodium-phosphate buffer, pH 7.0 was incubated for 2 min. The enzyme activity of *Bo*GH43_35 was determined by estimating the amount of released reducing sugar as mentioned in section 3.2.4.1. The thermostability of *Bo*GH43_35 was determined by incubating 500 µL of *Bo*GH43_35 (50 µg.mL^{-1}) at different temperatures (4, 25, 30, 35, 40 and 50°C) for 48 h. 10 µL aliquot of *Bo*GH43_35 (50 µg.mL^{-1}) was taken from incubated enzyme at different time intervals for 0.1 mL reaction mixture containing 1.0 % (w/v) wheat arabinoxylan and residual activity was determined by estimating the reducing sugar released described in section 3.2.4.1. The half-life ($t_{1/2}$) of *Bo*GH43_35 at the mentioned temperatures was calculated by plotting the residual activity versus the time of incubation. Thermal inactivation of *Bo*GH43_35 was calculated by considering that the enzyme follows first order kinetics and using first order kinetics equation, $\ln[A]=-kt+\ln[A]_0$, where A_0 and A are the initial and residual enzyme activity at different temperatures and corresponding time intervals, respectively, t is the time of incubation and k is the rate constant for enzyme inactivation and is calculated by obtaining the slope of linear plot. The half-life ($t_{1/2}$) of *Bo*GH43_35 was determined by employing the equation $t_{1/2}=\ln 2/k$ (Ahmed et al., 2023).

3.2.5.4 Influence of metal-ions and additives on *Bo*GH43_35 activity

Understanding the crucial role of metal-ions in enzyme activity is multifaceted and essential. Therefore, *Bo*GH43_35 was assayed by subjecting it to diverse metal-ions and additives at different concentrations to assess their influence. The enzyme was assayed by incubating 50 µL of *Bo*GH43_35 (50 µg.mL^{-1}) with different metal salts or additives at different concentrations for 90 min at 4°C. The metal salts such as NaCl, KCl, $CoCl_2$, $CaCl_2$, LiCl, $NiSO_4$, $CuSO_4$ and $MgSO_4$ at 1 mM and 2 mM, other additives such as SDS, EDTA, EGTA and Urea at 1 mM and 2 mM, Guanidine-HCl, PMSF at 5 mM and 10 mM, DMSO and glycerol at 5% (v/v) concentration were used. The effect of metal-ions or additives was determined by taking an aliquot 10 µL of *Bo*GH43_35 (50 µg.mL^{-1}) from incubated mixtures and adding to 90 µL (1.1%, w/v) of wheat arabinoxylan, low viscosity dissolved in 0.05 M sodium phosphate buffer, pH 7.0 and incubating at 37°C for 2 min. In parallel, the blank containing the substrate with the respective metal-ion or chemical agent without the enzyme was also assessed. The enzyme activity of *Bo*GH43_35 was determined by estimating the amount of released reducing sugar as mentioned in section 3.2.4.1. *Bo*GH43_35 activity without the addition of metal-ion or additive was considered as 100%.

3.2.5.5 Investigation of kinetic parameters of *Bo*GH43_35

The kinetic parameters of *Bo*GH43_35 were determined by conducting enzyme assays in 0.1 mL reaction mixture with varying concentrations (0.02-2.0%, w/v) of wheat arabinoxylan low viscosity and rye arabinoxylan insoluble at optimum temperature (37°C) and pH (7.0) for 2 min. The reaction was performed according to the method mentioned in section 3.2.4.1. The blank contained equivalent substrate concentration without enzyme. Assuming steady state conditions, the values for

Michaelis-Menten constant, K_M, maximum velocity, V_{max}, turnover number, K_{cat} and catalytic efficiency, K_{cat}/K_M were determined. All assays of *Bo*GH43_35 were carried out in triplicate. The Graphpad Prism software v8.4.3 was used to plot Michaelis-Menten graph and its double-reciprocal transformation, Lineweaver-Burk plot to determine the K_M and V_{max} values.

3.2.5.6 Melting point analysis of *Bo*GH43_35

The melting point of *Bo*GH43_35 was determined by incubating 1 mL of 50 µg.mL^{-1} *Bo*GH43_35 in 0.05 M sodium phosphate buffer, pH 7.0 at a temperature range, 25-65°C, for period of 5 min followed by taking absorbance at 280 nm (A_{280}) using a UV-Visible spectrophotometer (Multiskan Sky High, Thermo Scientific) at temperature interval of 5°C. The melting curve of *Bo*GH43_35 with absorbance at 280 nm versus temperature was plotted using Graphpad Prism software v8.4.3.

3.2.6 Functional characterization of *Bo*GH43_35

3.2.6.1 Analysis of mode of action and identification of *Bo*GH43_35 hydrolysed products

The mode of action of *Bo*GH43_35 and the pattern of wheat arabinoxylan hydrolysis were examined by performing TLC. The time-dependent hydrolysis analysis by TLC was set up in separate 400 µL reaction mixture containing 360 µL of 1% (w/v) wheat arabinoxylan (low viscosity) dissolved in 0.05 M sodium phosphate buffer, pH 7.0 and 40 µL of *Bo*GH43_35 (50 µg.mL^{-1}) were incubated at 37°C for 1 min, 5 min, 15 min, 30 min, 1 h, 2 h, 4 h, 6 h, 8 h, 10 h,12 h, 16 h and 24 h. A negative control with only wheat arabinoxylan, low viscosity without *Bo*GH43_35 was also set up. After each time interval, 100 µL of the reaction mixture was aliquoted for quantification of total reducing sugar as mentioned in section 3.2.4.1. The rest of the 300 µL reaction mixture

was stopped by adding twice the volume (600 µL) of chilled absolute ethyl alcohol then centrifuging at 13,000g at 4°C for 10 min. The supernatant obtained was gently taken in a new 1.5 mL Eppendorf tube and kept for drying at 60°C for 12 h. The dried hydrolysed samples were dissolved in 20 µL distilled water. The standards used for reference were 1 $mg.mL^{-1}$ solution of each L-arabinose, D-xylose, xylobiose, xylotriose, xylotetraose and xylopentaose. The hydrolysed samples (0.6 µL) and all the standards (0.6 µL) were applied to the TLC plate and the plate was dried in air after applying the samples. The solvent system used contained chloroform, glacial acetic acid and deionized water in the ratio 6:7:1. The spots were visualized by using a staining solution composed of 2 g diphenylamine, 2 mL aniline, 1 mL 37.5% HCl, 10 mL 85% H_3PO_4 and 100 mL ethyl acetate (Zhang et al., 2009). The stained TLC plate was kept in hot-air oven at 60°C until the spots of samples and standards were visible.

The TLC analysis of the time-dependent hydrolysis of arabinose-unsubstituted substrate *i.e.*, beechwood xylan by *Bo*GH43_35 was performed. The reaction mixture, 200 µL containing 180 µL of 1% (w/v) beechwood xylan in 0.05 M sodium phosphate buffer, pH 7.0 and 20 µL of *Bo*GH43_35 (50 $µg.mL^{-1}$) was incubated at 37°C for 1 min, 5 min, 30 min, 1 h, 6 h, 12 h and 24 h. The reactions were stopped by adding twice the volume (400 µL) of chilled absolute ethyl alcohol, followed by centrifugation at 13,000g at 4°C for 10 min. The samples were prepared by following the protocol as mentioned above. The hydrolysed samples (0.6 µL) as well as the xylooligosaccharide standards (0.6 µL) were applied on to the TLC plate. The mobile phase, the staining solution and the protocol followed was same as mentioned in section 3.2.6.1.

3.2.6.2 Analysis of *Bo*GH43_35 hydrolysed products by HPLC

High-performance liquid chromatography (HPLC) was used to analyse *Bo*GH43_35 hydrolysed products to determine the hydrolytic mechanism of *Bo*GH43_35. The reaction mixture, 1.0 mL containing 1% (w/v) wheat arabinoxylan, low viscosity in 0.05 M sodium phosphate buffer, pH 7.0 and 50 µL of *Bo*GH43_35 (0.05 $mg.mL^{-1}$) was incubated at 37°C for 12 h. Similar setup was kept as control where 50 µL of 0.05 M sodium phosphate buffer, pH 7.0 was added instead of *Bo*GH43_35. The reaction was stopped by adding two volumes of absolute ethanol which was further dried at 60°C for 12 h. The sample after drying was resuspended in 0.5 mL deionized water and filtered by passing it through 0.45 µm membrane using a syringe filter to remove insoluble impurities. Arabinose, xylose, xylobiose, xylotriose, xylotetraose and xylopentaose each of 1 $mg.mL^{-1}$ were used as standards for HPLC analysis. The prepared samples and standards were run through Rezex RSO-Oligosaccharide column (200 × 10 mm, Phenomenex, Inc. USA) coupled to the guard column (Rezex RSO-Oligosaccharide guard, 60 × 10 mm, Phenomenex, Inc. USA) connected to High Performance Liquid Chromatography (Shimadzu Corporation, Kyoto, Japan) attached with refractive index (RI) detector. The mobile phase of degassed deionized (Milli-Q) water was employed at a flow rate, 0.3 $mL.min^{-1}$ keeping the injection volume 20 µL for the samples.

3.2.6.3 TLC and MALDI-TOF MS analyses of hydrolysed xylooligosaccharides by *Bo*GH43_35

The mode of action of *Bo*GH43_35 against various xylooligosaccharides *viz.* xylobiose, xylotriose, xylotetraose and xylopentaose were also analysed by TLC. The reaction mixture consisted of 90 µL of the individual xylooligosaccharide (1.1 $mg.mL^{-}$

^{1}) with 10 µL of *Bo*GH43_35 (50 µg.mL^{-1}) and kept for 24 h at 37°C. The reaction was terminated by addition of twice the volume (200 µL) of chilled ethyl alcohol followed by centrifugation at 13000g for 10 min. The supernatant was transferred to fresh 1.5 mL Eppendorf tube and kept for drying at 60°C in a Hot-air oven for 12 h. The dried hydrolysed samples were dissolved in 20 µL deionized water. The hydrolysed samples and the xylooligosaccharide standards (0.6 µL each) were spotted on TLC plate, dried and developed for detection by following the protocol mentioned in section 3.2.6.1.

The *Bo*GH43_35 hydrolyzed xylooligosaccharide samples were subjected to Matrix Assisted Laser Desorption Ionization-Time of Flight Mass Spectrometry analysis (MALDI-TOF MS) by following the earlier reported protocol (Gavande et al., 2022). The hydrolysate (5 µL) was mixed with 5 µL of 2,5-Dihydroxybenzoic acid matrix (10 mg.mL^{-1}) prepared in 1:1 v/v acetonitrile:water and 0.1%, v/v trifluoroacetic acid. For the MALDI-TOF MS analysis, 2 µL of the prepared samples were spotted on stainless steel sample target plate, dried completely and then used for analysis. The spectra were obtained by employing MALDI-TOF MS Autoflex speed of Bruker Daltonics (Germany) in a positive ion mode. The default accelerating voltage of 20,000 volts was used. The delay for pulse ion extraction was set at 120 ns and the laser shot frequency at 2000 Hz.

3.2.6.4 Regioselectivity analysis of *Bo*GH43_35

α-L-Arabinofuranosidases are considered to cleave the non-reducing L-arabinofuranosyl (L-Araf) substitutions at O-2, O-3 or O-2/O-3 position of β-1,4-linked xylose backbone (Borsenberger et al., 2014). Proton nuclear magnetic resonance (^{1}H-NMR) of *Bo*GH43_35 hydrolysed wheat arabinoxylan sample was performed to determine the regioselectivity of *Bo*GH43_35 towards the different arabinose

substitutions. The reaction mixture, 1.0 mL containing 1% (w/v) wheat arabinoxylan, low viscosity in 0.05 M sodium phosphate buffer, pH 7.0 and 50 µL of *Bo*GH43_35 (0.05 $mg.mL^{-1}$) was incubated at 37°C for 12 h. Similar setup was kept as control where 50 µL of 0.05 M sodium phosphate buffer, pH 7.0 was added instead of *Bo*GH43_35. The *Bo*GH43_35 hydrolysed wheat arabinoxylan polysaccharide was precipitated by addition of 2 volumes (2 mL) of ice-cold absolute ethanol and then centrifuged at 13000g for 10 min. The precipitated wheat arabinoxylan was washed with 200 µL of ice-cold ethyl alcohol followed by freeze-drying by using a lyophilizer (ScanVac, Labogene, Denmark) for 12 h. Similarly, the sample preparation for untreated wheat arabinoxylan was done and was considered as control. The dried samples were then dissolved in 0.6 mL D_2O and the ^1H NMR spectra with 16 scans were collected at 25 ºC by using 600 MHz Nuclear Magnetic Resonance (NMR) Spectrometer (Bruker, ASCEND 600, Karlsruhe, Germany) containing a 5-mm probe. Analysis of the spectra was done using Topspin NMR software (Bruker, Karlsruhe, Germany). The regioselectivity of *Bo*GH43_35 was substantiated also by detecting *Bo*GH43_35 hydrolysed arabino-xylooligosaccharide (AXOS) substituted by arabinose at O-2 or O-3 positions. The AXOS *viz.*, 3^2-α-L-arabinofuranosyl-xylobiose (A^3X) and 2^3-α-L-arabinofuranosyl-xylotriose (A^2XX) were subjected to *Bo*GH43_35 mediated hydrolysis at 37 ºC for 12 h. The selectivity of linkage was confirmed by identifying the hydrolysed products on TLC plate and comparing them with the L-arabinose, D-xylose, xylobiose, xylotriose and xylotetraose as standards.

3.3 Results and Discussion

3.3.1 Purification of *Bo*GH43_35 by immobilized metal-ion affinity chromatography

The recombinant protein, *Bo*GH43_35 was purified by immobilized metal-ion affinity chromatography (IMAC) as described in Section 3.2.2 and then extensively dialyzed for removal of imidazole and salts. The purified *Bo*GH43_35 enzyme displayed a single, homogeneous protein band on SDS-PAGE with an observed molecular mass of approximately, 74 kDa, consistent with its theoretical molecular mass of 74.1 kDa showing that it expressed as a soluble protein.

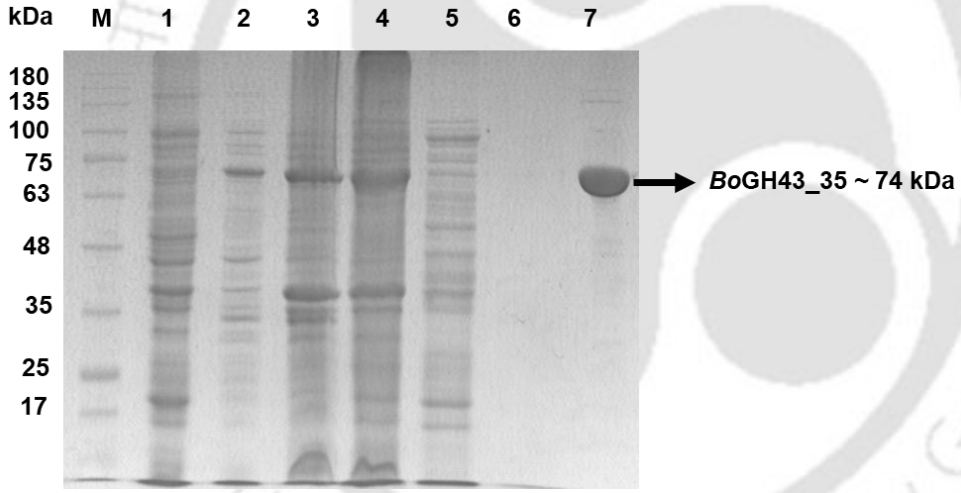

Fig. 3.1 Purification profile of recombinant *Bo*GH43_35 on SDS-PAGE (12%, w/v) gel. Lane M: Pre-stained protein marker (HiMedia Pvt. Ltd. India); Lane 1: Uninduced *E. coli.* BL21 (DE3) cell pellet; 2: Induced *E. coli*. BL21 (DE3) cell pellet; 3: Pellet of sonicated induced *E. coli.* BL21 (DE3) cells; 4: Induced *E. coli*. BL21 (DE3) sonicated cell extract; 5: Flow through from the column; 6: Last column wash and 7: Purified *Bo*GH43_35 (~74 kDa) after IMAC purification.

3.3.2 Purification fold analysis of *Bo*GH43_35

The protein concentration of *Bo*GH43_35 of 5.6 mL cell lysate obtained from 200 mL of LB culture was 7.5 $mg.mL^{-1}$ that yielded a specific activity of 1.5 $U.mg^{-1}$ (Table 3.1). This low specific activity of *Bo*GH43_35 in the crude lysate reflects the

presence of other cellular proteins and contaminants. These non-specific proteins and biomolecules are common in crude extracts and can interfere with enzyme assays, thus necessitating further purification. After purification of *Bo*GH43_35 by immobilized metal-ion affinity chromatography (IMAC) followed by dialysis, the protein concentration was 0.9 $mg.mL^{-1}$ in a total volume of 4.0 mL with a specific activity of 4.5 $U.mg^{-1}$, resulting in 3-fold purification (Table 3.1).

Table 3.1. Purification of *Bo*GH43_35 enzyme.

Purification step	Volume (mL)	*Bo*GH43_35			Protein conc. ($mg.mL^{-1}$)	SA[#] ($U.mg^{-1}$)	Fold Purification
		EA[*] ($U.mL^{-1}$)	Total Units	Overall yield (%)			
Cell lysate	5.6	11.6	64.9	100	7.5	1.5	1.0
IMAC	4.0	4.2	16.8	25.8	0.9	4.5	3.0

The enzyme activity of *Bo*GH43_35 was determined by using 1.0% (w/v) wheat arabinoxylan, low viscosity in 50 mM sodium phosphate buffer, pH 7.0 at 37ºC for 2 min.
[*] *Enzyme activity in* $U.mL^{-1}$ [#] *Specific activity in* $U.mg^{-1}$

3.3.3 Biochemical characterization of *Bo*GH43_35

3.3.3.1 Substrate specificity of *Bo*GH43_35

The substrate specificity of *Bo*GH43_35 against various natural and synthetic glycan substrates was assessed. It was observed that *Bo*GH43_35 is more specific towards xylan substrates with arabinose substitutions (Table 3.2). It displayed maximum specific activity against wheat arabinoxylan low viscosity (4.9±0.3 $U.mg^{-1}$). Wheat arabinoxylan, low viscosity contains arabinose and xylose in a ratio of 38:62 with a viscosity of ~10cSt and average molecular weight of 56.7 kDa (https://www.megazyme.com/arabinoxylan-wheat-flour-low-viscosity). In the case of rye arabinoxylan high viscosity (0.5%, w/v), *Bo*GH43_35 showed activity of 3.0±0.4 $U.mg^{-1}$. Although rye arabinoxylan high viscosity has a similar composition of xylose

and arabinose residues as that of wheat arabinoxylan, low viscosity, it is distinct from wheat arabinoxylan, low viscosity, due to its exceptionally high viscosity of ~95 cSt (~10 fold higher) and high molecular weight of 386 kDa at room temperature (https://www.megazyme.com/arabinoxylan-wheat-flour-high-viscosity). *Bo*GH43_35 also showed activity against beechwood xylan (2.3±0.5 U.mg^{-1}), which is composed majorly of xylose residues. However, lower enzyme activity was observed with larchwood xylan (1.9±0.2 U.mg^{-1}) and arabinan from sugar beet (1.0±0.2). It also showed activity against insoluble wheat arabinoxylan, displaying a specific activity, 1.5±0.1 U.mg^{-1}. *Bo*GH43_35 did not show any activity against cellulosic polysaccharides which makes it highly specific towards xylan substrates. The higher specificity of *Bo*GH43_35 for both arabinose-substituted and unsubstituted xylan, sets it apart from already reported GH43 xylanolytic enzyme such as a β-xylosidase (Gavande et al., 2024) which is mainly active on arabinose-unsubstituted xylan substrates such as corn cob xylan, beechwood xylan and an exo-β-xylosidase (Zhou et al., 2020) which could not hydrolyze wheat arabinoxylan but xylooligosaccharides to produce xylose. *Bo*GH43_35 was also active against *p*-Nitrophenyl-α-L-arabinofuranoside (*p*-NPAf) with specific activity of 1.4±0.1 U.mg^{-1}. It did not show enzyme activity against any other synthetic substrate. A β-xylosidase, *Bo*Xyl43A from *Bacteroides ovatus* was reported to be mainly specific for synthetic substrates such as *p*-NPX and *p*-NPAf (Zhou et al., 2020), designating it to be bifunctional showing β-xylosidase and α-L-arabinofuranosidase activities, respectively. However, a trifunctional enzyme from *P. curdlanolyticus* B-6 showed endo-xylanase, β-xylosidase and α-L-arabinofuranosidase activities having specific activity of 2.56 U.mg^{-1} against Birchwood xylan, 0.28 U.mg^{-1} against highly substituted wheat arabinoxylan and 0.20

U.mg^{-1} against rye arabinoxylan (Teeravivattanakit et al., 2016), preferring less substituted xylan for its activity. Two bifunctional enzymes, *Pp*xyl43A and *Pp*xyl43B from *Paenibacillus physcomitrellae* showing both β-xylosidase and α-L-arabinofuranosidase activities were characterized (Zhang et al., 2021). They reported that *Pp*xyl43A shows specific activity of 7.99 U.mg^{-1} against (*p*-NPX) and 1.52 U.mg^{-1} against (*p*-NPAf), whereas, *Pp*xyl43B shows 3.24 U.mg^{-1} against *p*-NPX and 1.42 U.mg^{-1} against *p*-NPAf indicating their bifunctionality.

Table 3.2. Substrate specificity of *Bo*GH43_35.

Substrates (1%, w/v)	Specific Activity ($U.mg^{-1}$)
Natural substrates	
Wheat arabinoxylan, low viscosity (Megazyme)	4.9±0.3
Rye arabinoxylan high viscosity (Megazyme)*	3.0±0.4
Xylan Beechwood (SRL)	2.3±0.5
Larchwood xylan (Megazyme)	1.9±0.2
Wheat arabinoxylan insoluble (Megazyme)	1.5±0.1
Arabinan from sugar beet (Megazyme)	1.0±0.2
4-O-methylglucuronoxylan (Carbosynth)	0.7±0.1
Xylan oat spelt (HiMedia)	0.5±0.2
CMC-Na salt (Sigma)	-
Synthetic substrates (2 mM)	
p-NP- α-L-arabinofuranoside	1.4±0.1
p-NP-β-D-xylopyranoside	-
p-NP-β-D-glucoside	-
p-NP-α-L-arabinopyranoside	-
p-NP-β-L-arabinopyranoside	-

**0.5% (w/v) of rye arabinoxylan high viscosity was used for enzyme assay. The enzymatic activity was performed in triplicates at 37°C for 2 min in 50 mM sodium phosphate buffer, pH 7.0 and ± indicates the standard error of mean (SEM) and the sample size, n=3.*

3.3.3.2 Investigating optimum pH and pH resilience of *Bo*GH43_35

With wheat arabinoxylan, low viscosity as the substrate, at 37°C, *Bo*GH43_35 showed two pH maxima with maximum specific activity at pH 7.0 (0.05 M sodium phosphate buffer), followed by pH 5.0 (in 0.05 M citrate phosphate buffer) as shown in Fig. 3.2a. It suggested that *Bo*GH43_35 is active under acidic and neutral conditions. The optimum pH of *Bo*GH43_35 is close to the physiological pH of the human large intestine that is in acidic to neutral range (pH 4-7). The maximum activity of

*Bo*GH43_35 at physiological pH ensures efficient hydrolysis of substrates like arabinoxylans in the colon, where these polysaccharides are most abundant (Meldrum & Yakubov, 2024). *Bo*GH43_35 demonstrates significant potential for use in prebiotic and functional food applications aimed at enhancing dietary fiber breakdown for better gut health. The pH stability analysis of *Bo*GH43_35 showed that it retains more than 80% of its specific activity after 90 min incubation between pH 4-5 in 0.05 M citrate phosphate buffer and when assayed at pH 7.0 (Fig. 3.2b). Moreover, it also retained its 80% activity at pH 6.5 when incubated for 90 min at 4°C (Fig. 3.2b). The optimum pH for *Bo*GH43_35 obtained in this study is consistent with other GH43 bifunctional *β*-xylosidase/ *α*-arabinosidase from *Humicola insolens*, where maximum activity was reported to be in acidic to neutral pH range (Yang et al., 2014). A GH51 bifunctional enzyme from *Alicyclobacillus* sp. containing α-L-arabinofuranosidase and endo-xylanase activities was reported to exhibit highest activity at pH 6.0 (W. Yang et al., 2015). The optimum pH of a bifunctional enzyme *Pp*xyl43A from *Paenibacillus physcomitrellae*, belonging to GH43 family, was 6.0 for *β*-xylosidase activity and 5.0 for *α*-L-arabinofuranosidase activity (X. J. Zhang et al., 2021). Whereas, the optimum pH of *Pp*xyl43B was more towards acidic pH range with *β*-xylosidase activity at pH 5.0 and *α*-L-arabinofuranosidase activity at pH 3.0. In contrast, the optimal pH of *Bo*GH43_35 aligns with the physiological pH of the human colon, which ranges from acidic to neutral (pH 4-7). *Bo*GH43_35's ability to function optimally in the pH range of the human colon makes it suitable for breaking down dietary fibers and promoting the growth of beneficial gut bacteria, such as *Bifidobacterium* and *Lactobacillus* (Meldrum & Yakubov, 2024).

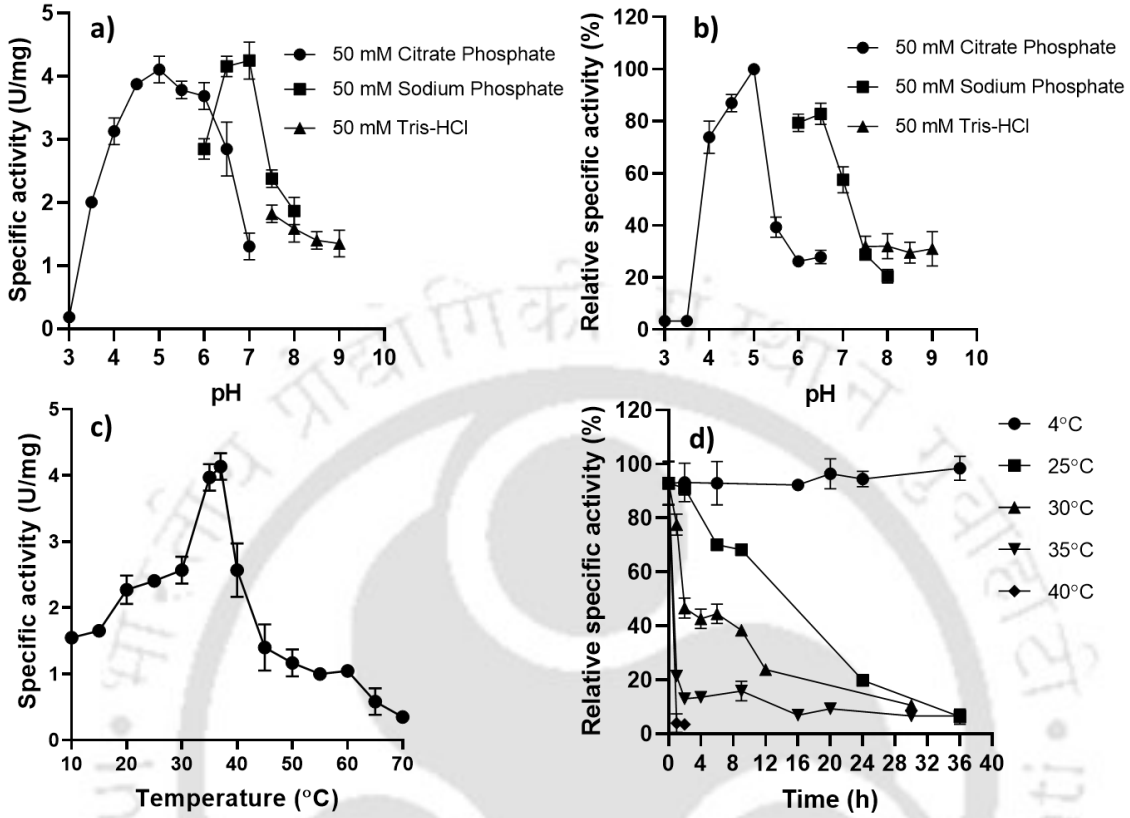

Fig. 3.2 Biochemical characterisation of *Bo*GH43_35. a) Optimum pH plot b) pH stability profile, c) Optimum temperature and d) thermal inactivation curve of *Bo*GH43_35. The data presented are averaged from three replicates, with error bars indicating ± Standard Deviation (SD).

3.3.3.3 Determination of optimum temperature and thermal inactivation of *Bo*GH43_35

The optimum temperature of *Bo*GH43_35 for enzymatic reactions was determined by carrying out enzyme assays at various temperatures in the range, 10-70°C. The highest specific activity of *Bo*GH43_35 was obtained at 37°C (Fig 3.2c). Usually, the optimum temperature of enzymes isolated from *Bacteroides ovatus* lie in the range of 30-40°C as reported by Wang et al. in 2022 (Wang et al., 2022). This might be attributed to the fact that *Bacteroides ovatus* is a human gut-microbe and the temperature of human gut is around 37°C. This is consistent with the results of a β-xylosidase, *Bo*Xyl43A from *Bacteroides ovatus* where maximum activity was obtained

at 35°C (Zhou et al., 2020). Another GH43 exo-β-1,4-xylosidase, *Bo*ExXyl43A from *Bacteroides ovatus* was reported exhibiting highest specific activity at 37°C (Gavande et al., 2024).

The thermal inactivation of *Bo*GH43_35 was measured in terms of residual specific activity (Fig 3.2d). *Bo*GH43_35 was stable at 25°C retaining ~75% activity till 8 h of incubation at 25°C showing half-life ($t_{1/2}$) of 9 h. However, the residual specific activity significantly decreased at 30°C and 35°C, revealing $t_{1/2}$ of 89 min and 45 min, respectively. Moreover, at 40°C and 50°C (data not shown), $t_{1/2}$ further reduced to 24 min and 22 min, respectively. It is not surprising to get low thermostability of *Bo*GH43_35 knowing that it has origin from *Bacteroides ovatus* which is a mesophilic bacterium. Likewise, half-life of 50 min of a rhamnogalacturonan lyase from the same source at 25°C was also reported (Wang et al., 2022). Moreover, *Bo*GH43_35 reported in the current study was stable for over 60 days at 4°C as shown in Fig. 3.2d.

3.3.3.4 Influence of metal-ions and additives on the enzyme activity of *Bo*GH43_35

Various metal-ions and additives were studied to explore their influence on enzyme activity of *Bo*GH43_35 using substrate, wheat arabinoxylan, low viscosity and the results are mentioned in Table 3.3. *Bo*GH43_35 activity was moderately reduced (70-80%) by 1 mM of Ca^{2+}, Mg^{2+} or Co^{2+} unlike enhanced activity of GH43 bifunctional xylosidase/arabinofuranosidase from gut bacterial genome in the presence Ca^{2+} ions (Xu et al., 2019). However, there was an inhibitory effect of Co^{2+} ions (Yang et al., 2015) and Mg^{2+} (Jordan et al., 2013) on the enzyme activity of bifunctional exo-α-L-arabinofuranosidase/endo-xylanase from *Alicyclobacillu*s sp. A4. Treatment of *Bo*GH43_35 by Cu^{2+} ions at only 1 mM concentration was enough to inactivate it

almost completely, echoing the reports by Jordan et al. in 2013 (Jordan et al., 2013). Sodium dodecyl sulfate (SDS), an anionic detergent also showed an inhibitory effect on the enzyme activity of *Bo*GH43_35. There was a reduction in enzyme activity of *Bo*GH43_35 in the presence of chaotropic agents such as NaCl and guanidine-HCl. However, there was a slight increase (~4 or 7%) or no significant change in the enzyme activity of *Bo*GH43_35 in the presence of chelating agents such as EDTA and EGTA. This slight augmentation in enzyme activity of *Bo*GH43_35 in the presence EDTA and EGTA suggests that metal-ions may not exist in the active-site of *Bo*GH43_35 and are not crucial for the enzyme activity, thereby evicting any probability of *Bo*GH43_35 being a metalloenzyme.

Table 3.3. Effect of metal-ions and additives on the enzyme activity of *Bo*GH43_35.

Metal-ion	Relative enzyme activity of *Bo*GH43_35 (%)	
	1 mM	2 mM
Control	100±2.1	100±2.5
Li^{+}	88.9±3.3	49.8±5
Ca^{2+}	79.3±2.4	64.6±3.7
Mg^{2+}	70.3±6.6	42.8±1.8
Co^{2+}	73.1±3.3	54.7±2.2
K^{+}	58.3±1.2	37.0±1.2
Ni^{2+}	55.4±4.6	39.5±3.7
Na^{+}	55.4±0.7	57.6±3.1
Cu^{2+}	1.2±2.1	-
EDTA	107.8±1.5	104±1.1
EGTA	100.8±1.9	95.9±1.7
Urea	76.1±5.2	45.0±0.7
SDS	14.9±2.1	7.8±2.5
Guanidine-HCl	49.4±9	21.5±1.9
DMSO (5%, v/v)	59.8±1.8	-
Glycerol (5%, v/v)	71.0±3.9	-

The assays were carried out in triplicates (n=3). Mean±SEM for each assay is shown in the table.

3.3.3.5 Kinetic parameters analysis of *Bo*GH43_35

The kinetic parameters (V_{max} and K_M) of *Bo*GH43_35 were determined under optimized conditions at 37°C and pH 7.0 against wheat arabinoxylan, low viscosity, were 5.4 U.mg^{-1} and 2.7 mg.mL^{-1} (Fig. 3.3a). *Bo*GH43_35 displayed V_{max} of 2.7 U.mg^{-1} and K_M of 1.9 mg.mL^{-1} against rye arabinoxylan, high viscosity (Fig. 3.3b). Low V_{max} of 2.7 U.mg^{-1} was achieved around 5 mg.mL^{-1} of substrate concentration and lower K_M signifies high substrate affinity. All the kinetic parameters are listed in Table 3.4. A previously reported multifunctional xylanolytic enzyme *Pc*Axy43B from *Paenibacillus curdlanolyticus* B-6 showed K_M of 0.51 mg.mL^{-1} against beechwood xylan showing high substrate affinity (Limsakul et al., 2021). *Bo*GH43_35 displayed turnover number, K_{cat} (sec^{-1}) of 6.6 sec^{-1} against wheat arabinoxylan and 3.3 sec^{-1} against rye arabinoxylan. The catalytic efficiency of *Bo*GH43_35 was 2.4 mL.mg^{-1}sec^{-1} against wheat arabinoxylan and 1.7 mL.mg^{-1}sec^{-1} against rye arabinoxylan.

Table 3.4. Kinetic parameters of *Bo*GH43_35 against different substrates

Substrate	V_{max} (U.mg^{-1})	K_M (mg.mL^{-1})	K_{cat} (sec^{-1})	K_{cat}/K_M (mL.mg^{-1}sec^{-1})
Wheat arabinoxylan	5.4	2.7	6.6	2.4
Rye arabinoxylan	2.7	1.9	3.3	1.7

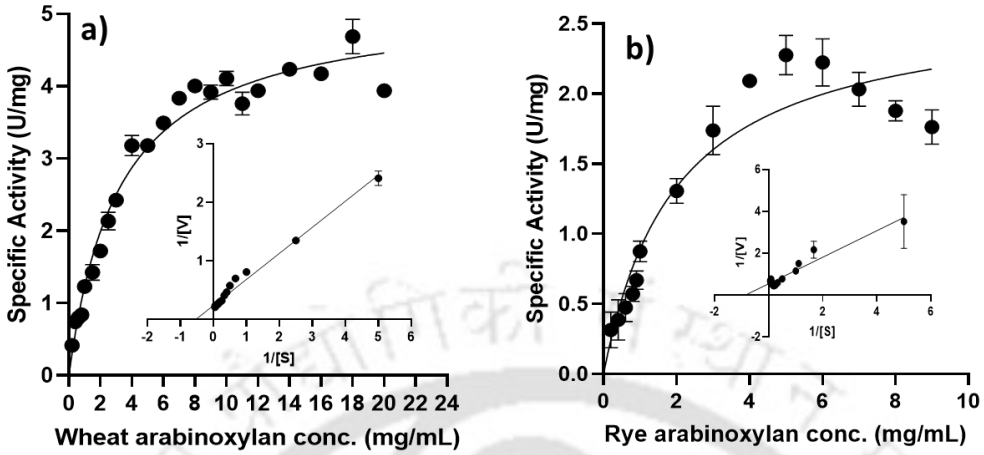

Fig. 3.3 Michaelis-Menten kinetics and Lineweaver Burk plot of *Bo*GH43_35 against (a) wheat arabinoxylan and (b) rye arabinoxylan. The inset shows the Lineweaver-Burk plot of *Bo*GH43_35 against respective substrates. The data presented are a mean of three biological replicates, with error bars indicating ± Standard Deviation (SD).

3.3.3.6 Melting point analysis of *Bo*GH43_35

*Bo*GH43_35 started to unfold as the temperature increased above 37°C. *Bo*GH43_35 completely unfolded above 45°C (Fig. 3.4). The complete denaturation of *Bo*GH43_35 at temperatures above 45°C can be attributed to the mesophilic nature of the source organism, *Bacteroides ovatus* which thrives at moderate temperatures, typically between 20°C to 45°C. The melting temperature (T_m) of *Bo*GH43_35 calculated by incorporating Boltzmann sigmoidal fitting to the plot was 41.0°C. The proximity of the T_m to the physiological temperature of the human colon suggests that *Bo*GH43_35 is marginally stable under in vivo conditions. This characteristic makes *Bo*GH43_35 suitable for applications in environments mimicking human gut conditions but less suited for high-temperature industrial processes without further stabilization. The thermostability of *Bo*GH43_35 can be enhanced by increasing global conformational rigidity by introducing random or site-directed mutations in the flexible residues within the active-site (Xie et al., 2014).

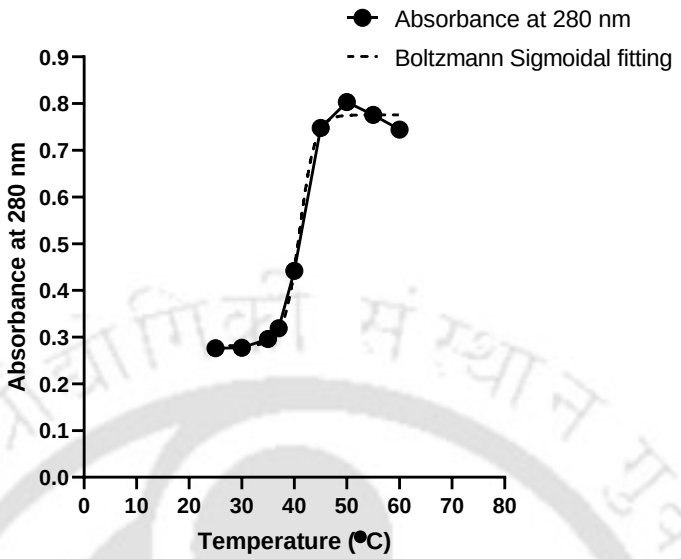

Fig. 3.4 Melting temperature plot of *Bo*GH43_35.

3.3.4 Mode of action analysis of *Bo*GH43_35

3.3.4.1 Analysis of mode of action and identification of *Bo*GH43_35 hydrolysed products

The TLC analysis of time-dependent wheat arabinoxylan hydrolysis displayed that initially, only arabinose is produced (till 1 h) when compared with standards, arabinose, xylose, xylobiose, xylotriose, xylotetraose and xylopentaose (Fig. 3.5a). After prolonged incubation of wheat arabinoxylan with *Bo*GH43_35 (after 1 h), xylobiose, xylotriose, xylotetraose, xylopentaose, xylohexaose and xyloheptaose were also produced. These results indicated initial α-L-arabinofuranosidase activity of *Bo*GH43_35 followed by endo-β-1,4-xylanase activity after the complete removal of arabinosyl side chains from xylan backbone. *Bo*GH43_35 produced 0.28 mg.mL^{-1} total reducing sugar (TRS) by hydrolyzing wheat arabinoxylan which remained constant after 12 h till 24 h of incubation (Fig 3.5b). However, the relative migration of *Bo*GH43_35 hydrolysed rye arabinoxylan products on TLC showed only one spot corresponding to arabinose throughout 24 h incubation (Fig 3.5c). Similarly, Yang et

al in 2015 reported about GH51 bifunctional exo-α-L-arabinofuranosidase/ endo-β-1,4-xylanase producing arabinose as the initial hydrolysed product followed by the production of xylooligosaccharides using wheat arabinoxylan as the substrates. There is no report in the literature describing a bifunctional xylanolytic enzyme, showing exclusively α-L-arabinofuranosidase activity against rye arabinoxylan and both α-L-arabinofuranosidase and endo-β-1,4-xylanase activities against wheat arabinoxylan. Although the arabinose-to-xylose ratios in both the arabinoxylans are same (38:62) but rye arabinoxylan has higher molecular weight (386 kDa) and higher intrinsic viscosity (~95 cSt) than wheat arabinoxylan (molecular weight 56.7 kDa and intrinsic viscosity 10 cSt). It is possible that the higher viscosity of rye arabinoxylan is restricting the access to enzyme for main chain cleavage thereby removing its endo-β-1,4-xylanase activity. All the hydrolysed products of rye arabinoxylan and wheat arabinoxylan by *Bo*GH43_35 were further analysed by HPLC.

To further confirm the endo-xylanase capacity of *Bo*GH43_35, the enzyme was incubated with the low substituted xylan derivative, beechwood xylan and the time-dependent hydrolysed products were analysed by TLC. The data confirmed the production of xylooligosaccharides (XOS) such as xylobiose, xylotriose and xylotetraose during the time course analysis (Fig. 3.5d). It was observed that these XOS were faint in the initial first hour of incubation however, they were clearly visible after 1 h and till 24 h. This result further confirms that *Bo*GH43_35 hydrolyzed beechwood xylan in a typical endo- mode confirming its endo-β-xylanase activity in addition to the primary α-L-arabinofuranosidase activity.

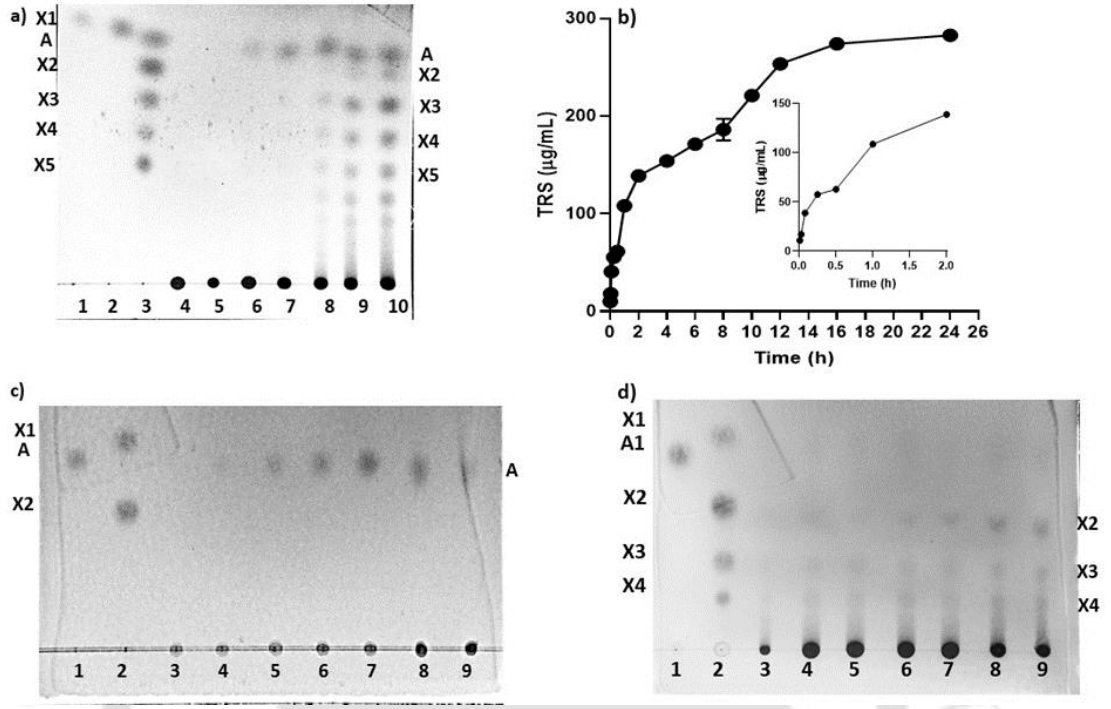

Fig. 3.5. a) TLC analysis of *Bo*GH43_35 hydrolysed products of wheat arabinoxylan. Lane 1. Xylose (X1) standard, 2- Arabinose (A) standard, 3- xylose (X1), xylobiose (X2), xylotriose (X3), xylotetraose (X4), xylopentaose (X5) standard, 4- unhydrolyzed wheat arbinoxylan, 5-1 min, 6- 5min, 7-1 h, 8-6 h, 9-12h and 10-24h hydrolysed product, b) Plot of total reducing sugar obtained at different time intervals by hydrolysing wheat arabinoxylan using *Bo*GH43_35, c) TLC analysis of *Bo*GH43_35 hydrolysed products of rye arabinoxylan. Lane 1. Arabinose (A) standard, 2- Xylose (X1) and xylobiose (X2) standard, 3- unhydrolyzed rye arbinoxylan, 4-1 min, 5- 5min, 6-1 h, 7-6 h, 8-12h and 9-24h hydrolysed product and d) TLC analysis of *Bo*GH43_35 hydrolysed products of beechwood xylan. Lane 1. Arabinose (A) standard, 2- Xylose (X1), xylobiose (X2), xylotriose (X3) and xylotetraose (X4) standard, 3- unhydrolyzed beechwood xylan, 4-1 min, 5- 5 min, 6-1 h, 7-6 h, 8-12 h and 9-24 h hydrolysed product.

3.3.4.2 Analysis of *Bo*GH43_35 hydrolysed products by HPLC

The supernatants containing *Bo*GH43_35 hydrolyzed products using wheat arabinoxylan or rye arabinoxylan were analysed by HPLC. The HPLC chromatogram of *Bo*GH43_35 hydrolysed products of wheat arabinoxylan showed major peaks of arabinose (retention time, 45.94 min), xylobiose (35.95 min), xylotriose (30.77 min), xylotetraose (26.79 min) and xylopentaose (23.76 min) as shown in Fig. 3.6a displaying

both α-L-arabinofuranosidase and endo-β-1,4-xylanase activity against wheat arabinoxylan. In the HPLC chromatogram, Fig. 3.6a, *Bo*GH43_35 hydrolyzed wheat arabinoxylan and gave arabinose (retention time: 45.94 min) at 5 min of reaction, whereas, very low intensities of the xylooligosaccharides were observed. The arabinose production confirmed α-L-arabinofuranosidase activity of *Bo*GH43_35. With the progress of the reaction, after 1 h, the hydrolysate showed the production of xylooligosaccharides such as xylobiose, xylotriose, xylotetraose, xylopentaose and xylohexaose depicting the endo-β-1,4-xylanase activity of *Bo*GH43_35. It was also noticed that there was no further increase in the production of arabinose after 6 h (Fig. 3.6a). However, the release of xylooligosaccharides increased and continued till 24 h implying that the removal of arabinose side-chains in 6 h increased the accessibility of *Bo*GH43_35 for cleaving β-1,4-linkages present in xylan. In the case of rye arabinoxylan hydrolyzed by *Bo*GH43_35, only the peak at 45.94 min corresponding to arabinose in the chromatogram was seen (Fig. 3.6b), showing exclusive α-L-arabinofuranosidase activity against rye arabinoxylan. There was no peak of xylose at retention time, 43.00 min in HPLC chromatogram (standard xylose shown in Fig. 3.6c) of wheat arabinoxylan and rye arabinoxylan (Fig. 3.6a and 3.6b), which rules out the possibility of *Bo*GH43_35 showing β-xylosidase activity as β-xylosidase hydrolyses shorter xylooligosaccharides into xylose.

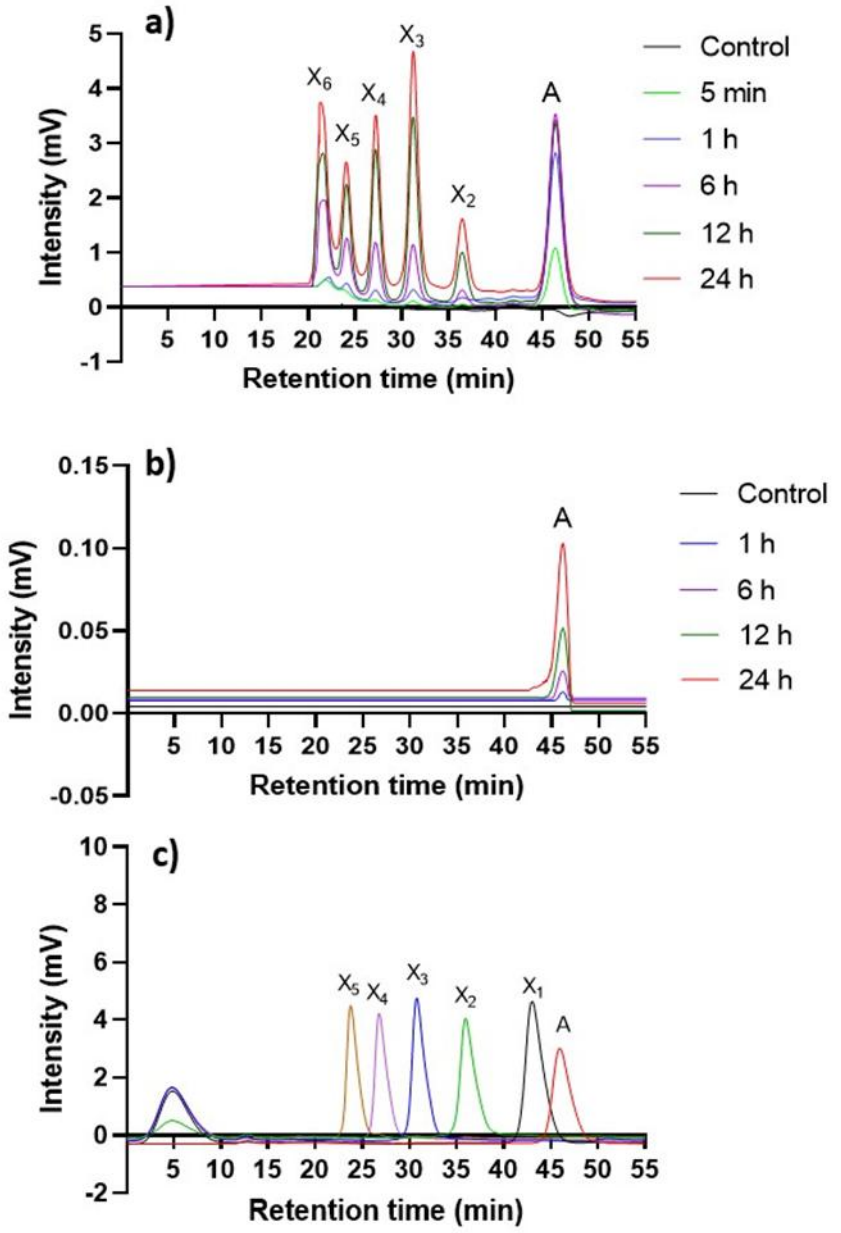

Fig. 3.6 HPLC analysis of *Bo*GH43_35 hydrolysed a) wheat arabinoxylan treated for 5 min, 1 h, 6 h, 12 h and 24 h, b) rye arabinoxylan treated for 1 h, 6 h, 12 h and 24 h and c) peaks of standards such as arabinose (retention time, 45.94 min), xylose (43.00 min), xylobiose (35.95 min), xylotriose (30.77 min), xylotetraose (26.79 min) and xylopentaose (23.76 min).

3.3.4.3 TLC and MALDI-TOF MS analysis of *Bo*GH43_35 hydrolysed xylooligosaccharides

The TLC analysis of the products released from the hydrolysis of xylooligosaccharides (xylopentaose, xylotetraose, xylotriose and xylobiose) by *Bo*GH43_35 after 24 h incubation showed that xylobiose was weakly hydrolyzed into xylose moiety, xylotriose was weakly hydrolysed into xylobiose and xylose (detected by MALDI-TOF MS but not visible in TLC), xylotetraose into xylotriose xylobiose and xylose and xylopentaose into xylotetraose, xylotriose, xylobiose and xylose (Fig. 3.7). The spots for xylobiose and xylose of the hydrolysed products were not detectable by naked eye in TLC but could be detected by MALDI-TOF MS analysis.

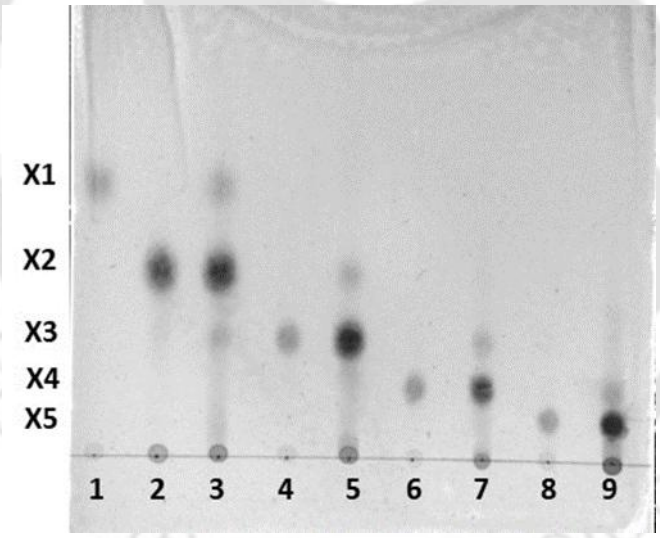

Fig. 3.7 TLC analysis of *Bo*GH43_35 hydrolysed xylooligosaccharides where Lane 1 is xylose standard, 2-Xylobiose standard, 3-hydrolyzed xylobiose, 4-xylotriose standard, 5-hydrolyzed xylotriose, 6-xylotetraose standard, 7-hydrolyzed xylotetraose, 8-xylopentaose standard and 9-hydrolyzed xylopentaose.

The Mass spectra of hydrolyzed xylobiose showed a major peak of unhydrolyzed xylobiose at *m/z*=305 and a very small peak of xylose at *m/z*=173 (Fig. 3.8a). This ruled out the possibility of *Bo*GH43_35 being a xylosidase as confirmed by the lack of activity against pNP-xylose. The spectra of hydrolyzed xylotriose showed a major peak

of unhydrolyzed xylotriose (*m/z*=437), xylobiose peak (*m/z*=305) and a small peak of xylose (*m/z*=173) as shown in Fig. 3.8b. The spectra of hydrolyzed xylotetraose showed a major peak of unhydrolyzed xylotetraose at *m/z*=569, xylotriose peak at *m/z*=437, and smaller peaks of xylobiose peak at *m/z*=305 and xylose at *m/z*=173 (Fig. 3.8c). The mass spectra of hydrolyzed xylopentaose showed a peak of unhydrolyzed xylopentaose (*m/z*=701), xylotetraose (*m/z*=569), xylotriose (*m/z*=437), xylobiose (*m/z*=305) and xylose (*m/z*=173) as depicted in Fig. 3.8d. Therefore, it can be inferred that *Bo*GH43_35 is an endo-β-xylanase as it displayed cleavage of xylopentaose and xylotetraose leading to production of shorter xylooligosaccharides.

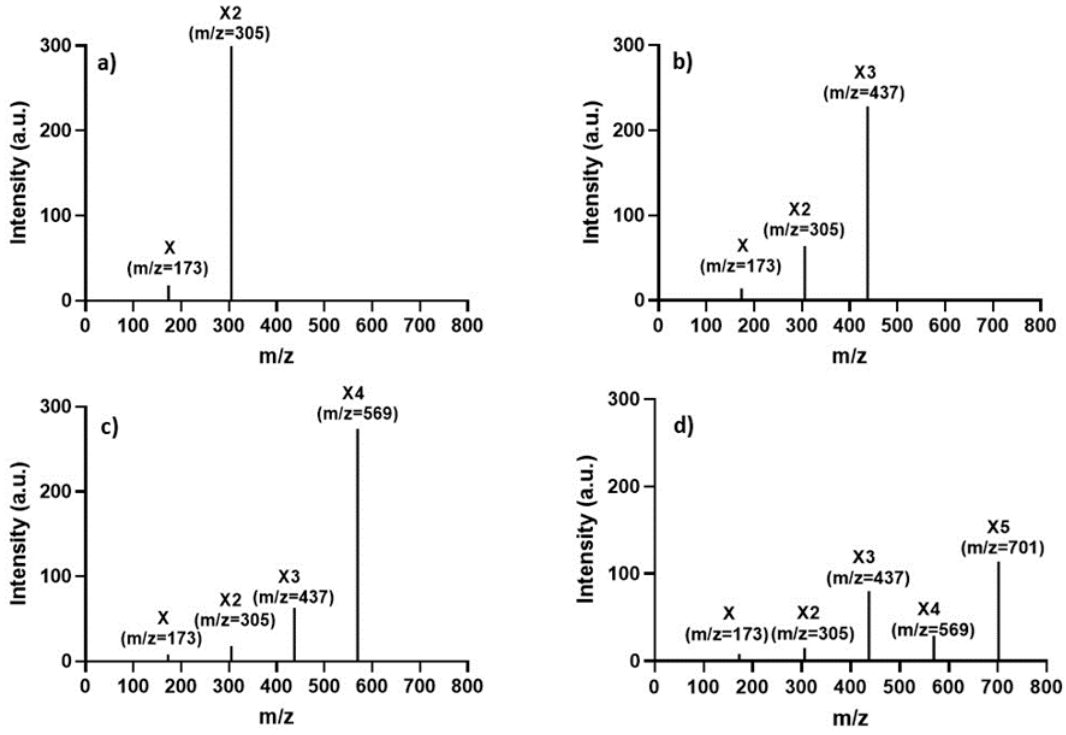

Fig. 3.8 MALDI-TOF MS analysis of *Bo*GH43_35 hydrolyzed a) xylobiose, b) xylotriose, c) xylotetraose and d) xylopentaose.

3.3.4.4 Regioselectivity analysis of *Bo*GH43_35

Arabinoxylan consists of β-D-1,4-linked xylopyranosyl residues substituted singly or doubly with L-arabinofuranose at α-1,2- and/or α-1,3- positions (Wilkens et al., 2017). Based on the α-L-arabinofuranosidase action at different types of arabinose substitutions, α-L-arabinofuranosidase is classified as type I, II and III (Thakur et al., 2020). Type I arabinofuranosidase releases L-arabinose bonded to O-2 or O-3 of mono-substituted (m) xylopyranosyl residues of arabinoxylan. Type II arabinofuranosidases are active on L-arabinose residues bonded to O-3 of di-substituted (d) arabinoxylan. The type III arabinofuranosidases can cleave both mono- and di-substituted xylopyranosyl residues of arabinoxylan. To investigate the preference of *Bo*GH43_35 for O-2 or O-3 of mono-substituted (m) and/or di-substituted (d), *Bo*GH43_35-treated and untreated wheat arabinoxylan were analysed by proton (^{1}H) NMR. The results showed that the chemical shift peaks at 5.23 ppm corresponded to m-α-(1 → 3)-L-arabinofuranose, 5.11 ppm to d-α-(1 → 2)-L-arabinofuranose and 5.06 ppm to d-α-(1 → 3)-L-arabinofuranose substitutions (Fig. 3.9a). The chemical shift signals of *Bo*GH43_35 treated arabinose-free wheat arabinoxylan displayed reduced intensity of only 5.23 ppm indicating the removal of L-arabinose from O-2 or O-3 position of mono-substituted (m) arabinoxylan. These results imply that *Bo*GH43_35 belongs to type I arabinofuranosidases. Three α-L-arabinofuranosidases belonging GH62_2 family from plant pathogenic fungi *viz.* NhaAbf62A from *Nectria haematococca*, SreAbf62A from *Sporisorium reilianum* and GzeAbf62A from *Gibberella zeae*, were also reported to be type I arabinofuranosidases (Sarch et al., 2019). A Bifidobacterial α-L-arabinofuranosidase isolated from *Bifidobacterium longum* subsp. *longum* has been

reported to show unique specificity for α-1,2-Araf in α-1,2/3-Araf doubly substituted arabinoxylan (Komeno et al., 2022).

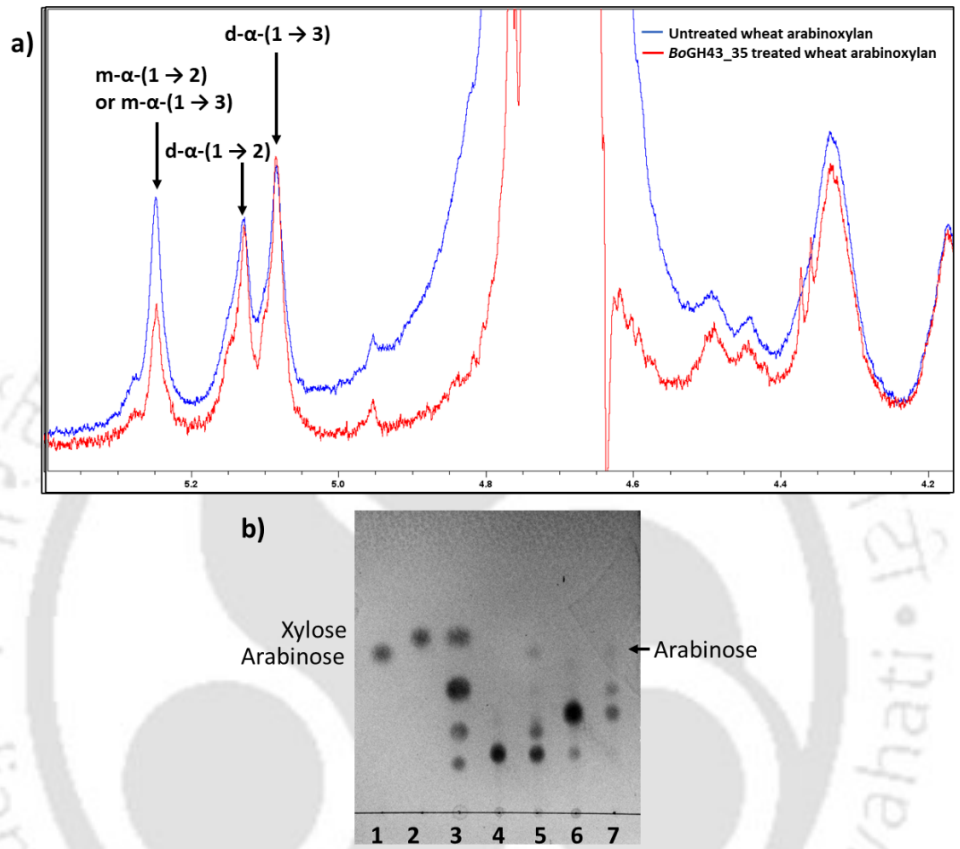

Fig. 3.9 Regioselectivity analysis of *Bo*GH43_35. a) Proton NMR of *Bo*GH43_35 untreated (in blue) and treated wheat arabinoxylan (in red) and b) TLC analysis showing regioselectivity of *Bo*GH43_35. Lanes: 1-Arabinose standard, 2-xylose standard, 3- mixture of xylose, xylobiose, xylotriose, xylotetraose standard, 4- A^2XX, lane 5- A^2XX + *Bo*GH43_35, 6- A^3X and 7- A^3X + *Bo*GH43_35

Furthermore, to elucidate the preference of α-L-arabinofuranosidase *Bo*GH43_35, for O-2 or O-3 position of the mono-substituted arabinoxylan, the TLC analysis of hydrolysed O-2 or O-3 substituted arabino-xylooligosaccharides *viz.* A^2XX (2^3-α-L-arabinofuranosyl-xylotriose having structural formula {α-L-Araf-(1 → 2)-β-D-Xylp-(1 → 4)-D-Xylp- β-D-Xylp-(1 → 4)-D-Xylp} and A^3X (3^2-α-L-arabinofuranosyl-xylobiose) with structural formula {α-L-Araf-(1→3)-β-D-Xylp-

(1→4)-D-Xylp} was performed (Fig. 3.9b). It was observed that there were spots near arabinose standard in lane 5 and lane 7 which indicated that *Bo*GH43_35 hydrolysed both A^2XX and A^3X substrates. This TLC analysis revealed that *Bo*GH43_35 acts at O-2 or O-3 substituted arabino-xylooligosaccharides classifying *Bo*GH43_35 as type I α-L-rabinofuranosidase and removes L-arabinose linked at O-2 or O-3 position of mono-substituted (m) arabinoxylan.

A schematic illustration of the mode of action of *Bo*GH43_35 on wheat arabinoxylan is depicted in Fig. 3.10. Wheat arabinoxylan consists of β-D-1,4-linked xylosyl residues substituted singly or doubly with L-arabinose residues at α-1,2- and/or α-1,3- positions. Initially, in first hour *Bo*GH43_35 predominantly removes α-1,2- or α-1,3-arabinofuranose (single substituted) present on xylopyranose residues of wheat arabinoxylan. After the removal of arabinose side-chains from wheat arabinoxylan, with the increase in incubation time (after 1 h), the endo-β-1,4-xylanase activity was observed which produces xylooligosaccharides such as xylobiose, xylotriose, xylotetraose, xylopentaose and xylohexaose, as shown in Fig. 3.10.

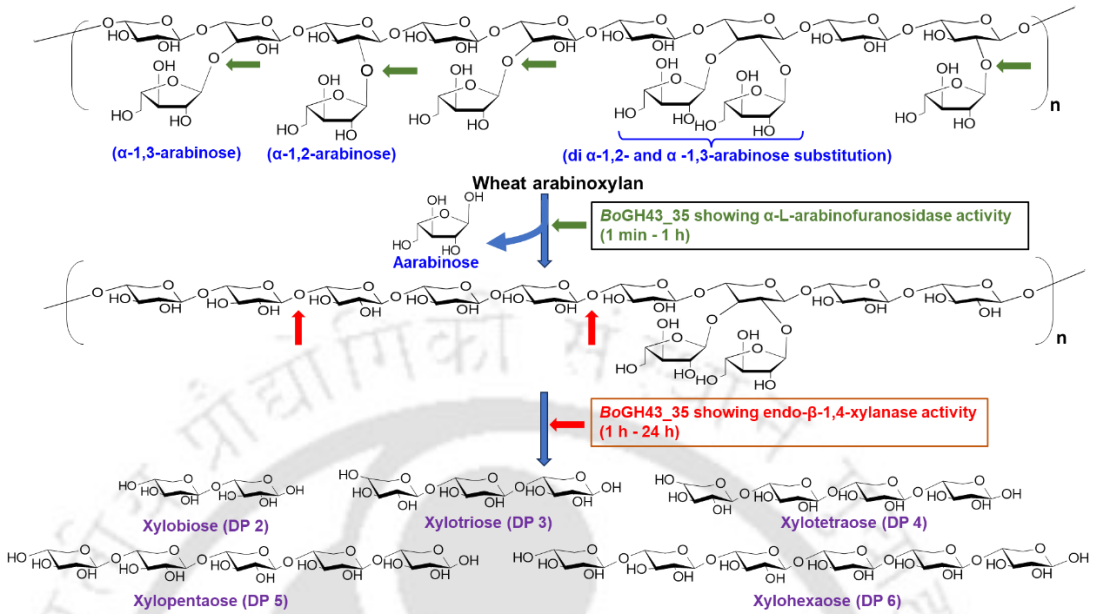

Fig. 3.10 Schematic illustration of wheat arabinoxylan cleavage pattern of bifunctional *Bo*GH43_35 showing α-L-arabinofuranosidase and endo-β-1,4-xylanase activities.

3.4 Conclusion

*Bo*GH43_35 from *B. ovatus* characterized in this study is a novel bifunctional α-L-arabinofuranosidase/endo-β-1,4-xylanase enzyme belonging to GH43 family. *Bo*GH43_35 expressed as a soluble protein of molecular mass 74.1 kDa. *Bo*GH43_35 showed mesophilic characteristics with maximum activity against wheat arabinoxylan at 37°C. *Bo*GH43_35 did not show any metal-ion dependence as its activity was not affected by the addition of metal-ions or any chelating agent. *Bo*GH43_35 hydrolysed wheat arabinoxylan with V_{max} 5.4 $U.mg^{-1}$ and K_M 2.7 $mg.mL^{-1}$. The melting temperature (T_m) of *Bo*GH43_35 was 41°C. The enzyme, *Bo*GH43_35 hydrolysed products of wheat arabinoxylan when subjected to TLC and HPLC analysis revealed its α-L-arabinofuranosidase as well as endo-β-1,4-xylanase activities. The release of xylotetraose, xylotriose and xylobiose from beechwood xylan and the release of shorter xylooligosaccharides from cleavage of xylopentaose and xylotetraose by *Bo*GH43_35 as analysed by TLC and MALDI-TOF MS confirmed its endo-β-1,4-xylanase activity. NMR analysis displayed that *Bo*GH43_35 removes L-arabinose at O-2 or O-3 position from mono-substituted arabinoxylan thereby categorizing it as type I α-L-arabinofuranosidase. This study makes *Bo*GH43_35 distinct from other GH43 xylanases characterized so far from *Bacteroides ovatus* ATCC 8483 owing to its initial type I α-L-arabinofuranosidase activity followed by endo-β-1,4-xylanase activity.

3.5 References

Ahmed, J., Kumar, K., & Goyal, A. (2023). A thermotolerant and pH stable rhamnogalacturonan acetylesterase (*Ct*Pae12B), a family 12 carbohydrate esterase from *Clostridium thermocellum* with broad substrate specificity. *International Journal of Biological Macromolecules*, *226*, 1560–1569. https://doi.org/10.1016/j.ijbiomac.2022.11.267

Borsenberger, V., Dornez, E., Desrousseaux, M.-L., Massou, S., Tenkanen, M., Courtin, C. M., Dumon, C., O'Donohue, M. J., & Fauré, R. (2014). A ^{1}H NMR study of the specificity of α-L-arabinofuranosidases on natural and unnatural substrates. *Biochimica et Biophysica Acta (BBA) - General Subjects*, *1840*(10), 3106–3114. https://doi.org/10.1016/j.bbagen.2014.07.001

Broekaert, W. F., Courtin, C. M., Verbeke, K., Van De Wiele, T., Verstraete, W., & Delcour, J. A. (2011). Prebiotic and other health-related effects of cereal-derived arabinoxylans, arabinoxylan-oligosaccharides, and xylooligosaccharides. *Critical Reviews in Food Science and Nutrition*, *51*(2), 178–194. https://doi.org/10.1080/10408390903044768

Collins, T., Gerday, C., & Feller, G. (2005). Xylanases, xylanase families and extremophilic xylanases. *FEMS Microbiology Reviews*, *29*(1), 3–23. https://doi.org/10.1016/j.femsre.2004.06.005

Fan, Z., Werkman, J. R., & Yuan, L. (2009). Engineering of a multifunctional hemicellulase. *Biotechnology Letters*, *31*(5), 751–757. https://doi.org/10.1007/s10529-009-9926-3

Fultz, R., Ticer, T., Ihekweazu, F. D., Horvath, T. D., Haidacher, S. J., Hoch, K. M., Bajaj, M., Spinler, J. K., Haag, A. M., Buffington, S. A., & Engevik, M. A. (2021). Unraveling the metabolic requirements of the gut commensal *Bacteroides ovatus*. *Frontiers in Microbiology*, *12*, 745469. https://doi.org/10.3389/fmicb.2021.745469

Gavande, P. V., Ji, S., Cardoso, V., M.G.A. Fontes, C., & Goyal, A. (2024). Reassigning the role of a mesophilic xylan hydrolysing family GH43 β-xylosidase from *Bacteroides ovatus*, *Bo*ExXyl43A as exo-β-1,4-xylosidase. *Current Research in Biotechnology*, *7*, 100191. https://doi.org/10.1016/j.crbiot.2024.100191

Gavande, P. V., Nath, P., Kumar, K., Ahmed, N., Fontes, C. M. G. A., & Goyal, A. (2022). Highly efficient, processive and multifunctional recombinant endoglucanase RfGH5_4 from *Ruminococcus flavefaciens* FD-1 v3 for recycling lignocellulosic plant biomasses. *International Journal of Biological Macromolecules*, *209*, 801–813. https://doi.org/10.1016/j.ijbiomac.2022.04.059

Jordan, D. B., Lee, C. C., Wagschal, K., & Braker, J. D. (2013). Activation of a GH43 β-xylosidase by divalent metal cations: Slow binding of divalent metal and high substrate specificity. *Archives of Biochemistry and Biophysics*, *533*(1–2), 79–87. https://doi.org/10.1016/j.abb.2013.02.020

Koh, A., De Vadder, F., Kovatcheva-Datchary, P., & Bäckhed, F. (2016). From dietary fiber to host physiology: Short-chain fatty acids as key bacterial metabolites. *Cell*, *165*(6), 1332–1345. https://doi.org/10.1016/j.cell.2016.05.041

Komeno, M., Yoshihara, Y., Kawasaki, J., Nabeshima, W., Maeda, K., Sasaki, Y., Fujita, K., & Ashida, H. (2022). Two α-L-arabinofuranosidases from *Bifidobacterium longum* subsp. *Longum* are involved in arabinoxylan utilization. *Applied Microbiology and Biotechnology*, *106*(5–6), 1957–1965. https://doi.org/10.1007/s00253-022-11845-x

Layne, E. (1957). Spectrophotometric and turbidimetric methods for measuring proteins. In *Methods in Enzymology* (Vol. 3, pp. 447–454). Elsevier. https://doi.org/10.1016/S0076-6879(57)03413-8

Leschonski, K. P., Mortensen, M. S., Hansen, L. B. S., Krogh, K. B. R. M., Kabel, M. A., & Laursen, M. F. (2024). Structure-dependent stimulation of gut bacteria by arabinoxylo-oligosaccharides (AXOS): A review. *Gut Microbes*, *16*(1), 2430419. https://doi.org/10.1080/19490976.2024.2430419

Limsakul, P., Phitsuwan, P., Waeonukul, R., Pason, P., Tachaapaikoon, C., Poomputsa, K., Kosugi, A., & Ratanakhanokchai, K. (2021). A novel multifunctional arabinofuranosidase/endoxylanase/β-xylosidase GH43 enzyme from *Paenibacillus curdlanolyticus* B-6 and its synergistic action to produce arabinose and xylose from cereal arabinoxylan. *Applied and Environmental Microbiology*, *87*(24), e01730-21. https://doi.org/10.1128/AEM.01730-21

Lowry, O. H., Rosebrough, N. J., Farr, A. L., & Randall, R. J. (1951). Protein measurement with the Folin phenol reagent. *The Journal of Biological Chemistry*, *193*(1), 265–275.

Margolles, A., & De Los Reyes-Gavilán, C. G. (2003). Purification and functional characterization of a novel α-L-arabinofuranosidase from *Bifidobacterium longum* B667. *Applied and Environmental Microbiology*, *69*(9), 5096–5103. https://doi.org/10.1128/AEM.69.9.5096-5103.2003

Meldrum, O. W., & Yakubov, G. E. (2024). Journey of dietary fiber along the gastrointestinal tract: Role of physical interactions, mucus, and biochemical transformations. *Critical Reviews in Food Science and Nutrition*, 1–29. https://doi.org/10.1080/10408398.2024.2390556

Mendis, M., & Simsek, S. (2014). Arabinoxylans and human health. *Food Hydrocolloids*, *42*, 239–243. https://doi.org/10.1016/j.foodhyd.2013.07.022

Nastasi, C., Candela, M., Bonefeld, C. M., Geisler, C., Hansen, M., Krejsgaard, T., Biagi, E., Andersen, M. H., Brigidi, P., Ødum, N., Litman, T., & Woetmann, A. (2015). The effect of short-chain fatty acids on human monocyte-derived dendritic cells. *Scientific Reports*, *5*(1), 16148. https://doi.org/10.1038/srep16148

Nelson, N. (1944). A photometric adaptation of the Somogyi method for the determination of glucose. *Journal of Biological Chemistry*, *153*(2), 375–380. https://doi.org/10.1016/S0021-9258(18)71980-7

Ríos-Covián, D., Ruas-Madiedo, P., Margolles, A., Gueimonde, M., De Los Reyes-Gavilán, C. G., & Salazar, N. (2016). Intestinal short chain fatty acids and their link with diet and human health. *Frontiers in Microbiology*, *7*. https://doi.org/10.3389/fmicb.2016.00185

Sarch, C., Suzuki, H., Master, E. R., & Wang, W. (2019). Kinetics and regioselectivity of three GH62 α-L-arabinofuranosidases from plant pathogenic fungi. *Biochimica et Biophysica Acta (BBA) - General Subjects*, *1863*(6), 1070–1078. https://doi.org/10.1016/j.bbagen.2019.03.020

Somogyi, M. (1945). A new reagent for the determination of sugars. *Journal of Biological Chemistry*, *160*(1), 61–68. https://doi.org/10.1016/S0021-9258(18)43097-9

Stoscheck, C. M. (1990). Quantitation of protein. *Methods in Enzymology*, *182*, 50–68. https://doi.org/10.1016/0076-6879(90)82008-p

Teeravivattanakit, T., Baramee, S., Phitsuwan, P., Waeonukul, R., Pason, P., Tachaapaikoon, C., Sakka, K., & Ratanakhanokchai, K. (2016). Novel trifunctional xylanolytic enzyme Axy43A from *Paenibacillus curdlanolyticus* strain B-6 exhibiting endo-xylanase, β-D-xylosidase, and arabinoxylan arabinofuranohydrolase activities. *Applied and Environmental Microbiology*, *82*(23), 6942–6951. https://doi.org/10.1128/AEM.02256-16

Thakur, A., Sharma, K., Jamaldheen, S. B., & Goyal, A. (2020). Molecular characterization, regioselective and synergistic action of first recombinant type III α-L-arabinofuranosidase of family 43 glycoside hydrolase (*Ps*GH43_12) from *Pseudopedobacter saltans*. *Molecular Biotechnology*, *62*(9), 443–455. https://doi.org/10.1007/s12033-020-00263-x

Wang, W., Wang, Y., Yi, H., Liu, Y., Zhang, G., Zhang, L., Mayo, K. H., Yuan, Y., & Zhou, Y. (2022). Biochemical characterization of two rhamnogalacturonan lyases from *Bacteroides ovatus* ATCC 8483 with preference for RG-I substrates. *Frontiers in Microbiology*, *12*, 799875. https://doi.org/10.3389/fmicb.2021.799875

Wang, X.-F., Chen, X., Tang, Y., Wu, J.-M., Qin, D.-L., Yu, L., Yu, C.-L., Zhou, X.-G., & Wu, A.-G. (2022). The therapeutic potential of plant polysaccharides in metabolic diseases. *Pharmaceuticals*, *15*(11), 1329. https://doi.org/10.3390/ph15111329

Wilkens, C., Andersen, S., Dumon, C., Berrin, J.-G., & Svensson, B. (2017). GH62 arabinofuranosidases: Structure, function and applications. *Biotechnology Advances*, *35*(6), 792–804. https://doi.org/10.1016/j.biotechadv.2017.06.005

Xie, Y., An, J., Yang, G., Wu, G., Zhang, Y., Cui, L., & Feng, Y. (2014). Enhanced enzyme kinetic stability by increasing rigidity within the active-site. *Journal of Biological Chemistry*, *289*(11), 7994–8006. https://doi.org/10.1074/jbc.M113.536045

Xu, B., Dai, L., Zhang, W., Yang, Y., Wu, Q., Li, J., Tang, X., Zhou, J., Ding, J., Han, N., & Huang, Z. (2019). Characterization of a novel salt-, xylose- and alkali-

tolerant GH43 bifunctional β-xylosidase/α-l-arabinofuranosidase from the gut bacterial genome. *Journal of Bioscience and Bioengineering*, *128*(4), 429–437. https://doi.org/10.1016/j.jbiosc.2019.03.018

Yang, W., Bai, Y., Yang, P., Luo, H., Huang, H., Meng, K., Shi, P., Wang, Y., & Yao, B. (2015). A novel bifunctional GH51 exo-α-L-arabinofuranosidase/endo-xylanase from *Alicyclobacillus sp.* A4 with significant biomass-degrading capacity. *Biotechnology for Biofuels*, *8*(1), 197. https://doi.org/10.1186/s13068-015-0366-0

Yang, X., Shi, P., Huang, H., Luo, H., Wang, Y., Zhang, W., & Yao, B. (2014). Two xylose-tolerant GH43 bifunctional β-xylosidase/α-arabinosidases and one GH11 xylanase from *Humicola insolens* and their synergy in the degradation of xylan. *Food Chemistry*, *148*, 381–387. https://doi.org/10.1016/j.foodchem.2013.10.062

Yang, X., Shi, P., Ma, R., Luo, H., Huang, H., Yang, P., & Yao, B. (2015). A New GH43 α-arabinofuranosidase from *Humicola insolens* Y1: Biochemical characterization and synergistic action with a xylanase on xylan degradation. *Applied Biochemistry and Biotechnology*, *175*(4), 1960–1970. https://doi.org/10.1007/s12010-014-1416-y

Yoo, S., Jung, S.-C., Kwak, K., & Kim, J.-S. (2024). The role of prebiotics in modulating gut microbiota: Implications for human health. *International Journal of Molecular Sciences*, *25*(9), 4834. https://doi.org/10.3390/ijms25094834

Zhang, X. J., Wang, L., Wang, S., Chen, Z. L., & Li, Y. H. (2021). Contributions and characteristics of two bifunctional GH43 β-xylosidase /α-L-arabinofuranosidases with different structures on the xylan degradation of *Paenibacillus physcomitrellae* strain XB. *Microbiological Research*, *253*, 126886. https://doi.org/10.1016/j.micres.2021.126886

Zhang, Z., Xiao, Z., & Linhardt, R. J. (2009). Thin layer chromatography for the separation and analysis of acidic carbohydrates. *Journal of Liquid Chromatography & Related Technologies*, *32*(11–12), 1711–1732. https://doi.org/10.1080/10826070902956402

Zhou, A., Hu, Y., Li, J., Wang, W., Zhang, M., & Guan, S. (2020). Characterization of a recombinant β-xylosidase of GH43 family from *Bacteroides ovatus* strain ATCC 8483. *Biocatalysis and Biotransformation*, *38*(1), 46–52. https://doi.org/10.1080/10242422.2019.1631813

Chapter 4

Structure and function analysis of bifunctional α-L-arabinofuranosidase/ endo-β-1,4-xylanase (*Bo*GH43_35) from *Bacteroides ovatus*

4.1 Introduction

The term 'hemicellulose' was coined by Schulze in 1891 to denote the fractions obtained from plant material by dilute alkali (Schulze, 1890). In nature, hemicellulose ranks as the second most abundant component of lignocellulosic polymers, next to cellulose. In the plant cell wall, it is closely associated with microfibrillar cellulose and lignin (Heredia et al., 1995). Based on the structural composition of hemicellulose, they are classified as xylan, xyloglucan, mannan, arabinan and β-glucans with mixed linkages (Qaseem et al., 2021). Xylan, a heteropolymer, is the major component of hemicellulosic polysaccharide and is composed of β-1,4-D-xylose backbone decorated with L-arabinofuranosyl, acetyl, glucuronyl, galactosyl and 4-O-methylglucuronyl

side-chains (Spiridon & Popa, 2008). Arabinoxylans have α-L-arabinofuranosyl substitutions at β-1,4-D-xylosyl residues through 1,2 and/or 1,3 glycosidic linkages (Mitchell et al., 2007). Thus, the β-D-xylosyl residues of the arabinoxylans are either unsubstituted, monosubstituted at O-2 position, monosubstituted at O-3 position or disubstituted at O-2 and O-3 positions (Broekaert et al., 2011). Additionally, at the O-5 position of some arabinose side chains, ferulic acid or *p*-coumaric acid is covalently attached (Pollet et al., 2010). Arabinoxylans have been of great importance in food production due to their functional properties such as the soluble arabinoxylans improve dough parameters in bread making (Buksa et al., 2012).

Arabinoxylans can be degraded by enzymatic catalysis. However, the substitutions present in arabinoxylan substrate and the presence of multiple types of bonds warrant concerted action of several enzymes to convert arabinoxylan to its constituent sugars (Sørensen et al., 2007). Arabinoxylan degrading enzymes are composed of glycoside hydrolases (GH) such as endo-β-1,4-xylanases (EC 3.2.1.8) and β-xylosidase that cleave the internal arabinoxylan backbone composed of β-1,4-linked xylose residues resulting in production of arabino-xylooligosaccharides and xylose residues, respectively (Wong et al., 1988). α-L-Arabinofuranosidases (EC 3.2.1.55) remove the arabinose substitutions from xylose main chain of arabinoxylans (Sturgeon, 1997). The glycoside hydrolases that display endo-β-1,4-xylanase activity are found in GH3, GH5, GH6, GH8, GH9, GH10, GH11, GH26, GH30, GH43, GH44, GH51, GH52, GH62 and GH141 families (http://www.cazy.org/Glycoside-Hydrolases.html). GH43 is one of the largest glycoside hydrolase families with 39 subfamilies (Mewis et al., 2016), accommodating 50,241 members, out of which only 229 are characterized

(http://www.cazy.org/GH43_characterized.html). GH43 enzymes perform hydrolysis of xylan substrates in a single-step reaction function by inverting-type mechanism (Smaali et al., 2006). The glycoside hydrolases that follow inverting-type reaction mechanism invert the anomeric configuration of carbon of the substrate (Sinnott, 1990). It occurs when a catalytic amino acid present at the active-site donates a proton to the anomeric carbon and the catalytic base oxidizes a water molecule by removing the proton which further promotes its attack on the anomeric carbon of the substrate. GH43 family also accommodates bifunctional xylanolytic enzymes such as β-xylosidase/α-L-arabinofuranosidases from *Clostridium stercorarium* (Sakka et al., 1993), rumen metagenome (Zhou et al., 2012), *Thermotoga thermarum* (Shi et al., 2013), *Bifidobacterium animalis* subsp. *lactis* BB-12 (Viborg et al., 2013), *Humicola insolens* (Yang et al., 2014).

The three-dimensional structure of N-terminal catalytic module of GH43 members, in all the subfamilies, display a similar five-bladed β-propeller fold (Lagaert et al., 2014). However, the difference in their structure lies at the C-terminal of GH43, where some of members have a β-sandwich fold, while others do not. Based on the occurrence of C-terminal domain and their amino acid sequence similarities, GH43 members are classified into different subfamilies from 1 to 39 (Mewis et al., 2016). The most frequently occurring non-catalytic module at the C-terminal of GH43 family is known as carbohydrate binding module of family 6 (CBM6). There are 271 members reported in GH43_35 with CBM6 at the C-terminal, of which 5 are characterized and structure of none have been determined (http://www.cazy.org/GH43_35_all.html). The common structural fold adopted by CBM6 is β-sandwich consisting of two opposing sheets of parallel or anti-parallel β-strands (Abbott et al., 2009).

B. ovatus is predominant human-gut microbe aiding the degradation of plant cell wall polysaccharides. Through complete genome analysis of *B. ovatus* ATCC 8483, a novel bifunctional α-L-arabinofuranosidase/endo-β-1,4-xylanase, *Bo*GH43_35 (GenBank Accession Number ALJ47148) belonging to glycoside hydrolase family 43 and subfamily 43_35 was identified. The gene encoding *Bo*GH43_35 (651 amino acid except signal peptide) from *B. ovatus* was cloned, expressed, purified to homogeneity by Immobilized Metal ion Affinity Chromatography (IMAC) purification technique and biochemically characterized. In this study, the structural and functional aspects of *Bo*GH43_35 were explored. The structural analysis of *Bo*GH43_35 gave insights about the secondary structure, three-dimensional structure and the conservation of functionally important residues at the active-site. The AF2 modeled three-dimensional structure of *Bo*GH43_35 when subjected to molecular dynamics simulation and ligand binding analysis by molecular docking study showed the interaction of *Bo*GH43_35 with its probable ligands. The change in the intrinsic fluorescence of *Bo*GH43_35 when bound to substrate, analysed by fluorescence spectroscopy was used to determine the association constant and number of binding sites. Moreover, the behaviour of *Bo*GH43_35 in solution was also analysed by determining its hydrodynamic radius and polydispersity index.

4.2 Materials and methods

4.2.1 Chemical, reagents and substrates

The chemical salts viz. sodium dihydrogen phosphate dibasic, sodium phosphate monobasic anhydrous, nickel sulphate, sodium chloride, calcium chloride, EDTA, IPTG, Imidazole, Luria-Bertani medium and kanamycin were purchased from Himedia Laboratories India Pvt Ltd. Wheat arabinoxylan (low viscosity) was procured from Megazyme Ltd., Ireland.

4.2.2 Amino acid sequence retrieval and analysis of *Bo*GH43_35

The full-length amino acid sequence of a novel bifunctional α-L-arabinofuranosidase/endo-β-1,4-xylanase, *Bo*GH43_35 belonging to GH43 family and subfamily 43_35 from *B. ovatus* ATCC 8483 with Genbank accession number ALJ47148 was recovered from NCBI database. The sequence similarity of *Bo*GH43_35 with its closest homologues was determined by BLASTp analysis of *Bo*GH43_35 against PDB database and UniProtKB/ SwissProt. SignalP 6.1 server was employed to predict the presence of signal peptide of *Bo*GH43_35 (https://services.healthtech.dtu.dk/services/SignalP-6.0/). The evolutionary analysis of *Bo*GH43_35 was studied by determining the phylogenetic tree with its closest homologues from GH43 family using Molecular Evolutionary Genetics Analysis 11 (MEGA 11) software (Tamura et al., 2021). The protein sequences of those closest homologues were extracted from UniProt database in FASTA format (https://www.uniprot.org/). Initial multiple sequence alignment of *Bo*GH43_35 was done by employing ClustalW, included in MEGA 11 software. The phylogenetic tree was constructed, with gap penalty 10 followed by Neighbour-Joining method and Poisson correction model using a bootstrap statistical assessment of 1000 replicates.

The conserved domain boundaries of *Bo*GH43_35 were predicted by employing NCBI-Conserved Domains Database (https://www.ncbi.nlm.nih.gov/cdd/) and InterProScan web service (https://www.ebi.ac.uk/interpro/search/sequence/). Clustal Omega (http://www.ebi.ac.uk/Tools/msa/clustalo/) was employed to execute multiple sequence alignment (MSA) of *Bo*GH43_35 with its homologous protein sequences to identify the evolutionary conserved and semi-conserved amino acid residues as well as the catalytic residues. The MSA results were later visualized and analyzed by Esprit 3.0 tool (https://espript.ibcp.fr/ESPript/cgi-bin/ESPript.cgi).

4.2.3 Homology modeling of *Bo*GH43_35 and energy minimization

The three-dimensional structure modeling of *Bo*GH43_35 was performed by using AlphaFold2 (AF2) server. The AF2, is a machine learning algorithm developed by DeepMind, that predicts the three-dimensional structure of a protein based on its amino acid sequence (Guo et al., 2022). The amino acid sequence of *Bo*GH43_35 (without signal peptide) was uploaded in AF2 server. Based on the per-residue confidence measure, i.e. the predicted local distance difference test (plDDT) score of the all the predicted models, the best modeled structure of *Bo*GH43_35 with highest plDDT score was obtained. The plDDT score denotes the confidence of the predicted structure. The modeled structure of *Bo*GH43_35 was subjected to Yet Another Scientific Artificial Reality Application (YASARA) server for overall energy minimization (https://www.yasara.org/minimizationserver.htm). YASARA server uses its inbuilt YASARA forcefield to carry out energy minimization and requires the protein model in PDB format. Energy minimization of the modeled structure is necessary to optimize the hydrogen bond networks and spatial arrangement of amino acid residues in order obtain lowest possible energy of the system (Land & Humble,

2018). The topology diagram of *Bo*GH43_35 structure was generated by uploading its PDB file in PDBSum database (Laskowski et al., 1997).

4.2.4 Three-dimensional structure validation and quality assessment of *Bo*GH43_35

The quality of the energy minimized three-dimensional structure of *Bo*GH43_35 was assessed by SAVESv6.1, a structure validation server (https://saves.mbi.ucla.edu/). The PDB file format of the *Bo*GH43_35 modeled structure was uploaded on UCLA-DOE LAB-SAVES v6.1 site to determine the ERRAT score, Verify3D score and Ramachandran plot generated by PROCHECK. ERRAT score is defined in terms of overall quality factor for the non-bonded atomic interactions, where a score higher than 80% implies higher quality of the protein structure (Colovos & Yeates, 1993). Verify3D computes the compatibility of 3D atomic model of a protein with its own amino acid sequence (Eisenberg et al., 1997). PROCHECK by Ramachandran plot analysis reveals the accuracy and stereochemical quality of the modeled structure (Laskowski et al., 1993). The modeled three-dimensional structure of *Bo*GH43_35 was also validated by ProSA web server (https://prosa.services.came.sbg.ac.at/prosa.php). It was achieved by submitting its atomic coordinates in PDB format in ProSA server which produces an energy plot showing the local model quality of the modeled structure of *Bo*GH43_35.

4.2.5 Determination of secondary structure composition of *Bo*GH43_35

The gene (1,956 bp) encoding *Bo*GH43_35 from *B. ovatus* including 57 bp sequence coding for N-terminal pHTP1-vector sequence with His-6 tag was expressed in *Escherichia coli* BL21 (DE3) cells and purified to homogeneity using Immobilized Metal-ion Affinity Chromatography as reported earlier (Chapter 3, Section 3.2.2). For

secondary structure analysis, *Bo*GH43_35 at a concentration of 0.1 mg/mL dissolved in 0.05 M sodium phosphate buffer (pH 7.0) was subjected to Circular Dichroism (CD) analysis and the spectrum in Far UV range (190-250 nm) was recorded using a spectropolarimeter (Jasco-81, Japan) equipped with Peltier temperature controller. The CD data were collected at 25ºC using a quartz cuvette of 1 mm path length and the scanning rate of 50 nm/min was kept constant to obtain the spectrum along with 1 nm bandwidth with an average of 5 scans. The CD data were processed to calculate Mean residual ellipticity (MRE) and plotted against the wavelength. The secondary structure content of *Bo*GH43_35 was estimated by a web-based K2D3 server (https://cbdm-01.zdv.uni-mainz.de/~andrade/k2d3/) as the percentage of α-helices, β-strands and coils.

The secondary structure elements of *Bo*GH43_35 was also evaluated by submitting its PDB format to online server, 2Struc (https://2struc.cryst.bbk.ac.uk/twostruc) and by submitting its sequence in FASTA format to server, PSIPRED 4.0 (http://bioinf.cs.ucl.ac.uk/psipred/) and predicted structures were compared with the secondary structure data obtained through CD analysis.

4.2.6 Molecular dynamic simulation of *Bo*GH43_35

The dynamic perturbations of AlphaFold2 predicted three-dimensional structure of *Bo*GH43_35 was studied by carrying out Molecular Dynamics (MD) simulation of *Bo*GH43_35 employing Gromacs v2019.6 software package (Berendsen et al., 1995) equipped in PARAM-ISHAN, a supercomputing facility at Indian Institute of Technology Guwahati, Guwahati, India. MD simulation of a protein enables the analysis of its conformational changes over time and its stability. The protein force

calculations of *Bo*GH43_35 was done by employing CHARMM36 all-atom force-field (Tabasi et al., 2023) and modified TIP3P water model. TIP3P water model is a 3-site rigid water molecule with charges and Lennard-Jones parameters (Boonstra et al., 2016). The 3D structure of *Bo*GH43_35 was placed in a cubic box of dimension of length, breadth and height 10.77 nm with 38389 water molecules for hydration. The single negative charge on total charge on *Bo*GH43_35 was neutralized by addition of one sodium counter ion. The steric clashes of the hydrated protein structure were eliminated by performing energy minimization using 50,000 iteration steps using the steepest descent method until the maximum force less than 1000 kJ/min/nm was achieved. Long-range electrostatic interactions were evaluated by using the Particle Mesh Ewald (PME) method. The non-bonded pair list cut-off was 1 nm. Two phases of sequential equilibration of the system were carried, each for 1,000 ps. The first stage of equilibration was isochoric and isothermal NVT ensemble with constant number of particles, volume and temperature of 300 K. The other stage was NPT (constant no. of particles, pressure and temperature) condition with pressure of 1 bar and temperature 300 K. A V-rescale, modified Berendsen thermostat (Berendsen et al., 1984) at 300 K was used to control system's temperature with a time constant of 0.1 ps. The Parrinello-Rahman barostat was used to keep the system's pressure constant with a time constant of 2 ps (Ke et al., 2022). After the equilibration, simulation for 200 ns was carried out and at every 2 fs, the equations of motion were integrated using a leapfrog integrator. The atomic coordinates were recorded every 1.0 ps and a trajectory file was generated for further analysis. Linear Constraint Solver (LINCS) algorithm was used for the correction of rotational bond lengths (Hess et al., 1997). Upon completion of 200 ns run, the generated trajectories were analyzed for structural stability in the solvent

system. The compactness of the *Bo*GH43_35 structure was evaluated by calculating radius of gyration (Rg) with *gmx gyrate* command. The alteration in the backbone of *Bo*GH43_35 was analysed by calculating the root mean square deviation (RMSD) by using *gmx rmsd* command. The structural flexibility was determined by root mean square fluctuation (RMSF) calculation with *gmx rmsf* command. The solvent accessible surface area (SASA) of *Bo*GH43_35 was computed by *gmx sasa* command and number of intramolecular H-bonds were determined by *gmx hbond* command. All the respective plots were generated by using the software GraphPad Prism 8.4.3 and MD simulated structure obtained was visualized by PyMOL v2.5.2.

4.2.7 Active-site and subsites prediction of *Bo*GH43_35

The theoretical active-site of *Bo*GH43_35 was identified using Computed Atlas of Surface Topography of proteins (CASTp) server (http://sts.bioe.uic.edu/castp/calculation.html) that provides insights into the volume and area of the binding pocket, along with the amino acid residues constituting it. The structure of *Bo*GH43_35 in its PDB format was submitted with a default probe radius of 1.4 Å to calculate solvent accessible surface area (Tian et al., 2018).

4.2.8 Binding analysis of *Bo*GH43_35 with ligands by Molecular Docking

The interactions of *Bo*GH43_35 with the probable ligands were assessed by molecular docking studies using AutoDock v4.2.7 integrated into MGL Tools (version 1.5.6). The active-site residues of *Bo*GH43_35 involved in the interaction with xylose and xylo-oligosaccharides (xylobiose, xylotriose, xylotetraose and xylopentaose) and arabinose, and arabinose substituted xylooligosaccharides (arabinoxylobiose and arabinoxylotriose) were also determined. The three-dimensional coordinates of xylo-

oligosaccharides and arabino-xylooligosaccharides were downloaded in xml format from PubChem database (http://www.ncbi.nlm.nih.gov) which was further converted to PDB format using Open Babel (O'Boyle et al., 2011). The most stable conformation of xylo-oligosaccharides and arabino-xylooligosaccharides were obtained by YASARA energy minimization server (https://www.yasara.org/minimizationserver.htm). Polar hydrogens were added to *Bo*GH43_35 (receptor), Kollman's charges were added to achieve energy minimization of the receptor and saved in PDBQT format. All the ligands were prepared by assigning torsion angles and saved in PDBQT format. The grid box of 65.6, 56.2, 54.7 coordinates with size of 38 x-points, 28 y-points and 30 z-points was used to cover the active-site of *Bo*GH43_35. The pre-docking energy grid maps for docking analysis were computed with the AutoGrid module of AutoDock v4.2.7 tools. Lamarckian Genetic Algorithm (LGA) search was conducted to generate 100 conformations of *Bo*GH43_35-ligand complexes with 25,000,000 as the maximum number of energy evaluation and 27,000 as the number of generations. The mutation rate was set as 0.02 and crossover rate as 0.80. The iterations of Solis & Wets local search were set as 300 (Roy et al., 2014). The best conformation of *Bo*GH43_35-ligand interaction based on the binding energy was studied and was visualized in PyMOL v2.5. The hydrophobic and polar contacts of the receptor-ligand interaction was generated by LigPlot+.

4.2.9 MD simulation of protein-ligand (*Bo*GH43_35-arabinose) complex

The best docked complex of *Bo*GH43_35 and arabinose having the lowest binding energy determined by molecular docking was chosen for integrity and stability analyses. *Bo*GH43_35-arabinose complex were simulated by Gromacs v2019.6 software package (Berendsen et al., 1995) equipped in PARAM-ISHAN, the

supercomputing facility at Indian Institute of Technology Guwahati, Guwahati, India. The all-atom protein force-field, CHARMM36 with modified TIP3P water model, was used for force calculations of the *Bo*GH43_35-arabinose complex whereas, the topology of arabinose was generated by employing SwissParam tool (http://www.swissparam.ch/) to make it compatible for CHARMM36 all-atom force-field. The *Bo*GH43_35-arabinose complex was embedded in cubic box with 26,434 solvent water molecules. The equilibration of the system was done as mentioned earlier in section 4.2.6. The first stage of equilibration included isochoric and isothermal NVT ensemble with constant number of particles, volume and temperature of 300 K followed by NPT (constant no. of particles, pressure and temperature) condition with pressure of 1 bar and temperature 300 K. After the equilibration of the system, the production run for 200 ns was performed at integration time, 2 fs. The atomic coordinates were recorded every 1.0 ps and a trajectory file was generated for subsequent analysis. The simulated complex, *Bo*GH43_35-arabinose was analysed for its average RMSD of the protein and ligand from the backbone, RMSF, Rg, SASA and number of intramolecular hydrogen bonds using GROMACS commands *gmx rmsd, gmx rmsf, gmx gyrate, gmx sasa* and *gmx hbond,* respectively. The MD simulation results of the complex was compared with that of individual simulation of *Bo*GH43_35 protein structure. The respective plots were generated by using the software GraphPad Prism 8.4.3 and MD simulated structure obtained was visualized in PyMOL v2.5.2.

4.2.10 Binding analysis of *Bo*GH43_35 and wheat arabinoxylan by Fluorescence spectroscopy

*Bo*GH43_35 showed a maximum specific activity of 4.9 U/mg against 1.0% (w/v) wheat arabinoxylan in 0.05 M sodium phosphate buffer, pH 7.0 at 37ºC and 2

min reaction time (Chapter 2, Section 3.3.3.2). Therefore, the change in the intrinsic fluorescence of *Bo*GH43_35 on binding to wheat arabinoxylan was studied by analysing its fluorescence spectra. *Bo*GH43_35 at a concentration of 674 µM (0.05 mg/mL) was incubated with wheat arabinoxylan at varying concentrations (0.15%, 0.20%, 0.35%, 0.4%, and 0.45%, w/v) in 0.05 M sodium phosphate buffer, pH 7.0 in 1000 µl reaction mixture at 4°C for 2 h. Their respective blanks were prepared by taking only wheat arabinoxylan in 0.05 M sodium phosphate buffer, pH 7.0 without adding *Bo*GH43_35, instead equal volume of 0.05 M sodium phosphate buffer, pH 7.0 was added. The fluorescence spectra were recorded using a fluorimeter (Fluoromax 3, Horiba Scientific, USA). The entrance and exit slit widths were kept 5.0 nm for both with 0.1 s integration time. The enzyme reaction samples were subjected to excitation at λ_{max}=295 nm for tryptophan fluorescence and their emission spectra were recorded in the wavelength range,300-450 nm (Ghosh et al., 2013). Averaged scans of 5 accumulations were recorded for each sample. Their respective blanks were also measured as a control in order to minimise the noise from the buffer and wheat arabinoxylan and were subtracted for correction. The inner filter effect, an error in fluorescence measurement, was minimized by the inbuilt instrument-based correction while computing the fluorescence intensity of samples as well as by keeping all the samples in appropriate dilutions (Sarzehi & Chamani, 2010). The association constant, K_a of *Bo*GH43_35 complex with wheat arabinoxylan was derived by modified Stern Volmer equation (Ghosh et al., 2013) as follows

$$\log\left(\frac{Fo - F}{F}\right) = \log Ka + n \times \log[Polysaccharide]$$

Where, the relative fluorescence intensity is given, Fo-F/F, where, Fo is initial fluorescence intensity of *Bo*GH43_35 and F is final fluorescence intensity of *Bo*GH43_35-wheat arabinoxylan complex. The change in Gibb's free energy was also determined by the equation as follows

$$\Delta G = -RTlnKa$$

Where, ΔG is the change in Gibb's free energy (kJoule $mole^{-1}$), R is the gas constant (Joule K^{-1} mol^{-1}), T is temperature in Kelvin and K_a is the association constant (M^{-1}) (Rezaei et al., 2024).

4.2.11 Size distribution analysis of *Bo*GH43_35 by Dynamic Light Scattering

The particle size of *Bo*GH43_35 and its behaviour in aqueous environment was analyzed by Dynamic Light Scattering (DLS), Litesizer 500, manufactured by Anton Paar (Graz, Austria). The purified *Bo*GH43_35 was centrifuged at 13,000 ×g, 10 min, 4 °C and filtered using a syringe filter with a membrane of pore size 0.25 µm (Pall Corporation, USA) to prepare samples at two different concentrations (0.5 and 1.0 mg/mL) in 0.05 M sodium phosphate buffer, pH 7.0. Both the dilutions of *Bo*GH43_35 were subjected to dynamic light scattering at backscatter angle (175°) with an average of 10 runs per sample analysis. The instrument was kept at a constant temperature, 25°C by using its inbuilt Peltier temperature controller. The apparent hydrodynamic diameter (D_h) and polydispersity index of *Bo*GH43_35 were derived from the DLS analysis. Additionally, D_h of *Bo*GH43_35 at 1.0 mg/mL (13 mM) with 13 mM arabinose was also determined.

The electrophoretic mobility and zeta potential of *Bo*GH43_35 were obtained by subjecting 600 µL each of 0.5 mg/mL, 1.0 mg/mL and 1.0 mg/mL with 13 mM

arabinose for the analysis. A total of 60 processed runs were performed at 25°C in an Omega electrode cuvette keeping equilibration time of 1 min in all the sample analysis. The values of electrophoretic mobility are related to zeta potential by Henry's equation,

$$\zeta = \frac{3\eta}{2\varepsilon F(Ka)} \mu_e$$

where, ζ is the zeta potential of proteins, η is the viscosity of the medium, ε is dielectric constant of water, *F(Ka)* is Henry's function and μ_e is the electrophoretic mobility of the protein (Jachimska et al., 2008). The zeta potential, ζ is the measure of net surface charge that a protein acquires in a particular environment. The surface charge of protein, whether positive or negative ξ, denotes the stability of protein in aqueous environment (Kumari et al., 2018).

4.3 Results and Discussion

4.3.1 Protein sequence retrieval of *Bo*GH43_35 and its analysis

The protein sequence of *Bo*GH43_35 from *B. ovatus* ATCC 8483 with locus tag Bovatus_02523 and GenBank Accession number ALJ47148 was retrieved from NCBI database (http://www.ncbi.nlm.nih). BLASTp analysis of *Bo*GH43_35 against PDB database showed highest percent identity of 28.13% with an alpha-L-arabinofuranosidase (*Ct*GH43) from *Acetivibrio thermocellus* ATCC 27405 (PDB ID: 5A8C) followed by 27.16% with a beta-xylosidase from an uncultured bacterium (PDB ID: 4MLG), 26.82% with a GH43_1 enzyme from *Xanthomonas citri* (PDB ID: 6XN0), 26.46% with a GH43 from an uncultured bacterium, 26.11% with a beta-1, 4-xylosidase from *Pseudopedobacter saltans* (PDB ID: 8HCJ) and 25.81% with GH43 beta-xylosidase/alpha-arabinofuranosidase Xsa43E from *Butyrivibrio proteoclasticus* (PDB ID: 4NOV) as given in Table 4.1. The phylogenetic analysis showed that *Bo*GH43_35 shares closest relationship and belongs to the same clade with that of xylosidase/arabinofuranosidase from *Thermoclostridium stercorarium* (Fig. 4.1). The branch length from the node is proportional to the divergence through evolution (Britton et al., 2007). Although there was some difference in branch lengths between them, showing some sequence divergence, but, 99% bootstrap value reflects high reliability of the evolutionary analysis. The MSA analysis of protein sequence of *Bo*GH43_35 with the sequences mentioned above (procured from PDB) determined the conserved as well as semi-conserved amino acid residues (Fig. 4.2). MSA with all the homologues revealed Asp34 and Glu251 as the catalytic residues, where Asp34 acts as a proton donor and Glu251 acts as a nucleophile. The full-length amino acid sequence of *Bo*GH43_35 was analysed which highlighted the presence of a 24 amino acid residue

long signal peptide at the N-terminal of *Bo*GH43_35. The gene encoding full length *Bo*GH43_35 (670 amino acids) excluding the signal peptide was cloned (Chapter 2, Section 2.3.3). *Bo*GH43_35 protein consisted of 670 amino acids containing a 19 amino acid sequence of pHTP1 vector including His_6-tag at the N-terminal (MGSSHHHHHHSSGPQQGLR) followed by GH43_XylA-like catalytic module (residue 38-363), CBM6A (residue 445-573) and CBM6B (residue 584 to 670) at the C-terminal.

Table 4.1. BLASTp analysis of amino acid sequence of *Bo*GH43_35.

Microorganism Name	Enzyme	Query cover (%)	Identity (%)	E-value	PDB ID
Clostridium thermocellum	Arabinofuranosidase	51	28.13	4e-09	5A8C
Butyrivibrio proteoclasticus	Arabinofuranosidase	39	25.81	2e-08	4NOV
Pseudopedobacter saltans	Xylosidase	57	26.11	2e-06	8HCJ
Uncultured bacterium	-	36	26.46	2e-06	5GLK
Uncultured bacterium	Xylosidase	34	27.16	3e-06	4MLG
Xanthomonas citri	Xylosidase	47	26.82	1e-05	6XN0

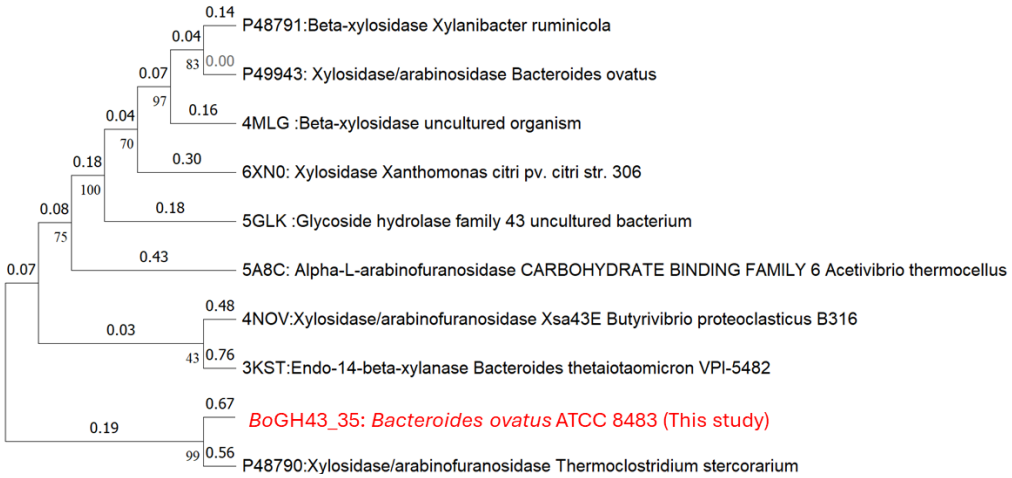

Fig. 4.1 Cladogram depicting a phylogenetic tree of *Bo*GH43_35 with its closest homologues by Neighbour-Joining method.

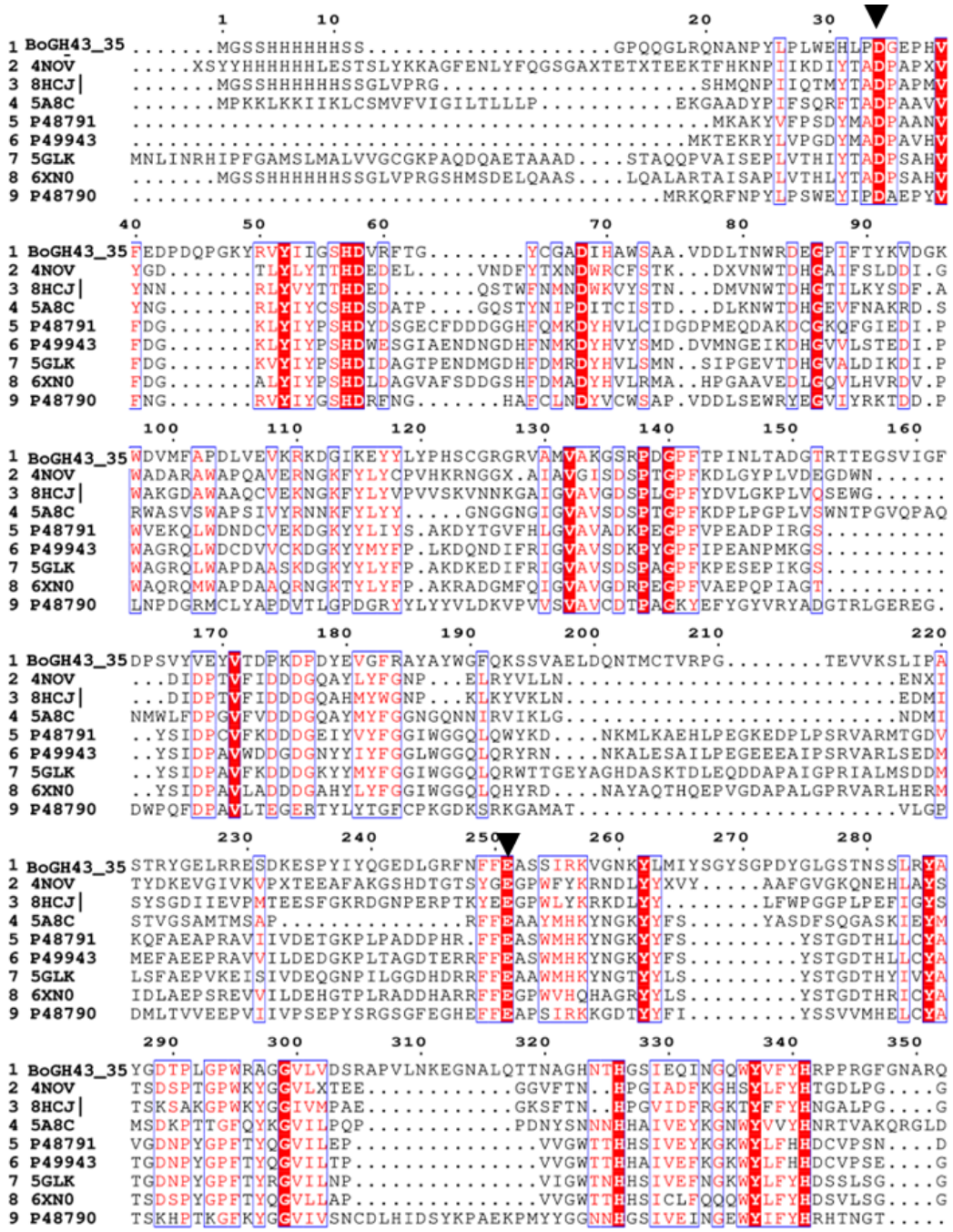

Fig. 4.2. MSA of *Bo*GH43_35 with homologous sequences. Amino acid residues represented with red color show conserved and amino acid residues with white color background show semi-conserved residues. The catalytic residues (Asp34 and Glu251) are displayed by black inverted triangle.

4.3.2 Three-dimensional structure of *Bo*GH43_35 by homology modeling

The accurate prediction of three-dimensional structure of a protein accelerates the understanding of protein structure and function relationships (Guo et al., 2022). Therefore, to get in-depth knowledge of *Bo*GH43_35 structure, it was modeled into a three-dimensional structure by AlphaFold2. The best AF2 modeled structure of *Bo*GH43_35 showed a pLDDT score of 94.4 and predicted Template Modeling (pTM) score of 0.927. The three-dimensional structure analysis of *Bo*GH43_35 displayed 5-bladed β-propeller fold adopted by N-terminal, GH43 catalytic module of *Bo*GH43_35 spanning from Met1-Asp363 (including 19 amino acid residues of pHTP1 vector with His_6-tag) as shown in Fig. 4.2a. The 5-bladed β-propeller fold is the conserved signature fold of GH43 members. Moreover, the catalytic amino acid residues, Asp34 and Glu251 were also present in the catalytic module and the two were 6.7 Å apart as shown in Fig. 4.2b depicting single-displacement or an inverting-type mechanism followed by *Bo*GH43_35. In single-displacement mechanism, a water molecule attacks the anomeric carbon of the substrate simultaneously with the acidic amino acid residue, donating a proton to the glycosidic oxygen and inverting the stereochemistry at the anomeric carbon (Mayes et al., 2016). The modeled structure of *Bo*GH43_35 also displayed that the two independently folded CBM6A (from Cys445- Lys573) and a C-terminal CBM6B (from Glu584-Lys670) took up jellyroll type β-sandwich fold. CBM6A of *Bo*GH43_35 consisted of four anti-parallel β-strands on one face and three anti-parallel β-strands on other face as shown Fig. 4.2c. The four anti-parallel β-strands are connected with loops of varying lengths. The jellyroll type β-sandwich fold adopted by C-terminal CBM6B consisted of 4 anti-parallel β-strands on one face and two anti-parallel β-strands on other face (Fig. 4.2c). Similar three-dimensional structure was

also observed for a GH43 α-L-arabinofuranosidase (GenBank Accession ID ABN52503.1) from *Clostridium thermocellum* (Sharma et al., 2021). The modeled structure of *Bo*GH43_35 was refined by energy minimization, which was used for further analysis. The numbering and nomenclature of the α-helices and β-strands involved in the formation of 5-bladed β-propeller fold and jellyroll type β-sandwich fold were corroborated by the topology diagram obtained by PDBSum server. The topology diagram of *Bo*GH43_35 showed that the 5-bladed β-propeller fold of *Bo*GH43_35 consists of 5 β-sheets (5 blades) in which one β-sheet (blade I) comprises 5 anti-parallel β-strands whereas, three β-sheets (blade II, III and IV) each containing four anti-parallel β-strands, whereas one β-sheet (blade V) is composed of only three anti-parallel β-strands (Fig. 4.2c).

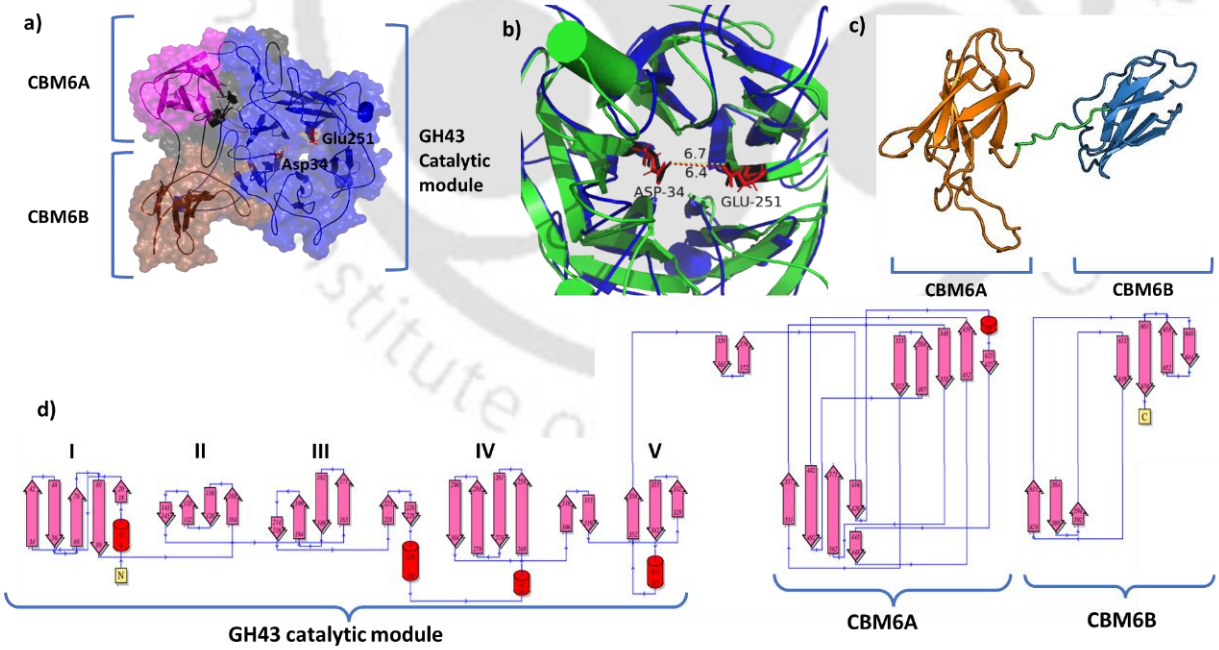

Fig. 4.2. a) Three-dimensional modeled structure of *Bo*GH43_35, b) bond length between the catalytic residues, Asp34 and Glu251, c) jellyroll type β-sandwich fold adopted by CB6A and CBM6B and d) topology diagram of *Bo*GH43_35 by PDBSum.

4.3.3 Quality assessment and validation of three-dimensional structure of *Bo*GH43_35

The energy minimized structure of *Bo*GH43_35 was validated using ERRAT, VERIFY 3D, Ramachandran plot by PROCHECK and ProSA. ERRAT plot shows the statistics of the non-bonded atomic interactions which is expressed as the percentage of the protein for which the calculated error value falls below the 95% rejection limit. The ERRAT plot of *Bo*GH43_35 produced satisfactory result with average overall quality factor of 92.3% (Fig. 4.3a). The Verify_3-D results revealed that 89% of amino acids of modeled structure of *Bo*GH43_35 has a 3D-1D score, ≥0.2 which indicated the compatibility of the amino acids with modeled structure (Fig. 4.3b). The quality of the modeled structure of *Bo*GH43_35 was also assessed by Ramachandran plot through PROCHECK, that gives a statistical report of the torsional angles of the amino acids of *Bo*GH43_35 structure. Based on the phi (φ) and psi (ψ) dihedral angles adopted by the amino acids of *Bo*GH43_35, they are depicted in the allowed (low-energy), generously allowed (moderate-energy) and disallowed region (high-energy). It was observed that modeled structure of *Bo*GH43_35 shows 89.1% of the amino acid residues are located in the most favoured region, 10.4% in additional allowed region, only 0.5% residues (Cys65, Arg345 and Asp504) in the generously allowed region and none of the amino acid residue was found in the disallowed region. This suggested that the amino acid residues in *Bo*GH43_35 structure adopt the favorable phi (φ) and psi (ψ) dihedral angles (Fig. 4.3c). ProSA results showed a Z-score of −9.5 of the modeled *Bo*GH43_35, implying that the *Bo*GH43_35 structure is error-free and falls within the range of experimentally determined X-ray crystallography structures (Fig. 4.3d). The energy profile of *Bo*GH43_35 generated by local energy plot, which assesses the overall

quality of modeled structure based on the amino acid sequence showed an overall negative energy value, indicating high quality of the modeled structure (Fig. 4.3e). Thus, all the results from ERRAT, Verify-3D, Ramachandran plot and PROSA confirmed that the generated model of *Bo*GH43_35 is reliable and of good quality and can be used for further studies.

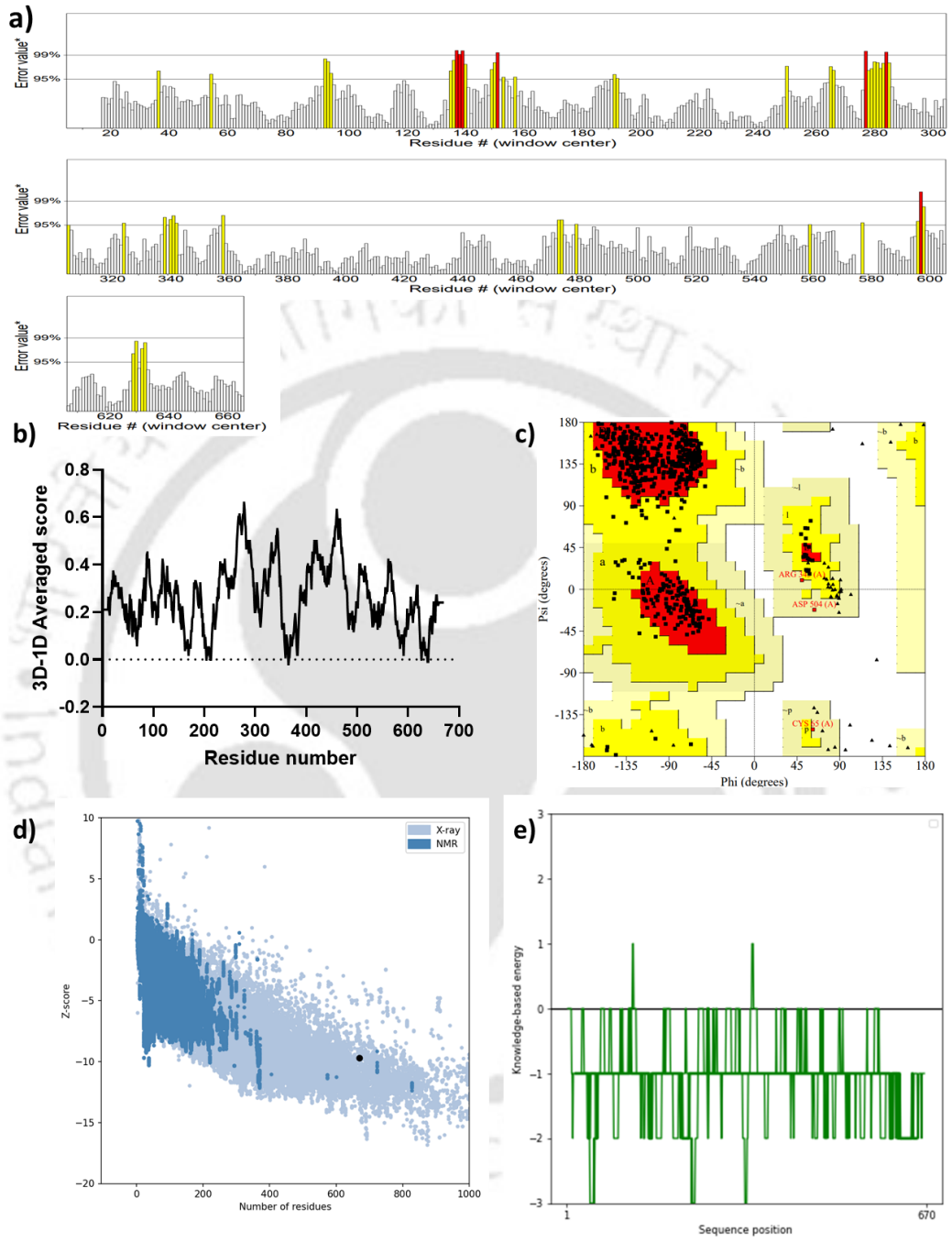

Fig. 4.3. Validation of three-dimensional structure of *Bo*GH43_35. a) Residue vs error value by ERRAT plot showing overall quality factor of 92.3%, b) Verify 3D plot showing 3D-1D score ≥0.2 of 89% c) Ramachandran plot using PROCHECK showing 89.1% residues in most favoured region, 10.4% in additional allowed region, only 0.5% residues in the generously allowed region and none of the amino acid residue in the disallowed region d) overall quality factor by ProSA analysis showing Z-score of -9.5 and e) overall negative energy by local energy plot.

4.3.4 Secondary structure analysis of *Bo*GH43_35

There are four hierarchies of a protein structure: primary, secondary, tertiary and quaternary structure. The three-dimensional structure and functional characteristics of a protein is determined by its tertiary and quaternary structure. Whereas, the secondary structure of a protein is a link between its primary and tertiary structure (Jiang et al., 2017). The purified *Bo*GH43_35 when subjected to secondary structure analysis by Circular Dichroism and analysed by the server, K2D3, displayed the presence of 2.2% α-helix, 28.9% β-strand and 68.9% random coil. A plot of Far-UV spectrum of *Bo*GH43_35 was generated as shown in (Fig. 4.4a). These results aligned with the composition of secondary structure elements of *Bo*GH43_35 predicted by PsiPred (Table 4.2) that revealed 2.3% α-helix, 35.3% β-strand and 63.2% random coil (Fig. 4.4b). Moreover, the secondary structure elements of the homology modeled structure of *Bo*GH43_35 by AF2 (2.0% α-helices, 34.7% β-strands and 63.3% random coils) were also in agreement with the above Psipred predicted and CD results. The agreement between experimental and computational results underscores the reliability and accuracy of secondary structure prediction of *Bo*GH43_35.

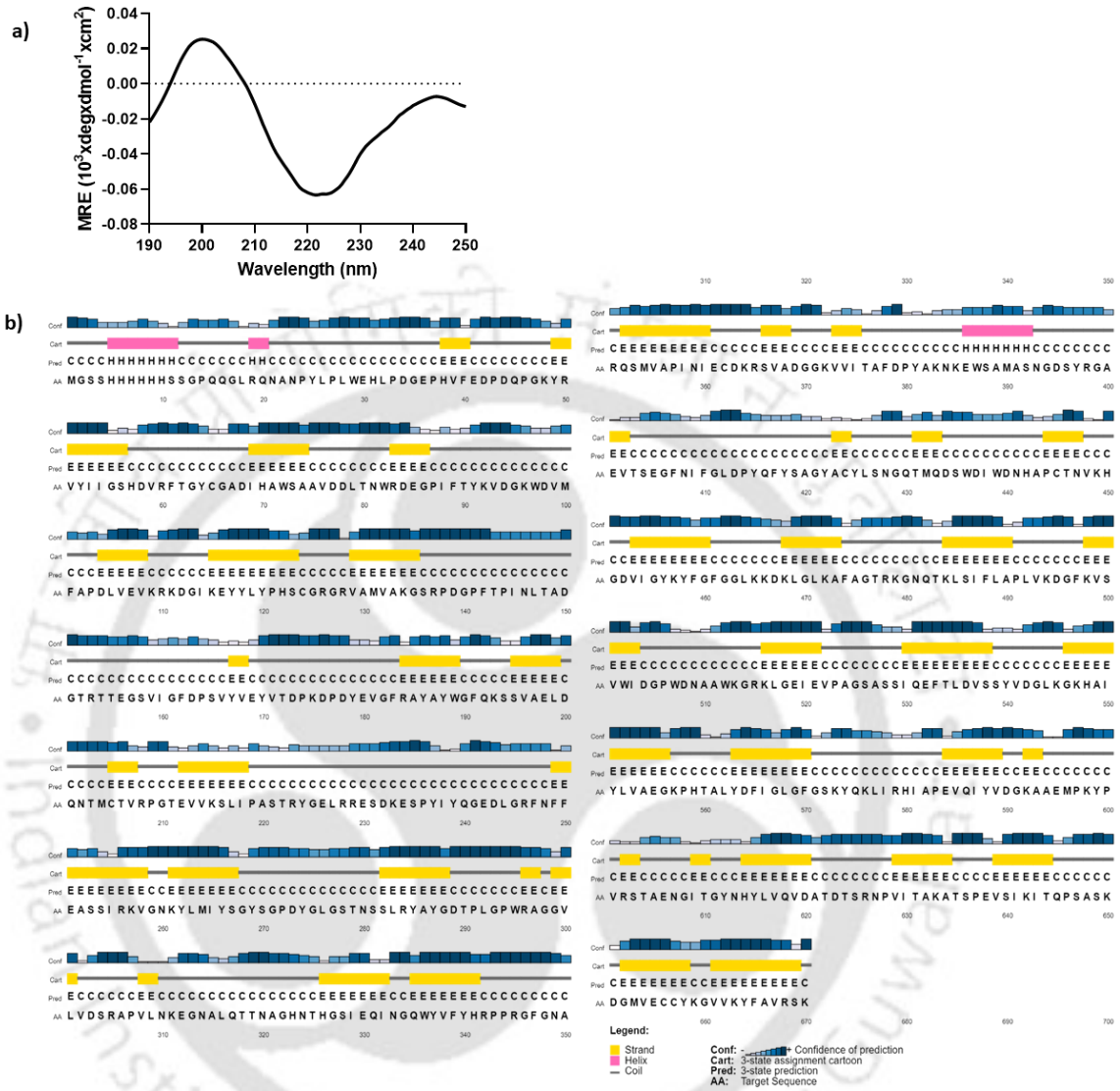

Fig. 4.4 Prediction of secondary structure composition of *Bo*GH43_35 by a) Far-UV (190-250 nm) spectrum of *Bo*GH43_35 and b) PDBSum server.

Table 4.2 Prediction of secondary structure of *Bo*GH43_35 through CD and web-based servers.

Server	α-helix (%)	β-Strand (%)	Coil (%)
PsiPred	2.3	35.3	62.2
2Struc	1.8	22.8	75.4
AlphaFold2	2.0	34.7	63.3
CD (K2D3)	2.2	28.9	68.9

4.3.5 Molecular dynamic simulation analysis of *Bo*GH43_35

Molecular Dynamics (MD) simulation provided a detailed information about the stability and compactness of the Alphafold2 modeled structure of *Bo*GH43_35. MD simulation of *Bo*GH43_35 was carried out for 200 ns. The result of MD simulation was analysed through radius of gyration versus time, a RMSD versus time, RMSF of the amino acid residues, solvent-accessible surface area, and number of intra-molecular hydrogen bonds plots. In the radius of gyration (*Rg*) against time plot, the average *Rg* value of *Bo*GH43_35 was found to be 2.69 nm (Fig. 4.5a). Initially, the rise in *Bo*GH43_35 RMSD value was seen up to 3 ns and then onwards the structure was stable till 200 ns with an average RMSD of 0.35 nm (Fig. 4.5b). Root mean square fluctuation computes the overall displacement of an atom or group of atoms relative to the initial structure of *Bo*GH43_35 submitted for MD simulation. The Cα root mean square fluctuations (RMSFs) versus amino acid residues plot was examined to observe the changes in the structure of *Bo*GH43_35 throughout the trajectory. It was found that there were uniform fluctuations in the alpha carbon atoms of *Bo*GH43_35 secondary structure, but the loops of N-terminal region of *Bo*GH43_35 were highly flexible (Fig. 4.5c). Another parameter, SASA was also analysed which remained stable in a range of 287-312 nm^2 with an average of 300 nm^2 (Fig. 4.5d). The average number of intramolecular hydrogen bonds within *Bo*GH43_35 was also calculated. It was found that there are 452 intra-molecular hydrogen bonds on average assisting *Bo*GH43_35 to achieve a stable confirmation (Fig. 4.5e). The superposition and alignment of AF2 three-dimensional modeled structure of *Bo*GH43_35 (hot pink color) with MD simulated structure at 200 ns (cyan color) overlapped well with an RMSD of 0.17 nm (Fig. 4.5f). The combination of stable *Rg*, low RMSD, stable RMSF, SASA and number

of H-bonds discerned for *Bo*GH43_35 modeled structure exhibited its stable conformation.

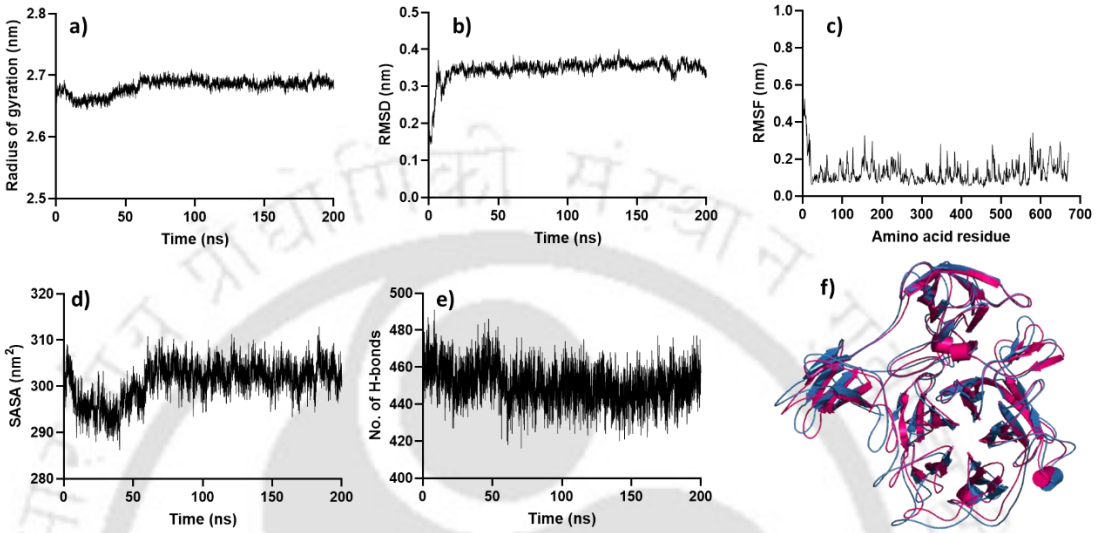

Fig. 4.5 MD simulation analysis of *Bo*GH43_35 showing, a) Compactness through Radius of gyration plot, b) Average deviation of protein's atomic position through Root Mean Square Deviation plot, c) Flexibility of individual amino acid residues through Root Mean Square Fluctuation plot, d) Surface area accessible to the solvent through SASA plot, e) Protein stability and number of hydrogen bonds through H-bonds plot and f) Superposition of initial *Bo*GH43_35 modeled structure (hot pink) and simulated structure after 200 ns (cyan blue) with RMSD of 0.17 nm.

4.3.6 Active-site and sub-sites prediction of *Bo*GH43_35

The CASTp server identified the active-site of *Bo*GH43_35 (Fig. 4.6a). The calculated surface area and volume of the identified active-site pocket are 66.55 $Å^2$ and 41.0 $Å^3$, respectively. The amino acid residues located in this pocket are Asp34, Tyr64, Cys65, Phe101, Ala102, Phe162, Asp163, Glu251, His323, Asn324, His326 and Arg351. The subsite of *Bo*GH43_35 was determined by visualizing *Bo*GH43_35-arabinoxylobiose complex in PyMOL (Fig. 4.6b). The non-reducing end of arabinoxylobiose is indicated by a negative number (-1), whereas, the reducing end is shown by positive numbers (+1 and +2). It was observed that the amino acid residues

involved in the binding of arabinose at -1 subsite are Phe250, Glu251, Ser267, Asn324 and Thr325 (Fig. 4.6b). The +1 subsite is composed of Asp34, Phe101, Ala102, Ala252 and His326, whereas, the +2 subsite is constituted by Asp163, Pro164, Ser165, Tyr188, Trp189, Ser253 and Ser254.

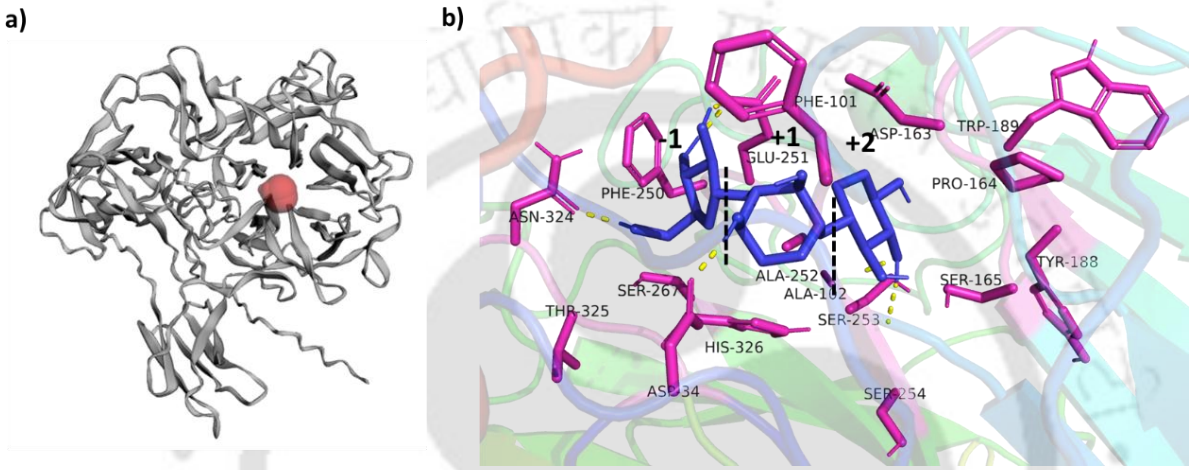

Fig. 4.6 a) Identification of active-site cavity of *Bo*GH43_35 by CASTp web-server, where active-site cavity is shown in red sphere and b) Subsite analysis of *Bo*GH43_35 with arabinoxylobiose.

4.3.7 Ligand binding analysis of *Bo*GH43_35

Binding analysis of *Bo*GH43_35 with its probable ligands (arabinose, arabinoxylobiose, arabinoxylotriose, xylose, xylobiose, xylotriose, xylotetraose and xylopentaose) was performed by Molecular docking using AutoDock v4.2.7 and the binding affinity in terms of Gibbs free Energy (kcal/mol) was compared in order to determine the best-docked complex. The interaction of *Bo*GH43_35 with the ligands revealed the amino acid residues involved in the formation of hydrogen bond and hydrophobic interactions. The binding affinity, the binding free energy of *Bo*GH43_35 with the ligand interactions are reported in Table 4.3. The results revealed maximum binding energy with arabinose (-5.01 kcal/mol) followed by arabinoxylobiose (-4.35 kcal/mol). The interaction analysis with xylooligosaccharides showed binding energy

of -4.65 kcal/mol with xylotriose, -4.18 kcal/mol with xylotetraose and -3.66 kcal/mol with xylobiose.

The surface view of the docking interaction of *Bo*GH43_35 with arabinose at the active-site cleft (Fig. 4.7a) showed that Ser165, Tyr188, Gly190, Ala252, Ser253 form hydrogen bonds with arabinose whereas, Pro164, Trp189, Glu251 are involved in hydrophobic interactions by (Fig. 4.7b). The 2-dimensional interaction of *Bo*GH43_35 with arabinose generated by LigPlot+ is showed that Ala252 forms H-bond with O, Tyr188 with O1, Asp163 and Gly190 with O2, Ser165 and Ser253 with O3 of arabinose (Fig. 4.7c). Arabinoxylobiose is accommodated in the active-site cleft of *Bo*GH43_35 (Fig. 4.7d) by forming H-bonds with Asp34, Ser165, Glu251 and involving Ala102, Asp163, Phe250, Ala252, Ser253, Ser267, Asn324, Thr325 and His326 in hydrophobic interactions (Fig. 4.7e). The 2D plot showed that Asp34 forms H-bond with O6, Glu251 with O7 and O8 and Ser165 with O9 of arabinoxylobiose (Fig. 4.7f). The molecular docking analysis revealed the accommodation of xylotriose in the active-site pocket of *Bo*GH43_35 (Fig. 4.7g) and displayed that Asp163, Glu251, Ala252 and Ser253 are involved in H-bond formation whereas, Pro164, Ser165, Tyr188, Trp189, Gly190, Phe250, Asn324 and His326 take part in hydrophobic interaction (Fig. 4.7h). The 2-D interaction of *Bo*GH43_35 with xylotriose generated by LigPlot+ showed that Asp163 forms H-bond with O5, O6 and O7 and Glu251 forms H-bond with O8 and O9 of xylotriose (Fig. 4.7i). It was also observed that xylotetraose can also be accommodated at the active-site of *Bo*GH43_35 (Fig. 4.7j) by involving Asp163, Gly190, Glu251, Ser253 and Arg351 in H-bond formation and through the hydrophobic interactions with Asp34, Pro164, Ser165, Tyr188, Trp189, Ala252, Asn324, Thr325, His326 and His341 (Fig. 4.7k). The 2-D interaction of *Bo*GH43_35 with xylotetraose generated by

LigPlot+ revealed that Asp163 forms H-bond with O6 and O9, Glu251 with O9, Arg351 with O12 of xylotetraose as shown in Fig. 4.7l. These results showed that the active-site cleft of *Bo*GH43_35 can accommodate xylooligosaccharides of the length xylotetraose though the most favourable binding was obtained with arabinose.

Table 4.3 Molecular docking interaction of *Bo*GH43_35 against its probable ligands

Ligand	Binding Energy (kcal/mol)	Residues forming Hydrogen bond	Residues involved in hydrophobic interactions
Arabinose	-5.02	Ser165, Tyr188, Gly190, Ala252, Ser253	Pro164, Trp189, Glu251
Arabinoxylobiose	-4.35	Asp34, Ser165, Glu251	Ala102, Asp163, Phe250, Ala252, Ser253, Ser267, Asn324, Thr325, His326
Arabinoxylotriose	-2.87	Asp163, Glu251, His326	Phe101, Ala102, Asp104, Pro164, Ser165, Ala252
Xylose	-3.38	Asp163, Gly190, Ser253	Pro164, Trp189, Phe249, Glu251, Ala252
Xylobiose	-3.66	Asp34, Glu251, Arg351, Thr325	Phe250, Ser267, Asn324
Xylotriose	-4.65	Asp163, Glu251, Ala252, Ser253	Pro164, Ser165, Tyr188, Trp189, Gly190, Phe250, Asn324, His326
Xylotetraose	-4.18	Asp163, Gly190, Glu251, Ser253, Arg351	Asp34, Pro164, Ser165, Tyr188, Trp189, Ala252, Asn324, Thr325, His326, His341
Xylopentaose	-1.92	Asp34, Asp104, Pro164, Ser165, Glu251, Ala252, Ser253, Asn324, Arg351	Cys65, Phe101, Ala102, Asp163, Thr325

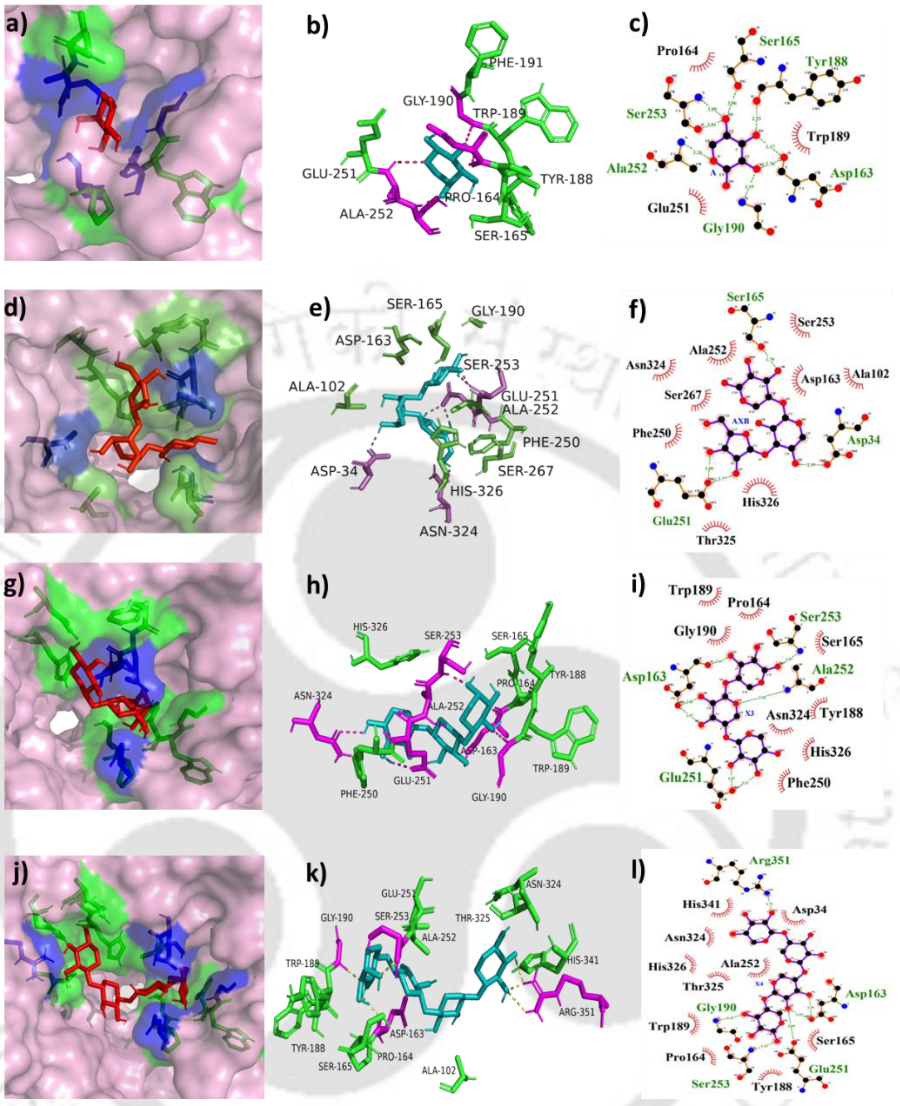

Fig. 4.7. Ligand binding analysis of *Bo*GH43_35. a) surface view of active-site cleft of *Bo*GH43_35 accommodating arabinose in red, H-bond forming residues in blue and residues involved in hydrophobic interaction in green colour, b) H-bond and hydrophobic interaction of *Bo*GH43_35 with arabinose in cyan, H-bond forming residues in purple and residues involved in hydrophobic interaction in green colour, c) 2-D interaction of *Bo*GH43_35 with arabinose, d) surface view of active-site cleft of *Bo*GH43_35 accommodating arabinoxylobiose in red, H-bond forming residues in blue and residues involved in hydrophobic interaction in green colour e) H-bond and hydrophobic interaction of *Bo*GH43_35 with arabinoxylobiose in cyan, H-bond forming residues in purple and residues involved in hydrophobic interaction in green colour, f) 2-D interaction of *Bo*GH43_35 with arabinoxylobiose, g) surface view of active-site cleft of *Bo*GH43_35 accommodating xylotriose in red, H-bond forming residues in blue and residues involved in hydrophobic interaction in green colour h) H-bond and hydrophobic interaction of *Bo*GH43_35 with xylotriose in cyan, H-bond forming residues in purple and residues involved in hydrophobic interaction in green colour, i) 2-D interaction of *Bo*GH43_35 with xylotriose, j) surface view of active-site cleft of *Bo*GH43_35 accommodating xylotetraose in red, H-bond forming residues in blue and residues involved in hydrophobic interaction in green colour and k) H-bond polar and hydrophobic interaction of *Bo*GH43_35 with xylotetraose in cyan, H-bond forming residues in purple and residues involved in hydrophobic interaction in green colour and l) 2-D interaction of *Bo*GH43_35 with xylotetraose.

4.3.8 MD simulation of *Bo*GH43_35-arabinose complex

The molecular dynamics (MD) simulation is of utmost importance in complete understanding of the association of protein and ligand. Therefore, MD simulation of the best conformation of the complex of *Bo*GH43_35 with arabinose (GH43_35-arabinose) was performed up to 200 ns and compared with the MD simulated *Bo*GH43_35 through various parameters. The structural stability of arabinose bound *Bo*GH43_35 was determined by analysing the radius of gyration, root-mean square deviation, root mean square fluctuations, solvent accessible surface area and number of hydrogen bonds plot. All these outcomes were compared with that of only *Bo*GH43_35. The radius of gyration of GH43_35-arabinose remained between 2.62-2.73 nm with average *Rg* of 2.68 nm (Fig. 4.8a). There was only slight reduction of ~0.01 nm in the *Rg* value compared to that of independently simulated *Bo*GH43_35 (2.69 nm) and it indicated a stable and compact GH43_35-arabinose complex. The average RMSD score of GH43_35-arabinose complex throughout the trajectory was 0.28 nm (Fig. 4.8b) showing a decrease of 0.07 nm as compared with 0.35 nm of only *Bo*GH43_35. This significant decrease in RMSD was indicative of stability of the GH43_35-arabinose complex throughout the trajectory. Additionally, the fluctuation of the ligand in the binding was computed by calculating its RMSD after a fit to the *Bo*GH43_35 backbone (Fig. 4.8c). It was observed that in the initial ~42 ns, the average RMSD was 0.25 nm, whereas, it increased to 4.8 nm later in the trajectory. These deviations suggest that arabinose is undergoing substantial conformational changes and is not maintaining a single stable conformation relative to the *Bo*GH43_35 backbone. The conformational flexibility of the amino acid residues of GH43_35-arabinose complex was anticipated

in terms of root mean square fluctuations for Cα atoms for all the residues (Fig. 4.8d). It was observed that there was fluctuation at the N-terminal region of the complex depicting higher flexibility. However, there was reduction in the Cα atoms' fluctuations of the catalytic residues such as Asp34 (from 0.11 nm to 0.09 nm) and Glu251 (from 0.12 nm to 0.09 nm) compared to that of individually simulated *Bo*GH43_35. The decrease in RMSF value showed rigidity in the catalytic residues when arabinose binds to *Bo*GH43_35. There was sharp increase in the RMSF value at the C-terminal of GH43_35-arabinose complex indicating flexibility of the loop region of CBM6B. An average hydrophobic SASA of GH43_35-arabinose complex was obtained to be 310 nm^2 (Fig. 4.8e). The increase in SASA of 10 nm^2 from the SASA of individual *Bo*GH43_35 (300 nm^2) implies exposure of the hydrophobic regions and expansion of *Bo*GH43_35 when arabinose binds to it. Additionally, the number of intramolecular hydrogen bonds of GH43_35-arabinose complex also decreased up to 442 from 452 of individual *Bo*GH43_35 (Fig. 4.8f). The decrease in number of hydrogen bonds indicate that mostly hydrophobic interactions are involved in stabilizing the complex suggesting weaker interactions between *Bo*GH43_35 and arabinose.

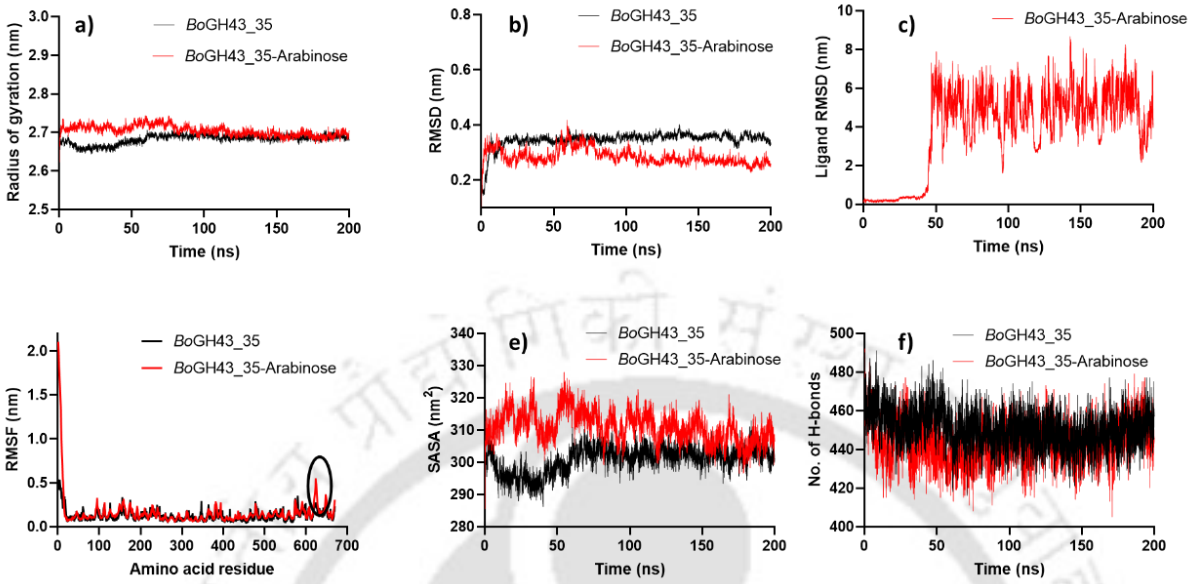

Fig. 4.8. MD simulation analysis of *Bo*GH43_35-arabinose complex shown in red and only *Bo*GH43_35 is shown in black after 200 ns simulation. a) Compactness analysis through Radius of gyration plot, b) Average deviation of protein's atomic position through Root Mean Square Deviation plot, c) Average deviation of the ligand, arabinose after a fit to the *Bo*GH43_35 backbone, d) Flexibility of individual amino acid residues through Root Mean Square Fluctuation plot, e) Surface area accessible to the solvent through Solvent Accessible Surface Area plot and f) Stability and Number of hydrogen bonds within the protein through H-bond plot.

4.3.9 Binding analysis of *Bo*GH43_35 and wheat arabinoxylan by Fluorescence spectroscopy

Fluorescence spectroscopy is routinely used to fetch structural and functional information of proteins. The presence of tryptophan residue, with an intrinsic fluorescence offers an advantage in monitoring fluorescence spectra of a protein without modifying it (Hellmann & Schneider, 2019). The change in tryptophan's local environment is assessed when a polysaccharide binds to a protein. The fluorescence spectra of *Bo*GH43_35 recorded in the presence of varying concentrations (0.15-0.5%, w/v) of wheat arabinoxylan, low viscosity revealed that there is reduction in the fluorescence intensity with increasing concentrations of wheat arabinoxylan (Fig. 4.9a).

Binding of wheat arabinoxylan lowered the fluorescence intensity of tryptophan emission spectrum of *Bo*GH43_35 from 1.31x 10^6 Coulomb per second/ MicroAmps at 0.15%, w/v wheat arabinoxylan to 6.63x10^5 Coulomb per Second (CPS)/ MicroAmpere (μA) at 0.45%, w/v wheat arabinoxylan. The association constant (K_a) of *Bo*GH43_35 with wheat arabinoxylan was derived from the plot of $\log\left(\frac{Fo-F}{F}\right)$ against log[Wheat arabinoxylan] (Fig. 4.9b) and it was found to be 3.11x10^2 M^{-1} as determined by the straight-line equation of the plot, i.e. y=2.2x + 2.49, where 2.2 is the average number of binding sites (n), indicating two binding sites on *Bo*GH43_35. The K_a =3.11x10^2 M^{-1} was determined by taking the antilog of 2.49. The two binding sites may be located at the GH43 catalytic module and CBM6A of *Bo*GH43_35 as CBM6B is devoid of a Trp residue. The change in Gibb's free energy (ΔG) of substrate binding was calculated to be -14.2 kJ $mole^{-1}$ by using the derived association constant. In a study, a CBM35 from *Clostridium thermocellum* showing K_a, 1.14x10^5 M^{-1}, ΔG -22.0 kJ $mole^{-1}$ and one binding site (n=0.79) against carob galactomannam was reported (Ghosh et al., 2013). The binding analysis of mannanase (Man5C) containing CBM35, Man5C-CBM35 from *Cellvibrio japonicas* against carob galactomannan and konjac glucomannan by Isothermal Titration Calorimetry (ITC), showed K_a 5.8x10^3 M^{-1} and 5.6x10^3 M^{-1}, respectively and number of binding sites one for CBM35 (Bolam et al., 2004).

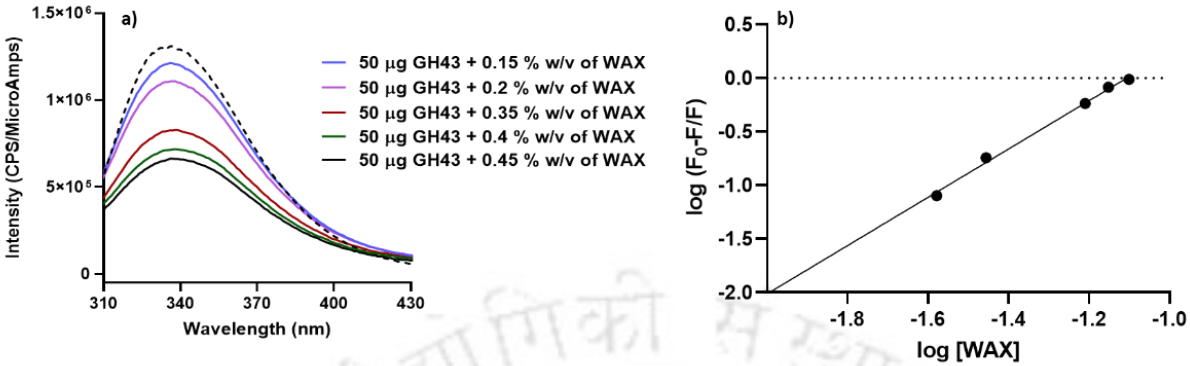

Fig. 4.9 a) Tryptophan fluorescence emission spectrum of *Bo*GH43_35 with or without wheat arabinoxylan and b) A linear plot of log [(Fo−F)/F] vs log [WAX] to derive association constant (K_a) from Stern-Volmer equation.

4.3.10 Size distribution analysis of *Bo*GH43_35 by Dynamic Light Scattering

The hydrodynamic diameter plot of *Bo*GH43_35 against size distribution at 0.5 and 1.0 mg/mL concentrations by DLS analysis revealed a single peak indicating the proteins' monodispersity in aqueous environment. The Polydispersity Index (PI), a measure of heterogeneity of protein's size distribution of *Bo*GH43_35 at 0.5 and 1 mg/mL were 25.2 and 27.3%, respectively, which are above the conventional threshold of 20%, therefore, confirming its monodispersity in aqueous solution. The hydrodynamic diameter (D_h) of *Bo*GH43 at both the concentrations was 8.01 nm (Fig. 4.10a), suggesting a hydrodynamic radius, R_h of 4.0 nm that is slightly larger than the radius of gyration, *Rg* of *Bo*GH43_35 (2.69 nm) obtained from MD simulation analysis. Higher R_h of *Bo*GH43_35, obtained by DLS suggested that the hypothetical sphere of the enzyme might be including the solvation layer of hydration at both 0.5 and 1.0 mg/mL protein concentrations in aqueous form. Similarly, in a study on the hydration shell of lysozyme, it was reported that there exists a hydration layer of ~1.2 nm around the lysozyme surface determined by depolarized light scattering (Perticaroli et al., 2015). The hydrodynamic radii of only *Bo*GH43_35 at 1.0 mg/mL (13 mM) and

*Bo*GH43_35 (13 mM) along with the 13 mM arabinose remained unaltered, i.e. 4.0 nm, as shown in Fig. 4.10b which corroborated with the result of unaffected radius of gyration of *Bo*GH43_35-arabinose complex, 2.68 nm obtained from MD simulation. There was no change in the hydrodynamic radius of *Bo*GH43_35 upon arabinose binding in the aqueous solution indicating no change in the enzyme conformation. The electrophoretic mobility of *Bo*GH43_35 at 0.5 and 1.0 mg/mL were found to be -0.72 and -0.73 µm.cm/V.s, respectively. The electrophoretic mobility implies the number of uncompensated charge on protein surface. The negligible difference in the value of electrophoretic mobility at both the concentrations suggested that *Bo*GH43_35 is stable and does not aggregate at these concentrations. The zeta potential, ξ value of *Bo*GH43_35 was -9.3 mV at 0.5 mg/mL and -9.4 mV at 1.0 mg/mL (Fig. 4.10c). The overall negative charge on *Bo*GH43_35 protein surface at both the concentrations indicate that the surface charge is independent of the concentration. This also confirms its solubility as well as stability in the aqueous environment. The overall surface charge of *Bo*GH43_35 at 1.0 mg/mL (13 mM) along with 13 mM arabinose, slightly reduced to -9.1 mV (Fig. 4.10d) indicating that the binding of arabinose to *Bo*GH43_35 results in compact structure of the complex, again corroborating the MD simulation results.

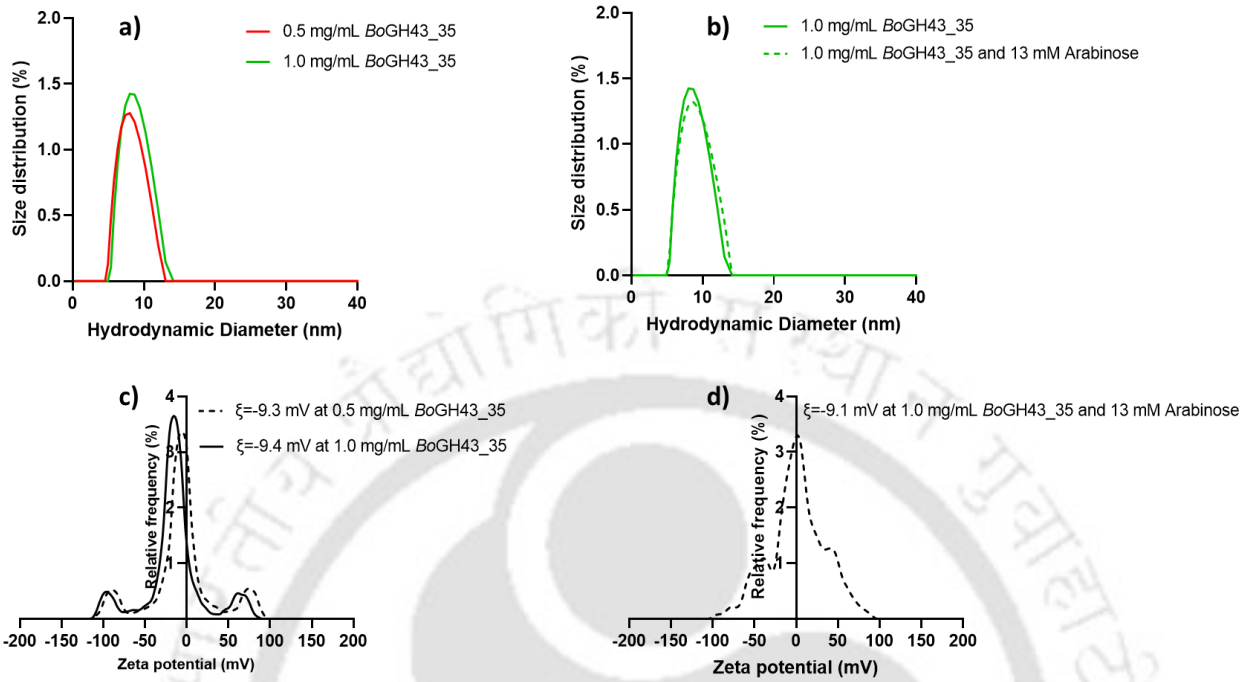

Fig. 4.10 DLS analysis of *Bo*GH43_35 for a) hydrodynamic diameter (D_h) at 0.5 and 1.0 mg/mL protein concentrations, b) hydrodynamic diameter (D_h) of only *Bo*GH43_35 at 1.0 mg/mL (13 mM) protein concentration and *Bo*GH43_35 at 1.0 mg/mL (13 mM) along with 13 mM arabinose, c) Surface charge (Zeta potential, ξ) of *Bo*GH43_35 at 0.5 mg/mL and 1.0 mg/mL protein concentrations and d) Surface charge of *Bo*GH43_35 at 1.0 mg/mL (13 mM) protein concentration added with 13 mM arabinose in 0.05 M sodium phosphate buffer, pH 7.0.

4.4 Conclusions

The amino acid sequence analysis of α-L-arabinofuranosidase/endo-β-1,4-xylanase, *Bo*GH43_35 from *B. ovatus* ATCC 8483 revealed 28.1% identity with α-L-arabinofuranosidase (*Ct*GH43) from *Clostridium thermocellum* ATCC 27405. MSA of *Bo*GH43_35 with its homologous sequences showed Asp34 and Glu251 as the catalytic residues. The three-dimensional structure of *Bo*GH43_35 generated by AlphaFold2 revealed the presence 5-bladed-β-propeller fold by catalytic module followed by two consecutive jellyroll type β-sandwich fold adopted by CBM6A and CBM6B. Secondary structure analysis of *Bo*GH43_35 by Circular Dichroism showed 2.2% α-helix, 28.9% β-sheet and 68.9% of random coil, which accorded with the results predicted from 2Struc and Psipred. MD simulation of AF2 modeled structure of *Bo*GH43_35 confirmed its stability, compactness and no deformity. Molecular docking of *Bo*GH43_35 with arabino-xylooligosaccharides and xylooligosaccharides revealed the active-site pocket forming residues and maximum binding affinity with arabinose. The comparative study of MD simulated structures of *Bo*GH43_35-arabinose complex and the only *Bo*GH43_35 revealed the stability of *Bo*GH43_35-arabinose docked complex. The catalytic residues in docked complex were also found stable with reduced RMSF. The binding analysis of *Bo*GH43_35 by fluorescence spectroscopy against wheat arabinoxylan showed association constant, K_a of 3.11×10^2 M^{-1} and presence of two binding sites. The DLS analysis of *Bo*GH43_35 indicated that there exists as a hypothetical sphere surrounded by a hydration shell in aqueous solution. The overall negative charge of *Bo*GH43_35 as determined by zeta potential on protein surface showed its stability and solubility in the aqueous environment.

4.5 References

Abbott, D. W., Ficko-Blean, E., Van Bueren, A. L., Rogowski, A., Cartmell, A., Coutinho, P. M., Henrissat, B., Gilbert, H. J., & Boraston, A. B. (2009). Analysis of the structural and functional diversity of plant cell wall specific family 6 Carbohydrate Binding Modules. *Biochemistry*, *48*(43), 10395–10404. https://doi.org/10.1021/bi9013424

Berendsen, H. J. C., Postma, J. P. M., Van Gunsteren, W. F., DiNola, A., & Haak, J. R. (1984). Molecular dynamics with coupling to an external bath. *The Journal of Chemical Physics*, *81*(8), 3684–3690. https://doi.org/10.1063/1.448118

Berendsen, H. J. C., Van Der Spoel, D., & Van Drunen, R. (1995). GROMACS: A message-passing parallel molecular dynamics implementation. *Computer Physics Communications*, *91*(1–3), 43–56. https://doi.org/10.1016/0010-4655(95)00042-E

Bolam, D. N., Xie, H., Pell, G., Hogg, D., Galbraith, G., Henrissat, B., & Gilbert, H. J. (2004). X4 modules represent a new family of Carbohydrate-binding Modules that display novel properties. *Journal of Biological Chemistry*, *279*(22), 22953–22963. https://doi.org/10.1074/jbc.M313317200

Boonstra, S., Onck, P. R., & Van Der Giessen, E. (2016). CHARMM TIP3P water model suppresses peptide folding by solvating the unfolded state. *The Journal of Physical Chemistry B*, *120*(15), 3692–3698. https://doi.org/10.1021/acs.jpcb.6b01316

Britton, T., Anderson, C. L., Jacquet, D., Lundqvist, S., & Bremer, K. (2007). Estimating divergence times in large phylogenetic trees. *Systematic Biology*, *56*(5), 741–752. https://doi.org/10.1080/10635150701613783

Broekaert, W. F., Courtin, C. M., Verbeke, K., Van De Wiele, T., Verstraete, W., & Delcour, J. A. (2011). Prebiotic and other health-related effects of cereal-derived arabinoxylans, arabinoxylan-oligosaccharides, and xylooligosaccharides. *Critical Reviews in Food Science and Nutrition*, *51*(2), 178–194. https://doi.org/10.1080/10408390903044768

Buksa, K., Ziobro, R., Nowotna, A., Praznik, W., & Gambuś, H. (2012). Isolation, modification and characterization of soluble arabinoxylan fractions from rye grain. *European Food Research and Technology*, *235*(3), 385–395. https://doi.org/10.1007/s00217-012-1765-0

Colovos, C., & Yeates, T. O. (1993). Verification of protein structures: Patterns of nonbonded atomic interactions. *Protein Science*, *2*(9), 1511–1519. https://doi.org/10.1002/pro.5560020916

Eisenberg, D., Lüthy, R., & Bowie, J. U. (1997). VERIFY3D: Assessment of protein models with three-dimensional profiles. In *Methods in Enzymology* (Vol. 277, pp. 396–404). Elsevier. https://doi.org/10.1016/S0076-6879(97)77022-8

Ghosh, A., Luís, A. S., Brás, J. L. A., Pathaw, N., Chrungoo, N. K., Fontes, C. M. G. A., & Goyal, A. (2013). Deciphering ligand specificity of a *Clostridium*

thermocellum family 35 Carbohydrate Binding Module (CtCBM35) for gluco- and galacto-substituted mannans and its calcium induced stability. *PLoS ONE*, *8*(12), e80415. https://doi.org/10.1371/journal.pone.0080415

Guo, H.-B., Perminov, A., Bekele, S., Kedziora, G., Farajollahi, S., Varaljay, V., Hinkle, K., Molinero, V., Meister, K., Hung, C., Dennis, P., Kelley-Loughnane, N., & Berry, R. (2022). AlphaFold2 models indicate that protein sequence determines both structure and dynamics. *Scientific Reports*, *12*(1), 10696. https://doi.org/10.1038/s41598-022-14382-9

Hellmann, N., & Schneider, D. (2019). Hands on: Using Tryptophan fluorescence spectroscopy to study protein structure. In A. E. Kister (Ed.), *Protein Supersecondary Structures* (Vol. 1958, pp. 379–401). Springer New York. https://doi.org/10.1007/978-1-4939-9161-7_20

Heredia, A., Jimnez, A., & Guillon, R. (1995). Composition of plant cell walls. *Zeitschrift Fer Lebensmittel-Untersuchung Und -Forschung*, *200*(1), 24–31. https://doi.org/10.1007/BF01192903

Hess, B., Bekker, H., Berendsen, H. J. C., & Fraaije, J. G. E. M. (1997). LINCS: A linear constraint solver for molecular simulations. *Journal of Computational Chemistry*, *18*(12), 1463–1472. https://doi.org/10.1002/(SICI)1096-987X(199709)18:12<1463::AID-JCC4>3.0.CO;2-H

Jachimska, B., Wasilewska, M., & Adamczyk, Z. (2008). Characterization of globular protein solutions by dynamic light scattering, electrophoretic mobility, and viscosity measurements. *Langmuir*, *24*(13), 6866–6872. https://doi.org/10.1021/la800548p

Jiang, Q., Jin, X., Lee, S.-J., & Yao, S. (2017). Protein secondary structure prediction: A survey of the state of the art. *Journal of Molecular Graphics and Modelling*, *76*, 379–402. https://doi.org/10.1016/j.jmgm.2017.07.015

Ke, Q., Gong, X., Liao, S., Duan, C., & Li, L. (2022). Effects of thermostats/barostats on physical properties of liquids by molecular dynamics simulations. *Journal of Molecular Liquids*, *365*, 120116. https://doi.org/10.1016/j.molliq.2022.120116

Kumari, A., Kaila, P., Tiwari, P., Singh, V., Kaul, S., Singhal, N., & Guptasarma, P. (2018). Multiple thermostable enzyme hydrolases on magnetic nanoparticles: An immobilized enzyme-mediated approach to saccharification through simultaneous xylanase, cellulase and amylolytic glucanotransferase action. *International Journal of Biological Macromolecules*, *120*, 1650–1658. https://doi.org/10.1016/j.ijbiomac.2018.09.106

Lagaert, S., Pollet, A., Courtin, C. M., & Volckaert, G. (2014). β-Xylosidases and α-L-arabinofuranosidases: Accessory enzymes for arabinoxylan degradation. *Biotechnology Advances*, *32*(2), 316–332. https://doi.org/10.1016/j.biotechadv.2013.11.005

Land, H., & Humble, M. S. (2018). YASARA: A tool to obtain structural guidance in biocatalytic investigations. In U. T. Bornscheuer & M. Höhne (Eds.), *Protein*

Engineering (Vol. 1685, pp. 43–67). Springer New York. https://doi.org/10.1007/978-1-4939-7366-8_4

Laskowski, R. A., Hutchinson, E. G., Michie, A. D., Wallace, A. C., Jones, M. L., & Thornton, J. M. (1997). PDBsum: A web-based database of summaries and analyses of all PDB structures. *Trends in Biochemical Sciences*, *22*(12), 488–490. https://doi.org/10.1016/S0968-0004(97)01140-7

Laskowski, R. A., MacArthur, M. W., Moss, D. S., & Thornton, J. M. (1993). PROCHECK: A program to check the stereochemical quality of protein structures. *Journal of Applied Crystallography*, *26*(2), 283–291. https://doi.org/10.1107/S0021889892009944

Mayes, H. B., Knott, B. C., Crowley, M. F., Broadbelt, L. J., Ståhlberg, J., & Beckham, G. T. (2016). Who's on base? Revealing the catalytic mechanism of inverting family 6 glycoside hydrolases. *Chemical Science*, *7*(9), 5955–5968. https://doi.org/10.1039/C6SC00571C

Mewis, K., Lenfant, N., Lombard, V., & Henrissat, B. (2016). Dividing the large glycoside hydrolase family 43 into subfamilies: A motivation for detailed enzyme characterization. *Applied and Environmental Microbiology*, *82*(6), 1686–1692. https://doi.org/10.1128/AEM.03453-15

Mitchell, R. A. C., Dupree, P., & Shewry, P. R. (2007). A novel bioinformatics approach identifies candidate genes for the synthesis and feruloylation of arabinoxylan. *Plant Physiology*, *144*(1), 43–53. https://doi.org/10.1104/pp.106.094995

O'Boyle, N. M., Banck, M., James, C. A., Morley, C., Vandermeersch, T., & Hutchison, G. R. (2011). Open Babel: An open chemical toolbox. *Journal of Cheminformatics*, *3*(1), 33. https://doi.org/10.1186/1758-2946-3-33

Perticaroli, S., Comez, L., Sassi, P., Paolantoni, M., Corezzi, S., Caponi, S., Morresi, A., & Fioretto, D. (2015). Hydration and aggregation of lysozyme by extended frequency range depolarized light scattering. *Journal of Non-Crystalline Solids*, *407*, 472–477. https://doi.org/10.1016/j.jnoncrysol.2014.07.017

Pollet, A., Delcour, J. A., & Courtin, C. M. (2010). Structural determinants of the substrate specificities of xylanases from different glycoside hydrolase families. *Critical Reviews in Biotechnology*, *30*(3), 176–191. https://doi.org/10.3109/07388551003645599

Qaseem, M. F., Shaheen, H., & Wu, A.-M. (2021). Cell wall hemicellulose for sustainable industrial utilization. *Renewable and Sustainable Energy Reviews*, *144*, 110996. https://doi.org/10.1016/j.rser.2021.110996

Rezaei, S., Meftah, H.-S., Ebtehajpour, Y., Rahimi, H. R., & Chamani, J. (2024). Investigation on the effect of fluorescence quenching of calf thymus DNA by piperine: Caspase activation in the human breast cancer cell line studies. *DNA and Cell Biology*, *43*(1), 26–38. https://doi.org/10.1089/dna.2023.0269

Roy, D., Kumar, V., Acharya, K. K., & Thirumurugan, K. (2014). Probing the binding of syzygium-derived α-glucosidase inhibitors with N- and C-terminal human

maltase glucoamylase by docking and Molecular Dynamics simulation. *Applied Biochemistry and Biotechnology*, *172*(1), 102–114. https://doi.org/10.1007/s12010-013-0497-3

Sakka, K., Kojima, Y., Kondo, T., Karita, S., Ohmiya, K., & Shimada, K. (1993). Nucleotide sequence of the *Clostridium stercorarium xynA* gene encoding xylanase A: Identification of catalytic and Cellulose Binding Domains. *Bioscience, Biotechnology, and Biochemistry*, *57*(2), 273–277. https://doi.org/10.1271/bbb.57.273

Sarzehi, S., & Chamani, J. (2010). Investigation on the interaction between tamoxifen and human holo-transferrin: Determination of the binding mechanism by fluorescence quenching, resonance light scattering and circular dichroism methods. *International Journal of Biological Macromolecules*, *47*(4), 558–569. https://doi.org/10.1016/j.ijbiomac.2010.08.002

Schulze, E. (1890). Zur Kenntniss der chemischen Zusammensetzung der pflanzlichen Zellmembranen. *Berichte Der Deutschen Chemischen Gesellschaft*, *23*(2), 2579–2583. https://doi.org/10.1002/cber.189002302151

Sharma, K., Fontes, C. M. G. A., Najmudin, S., & Goyal, A. (2021). Small angle X-ray scattering based structure, modeling and molecular dynamics analyses of family 43 glycoside hydrolase α-L-arabinofuranosidase from *Clostridium thermocellum*. *Journal of Biomolecular Structure and Dynamics*, *39*(1), 209–218. https://doi.org/10.1080/07391102.2019.1707119

Shi, H., Li, X., Gu, H., Zhang, Y., Huang, Y., Wang, L., & Wang, F. (2013). Biochemical properties of a novel thermostable and highly xylose-tolerant β-xylosidase/α-arabinosidase from *Thermotoga thermarum*. *Biotechnology for Biofuels*, *6*(1), 27. https://doi.org/10.1186/1754-6834-6-27

Sinnott, M. L. (1990). Catalytic mechanism of enzymic glycosyl transfer. *Chemical Reviews*, *90*(7), 1171–1202. https://doi.org/10.1021/cr00105a006

Smaali, I., Rémond, C., & O'Donohue, M. J. (2006). Expression in *Escherichia coli* and characterization of β-xylosidases GH39 and GH-43 from *Bacillus halodurans* C-125. *Applied Microbiology and Biotechnology*, *73*(3), 582–590. https://doi.org/10.1007/s00253-006-0512-5

Sørensen, H. R., Pedersen, S., Jørgensen, C. T., & Meyer, A. S. (2007). Enzymatic hydrolysis of wheat arabinoxylan by a recombinant "Minimal" enzyme cocktail containing β-xylosidase and novel endo-1,4-β-xylanase and α-L-arabinofuranosidase activities. *Biotechnology Progress*, *23*(1), 100–107. https://doi.org/10.1021/bp0601701

Spiridon, I., & Popa, V. I. (2008). Hemicelluloses: Major sources, properties and applications. In *Monomers, Polymers and Composites from Renewable Resources* (pp. 289–304). Elsevier. https://doi.org/10.1016/B978-0-08-045316-3.00013-2

Sturgeon, R. J. (Ed.). (1997). *Advances in Macromolecular Carbohydrate Research*. JAI Press.

Tabasi, M., Maghami, P., Amiri-Tehranizadeh, Z., Reza Saberi, M., & Chamani, J. (2023). New perspective of the ternary complex of nano-curcumin with β-lactoglobulin in the presence of α-lactalbumin: Spectroscopic and molecular dynamic investigations. *Journal of Molecular Liquids*, *392*, 123472. https://doi.org/10.1016/j.molliq.2023.123472

Tamura, K., Stecher, G., & Kumar, S. (2021). MEGA11: Molecular Evolutionary Genetics Analysis Version 11. *Molecular Biology and Evolution*, *38*(7), 3022–3027. https://doi.org/10.1093/molbev/msab120

Tian, W., Chen, C., Lei, X., Zhao, J., & Liang, J. (2018). CASTp 3.0: Computed atlas of surface topography of proteins. *Nucleic Acids Research*, *46*(W1), W363–W367. https://doi.org/10.1093/nar/gky473

Viborg, A. H., Sørensen, K. I., Gilad, O., Steen-Jensen, D. B., Dilokpimol, A., Jacobsen, S., & Svensson, B. (2013). Biochemical and kinetic characterisation of a novel xylooligosaccharide-upregulated GH43 β-D-xylosidase/α-L-arabinofuranosidase (BXA43) from the probiotic *Bifidobacterium animalis* subsp. *Lactis* BB-12. *AMB Express*, *3*(1), 56. https://doi.org/10.1186/2191-0855-3-56

Wong, K. K., Tan, L. U., & Saddler, J. N. (1988). Multiplicity of beta-1,4-xylanase in microorganisms: Functions and applications. *Microbiological Reviews*, *52*(3), 305–317. https://doi.org/10.1128/mr.52.3.305-317.1988

Yang, X., Shi, P., Huang, H., Luo, H., Wang, Y., Zhang, W., & Yao, B. (2014). Two xylose-tolerant GH43 bifunctional β-xylosidase/α-arabinosidases and one GH11 xylanase from *Humicola insolens* and their synergy in the degradation of xylan. *Food Chemistry*, *148*, 381–387. https://doi.org/10.1016/j.foodchem.2013.10.062

Zhou, J., Bao, L., Chang, L., Zhou, Y., & Lu, H. (2012). Biochemical and kinetic characterization of GH43 β- D -xylosidase/α- L -arabinofuranosidase and GH30 α- L -arabinofuranosidase/β- D -xylosidase from rumen metagenome. *Journal of Industrial Microbiology and Biotechnology*, *39*(1), 143–152. https://doi.org/10.1007/s10295-011-1009-5

Chapter 5

Application of a bifunctional α-L-arabinofuranosidase/endo-β-1,4-xylanase (*Bo*GH43_35) from *Bacteroides ovatus* in *Punica granatum* and *Citrus limetta* fruit juice clarification and enzymatic hydrolysis of their peel

5.1 Introduction

α-L-Arabinofuranosidases (EC 3.2.1.55) are one of the xylanolytic enzymes that break the terminal and non-reducing α-1,2-, α-1,3- and/or α-1,5-L-arabinofuranoside substitutions into α-L-arabinosides such as arabinoxylan, L-arabinan and the other polysaccharides that include arabinose (İlgü et al., 2018). α-L-Arabinofuranosidases and other hemicellulases like xylanase play a promising role in various agro-industrial processes such as in bioethanol industry (Maibam & Goyal, 2023), wine industry (Ravanal et al., 2012), paper and pulp industry (Viikari et al., 1994), improving the quality of bread (Xue et al., 2020), clarifying fruit juices (Chen et al., 2024) and increasing the digestibility of animal feedstuffs (Liu et al., 2011).

In fruit juice processing, clarity is one of the significant indicators for testing the quality of fruit juice (Chen et al., 2024). The action of xylanalytic enzymes on

freshly squeezed fruit juice helps in the clarification of the juice from excess polysaccharides that cause its effective liquefaction and hence improve its quality (Kaushal et al., 2021). Pomegranate (*Punica granatum*) fruit, belonging to Punicacea family, has gained a tremendous popularity in consumption owing to its numerous health-related properties such as antioxidant, anti-inflammatory and anti-hypertensivity (Kandylis & Kokkinomagoulos, 2020). Similarly, Mosambi or sweet lemon (*Citrus limetta*) contains fruitful amount of nutrients and vitamin C that have antioxidant properties (Singh & Das, 2021).

After the extraction of juices, fruit wastes are the commonly generated wastes from households and food-processing industries (Pathak et al., 2016). Among fruit wastes, peels, pulp and seeds account for approximately, 40% of the total mass of each fruit (Saheed et al., 2016). Interestingly, these discarded portions are rich in valuable bioactive compounds, such as carotenoids, polyphenols, dietary fibers, vitamins, enzymes and oils (Sagar et al., 2018). Owing to their health-promoting properties, researchers and food industries are exploring the possibility of using valuable ingredients of fruit peels in the preparation of functional food (Wanlapa et al., 2015). Pomegranate peel accounts for 40-50% of the total weight of the fruit with cellulose (35.3%), hemicellulose (29.3%), pectin (15.6%) and lignin (14.3%) (Jacqueline & Velvizhi, 2024). Similarly, mosambi or sweet lime (*Citrus limetta*) peel is a rich source of pectin (25-30%), cellulose (13.6%), hemicellulose (10%) and starch (7.1%) (B. Singh et al., 2022). These polymers are closely linked forming the structural framework of the plant cell wall (John et al., 2020).

The lignocellulosic fraction of both pomegranate peel (PP) and mosambi peel (MP) are being utilized for various industrial applications such as bioethanol production

(Sarkar et al., 2024), bio-gas through pyrolysis (Saadi et al., 2019) and butyric acid production (Wang et al., 2021). It was shown that pomegrante peel increases the feed intake and weight gain when fed to bull calves (Pathak et al., 2017). Moreover, the antioxidant activity in meat (Kotsampasi et al., 2014) and milk (Shabtay et al., 2012) improved significantly when animals were fed with pomegranate by-products. A recent report on utilizing the mosambi peel by enriching it with fatty acid producing strain *Aurantiochytrium* sp. ATCC 276 as a feed material for aquaculture farms appeared (Saikia et al., 2024). Mosammbi peel waste from juice processing industries is marketed as animal feed after drying and pelletization (John et al., 2020). However, the widespread valorization of fruit peels into animal feed on an industrial scale faces several hurdles. These challenges encompass logistical issues related to collection, transport and storage; operational difficulties in processing and standardization; and significant biochemical limitations (Haider et al., 2025). The biochemical challenges include increasing the digestibility of recalcitrant animal feed. The digestibility of feedstock consists of hydrolysis of cell wall biopolymers such as cellulose, hemicellulose, pectin and lignin (Figueiredo et al., 2019). This structural disruption is key to unlocking the encapsulated nutrients and making them more readily available for absorption by the animal.

The use of exogenous cell wall degrading enzymes are essential for making these feeds as ‘semi-digested’ (Bajaj & Mahajan, 2019). These cell wall degrading enzymes include cellulases and xylanases that act by degrading cellulose and hemicellulose present in cell wall of plant materials. Babalola et al. (2006) observed improved apparent nitrogen and fiber absorption as well as feed transit time by the application of xylanase in poultry feed (Babalola et al., 2006).

The current study elaborates on bridging the applications in juice clarification and feed improvement using a single, potent enzyme. The investigation involved evaluation of the impact of a bifunctional α-L-arabinofuranosidase/endo-β-1,4-xylanase (*Bo*GH43_35) cloned from *Bacteroides ovatus*, a bacterium known for its complex carbohydrate-degrading capabilities on pomegranate and sweet lime fruit juices. The study involved the assessment of the effectiveness of enzyme in clarifying the freshly extracted pomegranate and sweet lime juices. The clarification efficiency of juices was determined by measuring key parameters such as turbidity, transmittance and viscosity of the juices. Another application of *Bo*GH43_35 was explored in the enzymatic hydrolysis (saccharification) of the fruit peels generated as waste from the juice extraction process. Treating the peels with bifunctional α-L-arabinofuranosidase/endo-β-1,4-xylanase (*Bo*GH43_35) and exo-β-1,4-xylosidase (*Bo*ExXyl43A) from *Bacteroides ovatus* was also explored for breaking down of the hemicellulose components into simpler, soluble sugars, collectively measured as total reducing sugars. These resulting sugars represent a valuable intermediate product with significant potential for diverse downstream applications, including further processing into animal feed supplements, serving as a substrate for bioethanol fermentation, or being utilized as natural sweeteners in the food and beverage industries, thus contributing to a more circular and sustainable use of fruit resources.

5.2 Materials and Methods

5.2.1 Raw materials and chemicals

Pomegranate and Sweet lime were obtained from local market of Guwahati, Assam, India. Choline chloride, acetic acid, sodium chlorite, sulphuric acid, sodium azide, citric acid and sodium phosphate monobasic anhydrous, sodium dihydrogen phosphate dibasic, nickel sulphate and L-arabinose used were purchased from Himedia, Pvt. Ltd, India. Wheat arabinoxylan (low viscosity), D-xylose, xylobiose, xylotriose, xylotetraose and xylopentaose were procured from Megazyme Ltd., Ireland. Beechwood xylan and xylanase ex. *Aspergillus Niger* were purchased from Sisco Research Laboratories Pvt. Ltd., India.

5.2.2 Purification of *Bo*GH43_35 and BoExXyl43A, protein concentration and enzyme activity

The recombinant enzymes, bifunctional α-L-arabinofuranosidase/endo-β-1,4-xylanase (*Bo*GH43_35) and exo-β-1,4-xylosidase (*Bo*ExXyl43A) from *Bacteroides ovatus* were purified through immobilized metal-ion affinity chromatography (IMAC) following the methods reported earlier by (Shrivastava et al., 2025; Gavande et al., 2024). Both the enzymes, *Bo*GH43_35 and *Bo*ExXyl43A were expressed in by *E. coli* BL21 (DE3) cells, harbouring the respective recombinant plasmids by growing separately, in 400 mL Luria-Bertani (LB) medium. The LB medium was supplemented with 50 µg/mL kanamycin and kept at 37°C, 180 rpm till the cell growth reached mid-exponential phase (A_{600} = 0.6). After that, the cells were induced with 0.25 mM IPTG for *Bo*GH43_35 and 1 mM IPTG for *Bo*ExXyl43A and further grown at 24°C for 16 h. The overgrown cells were harvested by centrifugation (6,000g, 4°C) for 10 min, resuspended in 10 mL of 50 mM sodium phosphate buffer, pH 7.0 and sonicated at 33%

amplitude with pulse of 5 s on and 8 s off for 15 min using Sonics, Vibra cells. The sonicated cells were centrifuged at 12,000g, 4°C for 1 h followed by filtering the supernatants through 0.45 µm PVDF membrane using a syringe filter. The resulting supernatants were subjected for purification by using Ni^{2+} ion chelating column (HiTrap, GE Healthcare, USA). The resuspension buffer and equilibration buffer for *Bo*GH43_35 and *Bo*ExXyl43A purification was 50 mM Sodium phosphate buffer, pH 7.0, 300 mM NaCl, 60 mM imidazole and the elution buffer was composed of 50 mM Sodium phosphate buffer, pH 7.0, 300 mM NaCl, 300 mM imidazole. The purified recombinant proteins *Bo*GH43_35 and *Bo*ExXyl43A were dialysed using a dialysis membrane (with a Mol. Mass cut off 12 -14 kDa) in 50 mM sodium phosphate buffer, pH 7.0 to remove the solutes. The homogeneity of *Bo*GH43_35 and *Bo*ExXyl43A were verified by SDS-PAGE (12.0 %, w/v) as described in Chapter 2 (Section 2.2.14). The protein concentrations of both the purified proteins were determined by Bradford reagent (Bradford, 1976) and UV method by following the protocol mentioned in Chapter 3 (Section 3.2.3.2). The molar extinction co-efficient 134580 $M^{-1}cm^{-1}$for *Bo*GH43_35 (Shrivastava et al., 2025) and 85510 $M^{-1}cm^{-1}$ for *Bo*ExXyl43A were determined by Expasy Protparam (https://web.expasy.org/protparam/) and were used for the calculations.

The enzyme activity of both enzymes, *Bo*GH43_35 and *Bo*ExXyl43A, was determined by the quantification of reducing sugars using the methods of (Nelson, 1944) and (Somogyi, 1945). The substrates used for enzyme assays were wheat arabinoxylan, low viscosity (Megazyme) for *Bo*GH43_35 and beechwood xylan (SRL) for *Bo*ExXyl43A. The reaction mixture, 100 µL composed of 90 µL substrate (1.1%, w/v) dissolved in 50 mM Sodium phosphate buffer, pH 7.0 and 10 µL of *Bo*GH43_35

(1.0 mg/mL) or *Bo*ExXyl43A (0.6 mg/mL). For blank, 10 µL of 50 mM Sodium phosphate buffer, pH 7.0 was added instead of enzymes. The reaction was kept at 37°C for 2 min each for *Bo*GH43_35 and *Bo*ExXyl43A. The enzyme activity of *Bo*GH43_35 and *Bo*ExXyl43A was determined by following the protocol mentioned in Chapter 3 (Section 3.2.4). Similarly, the enzyme activity of commercial xylanase from *Aspergillus niger* was also calculated by taking 10 µL of 0.5 mg/mL commercial xylanase instead of previously mentioned enzymes. The enzyme activity of commercial xylanase was assessed against both 1%, w/v beechwood xylan and wheat arabinoxylan. The reaction time for enzyme activity determination was 2 min at 37°C. The standard curve of a mixture of equimolar L-arabinose and D-xylose was plotted for calculating the released amount of reducing sugar. All the enzyme assays were carried out in triplicate sets. The enzyme activity was estimated in units per millilitre ($U.mL^{-1}$). Enzyme activity ($U.mL^{-1}$) of *Bo*GH43_35 or *Bo*ExXyl43A refers to the quantity of enzyme per mL needed to release one µmole of arabinose/xylose per min. One unit (U or $\mu mole.min^{-1}$) of *Bo*GH43_35 or *Bo*ExXyl43A enzyme is the quantity of *Bo*GH43_35 or *Bo*ExXyl43A required to release one µmole of arabinose/xylose in one minute.

5.2.2.1 Fruit juice clarification by BoGH43_35

5.2.2.2 Preparation of puree for juice treatment

Mature and ripened fruit of pomegranate (2 kg) and mosambi or sweet lime (3 kg) were purchased from the local market of Guwahati, Assam, India. Fruits were washed under running tap water before removing the crown and peel. Fruit pulps were separated from the skin or peels manually and macerated using a blender to get a smooth textured puree. The puree obtained after the maceration process was strained through a strainer to separate the pulp from the juice.

5.2.2.3 Clarification of fruit juices

The effectiveness of purified bifunctional α-L-arabinofuranosidase/endo-β-1,4-xylanase, *Bo*GH43_35 (enzyme activity of 5.4 U/mL against wheat arabinoxylan) on the two fruit juice clarification was determined at various enzyme dose (0.25, 0.5 and 1.0 mg/mL) and incubation time *i.e.* enzyme with fruit juice (30 min, 1 h, 2 h, 3 h and 4 h). Each juice, 19 mL was separately added with 1 mL of enzyme, *Bo*GH43_35 of appropriate dilutions (5.4 U/mL; 0.25, 0.5 and 1.0 mg/mL) prepared in 50 mM sodium phosphate buffer, pH 7.0. The control was prepared by adding 1 mL 50 mM sodium phosphate buffer, pH 7.0 instead of *Bo*GH43_35. The clarification of fruit juices was carried out in triplicate sets of each enzyme dose and kept at 37°C and 120 rpm in shaking incubator for different time durations (30 min, 1 h, 2 h, 3 h and 4 h). At the end of enzymatic treatment, the enzyme in the sample was inactivated by heating the suspension at 60°C for 2 min followed by centrifugation at 6000g for 10 min. After that the transmittance, turbidity, TRS and viscosity of the enzyme treated and untreated fruit juices were determined.

5.2.2.4 Transmittance and reducing sugar determination of the fruit juice

The supernatants of the fruit juices obtained after centrifugation were used to determine the clarity of the juice by measuring percent transmittance (%T) at 660 nm using a spectrophotometer (Multiskan SkyHigh, Thermo Fisher Scientific, Waltham, MA, USA) using 50 mM Sodium phosphate buffer, pH 7.0 as a reference. The percent transmittance was considered a measure of the juice clarity.

The total reducing sugars (TRS) released after enzymatic treatment of fruit pulp were determined by taking 100 µL aliquot from each sample and following the protocol of (Nelson, 1944) and (Somogyi, 1945) mentioned in Chapter 3 (Section 3.2.4.3). The

TRS estimation was carried out by adding 100 µL of freshly prepared reagent D to 100 µL of hydrolysate. The solution was mixed and heated for 20 min in a boiling water bath. After 20 min cooling to room temperature (25°C), 100 µL of reagent C was added, followed by the addition of 700 µL distilled water to make the final volume of 1 mL. Finally, the absorbance at 500 nm (A_{500}) of the mixture was measured by a UV-visible spectrophotometer. D-xylose (0.01-0.1 mg/mL) was used as a standard to quantify the concentration of reducing sugar. The TRS concentration was calculated as described below,

$$\text{TRS concentration (mg/ml)} = \Delta A_{500} \times C \quad \ldots (\text{Eqn. } 5.1)$$

Where, ΔA_{500} = change in absorbance at 500 nm
C = 1 OD equivalent xylose concentration (mg/mL) from standard plot

5.2.2.5 Turbidity and viscosity determination of fruit juices

The turbidity of the two juices before and after enzyme treatment was determined using Turbidity meter (Orion AQ3010, Thermo Scientific). The juice (10 mL) of each fruit was added in the sample holder and turbidity was obtained in Nephelometric turbidity units (NTU) using 50 mM Sodium phosphate buffer, pH 7.0 as reference. The viscosity of fruit juices before and after enzyme treatment was determined using a capillary Ostwald viscometer under controlled room temperature conditions (25°C). To assess the viscosity (η_1) of the enzyme treated fruit juice, its density (ρ_1) was first measured. The viscosity was then calculated based on the Hagen-Poiseuille law for the laminar flow of incompressible fluids, following the methodology described by (Beaulieu et al., 2017). The relationship used for calculation is as follows:

$$\eta 1 = \eta 2 \frac{\rho 1 t 1}{\rho 2 t 2} \quad \ldots (\text{Eqn. } 5.2)$$

Where, η_1 is viscosity of fruit juice after enzyme treatment, ρ_1 is its density at 25°C, t_1 is the time it takes for a liquid to flow, under the influence of gravity, between two marked points on the viscometer (A and B), as illustrated in Fig. 5.1, t_2 is the corresponding flow time for the reference fluid (water here) of known viscosity (η_2) and density (ρ_2) to flow between the same two points at the same temperature.

5.2.3 Fruit peel biomass pretreatment

5.2.3.1 Processing of fruit peel

The pomegranate peels (PP) and mausambi peels (MP) generated as byproduct of fruit juice extraction were washed under tap water and dried at 80°C in an oven till a constant weight was achieved. Subsequently, the dried biomass was grinded using a grinder and stored in sealed bags at 25°C for further use.

5.2.3.2 Determination of holocellulose content of peels

The holocellulose content of both pomegranate and mausambi peels was determined following TAPPI (TAPPI, 1992) standard procedure. Two grams each of oven-dried and ground biomass (PP and MP) were separately transferred into a 250 mL Erlenmeyer flask containing 100 mL of deionized water. The flask was kept at 70°C in a shaking water bath and 1.5 g sodium chlorite and 5 mL of 10% (v/v) acetic acid were added to the suspension. The contents were gently stirred at every 10 min to ensure homogeneity. After 30 minutes, 5 mL of 10% (v/v) acetic acid was added. Subsequently, at hourly intervals over a duration of 4 hours, 1.5 g sodium chlorite and 5 mL acetic acid were added to the reaction mixture. Upon completion of the reaction, the mixture was cooled to 4°C and the resulting mixture was then filtered through a pre-weighed sintered glass funnel. The solid residue, comprising holocellulose fraction, was washed with water followed by acetone and air-dried to make it acetone-free and

dried in a 50°C oven for 24 h. The holocellulose content was calculated as a percentage based on the oven dry sample. The holocellulose content was expressed as a percentage of the initial oven-dried biomass weight.

$$\text{Holocellulose content (\%)} = \left(\frac{\text{Final weight}}{\text{Initial weight}}\right) \times 100 \qquad \ldots (\text{Eqn. 5.3})$$

5.2.3.3 Determination of cellulose content of peels

The cellulose content of PP and MP was determined from the holocellulose fraction obtained in the previous section 5.2.4.2, following the TAPPI (TAPPI, 1992). An accurately weighed 0.4 g sample of holocellulose was placed into a 250 mL glass beaker maintained at 20°C using a temperature-controlled water bath. A solution of sodium hydroxide (NaOH), 17.5% (approximately 4.4 N) was added in a stepwise manner at specific intervals. Specifically, the NaOH solution was added as follows: 3 mL at 0 minutes, 2 mL at 1 minute, 2 mL at 45 seconds, 7 mL at 15 seconds and finally 2 mL at 3 minutes. The mixture was gently stirred intermittently during the addition process to promote uniform mixing.

Following the final addition, the suspension was allowed to stand at 20°C for 30 minutes to complete the alkali treatment. Thereafter, 50 mL of distilled water was added, and the mixture was allowed to stand for an additional 40 minutes. The contents were then filtered through a pre-weighed sintered glass funnel under suction. The retained solid was washed with 5 mL of 8.3% (approximately 2 N) NaOH solution at 20°C, followed by transfer into a pre-weighed crucible.

Subsequently, the residue was thoroughly washed with approximately, 160 mL of distilled water under suction to remove residual alkali. The suction was temporarily discontinued and the crucible was filled with 2 N acetic acid, allowing the sample to

stand for 5 minutes to hydrolyze and remove the hemicellulosic components. After this step, the acetic acid was removed by reapplying suction, and the residue was repeatedly washed with distilled water until a neutral pH was achieved. The crucible containing the residue was then placed in a hot air oven and dried at 50°C to constant weight. The cellulose content was expressed as a percentage of the initial oven-dried sample weight.

5.2.3.4 Pretreatment of fruit peel biomass

For pretreatment of pomegranate peel (PP) and mosambi peel (MP), 1% H_2SO_4 (v/v) was separately added to 20 g PP and MP in 200 mL distilled water in 500 mL reagent bottle and autoclaved at 121°C, 15 psi for 15 min. Another set of pretreament of PP and MP was done by only autoclaving 20 g PP and MP in 200 mL distilled water without adding 1% (v/v) H_2SO_4. After cooling down, the pretreated PP and MP were filtered through muslin cloth and the hydrolysates (1 mL) were kept for further analysis of TRS. The solid fraction of the slurry was washed with tap water till neutral pH value was achieved. The solid fractions were dried in hot air oven at 50°C till constant weight was obtained. Then the dried powder was subjected to enzymatic saccharification.

5.2.3.5 Functional groups analysis of raw and pretreated fruit peel biomass

The functional group distribution in the raw and pretreated fruit peel biomasses was analyzed by Fourier Transform Infrared (FTIR) spectroscopy (Perkin Elmer, USA). Dried samples of raw fruit peels and pretreated fruit peels biomass were finely ground and mixed with KBr in 1:100 ratio (sample:KBr, w/w). The mixture was then compressed into translucent pellets using a hydraulic press operating at 15 tons of pressure. and their pellets were made under a 15-ton hydraulic press. FTIR spectra were recorded over the wavenumber range of 400–4000 cm^{-1} to identify characteristic

functional group vibrations and assess structural modifications induced by the pretreatment process.

5.2.4 Enzymatic hydrolysis of pretreated peels by *Bo*GH43_35 and *Bo*ExXyl43A

The pretreated fruit peels were used for saccharification by using various xylanolytic enzyme combinations. *Bo*GH43_35 (enzyme activity of 5.4 U/mL against wheat arabinoxylan, low viscosity, Megazyme), *Bo*ExXyl43A (enzyme activity of 9.3 U/mL against beechwood xylan, SRL) and commercial xylanase from *Aspergillus niger* (enzyme activity of 9.0 U/mL against beechwood xylan, SRL and 3.4 U/mL against wheat arabioxylan) were used for saccharification of raw and pretreated PP and MP. Raw PP, autoclaved PP and 1% (v/v) H_2SO_4 treated and autoclaved PP were three different types of PP used as biomass for saccharification. But for MP, only raw MP and autoclaved MP were used as biomass for saccharification. Because treating MP with 1% (v/v) H_2SO_4 treatment followed by autoclaving and subsequent drying solidified to a solid rock-like state. Due to this transformation, no further processing was carried out. Saccharification of raw and pretreated PP and MP was performed in 3 mL reaction mixure with 10%, w/v peel biomass loading in 50 mM sodium phosphate buffer, pH 7.0 and incubating at 37°C for 48 h. The volume of each enzyme loading is given in Table 5.1. A control contained 3 mL 50 mM sodium phosphate buffer, pH 7.0 with 10% w/v peel biomass without enzyme. At pH 7, *Bo*GH43_35 showed maximum stability in terms of specific activity (Chapter 3, section 3.3.3.2). Whereas, *Bo*ExXyl43A retained more than 60% of specific activity at pH 7 (Gavande et al., 2024), therefore 50 mM sodium phosphate buffer, pH 7 was chosen for saccharification. As *Bo*GH43_35 and *Bo*ExXyl43A are mesophilic enzymes, the optimum temperature of both the enzymes is 37°C. Therefore, 37°C was used for saccharification.

Table 5.1 Enzyme used for saccharification of peel biomass.

Enzyme	Enzyme loading	Volume used	Total volume (mL)
*Bo*GH43_35	5.4 U/g biomass	300 µL	3.0
*Bo*ExXyl43A	9.3 U/g biomass	300 µL	3.0
*Bo*GH43_35+*Bo*ExXyl43A	5.4 and 9.3 U/g biomass	150 µL each	3.0
Xylanase from *Aspergillus niger*	9.0 U/g biomass	300 µL	3.0

Biomass loading 10% w/v in 50 mM sodium phosphate buffer, pH 7.0 incubated at 37°C for 48 h.

5.2.5 Determination of TRS in enzyme treated peel hydrolysates

The total reducing sugar (TRS) released in the hydrolysates of enzyme treated peels was estimated by NS method (Nelson, 1944; Somogyi, 1945). The composition of the reagents used in determination of TRS is mentioned in Chapter 3 (Section 3.2.4.3). 100 µL of freshly prepared reagent D was added to 100 µL of hydrolysate. The solution was mixed and heated in a boiling water bath for 20 min. After cooling to room temperature (25°C), 100 µL of reagent C was added, followed by the addition of 700 µL distilled water to make the final volume, 1 mL. Finally, the absorbance at 500 nm (A_{500}) of the mixture was measured by a UV-visible spectrophotometer. D-Xylose (0.01-0.1 mg/mL) was used as a standard to quantify the concentration of reducing sugar.

5.2.6 Quantitative analysis of monosaccharides in peel biomass

The hydrolysate of peels after pretreatment and after the enzymatic saccharification was analyzed for the monosaccharide content. The glucose and xylose concentration in the saccharified hydrolysate was determined using High-Performance Liquid Chromatography (Shimadzu Corporation, Japan). Phenomenex Rezex ROA

(H+) (300 × 7.8 mm) column attached to guard column Phenomenex Rezex-ROA (H+) (50 × 7.8 mm) with refractive index detector (RID) was used. The chromatographic separation was performed under isocratic condition using a mobile phase of 5 mM H_2SO_4 at a flow rate of 0.6 mL/min. The column oven was maintained at 50°C and acquisition time 25 min was set as total run time for each sample analysis. All the samples were centrifuged at 13,000g for 15 min prior to subjecting them for analysis and 20 µL was used as injection volume of sample for each run. Quantification of reducing sugar was done by using a standard plot of D-xylose, L-arabinose and xylobiose.

5.3 Results and Discussion

5.3.1 Purification of bifunctional α-L-arabinofuranosidase/endo-β-1,4-xylanase, *Bo*GH43_35 and exo-β-1,4-xylosidase, *Bo*ExXyl43A

The enzymes, bifunctional α-L-arabinofuranosidase/endo-β-1,4-xylanase (*Bo*GH43_35) and exo-β-1,4-xylosidase (*Bo*ExXyl43A), purified by IMAC were subjected to SDS-PAGE analysis using 12%, w/v gel. *Bo*GH43_35 revealed a distinct single band corresponding to its respective molecular mass as reported earlier in Chapter 2, section 3.2.2 and *Bo*ExXyl43A gave single band corresponding to 37.2 kDa as reported earlier (Fig. 5.1). The total yield of purified enzymes, *Bo*GH43_35 and *Bo*ExXyl43A was determined to be 7.0±0.3 mg (35 mg/L LB) and 3.6±0.05 mg (18 mg/L LB), respectively, from 200 mL LB medium.

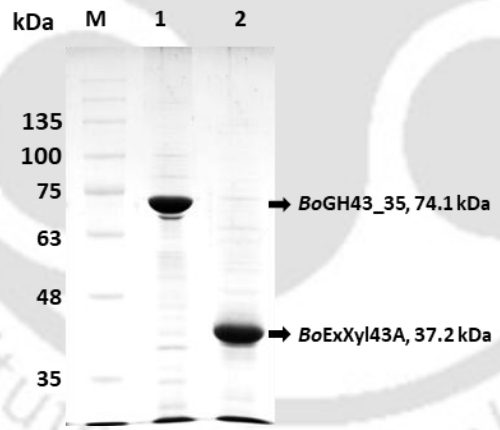

Fig. 5.1 SDS PAGE analysis of purified *Bo*GH43_35 and *Bo*ExXyl43A using 12% (w/v) gel. Lane M- Protein molecular mass marker (Himedia, India), Lane 1- Purified *Bo*GH43_35 and Lane 2- Purified *Bo*ExXyl43A

5.3.2 Assay of *Bo*GH43_35 and *Bo*ExXyl43A enzyme

The enzyme activity of purified *Bo*GH43_35 (1.0 mg/mL) against wheat arabinoxylan, low viscosity was determined to be 5.4 U/mL (specific activity 5.4 U/mg) and of *Bo*ExXyl43A (0.6 mg/mL) against beechwood xylan was 9.3 U/mL (specific activity 15.5 U/mg). The commercial xylanase from *Aspergillus niger* (0.5 mg/mL)

gave enzyme activity of 9.0 U/mL (specific activity 18 U/mg) and 3.4 U/mL (specific activity 6.8 U/mg) against wheat arabinoxylan and beechwood xylan, respectively.

5.3.3 Fruit juice clarification by *Bo*GH43_35

The potential of purified bifunctional α-L-arabinofuranosidase/endo-β-1,4-xylanase, *Bo*GH43_35 from *Bacteroides ovatus* was investigated in clarification of pomegranate and mausambi juices. The effect of various enzyme doses and incubation time were measured in terms of clarity or transmittance (%) at 660 nm, turbidity, reducing sugar and viscosity under same conditions for both fruit juices.

5.3.3.1 Effect of enzyme dose and incubation time on juice clarification

To determine the optimum enzyme dose for juice clarification was determined by varying the concentration of purified *Bo*GH43_35 (0.25 mg/mL, 0.5 mg/mL and 1.0 mg/mL) as mentioned in Table 5.2. The enzyme dose of 1 mg/mL worked best in terms of % transmittance and turbidity for both pomegranate and mosambi juices when incubated for 4 h (Fig. 5.2). The transmittance of pomegranate juice moderately increased from 75.8% in control to 81.5% and significantly from 17.9% in control to 46.5% in mosambi juice by 1 mg/mL *Bo*GH43_35 enzyme treatment. The turbidity of pomegranate juice reduced from 20.1 NTU in control to 3.8 NTU in 1 mg/mL *Bo*GH43_35 treated (Fig. 5.2a). The turbidity of mosambi juice reduced from 597 NTU in control to 290 NTU by 1 mg/mL *Bo*GH43_35 enzyme treatment (Fig. 5.2b). The transmittance increased and turbidity decreased for both pomegranate and mosambi juices after 4 h of incubation with 1 mg/mL *Bo*GH43_35 (Table 5.2). After 4 h of *Bo*GH43_35 treatment, the visual analysis showed clarified juices of pomegranate and mosambi as compared with their respective untreated juices (Fig. 5.3a and 5.3b,

respectively). The degradation of cell wall of fruits by hydrolytic enzymes makes the juice recovery easier (Nagar et al., 2012).

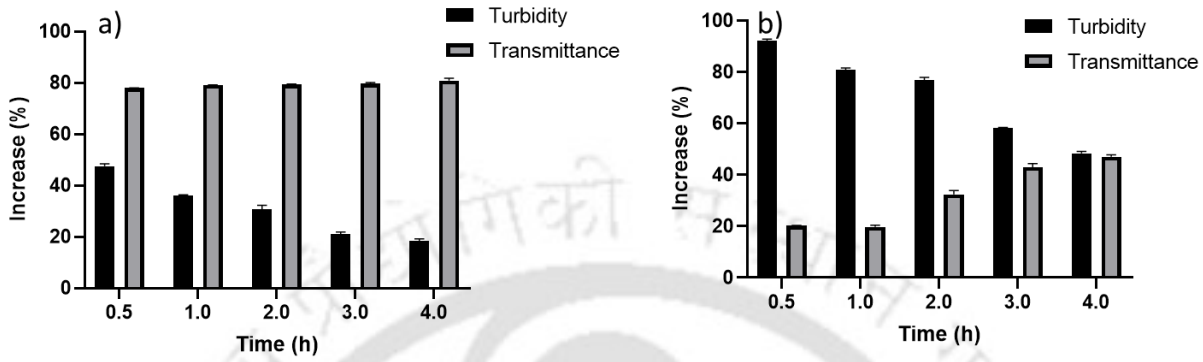

Fig. 5.2 Juice clarification by *Bo*GH43_35 (1 mg/mL, 5.4 U/mL against wheat arabinoxylan) with respect to relative turbidity (%) and transmittance (%) of (a) Pomegranate and (b) Mosambi or sweet lime using at 37°C.

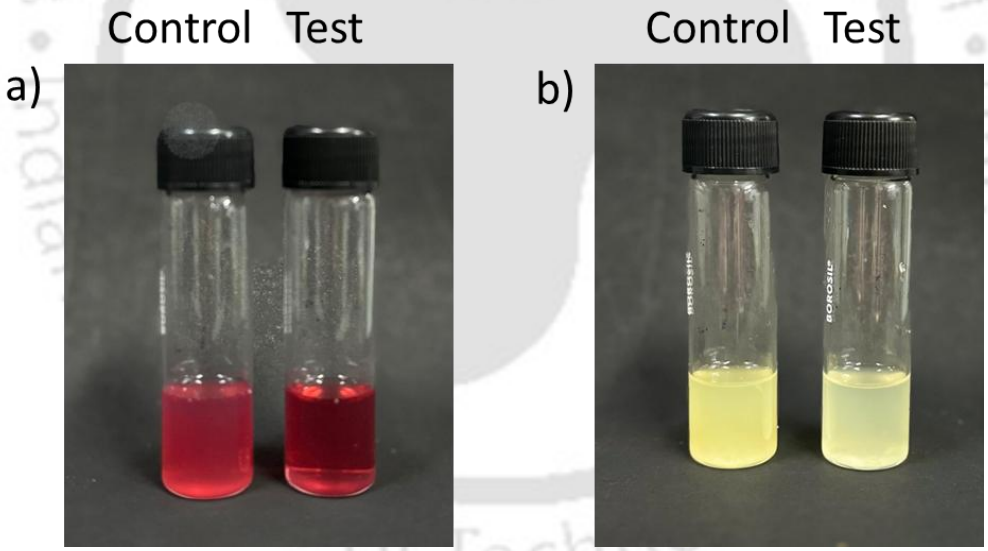

Fig. 5.3 Clarified juices of (a) Pomegranate and (b) Mosambi or sweet lime using *Bo*GH43_35 (1 mg/mL, 5.4 U/mL against wheat arabinoxylan) after 4 h incubation at 37°C.

The release of total reducing sugar was observed as *Bo*GH43_35 causes the breakdown of hemicellulose present in untreated fruit juice. It was found that 0.5 and 1.0 mg/mL of *Bo*GH43_35 produced 0.8 mg/mL of total reducing sugar in pomegranate juice after 2 h incubation (Table 5.2). With increase in incubation time of pomegranate

juice with *Bo*GH43_35, there was not much increase in reducing sugar production. However, 1 mg/mL of *Bo*GH43_35 was enough to produce 1.5 mg/mL of reducing sugar in mosambi juice with incubation of 30 min. With increase in time of incubation, there was no significant increase in reducing sugar production in mosambi juice. The treatment of fruit juices with *Bo*GH43_35 favors the degradation of xylan present in fruit cell wall into xylooligosaccharides. Consequently, more reducing sugar production indicates effective xyaln degradation leading to reduced turbidity and improved juice clarity (Dhiman et al., 2011).

The viscosity of fruit juices plays a crucial role during their preparation, as higher viscosity can slow down the filtration process and cloud particles may lead to clogging of the filtration equipment (Jacob et al., 2008). The treatment of fruit juice with hemicellulose degrading enzymes disintegrates the non-soluble hemicelluloses present in cell wall leading to drop in their viscosity (Tochi et al., 2009). The decrease in viscosity was observed in both pomegranate and mosambi juices when treated with purified *Bo*GH43_35. Pomegranate juice is not too viscous, therefore, there was slight reduction in the viscosity during all the incubation time. *Bo*GH43_35 at 0.5 mg/mL and 1.0 mg/mL reduced the viscosity of pomegranate juice from 1.2 cP to 0.99 cP and 0.98 cP, respectively at 4 h incubation. Whereas, significant decrease in viscosity from 4.3 cP to 2.8 cP, at 4 h incubation was observed in mosambi juice when treated with 1 mg/mL of *Bo*GH43_35 (Table 5.2).

Table 5.2 Treatment of fruit juices with *Bo*GH43_35 at 37°C for 4 h.

Time	Parameters	Pomegranate				Mosambi			
	*Bo*GH43_35 (mg/mL)	Control	0.25	0.5	1.0	Control	0.25	0.5	1.0
	Transmittance (%)	75.5±0.6	77.8±0.8	77.9±0.9	78.0±0.6	16.7±0.1	17.7±0.1	18.0±0.2	20.2±0.7
30 min	Turbidity (NTU)	14.1±0.1	8.9±0.3	7.8±0.1	6.8±0.2	538±4.2	528±3.5	526±1.4	493±4.2
	TRS (mg/mL)	0.6±0.1	0.6±0.1	0.6±0.1	0.7±0.1	1.3±0.1	1.4±0.1	1.4±0.1	1.5±0.1
	Viscosity (cP)	1.2±0.1	1.0±0.1	0.99±0.1	0.99±0.1	5.0±0.6	4.8±0.1	4.5±0.1	4.4±0.1
	*Bo*GH43_35 (mg/mL)	Control	0.25	0.5	1.0	Control	0.25	0.5	1.0
	Transmittance (%)	75.8±0.6	77.4±0.8	78.5±0.7	79.2±0.8	14.6±0.1	17.5±0.3	18.8±0.4	19.2±0.7
1 h	Turbidity (NTU)	13.8±0.6	7.9±0.4	6.7±0.4	5.0±0.2	595±3.1	561±3.5	542±1.4	484±4.2
	TRS (mg/mL)	0.6±0.1	0.7±0.1	0.7±0.1	0.8±0.1	1.3±0.1	1.4±0.1	1.4±0.1	1.5±0.1
	Viscosity (cP)	1.0±0.1	1.0±0.1	0.99±0.1	0.99±0.1	5.0±0.3	4.8±0.1	4.4±0	4.3±0
	*Bo*GH43_35 (mg/mL)	Control	0.25	0.5	1.0	Control	0.25	0.5	1.0
	Transmittance (%)	76.0±0.5	77.1±0.6	78.9±0.6	79.2±0.7	16.3±0.1	20.3±0.1	26.8±0.3	31.2±0.5
2 h	Turbidity (NTU)	14.5±0.2	8.2±0.1	7.0±0.2	4.6±0.2	598±2.3	556±3.5	542±1.4	464±4.2
	TRS (mg/mL)	0.6±0.1	0.7±0.1	0.8±0.0	0.8±0.1	1.3±0.1	1.4±0.1	1.5±0.1	1.5±0.1
	Viscosity (cP)	1.1±0.1	1.0±0	0.99±0	0.991±0	5.1±0.2	4.4±0.1	4.2±0.1	4.1±0
	*Bo*GH43_35 (mg/mL)	Control	0.25	0.5	1.0	Control	0.25	0.5	1.0
	Transmittance (%)	75.6±0.2	77.4±0.6	77.9±0.3	79.9±0.6	17.3±0.1	21.8±0.1	28.7±0.2	43.9±0.5
3 h	Turbidity (NTU)	19.4±0.4	11.2±0.3	8.8±0.2	4.2±0.2	593±1.7	464±2.7	388±1.9	346±2.9
	TRS (mg)	0.6±0.1	0.7±0.1	0.8±0.1	0.8±0.1	1.3±0.1	1.4±0.1	1.5±0.1	1.6±0.1
	Viscosity (cP)	1.1±0.1	0.997±0.1	0.997±0.1	0.985±0.1	4.3±0.1	3.8±0.1	3.4±0.1	3.4±0.1
	*Bo*GH43_35 (mg/mL)	Control	0.25	0.5	1.0	Control	0.25	0.5	1.0
	Transmittance (%)	75.8±0.2	76.7±0.7	79.4±0.1	80.9±0.3	17.97±0.1	23.2±0.2	34.2±0.2	47.0±0.5
4 h	Turbidity (NTU)	20.15±0.6	6.73±0.4	4.3±0.2	3.72±0.2	597±1.3	327.5±3.5	326±1.4	289±4.2
	TRS (mg/mL)	0.5±0.1	0.6±0.1	0.7±0.1	0.8±0.1	1.31±0.1	1.38±0.1	1.5±0.1	1.6±0.1
	Viscosity (cP)	1.2±0.1	0.99±0	0.99±0	0.98±0	4.3±0.2	2.9±0.0	2.8±0	2.8±0

19 mL fruit juice was treated with 1 mL of BoGH43_35 (5.4 U/mg against wheat arabinoxylan). All the treatments were done in triplicate sets.

5.3.4 Fruit peel biomass hydrolysis

5.3.4.1 Holocellulose and cellulose content in raw PP and MP

The raw PP contained 21.3% holocellulose per gram PP and 35.6% holocellulose per gram raw MP. Raw PP consisted of 31.7% cellulose and 3.9% hemicellulose. Whereas, raw MP consisted of 11.4% cellulose and 9.9% hemicellulose.

5.3.4.2 Fruit peel biomass recovery after pretreatment

The biomass recovery of PP and MP was calculated after employing both pretreatment methods (autoclaving and 1% (v/v) H_2SO_4 treatment followed by autoclaving). After complete drying of the biomasses, biomass recovery was calculated by using the following equation,

$$\text{Biomass recovery (\%)} = \left(\frac{\text{weight of pretreated biomass}}{\text{Initial weight of raw biomass}}\right) \times 100 \quad \ldots(\text{Eqn. 5.4})$$

The biomass recovery of 33.3% in PP autoclave and 37.2% in PP 1% (v/v) H_2SO_4 + autoclave was obtained. Whereas, 44.8% of biomass recovery was obtained after autoclave pretreatment of MP.

5.3.4.3 FT-IR analysis of raw and pretreated fruit peel biomass

The FTIR spectra of raw and pretreated PP displayed a distinct hydroxyl (OH) group stretching vibration peak at 3436 cm^{-1} (Fig. 5.4a) , which was similar to the peak obtained by OH stretching in other xylans (Sharma et al., 2020) depicting the presence of xylan in both raw and pretreaed PP. The band at 895 cm^{-1} is indicative of the β-configuration of the 1→4 glycosidic bond between xylopyranose (Xylp) units of the main xylan chains (Bian et al., 2012). There was slight reduction in the peak at 895 cm^{-1} resulting in the loss of xylose residues from the main chain after both

pretreatments of PP. The reduction in the peak at 1049 cm^{-1} of both the pretreatments suggested the loss of arabinose, monosaccharide constituent of the polysaaccharide as also reported earlier (Kačuráková et al., 2000). Therefore, it can be inferred that the branched xylan such as arabinoxylan showing peak at 1049 cm^{-1} was present the raw PP and the arabinose residues were lost after both the pretreatments. The symmetric stretching mode of the carboxyl group at 1415^{-1} revealed the presence of the glucuronic acid component and corroborated with the results of a previous report (Sharma et al., 2020). There was no alteration in the glucuronic acid peak by any of the pretreatment methods. The signal of residual water was observed at 1643 cm^{-1}, as previously reported by (Bian et al., 2012).

In case of MP, the FTIR spectrum of raw MP was devoid of peaks at 3436 cm^{-1} and 2929 cm^{-1}, indicating the absence of hydroxyl (OH) group stretching and symmetric CH stretching, respectively (Fig. 5.4b). However, these peaks were observed after treatment in MP after autoclave treatment of MP at 121°C, 15 psi for 15 min.. This may be attributed to the fact that heating exposes functional groups like hydroxyls (–OH) and methyl/methylene groups (–CH) during autoclave pretreatment.

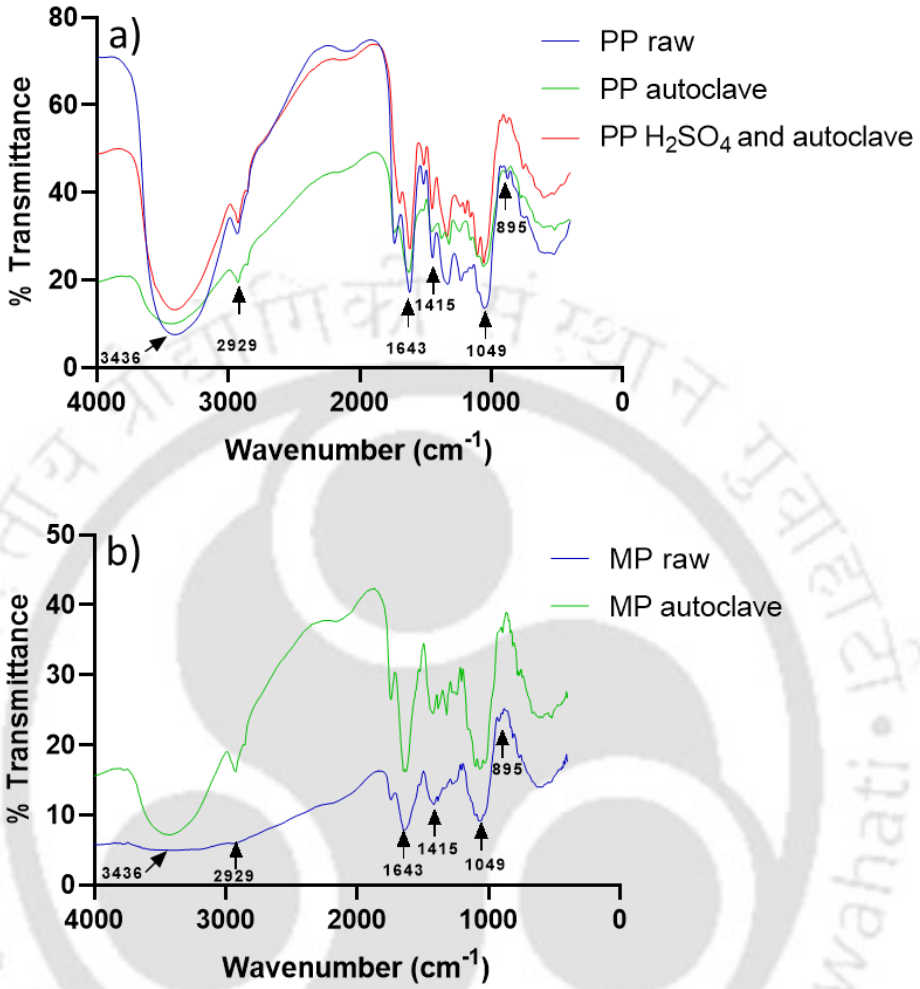

Fig. 5.4 FTIR spectra of raw and pretreated a) pomegranate peel and b) mosambi peel.

5.3.4.4 Total reducing sugars determination of raw and pretreated fruit peels

The total reducing sugar (TRS yield) of raw PP and MP determined before applying any pretreatment were 66 mg/g raw PP and 60 mg/g raw MP, respectively. The chemical or physico-chemical pretreatment process plays a crucial role in disrupting the intricate network of hydrogen and covalent bonds among the various components of lignocellulosic biomass. This structural alteration significantly reduces the inherent recalcitrance of the biomass, thereby enhancing its accessibility for subsequent enzymatic hydrolysis and bioconversion processes (Maibam & Goyal,

2022). The TRS loss in the liquid fraction obtained after the pretreatment methods was also determined (Table 5.3). TRS of the liquid fraction of PP and MP after autoclaving at 121°C for 15 min were 107.1 mg/g raw PP and 162.4 mg/g raw MP, respectively. Whereas, with the treatment of 1% (v/v) H_2SO_4 followed by autoclaving at 121°C, 15 psi for 15 min with PP and MP, TRS yield of 91.2 mg/g raw PP and 155.6 mg/g raw MP, respectively, in the liquid fraction after the pretreatment were obtained.

A pretreatment method should result in minimum loss of TRS yield in the pretreated liquid hydrolysate. Although the liquid fraction of both the pretreatment methods for PP and MP resulted in significant loss of TRS but both raw and pretreated peels were subjected to subsequent enzymatic saccharification for TRS production. The schematic presentation of PP ad MP processing for enzymatic saccharification is illustrated in Fig. 5.5.

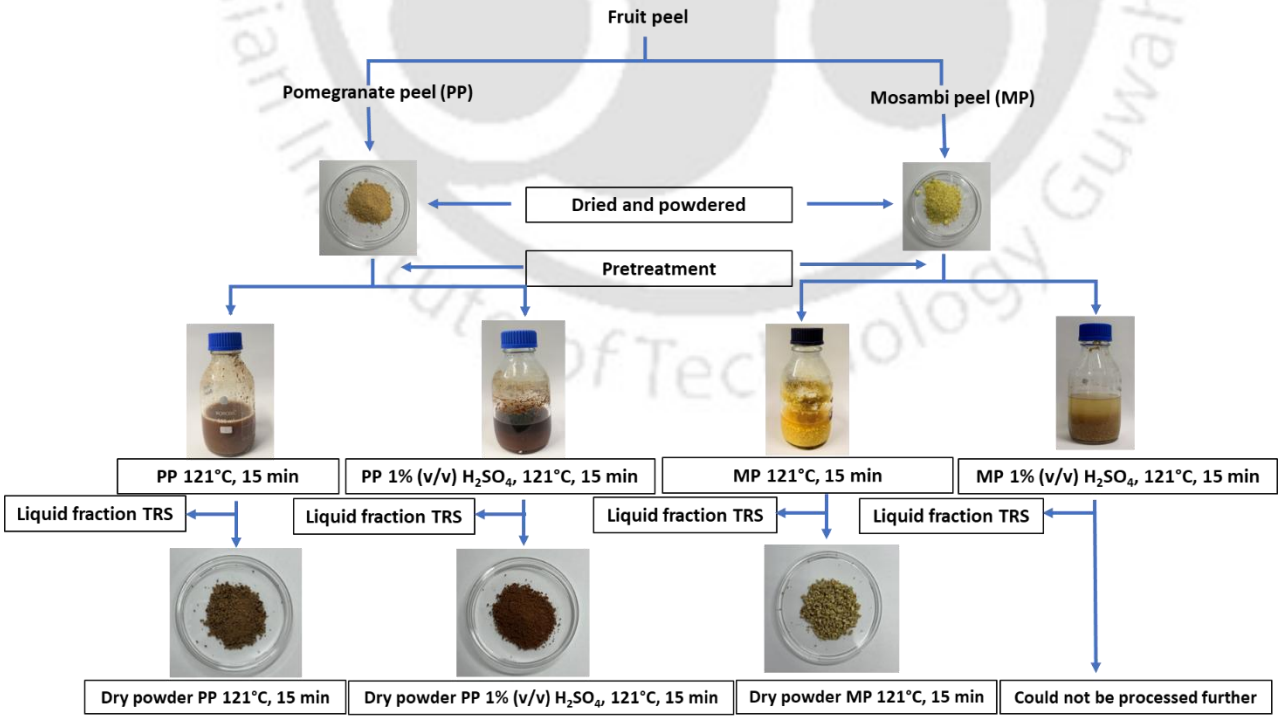

Fig. 5.5 Schematic presentation of fruit peel biomass pretreatment.

Table 5.3. Analysis of TRS and monosaccharides in raw biomass and released in liquid fraction after the pretreatment process.

Biomass	Pretreatment	TRS [a*] (mg/g raw biomass)	Xylose [b*] (mg/g raw biomass)
Pomegranate	Raw	66 mg/g raw PP	-
	Autoclave 121°C	107.1 mg/g raw PP	87 mg/g raw PP
	1% H_2SO_4 + Autoclave 121°C	91.2 mg/g raw PP	89 mg/g raw PP
Mosambi	Raw	60 mg/g raw MP	-
	Autoclave 121°C	162.4 mg/g raw MP	107 mg/g raw MP
	1% H_2SO_4 + Autoclave 121°C	155.6 mg/g raw MP	107 mg/g raw MP

[a]*:TRS: Total reducing sugar, TRS yield estimated by the method of Nelson (1944) and Somogyi (1945)*

[b]*: HPLC analysis*

5.3.4.5 Quantitative analysis of reducing sugar of raw and pretreated peels after saccharification by *Bo*GH43_35 and *Bo*ExXyl43A

The total reducing sugar of the enzymatic hydrolysates was analyzed by Nelson (1944) and Somogyi (1945) methods. The monosaccharide composition of raw and pretreated PP and MP afer enzymatic hydrolysis was determined using HPLC. The saccharification of raw and pretreated PP and MP using *Bo*GH43_35 and *Bo*ExXyl43A was carried out and the results are summarized in Table 5.4. *Bo*GH43_35 gave TRS yield of 558.0 mg/g raw PP for raw PP, whereas, *Bo*ExXyl43A gave TRS yield for raw PP of 563.8 mg/g raw PP. However, the enzyme combination, *Bo*GH43_35 + *Bo*ExXyl43A gave the highest TRS yield for raw PP (623.8 mg/g raw PP). Commercial xylanase yielded TRS of 558.0 mg/g raw PP. This shows that raw PP was efficiently converted to reducing sugars using enzyme combination, *Bo*GH43_35 + *Bo*ExXyl43A. For pomegranate peel, the highest xylose yield was 194.5 mg/g raw PP with the combination *Bo*GH43_35 and *Bo*ExXyl43A. *Bo*ExXyl43A treatment gave the highest xylobiose yield, 70.8 mg/g raw PP, suggesting that these enzymes efficiently break down xylan into both xylose and xylobiose. Pomegranate peel showed a higher TRS yield in the range of 154-373 mg/g raw PP across all pretreatments, likely due to

differences in its hemicellulose composition remaining after pretreatments. Raw mosambi peel when treated with *Bo*GH43_35 alone, yielded TRS of 471.2 mg/g raw MP. With the combination *Bo*GH43_35 and *Bo*ExXyl43A, TRS of 505.4 mg/g raw MP was obtained for raw MP. Commercial xylanase yielded TRS of 512.3 mg/g raw MP. For mosambi peel, the highest xylose yield was 255 mg/g raw MP for raw MP, observed when treated with *Bo*ExXyl43A alone. Xylose recovery was higher for raw MP with yield of 243 mg/g raw MP compared to 194 mg/g raw PP for raw PP, corroborating with the higher hemicellulose content in MP as compared to PP. Higher xylose recovery also indicated that mosambi hemicelluloses might be more susceptible to enzymatic hydrolysis.

Table 5.4 Quantification of monosaccharides in the enzyme saccharified hydrolysate at 48 h.

Biomass	Enzyme Treatment	TRS [a] (mg/g raw biomass)	Xylose [b] (mg/g raw biomass)	Arabinose [b] (mg/g raw biomass)	Xylobiose [b] (mg/g raw biomass)
Pomegranate peel (Raw)	*Bo*GH43_35	558.0 mg/g raw PP	180.6 mg/g raw PP	133.2 mg/g raw PP	66.2 mg/g raw PP
	*Bo*ExXyl43A	563.8 mg/g raw PP	123.7 mg/g raw PP	-	-
	*Bo*GH43_35+ *Bo*ExXyl43A	623.8 mg/g raw PP	194.5 mg/g raw PP	134.9 mg/g raw PP	70.8 mg/g raw PP
	Commercial xylanase	593.8 mg/g raw PP	132.2 mg/g raw PP	104.3 mg/g raw PP	58.0 mg/g raw PP
Pomegranate peel (Autoclave at 121°C, 15 min)	*Bo*GH43_35	334 mg/g raw PP	-	-	-
	*Bo*ExXyl43A	322.4 mg/g raw PP	-	-	-
	*Bo*GH43_35+ *Bo*ExXyl43A	373.9 mg/g raw PP	-	-	-
	Commercial xylanase	343.4 mg/g raw PP	-	-	-
Pomegranate peel (1% H_2SO_4 + Autoclave at 121°C, 15 min)	*Bo*GH43_35	154.1.0 mg/g raw PP	-	-	-
	*Bo*ExXyl43A	160.9 mg/g raw PP	-	-	-
	*Bo*GH43_35+ *Bo*ExXyl43A	178.8 mg/g raw PP	65.7 mg/g raw PP	-	-
	Commercial xylanase	177.2 mg/g raw PP	-	-	-
Mosambi peel (Raw)	*Bo*GH43_35	471.2 mg/g raw MP	246 mg/g raw MP	-	-
	*Bo*ExXyl43A	480.7 mg/g raw MP	255 mg/g raw MP	-	-
	*Bo*GH43_35+ *Bo*ExXyl43A	505.4 mg/g raw MP	243 mg/g raw MP	-	-
	Commercial xylanase	512.3 mg/g raw MP	-	-	-
Mosambi peel (Autoclave at 121°C, 15 min)	*Bo*GH43_35	230.3 mg/g raw MP	-	-	-
	*Bo*ExXyl43A	168.8 mg/g raw MP	-	-	-
	*Bo*GH43_35+ *Bo*ExXyl43A	238.8 mg/g raw MP	11.5 mg/g raw MP	-	-
	Commercial xylanase	198.8 mg/g raw MP	-	-	-

Each saccharification involved: Biomass loading 10% (w/v) in 50 mM sodium phosphate buffer, pH 7.0, 37°C for 48 h.

[a]TRS: Total reducing sugar, TRS yield estimated by the method of Nelson (1944) and Somogyi (1945)

[b]: HPLC analysis

- denotes 'no detectable amount of sugar

5.4 Conclusion

*Bo*GH43_35, a bifunctional α-L-arabinofuranosidase/endo-β-1,4-xylanase from *Bacteroides ovatus*, demonstrates its versatility and efficiency in two distinct yet interconnected applications: fruit juice clarification and enzymatic peel hydrolysis**.** The enzyme successfully improves juice transparency**,** reduces viscosity and enhances saccharification of fruit peels**,** paving the way for sustainable applications in food, bioenergy and waste management industries. The results demonstrated that *Bo*GH43_35 treatment improves juice clarity, especially at higher enzyme concentration (1.0 mg/mL) and longer incubation time (4 hours). Turbidity in pomegranate juice decreased from 20.1 NTU (control) to 3.8 NTU, while in mosambi juice, turbidity reduced from 597 NTU to 290 NTU. The percentage of light transmittance increased significantly, indicating enhanced juice clarity. The enzymatic treatment with *Bo*GH43_35 lowered the juice viscosity, making filtration and processing more efficient. The discarded waste peels of pomegranate and mosambi were subjected to enzymatic saccharification with *Bo*GH43_35 and *Bo*ExXyl43A (exo-β-1,4-xylosidase from *Bacteroides ovatus*), converting hemicellulose into soluble reducing sugars, which could serve as valuable substrates for various industrial applications**.** The combination of *Bo*GH43_35 and *Bo*ExXyl43A showed maximum TRS yield**,** confirming their synergistic action. Raw pomegranate peel (PP) and mosambi peel (MP) contained significant amounts of reducing sugars, with TRS yields of 66 mg/g raw PP and 60 mg/g raw MP. Enzymatic treatment of raw PP and raw MP resulted in the TRS yields of 623.8 mg/g raw PP and 505.4 mg/g raw MP. With continued research and industrial adoption, *Bo*GH43_35 has the potential to

revolutionize fruit processing and lignocellulosic biomass utilization, contributing to a more sustainable and efficient agro-industrial sector.

5.5 References

Babalola, T., Apata, D., & Atteh, J. (2006). Effect of β-xylanase supplementation of boiled castor seed meal-based diets on the performance, nutrient absorbability and some blood constituents of pullet chicks. *Tropical Science*, *46*(4), 216–223. https://doi.org/10.1002/ts.181

Bajaj, P., & Mahajan, R. (2019). Cellulase and xylanase synergism in industrial biotechnology. *Applied Microbiology and Biotechnology*, *103*(21), 8711–8724. https://doi.org/10.1007/s00253-019-10146-0

Beaulieu, L. Y., Logan, E. R., Gering, K. L., & Dahn, J. R. (2017). An automated system for performing continuous viscosity versus temperature measurements of fluids using an Ostwald viscometer. *Review of Scientific Instruments*, *88*(9), 095101. https://doi.org/10.1063/1.4990134

Bian, J., Peng, F., Peng, X.-P., Xu, F., Sun, R.-C., & Kennedy, J. F. (2012). Isolation of hemicelluloses from sugarcane bagasse at different temperatures: Structure and properties. *Carbohydrate Polymers*, *88*(2), 638–645. https://doi.org/10.1016/j.carbpol.2012.01.010

Bradford, M. M. (1976). A rapid and sensitive method for the quantitation of microgram quantities of protein utilizing the principle of protein-dye binding. *Analytical Biochemistry*, *72*(1–2), 248–254. https://doi.org/10.1016/0003-2697(76)90527-3

Chen, J., Wang, Q., Zhou, J., Yang, J., Xu, L., Huo, D., & Wei, Z. (2024). Optimization of α-L-arabinofuranosidase CcABF on clarification and beneficial active substances in fermented ginkgo kernel juice by artificial neural network and genetic algorithm. *Food Chemistry*, *450*, 139386. https://doi.org/10.1016/j.foodchem.2024.139386

Dhiman, S. S., Garg, G., Sharma, J., & Mahajan, R. (2011). Characterization of statistically produced xylanase for enrichment of fruit juice clarification process. *New Biotechnology*, *28*(6), 746–755. https://doi.org/10.1016/j.nbt.2010.11.004

Figueiredo, R., Araújo, P., Llerena, J. P. P., & Mazzafera, P. (2019). Suberin and hemicellulose in sugarcane cell wall architecture and crop digestibility: A biotechnological perspective. *Food and Energy Security*, *8*(3), e00163. https://doi.org/10.1002/fes3.163

Gavande, P. V., Ji, S., Cardoso, V., M.G.A. Fontes, C., & Goyal, A. (2024). Reassigning the role of a mesophilic xylan hydrolysing family GH43 β-xylosidase from *Bacteroides ovatus*, *Bo*ExXyl43A as exo-β-1,4-xylosidase. *Current Research in Biotechnology*, *7*, 100191. https://doi.org/10.1016/j.crbiot.2024.100191

Haider, M. W., Abbas, S. M., Saeed, M. A., Farooq, U., Waseem, M., Adil, M., Javed, M. R., Haq, I. U., & Osei Tutu, C. (2025). Environmental and utritional value of fruit and vegetable peels as animal feed: A comprehensive review. *Animal Research and One Health*, aro2.70002. https://doi.org/10.1002/aro2.70002

İlgü, H., Sürmeli, Y., & Şanlı-Mohamed, G. (2018). A thermophilic α-L-arabinofuranosidase from *Geobacillus vulcani* GS90: Heterologous expression, biochemical characterization, and its synergistic action in fruit juice enrichment. *European Food Research and Technology*, *244*(9), 1627–1636. https://doi.org/10.1007/s00217-018-3075-7

Jacob, N., Sukumaran, R. K., & Prema, P. (2008). Optimization of enzymatic clarification of sapodilla juice: A statistical perspective. *Applied Biochemistry and Biotechnology*, *151*(2–3), 353–363. https://doi.org/10.1007/s12010-008-8198-z

Jacqueline, P. J., & Velvizhi, G. (2024). Co-fermentation exploiting glucose and xylose utilizing thermotolerant *S. cerevisiae* of highly lignified biomass for biofuel production: Statistical optimization and kinetic models. *Biocatalysis and Agricultural Biotechnology*, *58*, 103197. https://doi.org/10.1016/j.bcab.2024.103197

John, I., Pola, J., Thanabalan, M., & Appusamy, A. (2020). Bioethanol production from musambi peel by acid catalyzed steam pretreatment and enzymatic saccharification: Optimization of delignification using Taguchi design. *Waste and Biomass Valorization*, *11*(6), 2631–2643. https://doi.org/10.1007/s12649-018-00565-x

Kačuráková, M., Capek, P., Sasinková, V., Wellner, N., & Ebringerová, A. (2000). FT-IR study of plant cell wall model compounds: Pectic polysaccharides and hemicelluloses. *Carbohydrate Polymers*, *43*(2), 195–203. https://doi.org/10.1016/S0144-8617(00)00151-X

Kandylis, P., & Kokkinomagoulos, E. (2020). Food applications and potential health benefits of pomegranate and its derivatives. *Foods*, *9*(2), Article 2. https://doi.org/10.3390/foods9020122

Kaushal, J., Khatri, M., Singh, G., & Arya, S. K. (2021). A multifaceted enzyme conspicuous in fruit juice clarification: An elaborate review on xylanase. *International Journal of Biological Macromolecules*, *193*, 1350–1361. https://doi.org/10.1016/j.ijbiomac.2021.10.194

Kotsampasi, B., Christodoulou, V., Zotos, A., Liakopoulou-Kyriakides, M., Goulas, P., Petrotos, K., Natas, P., & Bampidis, V. A. (2014). Effects of dietary pomegranate byproduct silage supplementation on performance, carcass characteristics and meat quality of growing lambs. *Animal Feed Science and Technology*, *197*, 92–102. https://doi.org/10.1016/j.anifeedsci.2014.09.003

Liu, N., Ru, Y. J., Tang, D. F., Xu, T. S., & Partridge, G. G. (2011). Effects of corn distillers dried grains with solubles and xylanase on growth performance and digestibility of diet components in broilers. *Animal Feed Science and Technology*, *163*(2), 260–266. https://doi.org/10.1016/j.anifeedsci.2010.11.004

Maibam, P. D., & Goyal, A. (2022). Pretreatment methods for overcoming biomass recalcitrance. In *Enzymes in the Valorization of Waste*. CRC Press.

Maibam, P. D., & Goyal, A. (2023). Designing of recombinant hydrolytic enzymes cocktail for effective saccharification of delignified rice straw. *Industrial Crops and Products*, *206*, 117727. https://doi.org/10.1016/j.indcrop.2023.117727

Nagar, S., Mittal, A., & Gupta, V. K. (2012). Enzymatic clarification of fruit juices (Apple, Pineapple, and Tomato) using purified *Bacillus pumilus* SV-85S xylanase. *Biotechnology and Bioprocess Engineering*, *17*(6), 1165–1175. https://doi.org/10.1007/s12257-012-0375-9

Nelson, N. (1944). A photometric adaptation of the somogyi method for the determination of glucose. *Journal of Biological Chemistry*, *153*(2), 375–380. https://doi.org/10.1016/S0021-9258(18)71980-7

Pathak, P. D., Mandavgane, S. A., & Kulkarni, B. D. (2016). Characterizing fruit and vegetable peels as bioadsorbents. *Current Science*, *110*(11), 2114–2123.

Pathak, P. D., Mandavgane, S. A., & Kulkarni, B. D. (2017). Valorization of pomegranate peels: A biorefinery approach. *Waste and Biomass Valorization*, *8*(4), 1127–1137. https://doi.org/10.1007/s12649-016-9668-0

Ravanal, M. C., Rosa, L., & Eyzaguirre, J. (2012). α-L-Arabinofuranosidase 3 from *Penicillium purpurogenum* (ABF3): Potential application in the enhancement of wine flavour and heterologous expression of the enzyme. *Food Chemistry*, *134*(2), 888–893. https://doi.org/10.1016/j.foodchem.2012.02.200

Saadi, W., Rodríguez-Sánchez, S., Ruiz, B., Souissi-Najar, S., Ouederni, A., & Fuente, E. (2019). Pyrolysis technologies for pomegranate (*Punica granatum L.*) peel wastes. Prospects in the bioenergy sector. *Renewable Energy*, *136*, 373–382. https://doi.org/10.1016/j.renene.2019.01.017

Sagar, N. A., Pareek, S., Sharma, S., Yahia, E. M., & Lobo, M. G. (2018). Fruit and vegetable waste: Bioactive compounds, their extraction, and possible utilization. *Comprehensive Reviews in Food Science and Food Safety*, *17*(3), 512–531. https://doi.org/10.1111/1541-4337.12330

Saheed, O. K., Jamal, P., Karim, M. I. A., Alam, Md. Z., & Muyibi, S. A. (2016). Utilization of fruit peels as carbon source for white rot fungi biomass production under submerged state bioconversion. *Journal of King Saud University - Science*, *28*(2), 143–151. https://doi.org/10.1016/j.jksus.2015.08.002

Saikia, D. K., Chikkaputtaiah ,Channakeshavaiah, & Velmurugan, N. (2024). Nutritional enrichment of fruit peel wastes using lipid accumulating Aurantiochytrium strain as feed for aquaculture in the North-East Region of India. *Environmental Technology*, *45*(6), 1215–1233. https://doi.org/10.1080/09593330.2022.2139638

Sarkar, R., Nain, L., Dutta, A., Kundu, A., & Saha, S. (2024). Unraveling the utilization feasibility of citrus peel solid distillation waste as potential source for antioxidant as well as bioethanol. *Biomass Conversion and Biorefinery*, *14*(21), 27379–27391. https://doi.org/10.1007/s13399-022-03367-3

Shabtay, A., Nikbachat, M., Zenou, A., Yosef, E., Arkin, O., Sneer, O., Shwimmer, A., Yaari, A., Budman, E., Agmon, G., & Miron, J. (2012). Effects of adding a

concentrated pomegranate extract to the ration of lactating cows on performance and udder health parameters. *Animal Feed Science and Technology*, *175*(1), 24–32. https://doi.org/10.1016/j.anifeedsci.2012.04.004

Sharma, K., Khaire, K. C., Thakur, A., Moholkar, V. S., & Goyal, A. (2020). Acacia xylan as a substitute for commercially available xylan and its application in the production of xylooligosaccharides. *ACS Omega*, *5*(23), 13729–13738. https://doi.org/10.1021/acsomega.0c00896

Shrivastava, M., Aishwarya, A., Fontes, C. M. G. A., & Goyal, A. (2025). A novel bifunctional type I α-L-arabinofuranosidase of family 43 glycoside hydrolase (*Bo*GH43_35) from *Bacteroides ovatus* with endo-β-1,4-xylanase activity. *Carbohydrate Research*, *552*, 109432. https://doi.org/10.1016/j.carres.2025.109432

Singh, B., Garg, N., Mathur, P., Soni, S. K., Vaish, S., & Kumar, S. (2022). Microbial production of multienzyme preparation from mosambi peel using Trichoderma asperellum. *Archives of Microbiology*, *204*(6), 313. https://doi.org/10.1007/s00203-022-02913-x

Singh, V., & Das, C. (2021). Clarification of citrus fruit (Mosambi) juice by hybrid (Pretreatment and Membrane) process. *Materials Today: Proceedings*, *47*, 1384–1388. https://doi.org/10.1016/j.matpr.2021.02.435

Somogyi, M. (1945). A new reagent for the determination of sugars. *Journal of Biological Chemistry*, *160*(1), 61–68. https://doi.org/10.1016/S0021-9258(18)43097-9

Tochi, B., Zhang, W., Shi-Ying, X., & Zhang, W. (2009). The influence of a pectinase and pectinase/hemicellulases enzyme preparations on percentage pineapple juice recovery, particulates and sensory attributes. *Pakistan Journal of Nutrition*, *8*. https://doi.org/10.3923/pjn.2009.1184.1189

Viikari, L., Kantelinen, A., Sundquist, J., & Linko, M. (1994). Xylanases in bleaching: From an idea to the industry. *FEMS Microbiology Reviews*, *13*(2–3), 335–350. https://doi.org/10.1111/j.1574-6976.1994.tb00053.x

Wang, T., Zhao, Q., Li, C., He, F., Jiang, L., & Aisa, H. A. (2021). Integrating chemical and biological catalysis for simultaneous production of polyphenolics and butyric acid from waste pomegranate peels. *Science of The Total Environment*, *778*, 146095. https://doi.org/10.1016/j.scitotenv.2021.146095

Wanlapa, S., Wachirasiri, K., Sithisam-ang, D., & Suwannatup, T. (2015). Potential of selected tropical fruit peels as dietary fiber in functional foods. *International Journal of Food Properties*, *18*(6), 1306–1316. https://doi.org/10.1080/10942912.2010.535187

Xue, Y., Cui, X., Zhang, Z., Zhou, T., Gao, R., Li, Y., & Ding, X. (2020). Effect of β-endoxylanase and α-arabinofuranosidase enzymatic hydrolysis on nutritional and technological properties of wheat brans. *Food Chemistry*, *302*, 125332. https://doi.org/10.1016/j.foodchem.2019.125

LIST OF PUBLICATIONS

Publication from the Thesis

Research Articles

1. **Madhulika Shrivastava** and Arun Goyal (2025) Unveiling the structural and functional perspectives of a bifunctional α-l-arabinofuranosidase/endo-β-1,4-xylanase (*Bo*GH43_35) from *Bacteroides ovatus*. *Archives of Biochemistry and Biophysics*, 764, 110232.
2. **Madhulika Shrivastava**, Aishwarya Aishwarya, Carlos M.G.A. Fontes and Arun Goyal (2025) A novel bifunctional type I α-L-arabinofuranosidase of family 43 glycoside hydrolase (*Bo*GH43_35) from *Bacteroides ovatus* with endo-β-1,4-xylanase activity. *Carbohydrate Research*, 552, 109432.

Publication from other collaborations

1. **Madhulika Shrivastava**, Yumnam Robinson Singh and Arun Goyal (2024) Structure analysis of a putative exo-rhamnogalacturonan lyase of the polysaccharide lyase family 26 from *Bacteroides thetaiotaomicron* by computational methods. *Journal of Proteins and Proteomics*, 1-16.

Book chapters

1. **Madhulika Shrivastava** and Arun Goyal. (2024). Fundamentals and Industrial Applications of Modern Genetic Engineering. In *Industrial Microbiology and Biotechnology Vol III: An Insight into Current Trends* (pp. 35-52). Singapore: Springer Nature Singapore.
2. **Madhulika Shrivastava,** Premeshworii D. Maibam, Aishwarya Aishwarya and Arun Goyal (2024). Hemicellulases and auxiliary activities for biomass hydrolysis. In *Handbook of Biorefinery Research and Technology: Biomass Logistics to Saccharification* (pp. 731-753). Dordrecht: Springer Netherlands.

LIST OF CONFERENCES

Conferences/Symposia

1. **Madhulika Shrivastava**, Aishwarya Aishwarya, Carlos M.G.A. Fontes and Arun Goyal (2024) A novel bifunctional α-L-arabinofuranosidase / endo-β-1,4-xylanase, a family 43 glycoside hydrolase from *Bacteroides ovatus* with Type I arabinofuranosidase activity. IX International Conference on Sustainable Energy and Environmental Challenges, 13-15th December, 2024, IIT Mandi, Himachal Pradesh, India. (Best Paper Award)
2. **Madhulika Shrivastava** and Arun Goyal (2024) Structural and functional characterization of a novel α-L-arabinofuranosidase with endo-β-1,4-xylanase activity of glycoside hydrolase family 43 from Bacteroides ovatus. Association of Carbohydrate Chemists and Technologists, India (ACCTI-2024). Dec 4-6, 2024, Gauhati University, Assam, India.
3. **Madhulika Shrivastava**, Aishwarya Aishwarya, Carlos M.G.A. Fontes and Arun Goyal (2024) A novel bifunctional α-L-arabinofuranosidase / endo-β-1,4-xylanase, a family 43 glycoside hydrolase from *Bacteroides ovatus* with Type I arabinofuranosidase activity. Research and Industrial Conclave (RIC-2024). Aug 9-11, 2024, Indian Institute of Technology Guwahati, Assam, India.
4. **Madhulika Shrivastava**, Jebin Ahmed and Arun Goyal (2023) Isolation and structure characterization of recombinant Rhamnogalacturonan exolyase from *Bacteroides thetaiotaomicron* expressed as inclusion bodies in *E. coli*. Research and Industrial Conclave (RIC-2023). May 14-16, 2023, Indian Institute of Technology Guwahati, Assam, India.
5. **Madhulika Shrivastava**, Jebin Ahmed and Arun Goyal (2022) Solubilization, refolding and characterization of recombinant Rhamnogalacturonan exolyase from *Bacteroides thetaiotamicron* expressed as inclusion bodies in *E. coli*. International Carbohydrate Conference (CARBO XXXVI). December 05-07, 2022, Indian Institute of Technology Powai, Mumbai, India.
6. **Madhulika Shrivastava**, Kedar Sharma and Arun Goyal (2021) Construction of bi-functional chimeric enzyme by fusing from α-L-arabinofuranosidase from *Pseudopedobacter saltans* (*Ps*GH43_12) and endo-1,4-β-xylanase *Clostridium thermocellum* (*Ct*GH11A). International conference on advances in chemistry and biology of carbohydrates (CARBO XXXV). December 04-05, 2021, Dehradun, Uttrakhand, India.
7. **Madhulika Shrivastava**, Kedar Sharma and Arun Goyal (2021) Development and in-silico characterization of a bi-functional chimeric enzyme by fusing α-L-arabinofuranosidase from *Pseudopedobacter saltans* (*Ps*GH43_12) and endo-1,4-β-xylanase from *Clostridium thermocellum* (*Ct*GH11A) using protein engineering. Research & Industrial Conclave 2022"An amalgamation of Academia, Industry & Start-up". January 20-23, 2022, Indian Institute of Technology Guwahati, India

Awards and Honours

1. Awarded with '**Best paper award**' at IX International Conference on Sustainable Energy and Environmental Challenges, 13-15th December, 2024, IIT Mandi, Himachal Pradesh, India, for the article "**Madhulika Shrivastava**, Aishwarya Aishwarya, Carlos M.G.A. Fontes and Arun Goyal (2024) A novel bifunctional α-L-arabinofuranosidase/endo-β-1,4-xylanase, a family 43 glycoside hydrolase from *Bacteroides ovatus* with Type I arabinofuranosidase activity.

VITAE

Ms Madhulika Shrivastava was born on December 25, 1994 in Hathwa, Bihar, India. She passed the Secondary School Examination (10th Standard) conducted by Central Board of Secondary Education (CBSE) in 2011 and Higher Secondary Education (12th Standard) conducted by Central Board of Secondary Education (CBSE) in 2013. She completed B.Sc. Biotechnology from Mount Carmel College, Bengaluru, Karnataka, India in 2016. She qualified Combined Entrance Examination for Biotechnology (2016) and did M.Sc. in Industrial Biotechnology from Sardar Patel University, Anand, Gujarat, India.

Ms Madhulika Shrivastava qualified Graduate Aptitude Test in Engineering (GATE) 2018 and joined the Ph.D. programme in July 2020 at Department of Biosciences and Bioengineering, Indian Institute of Technology Guwahati, Guwahati 781039, Assam, India. She received an Institute fellowship for her Ph.D tenure under the scheme run by the Ministry of Education, Govt. of India. She delivered PhD Synopsis Seminar on her thesis work on May 08, 2025, and submitted the PhD thesis on May 20, 2024.